USGS
science for a changing world

National Climate Change and Wildlife Science Center

Application of the Precipitation-Runoff Modeling System (PRMS) in the Apalachicola–Chattahoochee–Flint River Basin in the Southeastern United States

Scientific Investigations Report 2013–5162

U.S. Department of the Interior
U.S. Geological Survey

Cover. All photographs by Alan M. Cressler, U.S. Geological Survey, unless noted otherwise.
Top left: Chattahoochee National Forest, White County, Georgia
Top right: Chattahoochee River, Fulton and Cobb Counties, Georgia
Middle left: Apalachicola River, Franklin County, Florida
Middle right: Woodruff Lock and Dam, Gadsden and Jackson Counties, Florida
Bottom left: Shinyrayed pocketbook Hamiota subangulata (Andrea Fritts, University of Illinois)
Bottom right: Black banded darter

Application of the Precipitation-Runoff Modeling System (PRMS) in the Apalachicola–Chattahoochee–Flint River Basin in the Southeastern United States

By Jacob H. LaFontaine, Lauren E. Hay, Roland J. Viger, Steve L. Markstrom, R. Steve Regan, Caroline M. Elliott, and John W. Jones

National Climate Change and Wildlife Science Center

Scientific Investigations Report 2013–5162

U.S. Department of the Interior
U.S. Geological Survey

U.S. Department of the Interior
SALLY JEWELL, Secretary

U.S. Geological Survey
Suzette M. Kimball, Acting Director

U.S. Geological Survey, Reston, Virginia: 2013

Suggested citation:
LaFontaine, J.H., Hay, L.E., Viger, R.J., Markstrom, S.L., Regan, R.S., Elliott, C.M., and Jones, J.W., 2013, Application of the Precipitation-Runoff Modeling System (PRMS) in the Apalachicola–Chattahoochee–Flint River Basin in the southeastern United States: U.S. Geological Survey Scientific Investigations Report 2013–5162, 118 p., http://pubs.usgs.gov/sir/2013/5162/.

Contents

Figures

Tables

Conversion Factors and Datums

SI to Inch/Pound

Multiply	By	To obtain
	Length	
millimeter (mm)	0.03937	inch
meter (m)	3.281	foot (ft)
kilometer (km)	0.6214	mile (mi)
kilometer (km)	0.5400	mile, nautical (nmi)
meter (m)	1.094	yard (yd)
	Area	
square kilometer (km^2)	247.1	acre
square kilometer (km^2)	0.3861	square mile (mi^2)
	Potential evapotranspiration	
millimeter per day (mm/d)	0. 03937	inch per day (in/d)

Temperature in degrees Celsius (°C) may be converted to degrees Fahrenheit (°F) as follows:

$$°F = (1.8 \times °C) + 32$$

Vertical coordinate information is referenced to the North American Vertical Datum of 1988 (NAVD 88)

Horizontal coordinate information is referenced to the North American Datum of 1983 (NAD 83)

Altitude, as used in this report, refers to distance above the vertical datum.

Abbreviations

ACFB	Apalachicola–Chattahoochee–Flint River Basin
COOP	cooperative network
CBH	climate by HRU
CF	Coastal Plain in Floridan aquifer system outcrop area
CR	Coastal Plain outside Floridan aquifer system outcrop area
DEM	digital elevation model
FORE-SCE	FORcasting SCEnarios
GCM	general circulation model
GIS	geographic information system
GUI	graphical user interface
HRU	hydrologic response unit
HSPF	Hydrologic Simulation Program Fortran
K	permeability
MS	Mainstem Apalachicola, Chattahoochee, and Flint Rivers
MODFE	MODular Finite-Element software
NAWQA	National Water-Quality Assessment Program
NCCWSC	National Climate Change and Wildlife Science Center
NRMSE	normalized root mean square error
NHD	National Hydrography Dataset
NLCD	National Land Cover Dataset
NOAA	National Oceanic and Atmospheric Administration
NS	Nash-Sutcliffe Model Efficiency Index
NWI	National Wetland Inventory
PD	Blue Ridge and Piedmont developed
PET	potential evapotranspiration
PR	Blue Ridge and Piedmont rural
PRISM	Parameter-elevation Regressions on Independent Slopes Model
PRMS	Precipitation-Runoff Modeling System
SCE	shuffled complex evolution
SERAP	Southeast Regional Assessment Project
SR	solar radiation
TM	Thematic Mapper
USACE	U.S. Army Corps of Engineers
USGS	U.S. Geological Survey
WRS	worldwide reference system

Application of the Precipitation-Runoff Modeling System (PRMS) in the Apalachicola–Chattahoochee–Flint River Basin in the Southeastern United States

By Jacob H. LaFontaine, Lauren E. Hay, Roland J. Viger, Steve L. Markstrom, R. Steve Regan, Caroline M. Elliott, and John W. Jones

Abstract

A hydrologic model of the Apalachicola–Chattahoochee–Flint River Basin (ACFB) has been developed as part of a U.S. Geological Survey (USGS) National Climate Change and Wildlife Science Center effort to provide integrated science that helps resource managers understand the effect of climate change on a range of ecosystem responses. The hydrologic model was developed as part of the Southeast Regional Assessment Project using the Precipitation Runoff Modeling System (PRMS), a deterministic, distributed-parameter, process-based system that simulates the effects of precipitation, temperature, and land use on basin hydrology.

The ACFB PRMS model simulates streamflow throughout the approximately 50,700 square-kilometer basin on a daily time step for the period 1950–99 using gridded climate forcings of air temperature and precipitation, and parameters derived from spatial data layers of altitude, land cover, soils, surficial geology, depression storage (small water bodies), and data from 56 USGS streamgages. Measured streamflow data from 35 of the 56 USGS streamgages were used to calibrate and evaluate simulated basin streamflow; the remaining gage locations were used for model delineation only. The model matched measured daily streamflow at 31 of the 35 calibration gages with Nash-Sutcliffe Model Efficiency Index (NS) greater than 0.6. Streamflow data for some calibration gages were augmented for regulation and water use effects to represent more natural flow volumes. Time-static parameters describing land cover limited the ability of the simulation to match historical runoff in the more developed subbasins.

Overall, the PRMS simulation of the ACFB provides a good representation of basin hydrology on annual and monthly time steps. Calibration subbasins were analyzed by separating the 35 subbasins into five classes based on physiography, land use, and stream type (tributary or mainstem). The lowest NS values were rarely below 0.6, whereas the median NS for all five classes was within 0.74 to 0.96 for annual mean streamflow, 0.89 to 0.98 for mean monthly streamflow, and 0.82 to 0.98 for monthly mean streamflow. The median bias for all five classes was within –4.3 to 0.8 percent for annual mean streamflow, –6.3 to 0.5 percent for mean monthly streamflow, and –9.3 to 1.3 percent for monthly mean streamflow. The NS results combined with the percent bias results indicated a good to very good streamflow volume simulation for all subbasins.

This simulation of the ACFB provides a foundation for future modeling and interpretive studies. Streamflow and other components of the hydrologic cycle simulated by PRMS can be used to inform other types of simulations; water-temperature, hydrodynamic, and ecosystem-dynamics simulations are three examples. In addition, possible future hydrologic conditions could be studied using this model in combination with land cover projections and downscaled general circulation model results.

Introduction

The U.S. Geological Survey (USGS) National Climate Change and Wildlife Science Center (NCCWSC; *http://nccwsc.usgs.gov/*) is supporting a series of regional assessments that provide integrated science that is useful to resource managers to understand the effect of climate change on a range of ecosystem responses. The chosen methodology is to link simulation models that span a broad range of scales and themes; from planetary general circulation models (GCMs) to local models of landscape dynamics and biota (fig. 1). The USGS Southeast Regional Assessment Project (SERAP; *http://serap.er.usgs.gov*) is the first regional assessment to be funded by the NCCWSC. SERAP has been developed in close coordination with recently formed Department of the Interior Landscape Conservation Cooperatives (*http://www.doi.gov/lcc/index.cfm*) to ensure that its products meet the needs of resource managers in the southeastern United States. Scientists associated with SERAP have developed regional models and other science tools to help environmental resource managers assess potential effects of climate change on land cover, ecosystems, and priority species in the region.

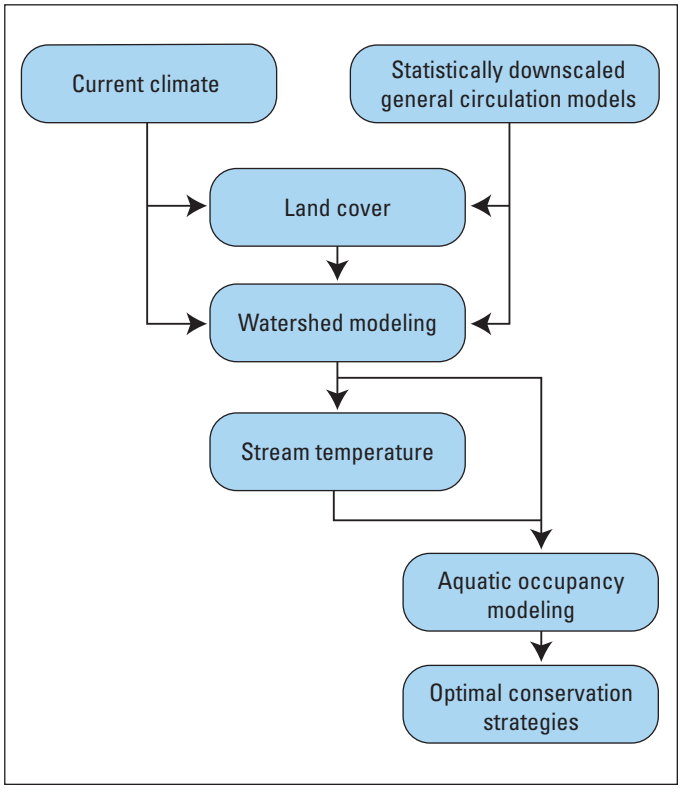

Figure 1. Southeast Regional Assessment Project data flow showing the various linkages of climate, landscape, and biota dynamics to watershed modeling.

One component of SERAP is the development of a hydrologic model for the Apalachicola–Chattahoochee–Flint River Basin (ACFB) (fig. 2). The basin is home to numerous fish and wildlife species of conservation concern and is regionally important for water supply. In recent decades, competing demands of municipal, industrial, and agricultural water use; ecological needs of fishes and mussels; and economic development have resulted in conflict and discussions between stakeholders in Alabama, Florida, and Georgia over water allocation in the ACFB (U.S. Army Corps of Engineers, 1997). Potential impacts on the various ecosystems within the ACFB caused by land cover changes (urbanization and vegetation) and possible climate change are being addressed as part of SERAP. The hydrologic model of the ACFB, developed as part of SERAP, will be used to determine how the basin potentially is affected by changes in land cover and by climate change.

Purpose and Scope

This report documents the development and calibration of a hydrologic model to simulate the potential impacts of land cover and climate change on the hydrology of the ACFB. The hydrologic model is developed using the USGS Precipitation Runoff Modeling System (PRMS; Leavesley and others, 1983; Markstrom and others, 2008), a deterministic, distributed-parameter, process-based model used to simulate the effects of precipitation, temperature, and land use on basin hydrology. The ACFB is divided into subareas called hydrologic response units (HRUs) in which the components of flow (groundwater (saturated zone), subsurface (unsaturated zone), and surface runoff) are computed in response to precipitation, air temperature, and land and subsurface characteristics of the basin (Leavesley and others, 1983). Daily maximum and minimum temperature and precipitation data on an approximately 12-kilometer (km) grid for 1950–99 are used as climatic forcings for PRMS.

Description of the Study Area

The ACFB includes three major rivers—the Apalachicola, Chattahoochee, and Flint Rivers (fig. 2). The Chattahoochee River begins in the mountains of northeastern Georgia and flows southwest through metropolitan Atlanta to the Alabama-Georgia border, where the river flows southward to Lake Seminole on the Florida-Georgia border. The Flint River begins in north-central Georgia, just south of Atlanta, and flows south to Lake Seminole. The Apalachicola River begins at Lake Seminole, which is the confluence of the Chattahoochee and Flint Rivers, and flows southward through Florida to the Gulf of Mexico. The Chattahoochee River is regulated by four U.S. Army Corps of Engineers (USACE) projects and eight run-of-the-river dams (not operated to regulate flow), while the Flint River is relatively unregulated with just two run-of-the-river dams (U.S. Army Corps of Engineers, 1997). The Apalachicola River has one USACE project (Lake Seminole) at its headwaters; one other impoundment in the basin, Dead Lakes, is present on the Chipola River.

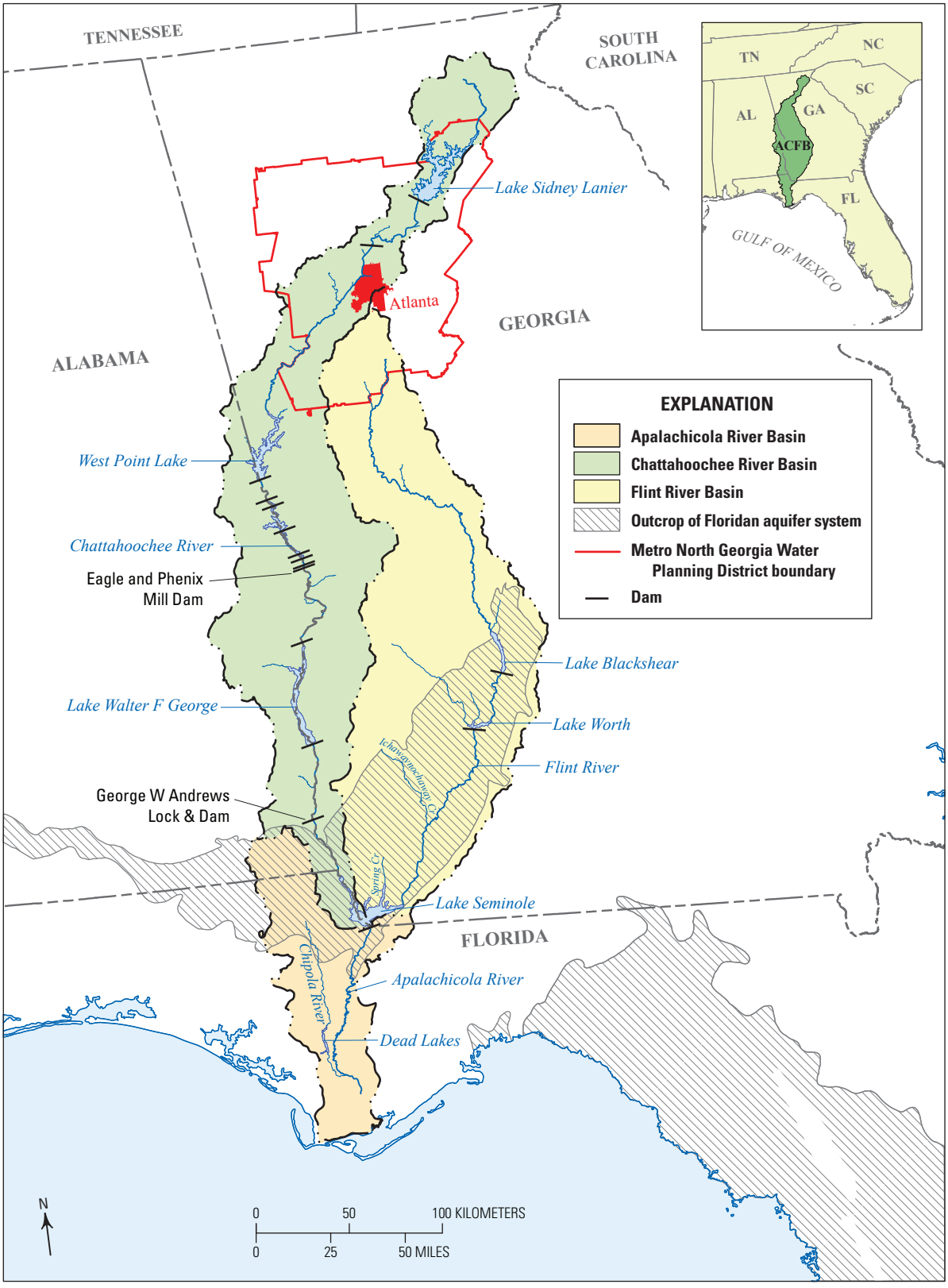

Base modified from U.S. Geological Survey 1:2,000,000-scale digital data, 1990–1994

Figure 2. Location of Apalachicola–Chattahoochee–Flint River Basin (ACFB).

The Chattahoochee and Flint River Basins are approximately the same size, covering 22,600 and 21,900 square kilometers (km^2), respectively; the Apalachicola River Basin, not including the Chattahoochee and Flint River Basins, is approximately 6,200 km^2. Land cover types and percentages in the ACFB, based on the 2001 and 2006 National Land Cover Datasets (NLCD), are shown in table 1. The ACFB is nearly half covered with forest, with about a tenth of the basin being developed (high-, medium-, or low-density) land and just over a tenth being cultivated crops. The majority of the developed land is in the Chattahoochee River Basin, with most attributed to metropolitan Atlanta. Nearly two-thirds of the cultivated cropland is located in the Flint River Basin, almost all of which is located in the lower Flint River Basin. This substantial amount of cropland in the lower Flint River Basin is irrigated by groundwater and surface-water withdrawals; the amount of these withdrawals varies depending on precipitation in the area. Irrigation withdrawals can account for more than 95 percent of total water use in some counties in southwestern Georgia (Fanning and Trent, 2009).

The ACFB includes the Blue Ridge, Piedmont, and Coastal Plain physiographic provinces (fig. 3). In the ACFB, the Blue Ridge and Piedmont physiographic provinces are present in the northern half of the basin and are underlain by crystalline rock; the Coastal Plain physiographic province is present in the southern half of the basin and is underlain by sedimentary rocks and unconsolidated sediments (Couch and others, 1995). The sedimentary rocks and sediments in the Coastal Plain are more permeable than the crystalline rocks of the Blue Ridge and Piedmont, thus allowing water to move more rapidly through them. This difference in permeability results in a marked difference in the hydrologic behavior of streams between these parts of the basin. According to the base-flow index map, which indicates the fraction of streamflow attributed to non-storm runoff (fig. 4; Wolock, 2003), the base-flow fraction of streamflow in the ACFB ranges from 37 to 75 percent of total streamflow. The areas having the largest fractions of streamflow attributed to base flow are in the mountainous northernmost part of the Chattahoochee River Basin, the middle Flint River Basin, and the

Table 1. Land cover percentages by river basin in the Apalachicola–Chattahoochee–Flint River Basin (ACFB).

[km^2, square kilometer; NLCD, National Land Cover Dataset]

Land-cover type	Land-cover percentage			
	Apalachicola River Basin[1]	Chattahoochee River Basin[2]	Flint River Basin[3]	ACFB[4]
2001 NLCD				
Developed	4.6	12.8	6.9	9.3
Forest	33.5	55.7	43.4	47.6
Cultivated crops	9.4	5.1	20.6	12.3
Hay/pasture	5.0	8.9	8.7	8.3
Water	1.6	2.8	1.0	1.9
Barren	0.1	0.5	0.2	0.3
Shrub/scrub/herb	12.8	10.0	8.9	9.9
Wetlands	33.0	4.2	10.3	10.4
2006 NLCD				
Developed	4.6	13.8	7.3	9.9
Forest	33.8	55.0	43.6	47.5
Cultivated crops	9.6	4.9	20.5	12.2
Hay/pasture	4.7	8.4	8.5	8.0
Water	1.7	2.9	1.0	1.9
Barren	0.1	0.3	0.2	0.2
Shrub/scrub/herb	12.7	10.6	8.8	10.1
Wetlands	32.8	4.1	10.1	10.2

[1] Drainage area = 6,200 km^2.

[2] Drainage area = 22,600 km^2.

[3] Drainage area = 21,900 km^2.

[4] Drainage area = 50,700 km^2.

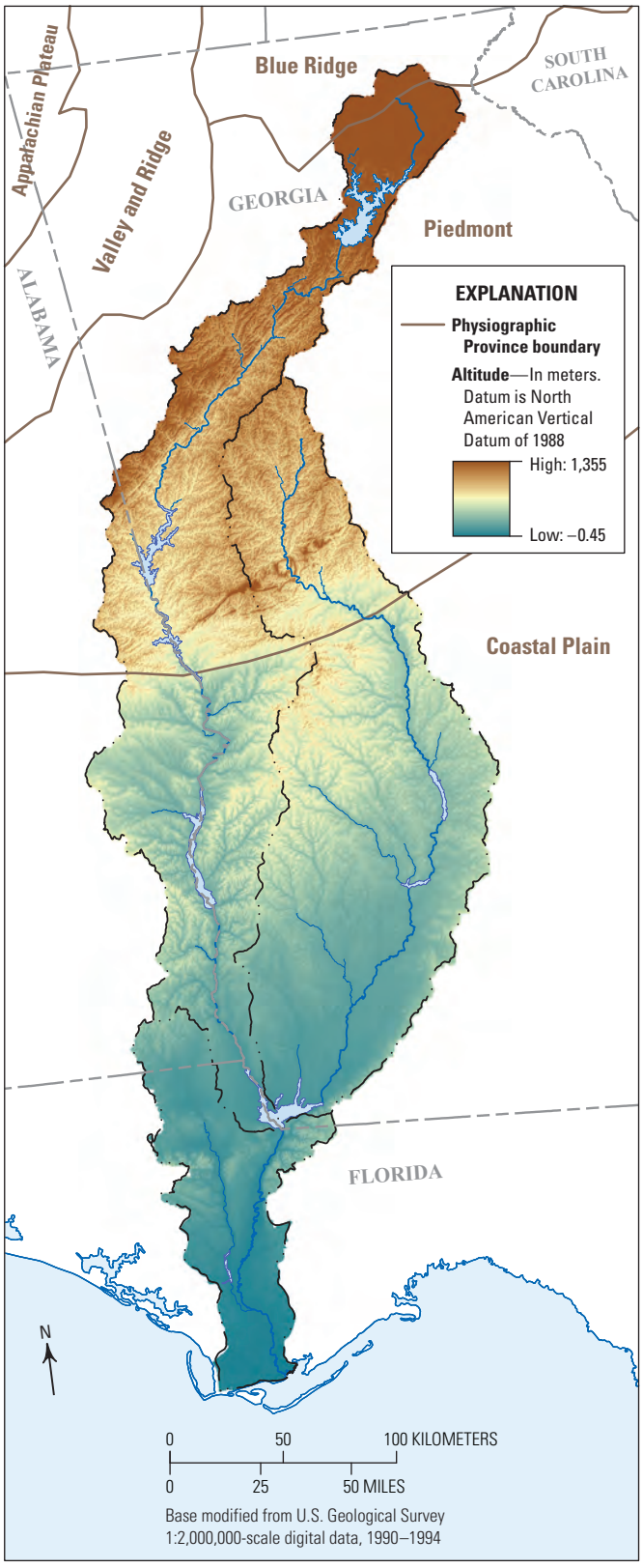

Figure 3. Altitude range and physiographic provinces of the Apalachicola–Chattahoochee–Flint River Basin.

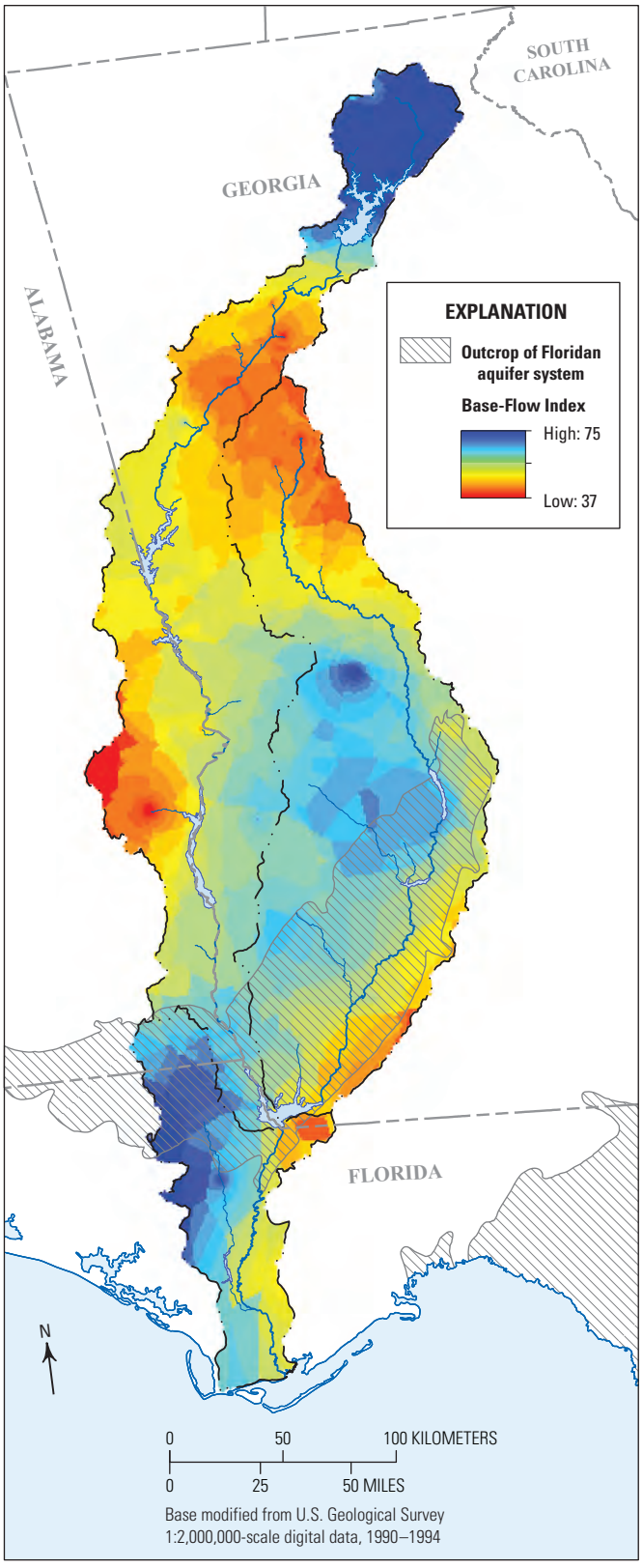

Figure 4. Base-flow index (adapted from Wolock, 2003).

northwestern part of the Apalachicola River Basin. Some of the streams in the lower parts of the Chattahoochee and Flint River Basins are located where the Floridan aquifer system crops out (fig. 2), with some of the streams actually incised into the Floridan aquifer system.

The ACFB is characterized by a warm and humid temperate climate. The ACFB has a generally north-south direction and spans approximately 590 km. Because of this substantial areal range and surface altitudes that range from greater than 1,300 meters (m) in the northern area to sea level at the mouth of the ACFB, air temperature and precipitation are not areally constant across the basin. Annual precipitation in the basin averages about 1,270 millimeters (mm), with totals substantially higher in the mountains in the northernmost part of the basin (about 1,780 mm) and along the Gulf of Mexico in the southernmost part of the basin (about 1,520 mm); totals are relatively close to the basin average across the middle part (data accessed June 6, 2011, at *http://www.sercc.com/climateinfo/historical/historical.html*). Precipitation totals in the ACFB are generally lower in the fall (September to November) compared to the rest of the year. Maximum daily summer (June to August) temperatures are around 29.4 degrees Celsius (°C) in the northern part of the basin and 32.2 °C in the southern part. Daily minimum summer temperatures range from 17.2 °C in the northern part of the basin to 21.7 °C in the southern part. Average winter daily minimum and maximum temperatures for winter (December to February) range from 0 to 12.2 °C and from 6.7 to 18.3 °C in the northern and southern parts of the basin, respectively.

Previous Investigations

The ACFB has been the focus of many studies describing the basin's geohydrology, ecology, and water quality. USGS scientists selected the ACFB to be studied as part of the National Water-Quality Assessment (NAWQA) Program in the early 1990s (Wangsness, 1997). As part of the NAWQA Program, USGS scientists have documented influences on the basin's aquatic ecosystems (Couch and others, 1995), water-quality conditions (Frick and others, 1998), and identification of nutrient sources in the basin (Frick and others, 1996). An extensive list of the studies conducted as part of the NAWQA Program are provided at *http://ga.water.usgs.gov/nawqa/publications.html*. Groundwater resources of the ACFB were discussed in a series of USGS reports in the mid-1990s (Torak and McDowell, 1996; Chapman and Peck, 1997a, b; Mayer, 1997). Further groundwater studies were completed in portions of the lower ACFB, mainly where the Floridan aquifer system crops out (fig. 2), to simulate stream-aquifer relations and the effects of groundwater pumpage on streamflow (Albertson and Torak, 2002; Mosner, 2002; Jones and Torak, 2006). The relation of aquatic habitats to river flows in the Apalachicola River floodplain were studied by Light and others (1998).

Hydrologic models have been developed for various parts of the ACFB using a variety of software packages. PRMS was used by Viger and others (2010) to simulate the hydrology of the upper Flint River Basin. Viger and others (2011) also published a separate paper on the hydrologic effects of urbanization and climate change on the upper Flint River Basin using PRMS. Their effort was part of a larger study by Hay and others (2011) that used PRMS to simulate the impacts of climate change on 14 basins across the United States. Walker and others (2011) also analyzed the impact of climate change on the 1.5-year flood (0.67 exceedance probability) for these same 14 basins that included the upper Flint River Basin.

Hydrologic models have been developed using the Hydrologic Simulation Program Fortran (HSPF) software for the headwaters of the Chattahoochee and Flint Rivers (Hummel and others, 2003), the Flint River Basin (Zhang and others, 2005), the mainstem portion of the lower Flint River Basin (Wen and others, 2007; Wen and Zhang, 2009), Ichawaynochaway Creek (Zeng and Wen, 2005), and Spring Creek (Zhang and Wen, 2005). The models of the lower Flint River, Ichawaynochaway Creek, and Spring Creek were coupled with groundwater models using the MODular Finite-Element (MODFE) software (Jones and Torak, 2006). Wen and Zhang (2009) also computed monthly estimates of agricultural water-use impacts on streamflow for the lower Flint River Basin for both drought and normal years. These estimations were used to augment the USGS streamflow data to more closely represent flow volumes without water use effects for model calibration.

An unimpaired flow dataset was developed for the ACFB by the U.S. Army Corps of Engineers (1997) for use as input to reservoir system models. The USACE defined these unimpaired flows as historically observed flows, modified to account for the management of surface-water reservoirs and for withdrawals and returns of water from municipal, industrial, thermal-power, and agricultural water uses. Gaps in the streamflow record were filled using regressions from existing observations so that each node (streamgage location or reservoir outlet) in the USACE dataset had daily streamflow for the period 1939 to 1993. The USACE dataset has been updated through 2008 and is the basis for several studies about water allocation and operational planning in the ACFB (Leitman and others, 2003; Zeng and others, 2009).

A coarse spatial-scale model of the ACFB was developed using a monthly time step by Georgakakos and Yao (2000) to assess the impacts of potential climate change and major water uses on watershed hydrology. The model simulates water levels of the USACE-operated reservoirs in the basin in response to future climate change scenarios. The ACFB was also the focus of a study on the alterations to flow regimes resulting from predicted climate change (Gibson and others, 2004). At an even coarser scale, the Water Supply Stress Index Model has been developed to predict water availability and stress at a monthly time step through the year 2030 across 13 southeastern States (*http://www.fs.fed.us/ccrc/tools/wassi.shtml*, accessed May 19, 2011).

Each of the models just described has provided hydrologic simulations and information for parts of the ACFB at similar temporal and spatial resolutions or for the entire ACFB at coarser temporal and spatial resolutions than the model documented herein. Although comparing simulations of various parts of the ACFB developed using differing tools and software packages is possible, this may not be informative because of structural differences between the models. To avoid the potential effects caused by these differences, the PRMS model of the ACFB was delineated, parameterized, and calibrated consistently across the study area so that valid comparisons can be made between model nodes throughout the basin. An extension of PRMS developed in Viger and others (2010) accounts for the effect of a large number of water-holding depressions in the land surface on the hydrologic response of a basin, which is necessary in studying the ACFB. Viger and others (2011) incorporated three emissions scenarios with five GCMs from the Intergovernmental Panel on Climate Change and projections of urbanization from the FORcasting SCEnarios of future land cover (FORE-SCE) model to simulate the hydrologic condition of the upper Flint River Basin through the year 2050 using PRMS. This report provides a consistently developed, finer spatial and temporal resolution, simulation of hydrology in the ACFB beyond other studies previously mentioned.

Precipitation-Runoff Modeling System (PRMS)

For this study, the PRMS (Leavesley and others, 1983; Markstrom and others, 2008) was chosen to simulate hydrology in the ACFB. Specifically, this PRMS application was developed to represent the overall water balance and hydrologic processes within the ACFB for further use by SERAP to study the effects of climate and land cover change on the ACFB hydrologic system. Because the ACFB spans a relatively large area, many factors were considered to properly subdivide and parameterize the model. Land cover types ranging from forest to agriculture to urban are present in the ACFB and each affect the hydrologic cycle in different ways. In order to represent each part of the basin accurately, the hydrologic model must account not only for the modeled outflow for the entire basin, but also flows at nodes (streamgage locations and large reservoir inlets and outlets) throughout the basin.

The PRMS is a deterministic, distributed-parameter, physical-process-based hydrologic modeling system. Its primary objectives are to (1) simulate land-surface hydrologic processes, including evapotranspiration, runoff, infiltration, interflow, snowpack, and soil moisture on the basis of distributed climate information (temperature, precipitation, and solar radiation); (2) simulate hydrologic water budgets at the watershed scale with temporal scales ranging from days to centuries; (3) integrate with models used for natural-resource management or other scientific disciplines; and (4) provide a modular design that allows the user to select alternative hydrologic-process algorithms from either the standard module library or user-provided provisional modules. Figure 5 shows a schematic of how the PRMS simulates the hydrologic cycle.

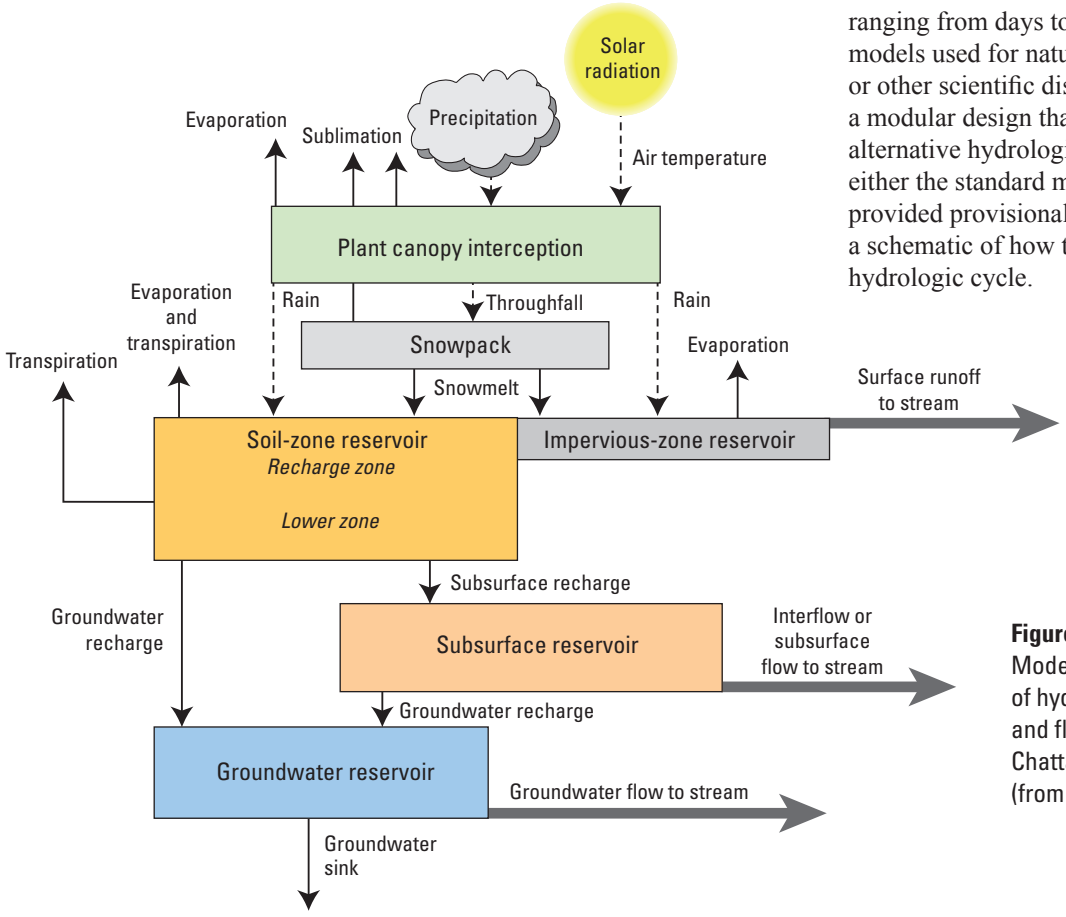

Figure 5. Precipitation-Runoff Modeling System conceptualization of hydrologic-cycle components and fluxes in the Apalachicola–Chattahoochee–Flint River Basin (from Markstrom and others, 2008).

PRMS models are developed using digital elevation models (DEM) and spatial datasets for land cover type, imperviousness, and canopy cover. Soils information and shallow permeability maps are used to develop subsurface parameters, and extended low-flow periods of measured streamflow are used to develop groundwater parameters. Using the DEM, the basin of interest is divided into subareas called HRUs in which the components of flow (groundwater (saturated zone), subsurface (unsaturated zone), and surface runoff) are computed in response to precipitation, air temperature, and land surface and subsurface characteristics of the basin (Leavesley and others, 1983). In smaller basins, where the time of travel from headwaters to the basin outlet is less than 1 day, the hydrologic responses of the HRUs are summed on a daily time step to simulate daily streamflow for the basin. In larger basins, where the time of travel from headwaters to the basin outlet exceeds 1 day, additional PRMS algorithms are used to more appropriately simulate the routing and timing of streamflow.

The PRMS simulates a daily time series of streamflow at the basin outlet as well as at any HRU or stream segment within the basin. Many variables are computed in a PRMS simulation and can also be output for subsequent analysis (Markstrom and others, 2011). For example, the user can compare the contributions of groundwater flow, subsurface flow, and surface runoff at points throughout the basin to determine which is dominant or to study how these components of flow vary through time or by season. These types of ancillary analyses may prove useful when simulating projections of land cover or climate change.

The ACFB PRMS application was developed to provide a simulation of the natural hydrologic processes of the basin in response to climate, subsurface characteristics, and land cover. The ACFB PRMS model covers 49,700 km^2 of the approximately 50,700 km^2 that compose the ACFB. The model does not include the part of the basin located along the coastline subject to tidal effects (fig. 6).

PRMS Conceptualization

To utilize available information and provide output at useful locations, the ACFB PRMS model HRUs and stream segments had to be developed at an appropriate spatial resolution. Nodes including streamgages and inlets and outlets of large reservoirs were used to divide the basin into these units.

ACFB Streamgages, Streamflow Data, and Large Impoundments

The USGS streamgaging network (*http://waterdata.usgs.gov/*, accessed January 5, 2011) currently has 169 streamgages with available daily-flow data in the ACFB. Of these 169 gages, 56 were considered for the development of the PRMS model based on a minimum drainage area of 25 km^2 and a minimum of 10 years of continuous daily-flow record

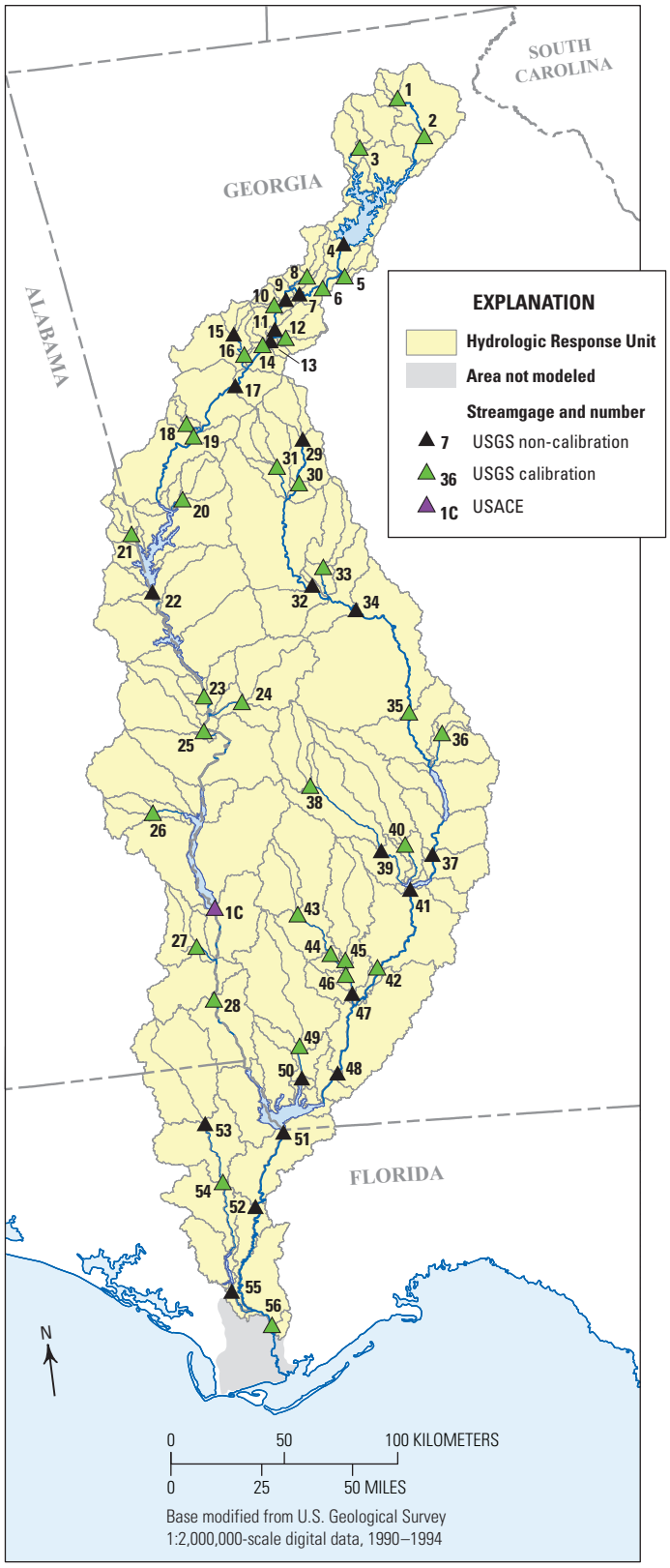

Figure 6. Precipitation-Runoff Modeling System hydrologic response units, stream network, and U.S. Geological Survey (USGS) streamgages. [USACE, U.S. Army Corps of Engineers]

during the simulation period 1950–99. These 56 gages (table 2) were used for model delineation and their locations are shown in figure 6. Daily mean streamflow data from 35 of the 56 streamflow locations were used to calibrate and evaluate the hydrologic model. Data from another 5 of the 56 streamflow locations were used for flow substitution in the hydrologic model, and the remaining 16 streamflow locations were used for model delineation only. Not all stations selected had data for the entire primary calibration period (1989–99), particularly stations 02339225, 02343300, and 02346500 (table 2); however, the stations that had older data only were in undeveloped parts of the basin where landscape changes over time were considered not substantial. Streamflow data were retrieved and formatted for the hydrologic model using Downsizer, a graphical user interface (GUI) developed by Ward-Garrison and others (2009). The streamgage on the Apalachicola River near Sumatra, Florida (station number 02359170) is the farthest downstream in the ACFB and is the location of the model outlet. Streamflow data provided by the USACE for the Chattahoochee River at the outlet of Walter F. George reservoir were used in the absence of USGS streamflow data (figs. 1 and 6; *http://water.sam.usace.army.mil/acfframe.htm*, accessed January 5, 2011).

The ACFB has a total of 15 mainstem impoundments and one tributary lake that were considered candidate lake HRUs during model development. The Chattahoochee River has 12 of these mainstem impoundments whose dates of construction range from as early as 1834 (Eagle and Phoenix Mill Dam) to 1974 (West Point Lake; fig. 2). Within the Chattahoochee River Basin, the USACE operates one reservoir completed in 1954 (Lake Sidney Lanier), two completed in 1963 (Lake Walter F. George and George W. Andrews Lock and Dam), and one completed in 1974 (West Point Lake) (U.S. Army Corps of Engineers, 1997). The Flint River has two mainstem impoundments (Lakes Blackshear and Worth; fig. 2). The USACE operates the Jim Woodruff dam (completed in 1954) at the head of the Apalachicola River. This river also has an associated water body (Dead Lakes) along a tributary, the Chipola River (fig. 2), which was delineated during model development. Of these 16 impoundments located throughout the ACFB, 11 were used for model delineation only and were represented as nodes in the PRMS modeling structure (table 3); the remaining 6 impoundments were delineated as lake HRUs. When the PRMS calibration encountered one of these nodes, simulated flow was replaced with actual flow data so that the calibration could continue downstream. These data were replaced during the calibration process so that the model parameters would not be adjusted to try and match unregulated runoff processes to a release schedule downstream of an impoundment. The calibration process would then be focused on that portion of the basin from the outlet of the impoundment to the calibration location further downstream. Thus, the flow replacement was a temporary measure used for calibration only and then was removed once the calibration was complete.

Stream Network Development

The model stream network was developed at a resolution similar to the drainage density and structure of the USGS National Hydrography Dataset (NHD, 1:100,000 scale) flow lines; this scale was relevant for its intended uses in the SERAP aquatic occupancy and hydrologic modeling effort (Peterson and others, 2010). To create this stream network, a DEM of the ACFB and two software programs, Bldgrds and Netrace (Miller, 2008), were used to create a systematic attributed stream network. Bldgrds and Netrace have adjustable parameters that were calibrated to yield networks reflective of actual drainage patterns in the area and that were appropriate for the modeling efforts in the southeastern United States. A 1 arc-second National Elevation Dataset DEM (Gesch, 2007) for the ACFB was resampled to 30 m to create the altitude base data for the channel network (*http://ned.usgs.gov/*, accessed February 9, 2010).

Bldgrds was used to hydrologically condition the input altitude grid to produce a depressionless DEM. This process adjusted altitudes with filling and cutting algorithms and determined flow directions and accumulations for each DEM cell using the D-Infinity algorithm (Tarboton, 1997), which divides each cell into eight triangular facets and assigns the flow direction of the steepest flow path. Additional files are created in this process including surface gradient, contour length per cell, and the number of nearby inflowing cells (Miller, 2008). The second program, Netrace, was used in conjunction with the flow direction and flow accumulation grids from Bldgrds to delineate the channel network and dynamically segment and attribute the network based on DEM-derived channel and valley morphology (Miller, 2008). The drainage network was then simplified by removing all stream segments but one above each headwater streamgage and any stream segment that did not have a streamgage located upstream of it. Although stream segments between streamgages and confluences were also merged for further simplification, the stream segments were divided at inlets and outlets of the large impoundments listed in table 3; this final network consisted of 128 segments.

Hydrologic Response Unit Development

Once the drainage network was created and the nodes throughout the basin were identified (streamgages and large reservoir inlets and outlets), the HRUs were delineated. The model HRUs were created using the GIS Weasel software developed by Viger and Leavesley (2007). Generally, the HRUs were created by dividing the local contributing area into each segment by the respective segment. Because of basin geometry, a stream segment could have zero to several HRUs connected to it, but in most cases, there are two HRUs for each stream segment. Two HRUs were delineated upstream of each headwater streamgage. By using the large impoundments as HRUs, it was possible to more accurately simulate

Table 2. Streamflow gages used in Apalachicola–Chattahoochee–Flint River Basin model development.

[ID, identification; km², square kilometer; point of interest type: C, calibration; FS, flow substitution; D, delineation only; USGS, U.S. Geological Survey; USACE, U.S. Army Corps of Engineers]

Stream-gage number (fig. 6)	Station number	Short ID	Station name	Drainage area (km²)	Point of interest type	Period of discharge record
			USGS streamflow gages			
1	02330450	cha01	Chattahoochee River at Helen, GA	116	C	1981–2010
2	02331600	cha02	Chattahoochee River near Cornelia, GA	815	C	1957–2010
3	02333500	che01	Chestatee River near Dahlonega, GA	396	C	1929–2010
4	02334430	cha03	Chattahoochee River at Buford Dam, near Buford, GA	2,690	FS	1942–2010
5	02334885	suw01	Suwanee Creek at Suwanee, GA	122	C	1984–2010
6	02335000	cha04	Chattahoochee River near Norcross, GA	3,030	C	1903–1946; 1956–2010
7	02335450	cha05	Chattahoochee River above Roswell, GA	3,160	D	1941–1960; 1976–2010 (1941–1960 at station 02335500)
8	02335700	big01	Big Creek near Alpharetta, GA	186	C	1960–2010
9	02335815	cha06	Chattahoochee River below Morgan Falls Dam, GA	3,550	D	2001–2010
10	02335870	sop01	Sope Creek near Marietta, GA	75.6	C	1984–2010
11	02336000	cha07	Chattahoochee River at Atlanta, GA	3,750	D	1928–2010
12	02336300	pea01	Peachtree Creek at Atlanta, GA	225	C	1958–2010
13	02336490	cha08	Chattahoochee River at GA 280, near Atlanta, GA	4,120	FS	1981–2010
14	02336635	nik01	Nickajack Creek at US 78/278, near Mableton, GA	81.5	C	1995–2010
15	02336968	nos01	Noses Creek at Powder Springs Road, Powder Springs, GA	115	D	1998–2010
16	02337000	swt01	Sweetwater Creek near Austell, GA	637	C	1937–2010
17	02337170	cha09	Chattahoochee River near Fairburn, GA	5,330	D	1965–2010
18	02337500	snk01	Snake Creek near Whitesburg, GA	91.9	C	1954–2010
19	02338000	cha10	Chattahoochee River near Whitesburg, GA	6,290	C	1938–1954; 1965–2010
20	02338660	new01	New River at GA 100, near Corinth, GA	329	C	1978–2010
21	02339225	weh01	Wehadkee Creek below Rock Mills, AL	156	C	1978–1990
22	02339500	cha11	Chattahoochee River at West Point, GA	9,190	FS	1896–2010
23	02341505	cha12	Chattahoochee River at US 280, near Columbus, GA	12,100	C	1929–2010 (1929–2002 at station 02341500)
24	02341800	upt01	Upatoi Creek near Columbus, GA	885	C	1968–2010
25	02342500	uch01	Uchee Creek near Fort Mitchell, AL	834	C	1946–2010
26	02342933	cow01	South Fork Cowikee Creek near Batesville, AL	290	C	1963–1971; 1974–2010
27	02343300	abb01	Abbie Creek near Haleburg, AL	378	C	1958–1971; 1974–1993
28	02343801	cha13	Chattahoochee River near Columbia, AL	21,300	C	1975–2010
29	02344350	fln01	Flint River near Lovejoy, GA	337	D	1985–2010

Table 2. Streamflow gages used in Apalachicola–Chattahoochee–Flint River Basin model development.—Continued

[ID, identification; km², square kilometer; point of interest type: C, calibration; FS, flow substitution; D, delineation only; USGS, U.S. Geological Survey; USACE, U.S. Army Corps of Engineers]

Stream-gage number (fig. 6)	Station number	Short ID	Station name	Drainage area (km²)	Point of interest type	Period of discharge record
			USGS streamflow gages			
30	02344500	fln02	Flint River near Griffin, GA	704	C	1937–2010
31	02344700	lin01	Line Creek near Senoia, GA	261	C	1964–2010
32	02346180	fln03	Flint River near Thomaston, GA	3,160	D	1966–1992
33	02346500	pot01	Potato Creek near Thomaston, GA	482	C	1937–1971
34	02347500	fln04	Flint River at US 19, near Carsonville, GA	4,790	D	1911–1923; 1928–1931; 1937–2010
35	02349605	fln05	Flint River at GA 26, near Montezuma, GA	7,560	C	1904–1912; 1930–2010
36	02349900	tur01	Turkey Creek at Byromville, GA	116	C	1958–2010
37	02350512	fln06	Flint River at GA 32, near Oakfield, GA	10,000	D	1929–1958; 1987–2010
38	02350600	kin01	Kinchafoonee Creek at Preston, GA	510	C	1951–1977; 1987–2002
39	02350900	kin02	Kinchafoonee Creek at Pinewood Road, near Dawson, GA	1360	D	1985–2010
40	02351890	muc01	Muckalee Creek at GA 195, near Leesburg, GA	937	C	1979–2010
41	02352500	fln07	Flint River at Albany, GA	13,700	FS	1901–1921; 1929–2010
42	02353000	fln08	Flint River at Newton, GA	14,900	C	1938–1950; 1956–2010
43	02353400	pac01	Pachitla Creek near Edison, GA	487	C	1959–1971; 1988–2010
44	02353500	ich01	Ichawaynochaway Creek at Milford, GA	1,600	C	1939–2010
45	02354500	chk01	Chickasawhatchee Creek at Elmodel, GA	828	C	1939–1949; 1995–2010
46	02354800	ich02	Ichawaynochaway Creek near Elmodel, GA	2,590	C	1995–2010
47	02355350	ich03	Ichawaynochaway Creek below Newton, GA	2,690	D	1937–1947; 1995–2010
48	02356000	fln09	Flint River at Bainbridge, GA	19,600	D	1907–1913; 1928–1971; 2001–2010
49	02357000	spr01	Spring Creek near Iron City, GA	1,260	C	1937–1971; 1982–2010
50	02357150	spr02	Spring Creek near Reynoldsville, GA	1,610	D	1998–2010
51	02358000	apa01	Apalachicola River at Chattahoochee, FL	44,500	FS	1928–2010
52	02358700	apa02	Apalachicola River near Blountstown, FL	45,600	D	1957–2010
53	02358789	chp01	Chipola River at Marianna, FL	1,200	D	1999–2010
54	02359000	chp02	Chipola River near Altha, FL	2,020	C	1921–1927; 1929–1931; 1943–2010
55	02359051	chp03	Chipola River at Cockran Landing, FL	3,120	D	1991–1995, 1998–2010
56	02359170	apa03	Apalachicola River near Sumatra, FL	49,700	C	1977–2010
			USACE streamflow gage			
1C	AL01432	cha12.2	Chattahoochee River outflow from Lake Walter F. George	19,400	FS	1964–2010

Table 3. Water bodies in the Apalachicola–Chattahoochee–Flint River Basin that are hydrologic model delineation points.

[ID, identifier; km², square kilometer]

ID	National Inventory of Dams ID	Impoundment name	River impounded	Drainage area (km²)	Year established
WB1	GA00824	Lake Lanier	Chattahoochee River	2,690	1958
WB2	GA00842	Bull Sluice Lake	Chattahoochee River	3,470	1903
WB3	GA00820	West Point Lake	Chattahoochee River	8,750	1974
WB4	GA00830	Lake Harding	Chattahoochee River	11,000	1926
WB5	GA00838	North Highlands	Chattahoochee River	12,100	1898
WB6	AL01432	Lake Walter F. George	Chattahoochee River	19,300	1962
WB7	AL01433	George W. Andrews Lock & Dam	Chattahoochee River	21,300	1963
WB8	GA00831	Lake Blackshear	Flint River	9,710	1930
WB9	GA00835	Lake Worth	Flint River	13,700	1921
WB10	FL00435	Lake Seminole	Apalachicola River	44,500	1952
WB11	FL00103	Dead Lakes	Chipola River	3,120	1962

evapotranspiration from the water surface of the impoundments as well as the surface-water routing through them. Nine of the 11 impoundments listed in table 3 were superimposed as additional HRUs; the remaining 2 impoundments (Bull Sluice Lake and George W. Andrews Lock and Dam) were represented by additional nodes in the drainage network and the associated contributing areas only. The final HRU map consisted of 258 individual units ranging in size from 1.4 to 1,950 km² with an average size of 193 km² (fig. 6).

PRMS Parameterization

PRMS is a distributed-parameter hydrologic model (fig. 5). Many of the model parameters are areally distributed across the landscape and vertically through the soil profile in order to represent various basin characteristics. The parameters describe the plant canopy, land surface reservoirs (surface depressions and impervious zone), stream network, and the soil zone, subsurface, and groundwater reservoirs. For this model, the subsurface and groundwater reservoirs have the same spatial delineations (shape and size) as the HRUs. Using several geographic information system (GIS) data layers and the USGS streamflow data, the initial model parameter values were computed for those listed in table 4. Soil-zone, subsurface, and groundwater-reservoir parameters were computed using the SSURGO soils database (*http://www.soils.usda.gov/survey/geography/ssurgo/*, accessed January 5, 2011), maps of near-surface (on the order of 100 m depth) permeability compiled by Gleeson and others (2011), and hydrographs of USGS streamgages.

Streamflow Routing

The drainage network comprising 128 segments was used to route streamflow in the model because the time-of-travel of runoff from the headwaters of the basin to the model outlet is several days. To simulate this process, the Muskingum routing module was used (Mastin and Vaccaro, 2002). The routing parameter **K_coef** was computed using the GIS Weasel (Viger and others, 2010) and the routing parameter **x_coef** was set to an initial value of 0.2 for all stream segments based on past modeling experience and then was included in the model calibration. The **K_coef** is approximately equal to the travel time, in hours, of streamflow through each stream segment and was computed using the following procedure and assumptions:

Travel time through a stream segment computed as

$$K\_coef = \frac{flowlength}{V \times 3,600}, \quad (1)$$

where

K_coef is the travel time through a stream segment, in hours;

flowlength is the length of a stream segment, in feet;

V is the average velocity in the cross section, in feet per second; and

3,600 is the conversion factor from seconds to hours.

Table 4. Parameter values derived from geographic information system processes.

[Dimension: ngw, parameter value is by groundwater reservoir; nhru, parameter value is by hydrologic response unit (HRU); nsegment, parameter value is by stream segment; nssr, parameter value is by subsurface reservoir; one, parameter value is applied to entire basin; GWR, groundwater reservoir; ET, evapotranspiration]

Parameter name	Parameter description	Dimension	Units
basin_area	Area of basin	one	Acres
basin_lat	Latitude of centroid of basin	one	Degrees
cov_type	Vegetation cover type for each HRU (0=bare soil; 1=grasses; 2=shrubs; 3=trees)	nhru	None
covden_sum	Summer vegetation cover density for the major vegetation type in each HRU	nhru	Decimal fraction
covden_win	Winter vegetation cover density for the major vegetation type in each HRU	nhru	Decimal fraction
dprst_area	Aggregate sum of surface depression areas of each HRU	nhru	Acres
dprst_flow_coef	Coefficient in linear flow routing equation for open surface depressions	nhru	Decimal fraction
dprst_seep_rate_clos	Coefficient used in linear seepage flow equation for closed surface depressions	nhru	Decimal fraction
dprst_seep_rate_open	Coefficient used in linear seepage flow equation for open surface depressions	nhru	Decimal fraction
fastcoef_lin	Linear coefficient in equation to route preferential-flow storage down slope for each HRU	nhru	1/day
gwflow_coef	Linear coefficient in the equation to compute groundwater discharge for each GWR	ngw	1/day
hru_area	Area of each HRU	nhru	Acres
hru_aspect	Aspect of each HRU (tilt from horizontal plane)	nhru	Degrees
hru_deplcrv	Index number for the snowpack areal depletion curve associated with each HRU	nhru	None
hru_elev	Mean elevation for each HRU	nhru	Meters
hru_lat	Latitude of each HRU	nhru	Degrees
hru_percent_imperv	Fraction of each HRU area that is impervious	nhru	Decimal fraction
hru_segment	Segment index to which an HRU contributes lateral flows (surface runoff, interflow, and groundwater discharge)	nhru	None
hru_slope	Slope of each HRU, specified as change in vertical length divided by change in horizontal length	nhru	Decimal fraction
jh_coef_hru	Air temperature coefficient used in Jensen-Haise potential ET computations for each HRU	nhru	Degrees Fahrenheit
K_coef	Travel time of flood wave from one segment to the next downstream segment	nsegment	Hours
rad_trncf	Transmission coefficient for short-wave radiation through the winter vegetation canopy	nhru	Decimal fraction
slowcoef_lin	Linear coefficient in equation to route gravity-reservoir storage down slope for each HRU	nhru	1/day
snarea_thresh	Maximum threshold snowpack water equivalent below which the snow-covered-area curve is applied; varies with elevation	nhru	Inches
snow_intcp	Snow interception storage capacity for the major vegetation type in each HRU	nhru	Inches
soil_moist_max	Maximum available water holding capacity of capillary reservoir from land surface to rooting depth of the major vegetation type of each HRU	nhru	Inches

Table 4. Parameter values derived from geographic information system processes.—Continued

[Dimension: ngw, parameter value is by groundwater reservoir; nhru, parameter value is by hydrologic response unit (HRU); nsegment, parameter value is by stream segment; nssr, parameter value is by subsurface reservoir; one, parameter value is applied to entire basin; GWR, groundwater reservoir; ET, evapotranspiration]

Parameter name	Parameter description	Dimension	Units
soil_rechr_max	Maximum storage for soil recharge zone (upper portion of capillary reservoir where losses occur as both evaporation and transpiration); must be less than or equal to soil_moist_max	nhru	Inches
soil_type	Soil type of each HRU (1=sand; 2=loam; 3=clay)	nhru	None
soil2gw_max	Maximum amount of the capillary reservoir excess that is routed directly to the GWR for each HRU	nhru	Inches
srain_intcp	Summer rain interception storage capacity for the major vegetation type in each HRU	nhru	Inches
sro_to_dprst	Fraction of pervious and impervious surface runoff that flows into surface depression storage; the remainder flows to a stream network	nhru	Decimal fraction
ssr2gw_rate	Linear coefficient in equation used to route water from the gravity reservoir to the GWR for each HRU	nssr	1/day
tmax_adj	Adjustment factor for each HRU to maximum measured temperature estimated based on slope and aspect	nhru	Degrees Fahrenheit
tmin_adj	Adjustment factor for each HRU to minimum measured temperature estimated based on slope and aspect	nhru	Degrees Fahrenheit
tosegment	Index of downstream segment to which the segment streamflow flows	nsegment	None
wrain_intcp	Winter rain interception storage capacity for the major vegetation type in each HRU	nhru	Inches

The Manning Equation is used to obtain the average velocity, V (Gray, 1973):

$$V = \frac{1.49}{n} \times R^{2/3} \times S^{1/2}, \quad (2)$$

where

R is the hydraulic radius, in feet;

S is the water surface slope, in feet per foot; and

n is a roughness coefficient.

The portion of the equation $\frac{1.49}{n} \times R^{2/3}$ was precalculated using assumptions about hydraulic radius and roughness as a function of Strahler stream order (Horton, 1945). A value of 12.89 was used for first order streams, 30.23 was used for second and third order streams, and 67.31 was used for fourth order streams and larger. The appropriate value was then multiplied by the square root of the slope of each stream segment to obtain initial values of the **K_coef** parameter for all segments; this parameter was adjusted during the calibration process while preserving the initial value distribution.

Surface Parameters

General HRU characteristics, such as size, altitude, slope, and aspect, were calculated from the DEM used to delineate the basin. Land cover characteristics, such as impervious area, canopy density, and land cover type, were obtained from the 2001 NLCD (Homer and others, 2007) and summarized per HRU. For land cover type, each HRU was assigned one of four vegetation cover classes (bare soil, grasses, shrubs, trees) based on the dominant land cover type, defined as having the largest percentage of HRU area. Also derived were the parameters **covden_sum** and **covden_win**, which represent the percentage of the HRU area covered by vegetation in summer and winter, respectively.

Surface Depressions

The PRMS includes the capability to simulate the hydrology of surface depressions to account for the impact of numerous, small, unregulated water bodies on the movement of water within each HRU. Although the impact of individual surface depressions may be negligible, the impact of numerous surface depressions can have a substantial collective effect on the hydrologic response of an HRU. The data used to estimate HRU surface-depression storage capacity were derived using the following process.

Suitable cloud-free imagery collected during a normal-to-slightly wet period were selected from the archive of available Landsat 5 Thematic Mapper (TM) imagery (*http://landsat.usgs.gov*). For the ACFB, five different images were mosaicked to obtain full geographic coverage. The image dates and worldwide reference system path/row locations (National Aeronautics and Space Administration, 2011) are shown in table 5.

Landsat TM images from April 2010 were chosen because examination of National Oceanic and Atmospheric Administration (NOAA) climate data suggested that this was a relatively wet period and would provide current information, at the time of dataset development, about the maximum possible extent of water storage in surface depressions. An image sample covering a portion of the upper Flint River Basin is shown in figure 7*A*. Although the data were already georeferenced to the highest precision available in the database, visual inspection of preliminary results revealed the need for additional correction of scene geometry for two of the satellite images. ENVI image processing software (*http://www.exelisvis.com/ProductsServices/ENVIPlatform.aspx*, accessed October 4, 2011) was used to rectify those scenes to ensure results generated from each image could be later combined to produce a cohesive image for the entire ACFB.

Prior to defining surface depressions using the Landsat TM imagery, a land cover analysis eliminated areas such as shadows and dark, bare ground that commonly result in erroneous identification of depressions. First, a DEM was processed to derive slope and aspect data layers for each Landsat TM scene. These derived layers were then "stacked" with reflectance data for each Landsat scene (table 6) and input for processing to land cover on a scene-by-scene basis using the classification tree approach detailed in Loh (2008). In this process, polygons delineating areas of particular land cover types in each image are created through visual interpretation and on-screen digitizing. These polygons "train" the classifier to build individual classification rules (that is, a decision tree) for each image. A portion of the decision tree used to derive the land cover for one scene is shown in figure 8. These rule sets were applied to their corresponding image to produce individual, scene-based land cover maps (fig. 7*B*).

Table 5. Image collection date, worldwide reference system (WRS) path and row for Landsat Thematic Mapper images used for surface water body identification (National Aeronautics and Space Administration, 2011).

Image date	WRS Path	WRS Row
04/02/2010	18	38
04/09/2010	19	36
04/09/2010	19	37
04/09/2010	19	38
04/09/2010	19	39

Table 6. Classification input variables created for each image scene for the Apalachicola–Chattahoochee–Flint River Basin study area (Landsat 5 Thematic Mapper imagery [*http://landsat.usgs.gov*]).

Variable	Description
Band 1	Thematic Mapper blue band
Band 2	Thematic Mapper green band
Band 3	Thematic Mapper red band
Band 4	Thematic Mapper near infrared band
Band 5	Thematic Mapper mid-infrared band
Band 7	Thematic Mapper shortwave infrared band
NDVI	Normalized Difference Vegetation Index
MNDWI	Modified Normalized Difference Wetness Index
TC1	Thematic Mapper tasseled cap component 1 (brightness)
TC2	Thematic Mapper tasseled cap component 2 (greenness)
TC3	Thematic Mapper tasseled cap component 3 (wetness)
TC4	Thematic mapper tasseled cap component 4 (other)
Slope	Slope (percent) derived from National Elevation Data
Aspect	Aspect (cardinal direction) derived from National Elevation Data
Elevation	Elevation from National Elevation Data

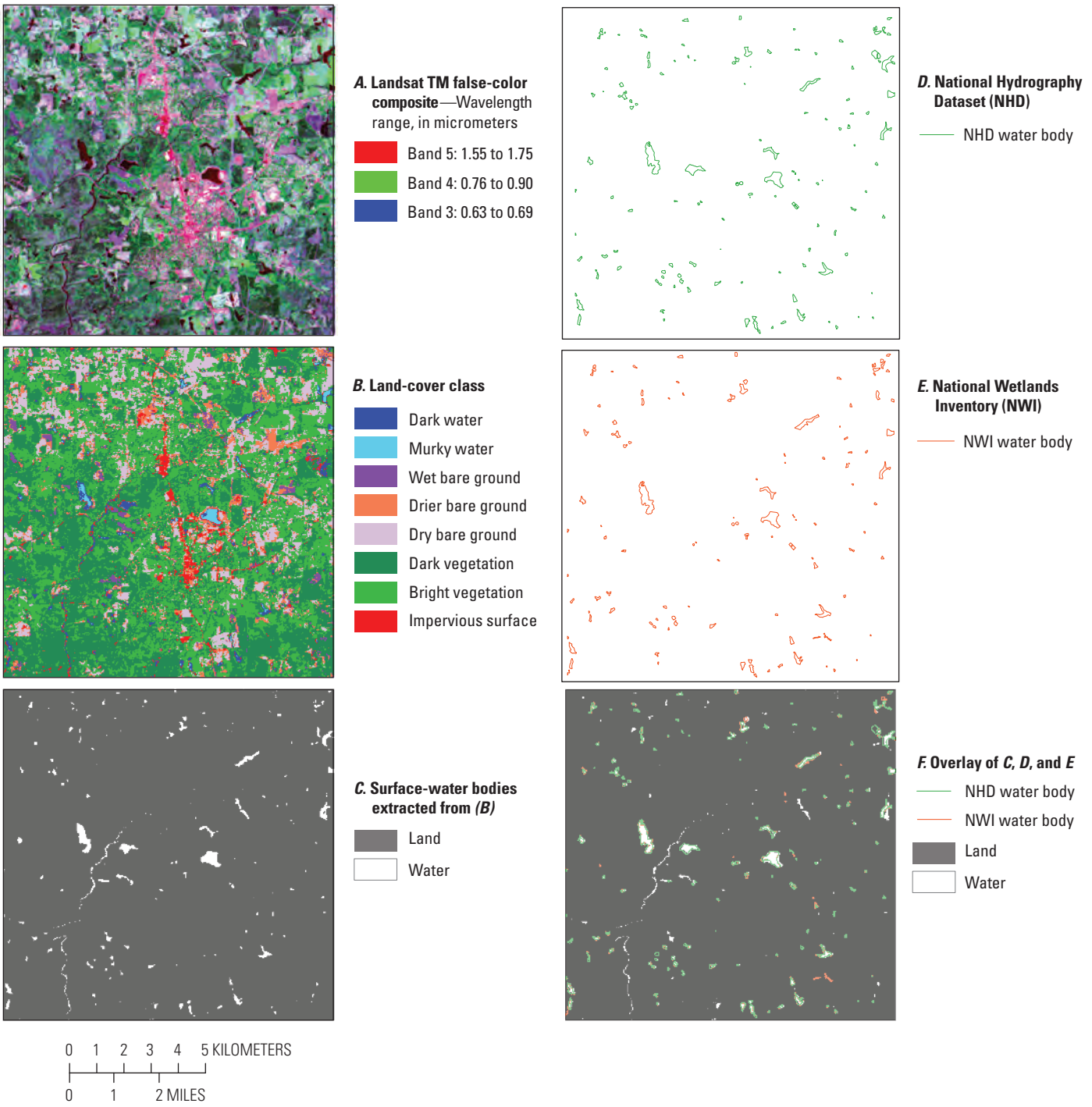

Figure 7. Imagery of surface depression storage input and output analysis. *A*, Sample Landsat thematic mapper (TM) image shown as a false color composite (bands 5, 4, and 3 as red, green and blue, respectively); *B*, Land cover map derived from the imagery and digital elevation model (DEM) as described in the text; *C*, Binary map of water body/non-water body extracted from the land cover layer (*B*); *D*, Water bodies in the sample area extracted from the National Hydrography Dataset (NHD); *E*, Water bodies extracted from the National Wetland Inventory (NWI); *F*, sample area illustrating that water bodies missing in the NWI and NHD are accounted for in the data extracted from satellite.

All classes except water were then eliminated from the land cover datasets, yielding a binary layer of 1 to indicate water and 0 to indicate its absence (for example, fig. 7*C*). Although no data were available for a formal accuracy assessment of the land cover analysis, visual assessment across the ACFB showed that the output provides a more up-to-date representation of surface-water storage than is available in any existing, standard database. This improved representation is illustrated in figure 7*D*–*F*, where water bodies delineated in the NHD (fig. 7*D*) and the National Wetland Inventory (NWI; fig. 7*E*) are overlain with the surface-water-body data generated for the sample area (fig. 7*F*). Many water bodies of various sizes were added to the database through this processing. The surface-water-body results for all images were merged to yield a single surface-water-body coverage for the entire ACFB (fig. 9). This coverage was then used to compute the amount of depression storage and parameters related to flow characteristics in and out of these depressions throughout the basin. The development of these parameters is further discussed in Viger and others (2010).

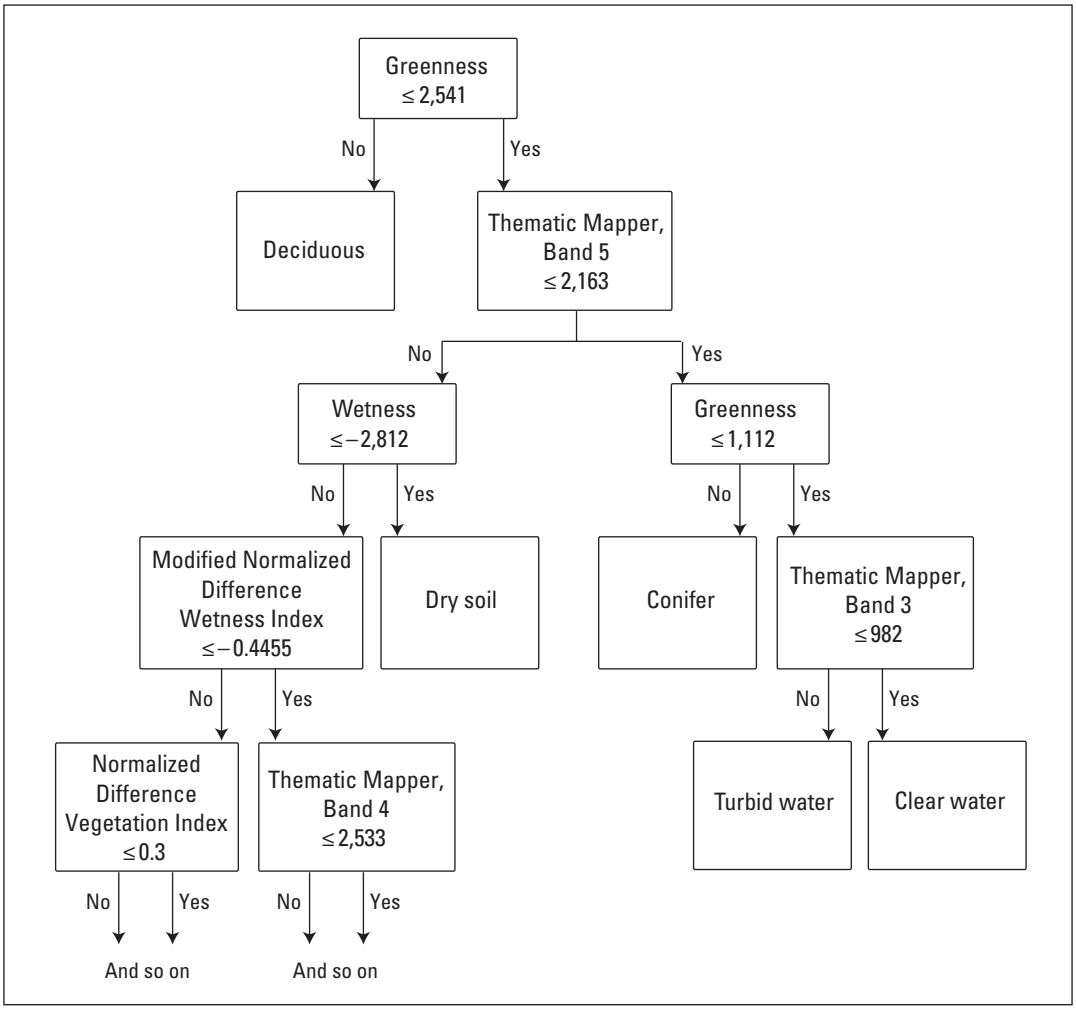

Figure 8. Decision tree used to derive land cover from remote sensed imagery.

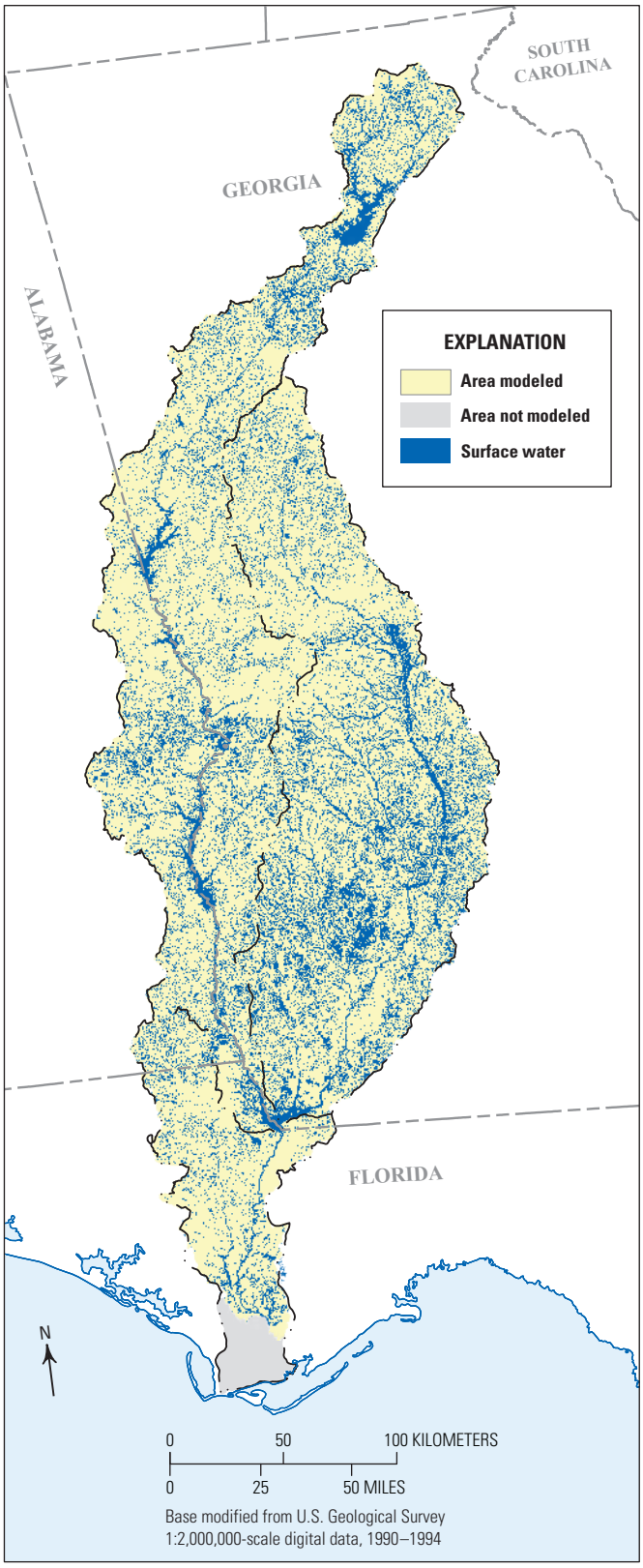

Figure 9. Surface-water-body map generated for the Apalachicola–Chattahoochee–Flint River Basin.

Subsurface Parameters

The PRMS Soil-Zone Module **soilzone** conceptualizes the active soil profile and shallow subsurface as a single layer, with three reservoirs (capillary, preferential-flow, and gravity) at the HRU spatial resolution (Markstrom and others, 2008). Actual capillary, preferential-flow, and gravity reservoirs are all contained within the same physical space, but in the model are represented by separate storage reservoirs for computational purposes, as described next.

The capillary reservoir represents water held in the soil zone by capillary forces between the wilting and field-capacity thresholds. Water is removed from this reservoir by evaporation and transpiration. The preferential-flow reservoir represents soil zone water between field capacity and saturation that is available for fast interflow through relatively large openings in the soil of each HRU. The gravity reservoir represents water in the soil zone between field-capacity and saturation thresholds that is not subject to the preferential-flow threshold. Water in the gravity reservoir can be discharged to a stream, a downslope groundwater reservoir, and (or) a groundwater sink. Water in the gravity reservoir also is available for downslope flow within the soil zone.

The parameters used to compute and move gravity drainage from gravity reservoirs to the associated groundwater and subsurface reservoirs are related to permeability (K) and slope and are defined in table 7 (Markstrom and others, 2008). Traditionally, parameters listed in table 7 have been set based on default values, local user knowledge, and (or) calibration. In Viger and others (2010), these parameters were defined for the upper Flint River Basin on the basis of "hydrogeological" groupings derived from GIS maps of surficial geology. These groupings were used, in collaboration with hydrogeologic experts, to estimate K and permeability values for the soil column associated with each group. The estimates then were used to heuristically define parameters indicating the flux rates between HRUs and the subsurface within the basin. In the PRMS, fluxes are volumes expressed as water depth, in inches, over a unit of area; the volumes are expressed per time step. In this case, the inches associated with a given flux parameter value is an indication of the volume of water that can pass during a given time step. The estimated parameter values were not expected to be highly accurate in magnitude, but instead, were expected to be valid in their degree of spatial variation throughout the ACFB. The magnitudes of these parameter values were resolved through the calibration process, which preserves the spatial pattern across HRUs while adjusting the magnitude of the values.

In this study, near-surface permeability maps for North America from Gleeson and others (2011) were used to provide K values for the ACFB study area (fig. 10). The near-surface

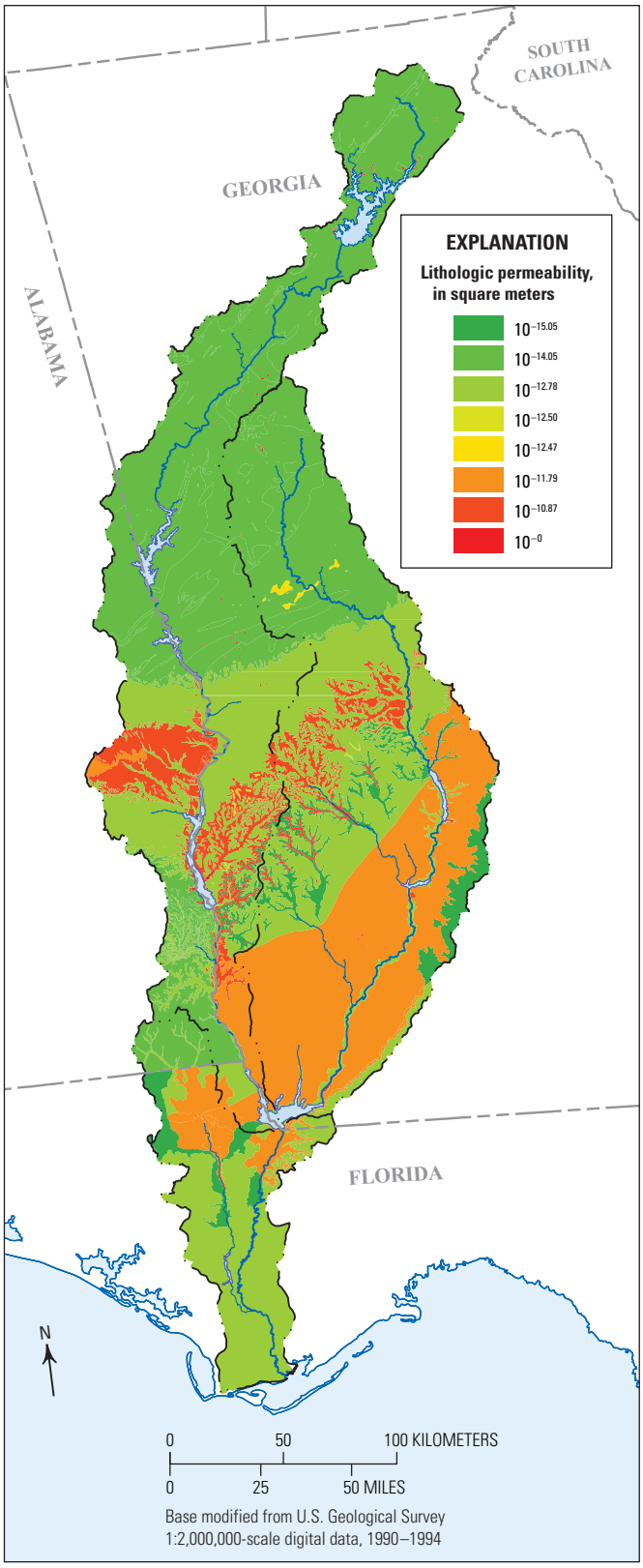

Figure 10. Lithologic permeability values in the Apalachicola–Chattahoochee–Flint River Basin based on near-surface permeability maps for North America (from Gleeson and others, 2011).

permeability maps are a combination of lithologic maps and compilations of near-surface permeability values from hydrogeologic models. Area-weighted K values were calculated for each HRU and used in conjunction with HRU-based slope values to produce the range of initial estimates for each parameter based on the default range listed in table 7. For each parameter, the range in HRU values was determined based on the ”relative to” descriptions shown the table. For example, parameters set relative to K are scaled based on their default range shown in table 7. The mean areal parameter value for all HRUs, instead of individual HRU parameter values, was then calibrated using the Luca software (Hay and Umemoto, 2006), which uses the Shuffled Complex Evolution (SCE; Duan and others, 1992, 1993, 1994) global search algorithm. Each time SCE generates a value for the mean, individual HRU parameter values are generated based on the new mean such that the mean-value distribution is preserved.

Parameters pertaining to the groundwater reservoir were developed using USGS streamflow data and methodologies similar to those described by Rutledge (1998). USGS streamgage locations relatively free of anthropogenic effects were selected for this analysis. If a certain streamgage location had a long-term period of record that started free of anthropogenic effects and then became affected later, only the early portion of the record was analyzed. For these records, the slopes of base-flow recessions were analyzed for extended dry periods for each year of record. These slopes were used to spatially distribute initial values of the **gwflow_coef** parameter, which is a factor applied to the groundwater reservoir of each HRU to compute the groundwater component of runoff.

PRMS Climate Input Data

PRMS requires the input of daily maximum and minimum air temperatures and daily precipitation time-series data. Typically, such data are compiled from stations in and around the basin from NOAA’s National Weather Service Cooperative Observer Program (COOP; National Oceanic and Atmospheric Administration, 2009). These point-station data are then distributed to each HRU based on one of the distribution algorithms available from PRMS.

For this study, daily climate inputs were developed for the PRMS model using a gridded temperature and precipitation dataset developed by Maurer and others (2002). This gridded product was chosen because it is consistent across the project tasks of SERAP. The daily precipitation and temperature grids were developed for the conterminous United States for 1950–99 using an approximately 12×12-km grid-cell size. Maurer and others (2002) used the NOAA COOP stations, which cover the United States with an average density of about one station per 700 km^2, to develop the grids.

Table 7. Parameter values set using the hydraulic permeability (K) values from the near-surface permeability maps (Gleeson and others, 2011).

[HRU, hydrologic response unit]

Parameter name	Parameter description	Units	Default range	Relative to
Parameters used to compute and move gravity drainage from gravity reservoirs to the associated ground-water reservoir				
soil2gw_max	The maximum amount of the soil water excess for an HRU that is routed directly to the associated groundwater reservoir each day.	Inches	0.0 to 0.1	K
ssr2gw_exp	Coefficient in equation used to route water from the subsurface reservoirs to the groundwater reservoirs	Unitless	0.0 to 3.0	K
ssr2gw_rate	Coefficient in equation used to route water from the subsurface reservoirs to the groundwater reservoirs	1/day	0.0 to 1.0	K×(1–slope)
Parameters used to compute and remove fast (slow) interflow from preferential-flow (gravity) reservoirs				
fastcoef_lin	Linear preferential flow routing coefficient for fast interflow	1/day	0.0 to 1.0	K×slope
fastcoef_sq	Non-Linear preferential flow routing coefficient for fast interflow	Unitless	0.0 to 1.0	K×slope
slowcoef_lin	Linear gravity-flow reservoir flow routing coefficient for slow interflow	1/day	0.0 to 1.0	fastcoef_lin/2.0
slowcoef_sq	Non-Linear gravity-flow reservoir flow routing coefficient for slow interflow	Unitless	0.0 to 1.0	fastcoef_sq

Maurer and others (2002) computed daily precipitation totals that were assigned to each day based on the time of observation for the station; therefore, a fraction of each daily precipitation total was applied to the previous day. Maurer and others (2002) then scaled the gridded daily precipitation data to match the long-term average of the Parameter-elevation Regressions on Independent Slopes Model (PRISM) climatology (Daly and others, 1994, 1997). Maurer and others (2002) derived the minimum and maximum daily temperature grids using the same algorithm as for precipitation, and lapsed the results (at –6.5 °C per km) to the grid cell mean altitude. Maurer and others (2002) interpolated temperatures at each time step by fitting an asymmetric spline through the daily maxima and minima.

PRMS Climate Module

The PRMS climate module (**climate_hru**) was developed to provide new functionality to use climate data distributed to the HRUs prior to running PRMS. For this study, the gridded climate data were spatially transferred to the model HRUs using an area-weighted averaging algorithm for each time step for daily maximum and minimum temperature and precipitation using the USGS Geo Data Portal (*http://cida.usgs.gov/gdp/*) (Blodgett and others, 2011).

The PRMS normally requires three input files: the Control File, Parameter File, and Data File. Module **climate_hru** reads values of precipitation (**hru_ppt**), maximum and minimum air temperature (**tmaxf and tminf**, respectively), potential evapotranspiration (**potet**), and (or) potential solar radiation (**swrad**) by HRU, from a separate climate-by-HRU (CBH) file. These files use the same format as the PRMS Data File. For comparison purposes, station data can also be included in the PRMS Data File.

The time period specified in each CBH file can vary, as long as values for the full simulation period are included within each file. These preprocessed values can be computed and distributed using any user-determined method. For example, precipitation can be distributed from a time-series grid, such as from a GCM or radar dataset, to each HRU using weights derived from an overlay analysis between the time-series grid and the HRU map. PRMS uses CBH file(s) when one or more of four control parameters—**temp_module**, **precip_module**, **et_module**, and **solrad_module**—are set to **climate_hru** in the Control File. The filename and location for the CBH file of each data type is specified in the Control File; these filenames are limited to 128 characters.

There is no allowance for missing values when using the **climate_hru** module, and thus, care is required to ensure that values for all HRUs and time steps are valid. Air temperatures can be specified as either degrees Fahrenheit or Celsius; the parameter **temp_units** must be set to 0 for Fahrenheit or 1 for Celsius in the Parameter File. Precipitation adjustment factors can be applied per subbasin or per HRU. If the parameter **adj_by_hru** (in the Parameter File) is equal to 0, precipitation will be adjusted by subbasin; if it is equal to 1, precipitation will be adjusted by HRU. Parameters and variables for module **climate_hru** are described in tables 8 and 9, respectively.

Table 8. Input parameters to precipitation, temperature, solar radiation, and potential evapotranspiration distribution module, climate_hru.

[HRU: hydrologic response unit; **one**, a constant; **nhru**, number of HRUs; **nmonths**, number of months in a year; **ntemp**, number of air temperature measurement stations; **nrain**, number of precipitation measurement stations; **nsub**, number of subbasins; **temp_units**: 0=degrees Fahrenheit; 1=degrees Celsius]

Parameter name	Description	Dimension variable	Units	Type	Range	Default value
		Input parameters				
adj_by_hru	Flag to indicate whether to adjust precipitation and air temperature by HRU or subbasin (0=subbasin; 1=HRU)	**one**	None	Integer	0 or 1	1
hru_area	Area of each HRU	**nhru**	Acres	Real	0.01 to 1.0E9	1.0
hru_subbasin	Index of subbasin assigned to each HRU	**nhru**	None	Integer	0 to 0	0
rain_adj	Monthly factor to adjust measured precipitation on each HRU to account for differences in elevation, etc.	**nhru, nmonths**	Decimal fraction	Real	0.2 to 5.0	1.0
rain_sub_adj	Rain adjust factor for each subbasin for each month	**nsub, nmonths**	Decimal fraction	Real	0.0 to 1.0	1.0
snow_adj	Monthly factor to adjust measured precipitation on each HRU to account for differences in elevation, etc.	**nhru, nmonths**	Decimal fraction	Real	0.2 to 5.0	1.0
snow_sub_adj	Snow adjust factor for each subbasin for each month	**nsub, nmonths**	Decimal fraction	Real	0.0 to 1.0	1.0
temp_units	Units for measured temperature (0=Fahrenheit; 1=Celsius)	**one**	None	Integer	0 or 1	0
tmax_adj	Adjustment to maximum air temperature for each HRU, estimated based on slope and aspect	**nhru**	**temp_units**	Real	–10.0 to 10.0	0.0
tmax_allrain	If maximum air temperature of an HRU is greater than or equal to this value (for each month, January to December), precipitation is assumed to be rain, in degrees Celsius or Fahrenheit, depending on units of data	**nmonths**	**temp_units**	Real	0.0 to 90.0	40.0
tmax_allsnow	If HRU maximum air temperature is less than or equal to this value, precipitation is assumed to be snow, in degrees Celsius or Fahrenheit, depending on units of data	**one**	**temp_units**	Real	–10.0 to 40.0	32.0
tmin_adj	Adjustment to minimum air temperature for each HRU, estimated based on slope and aspect	**nhru**	**temp_units**	Real	–10.0 to 10.0	0.0
		Control parameters				
potet_day	File name of daily time series of potential evapotranspiration for each HRU	**one**	None	Character	None	None
precip_day	File name of daily time series of precipitation for each HRU	**one**	None	Character	None	None
swrad_day	File name of daily time series of solar radiation for each HRU	**one**	None	Character	None	None
tmax_day	File name of daily time series of maximum air temperature for each HRU	**one**	None	Character	None	None
tmax_day	File name of daily time series of minimum air temperature for each HRU	**one**	None	Character	None	None

Table 9. Variables used in precipitation, temperature, solar radiation, and potential evapotranspiration distribution module, climate_hru.

[HRU: hydrologic response unit; **one**: a constant; **ndays**: maximum number of days in a year; **nhru**: number of HRUs; **ntemp**: number of air temperature measurement stations; **nrain**: number of precipitation measurement stations; **temp_units**: 0=degrees Fahrenheit; 1=degrees Celsius; ET: evapotranspiration]

Variable name	Description	Dimension	Units	Type
	Input variables			
active_hrus	Number of active HRUs	**one**	None	Integer
basin_area_inv	Inverse of total basin area as sum of HRU areas	**one**	1/acres	Real
hru_cossl	Cosine of each HRU slope	**nhru**	None	Real
hru_route_order	Routing order for HRUs	**nhru**	None	Integer
soltab_basinpotsw	Potential daily shortwave radiation for basin centroid on a horizontal surface	**ndays**	Langleys	Real
soltab_potsw	Potential daily shortwave radiation for each HRU	**ndays**, **nhru**	Langleys	Real
	Output variables			
basin_horad	Potential shortwave radiation for the basin centroid	**one**	Langleys	Real
basin_obs_ppt	Basin area-weighted measured average precipitation for basin	**one**	Inches	Real
basin_potet	Basin area-weighted average of potential ET	**one**	Inches	Real
basin_potsw	Area-weighted average of potential shortwave radiation for the basin	**one**	Langleys	Real
basin_ppt	Basin area-weighted adjusted average precipitation for basin	**one**	Inches	Real
basin_rain	Basin area-weighted adjusted average rain for basin	**one**	Inches	Real
basin_snow	Basin area-weighted adjusted average snow for basin	**one**	Inches	Real
basin_temp	Basin area-weighted average air temperature	**one**	**temp_units**	Real
basin_tmax	Basin area-weighted maximum air temperature	**one**	**temp_units**	Real
basin_tmin	Basin area-weighted minimum air temperature	**one**	**temp_units**	Real
hru_ppt	Adjusted precipitation on each HRU	**nhru**	Inches	Real
hru_rain	Computed rain on each HRU	**nhru**	Inches	Real
hru_snow	Computed snow on each HRU	**nhru**	Inches	Real
newsnow	New snow on HRU (0=no; 1=yes)	**nhru**	None	Integer
orad	Measured or computed solar radiation on a horizontal surface	**one**	Langleys	Real
potet	Potential ET on an HRU	**nhru**	Inches	Real
pptmix	Precipitation mixture (0=no; 1=yes)	**nhru**	None	Integer
prmx	Proportion of rain in a mixed event	**nhru**	Decimal fraction	Real
solrad_tmax	Basin maximum air temperature for use with solrad radiation	**one**	**temp_units**	Real
solrad_tmin	Basin minimum air temperature for use with solrad radiation	**one**	**temp_units**	Real
swrad	Computed shortwave radiation for each HRU	**nhru**	Langleys	Real
tavgc	HRU adjusted average air temperature	**nhru**	Degrees Celsius	Real
tavgf	HRU adjusted average air temperature	**nhru**	Degrees Fahrenheit	Real
tmaxc	HRU adjusted maximum air temperature	**nhru**	Degrees Celsius	Real
tmaxf	HRU adjusted maximum air temperature	**nhru**	Degrees Fahrenheit	Real
tminc	HRU adjusted minimum air temperature	**nhru**	Degrees Celsius	Real
tminf	HRU adjusted minimum air temperature	**nhru**	Degrees Fahrenheit	Real

Limitations of Gridded Climate Data

As part of SERAP, precipitation and air temperature projections were statistically downscaled from 16 spatially coarse GCMs to the finer-resolution gridded observations developed by Maurer and others (2002), Dalton and Jones (2010), and Stoner and others (2012). The PRMS model for the ACFB was developed, in part, to produce projections of future hydrologic conditions using these downscaled projections of precipitation and temperature. Therefore, the PRMS ACFB model needed to be developed using the gridded data from Maurer and others (2002).

A comparison of the Maurer and others (2002) grids of historical data with station data typically used for PRMS models yielded some differences, precipitation distribution being the most substantial. When the gridded dataset was developed in Maurer and others (2002), precipitation was assumed to be constant over each day and was therefore partitioned based on the reporting time at each observation station. A portion of each day's precipitation total was assigned to the previous day and the remainder was kept on the reporting day. This assumption may be appropriate in other parts of the country, because this is a national dataset, but in the ACFB it had the effect of lengthening and dampening the precipitation events. The magnitude difference between the station and gridded forcings are confirmed by Mannshardt-Shamseldin and others (2010), who compared extreme value distributions from point-sources (stations) with gridded precipitation data. The results from their study confirm that "return values computed from rain gage data are typically higher than those computed from gridded data," with "the rain gage data exhibiting return values sometimes two to three times that of the gridded data."

A comparison of simulations using gridded climate data and interpolated station climate data was done for the ACFB PRMS model. Example simulations are shown for the Peachtree Creek at Atlanta, Georgia subbasin (pea01; USGS streamgage 02336300) in figure 11. The comparison of simulations using gridded and station data sources indicates that peak precipitation occurs 1 day earlier for gridded data than station data and the magnitude of the simulated streamflow event is reduced relative to the streamgage observations. In addition, when using the gridded data, the length of the precipitation event is 2 days longer but the precipitation event ends on the same day as the station data interpolated by PRMS. A simple shift in the gridded data by 1 day would therefore not be adequate to match the station data because the precipitation event based on the gridded data ends on the same day as the station data.

Figure 11*B* compares the streamflow from the PRMS model in the Peachtree Creek at Atlanta, Georgia, subbasin simulated when using the gridded and station data as input, along with the measured streamflow The simulated storm

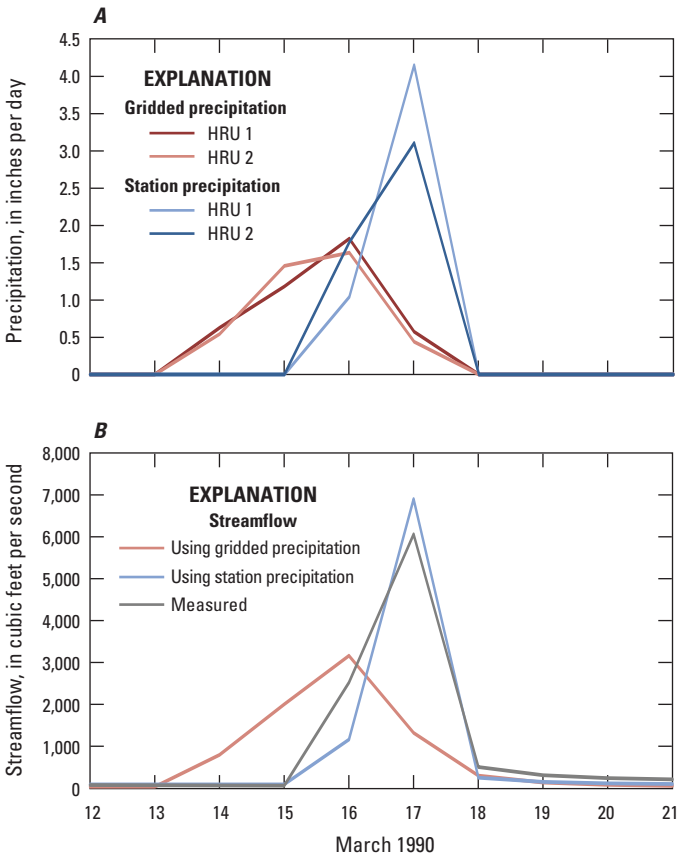

Figure 11. Comparison of *A,* daily precipitation and *B,* daily streamflow, using station precipitation versus gridded precipitation for March 12–21, 1990, in the Peachtree Creek at Atlanta subbasin (pea01, USGS streamgage 02336300). [HRU, hydrologic response unit]

hydrographs using the gridded dataset show earlier flow increases, smaller peak flows, and longer lasting events compared to the measured and station-forced streamflow storm hydrographs. Therefore, PRMS model calibration using the gridded data as forcings must consider these limitations to keep the calibration process from (1) overcompensating for the difference in flow timing because of issues related to the gridded inputs and (2) adjusting the model parameters to physically unrealistic values.

The example shown in figure 11 is in agreement with the findings of Mannshardt-Shamseldin and others (2010) in that the peak precipitation for this event was approximately twice as great for the station data as for the gridded data. The peak storm streamflow also is about twice as large for the station data as for the gridded data. This known limitation in the predictive capability of models using the gridded data forcings to reproduce measured streamflow magnitudes and timing must be considered when interpreting model results to avoid unrealistic expectations of model performance.

Calibration of PRMS Model in the ACFB

An automated parameter estimation procedure was combined with a geographically nested approach to calibrate the ACFB PRMS model (table 10). Parameters were calibrated in two phases, with a total of four steps, using the Luca software (Hay and others, 2006; Hay and Umemoto, 2006), which contains a multiple-objective, stepwise, automated procedure for PRMS calibration and an associated GUI. The software was developed to automate the calibration of a PRMS model with one streamflow gage. Because this application has 35 streamflow gages in the calibration strategy, additional scripts had to be developed to accommodate expansion of existing software capabilities. The first phase of calibration involved matching simulated and measured solar radiation (SR) and potential evapotranspiration (PET) in the ACFB. The second phase of calibration involved matching simulated and measured streamflow volumes and timing in the ACFB.

Phase 1: Solar Radiation and Potential Evapotranspiration Calibration

The first phase of model calibration consisted of comparing simulated SR and PET from the 1989–99 period to measured historical data provided in Farnsworth and Thompson (1982; table 10). The north-south extent of the ACFB covers about 5 degrees of latitude, making basin-wide (non-spatial) parameters for SR and PET inappropriate. Figure 12 shows the four subareas used for SR and PET calibration: the upper and middle Chattahoochee River Basin (cha10 and cha13), the Flint River Basin (fln09), and the Apalachicola River Basin combined with the lower portions of both the Chattahoochee and Flint River Basins (apa03). Historical mean-monthly SR and PET for each of these subareas were calculated based on the methodology presented in Hay and others (2006). Values of SR are similar for subareas cha10, cha13, and fln09, with the apa03 subarea having lower SR values than the others in the summer months (fig. 13*A*). Values of PET are similar for subareas apa03, cha13, and fln09, with the cha10 subarea having lower PET values for all months (fig. 13*B*). The difference between the cha10 subarea PET values and the rest of the basin is an average of –0.012 inch per day (–0.305 millimeter per day), which is a difference of approximately 5 percent in the summer months and almost 30 percent in winter months.

Table 10 lists the parameters used to calibrate the model state during the SR and PET phase of the calibration. Although these parameters also influence the other PRMS outputs, the calibration procedure focused on their role in calculating SR and PET. The objective function used by Luca to calibrate mean monthly SR and PET values produced in PRMS is described as

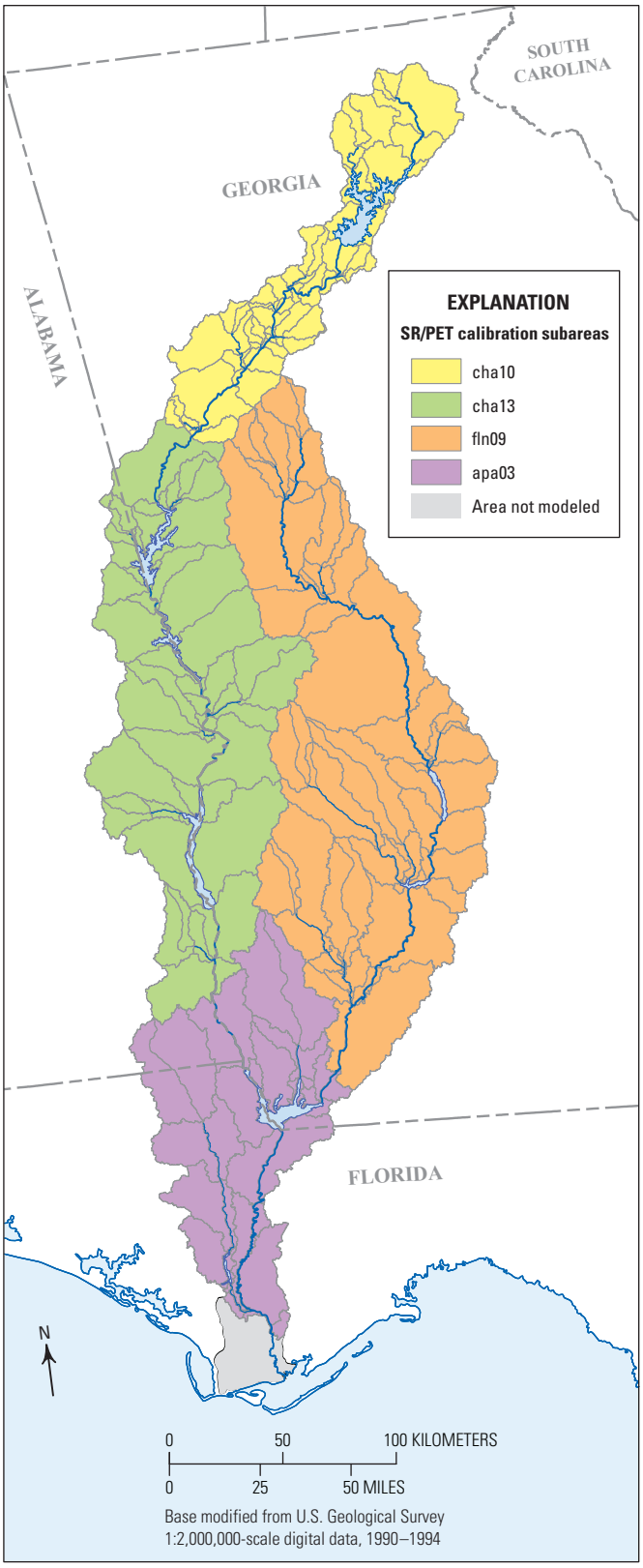

Figure 12. Apalachicola–Chattahoochee–Flint River Basin subbasins for solar radiation and potential evapotranspiration calibrations.

Table 10. Calibration procedure using the Luca software.

Calibration data set (model state)	Objective function(s)	Parameters used to calibrate model state	Parameter range	Parameter description
Phase 1				
Step 1—Solar radiation				
Basin mean monthly solar radiation (SR)	Absolute difference	dday_intcp	–60 to 10	Intercept in temperature degree-day relation
		dday_slope	0.2 to 0.9	Slope in temperature degree-day relation
		tmax_index	50 to 90	Index temperature used to determine precipitation adjustments to solar radiation, units specified by tmax_index parameter
Step 2—Potential evapotranspiration				
Basin mean monthly-potential evapo-transpiration (PET)	Absolute difference	jh_coef	0.005 to 0.09	Coefficient used in Jensen-Haise PET computations
Phase 2				
Step 1—Annual and monthly water balance				
Annual and monthly streamflow volume	Normalized root mean square error: 1. Annual mean 2. Monthly mean 3. Mean monthly	rain_adj	0.2 to 5	Precipitation adjustment factor for rain days
Step 2—Daily timing using 3-day moving average				
Daily streamflow timing	Normalized root mean square error: 1. Three-day moving average	dprst_flow_coef	0 to 0.5	Coefficient in depression flow routing computations
		dprst_seep_rate_open	0 to 0.1	Coefficient in depressions seepage flow computations
		fastcoef_lin	0 to 1	Linear preferential-flow routing coefficient
		fastcoef_sq	0 to 1	Non-linear preferential-flow routing coefficient
		gwflow_coef	0.001 to 0.05	Groundwater routing coefficient
		K_coef	0 to 48	Travel time through stream segment, hours
		op_flow_thres	0.6 to 1	Fraction of maximum open surface depression storage above which flow occurs
		pref_flow_den	0 to 0.1	Preferential flow pore density
		sat_threshold	1 to 40	Soil saturation threshold, above field-capacity threshold, inches
		slowcoef_lin	0 to 1	Coefficient to route gravity-flow storage down slope, 1/day
		slowcoef_sq	0 to 1	Coefficient to route gravity-flow storage downslope
		smidx_coef	0 to 1	Coefficient in nonlinear surface runoff contribution area algorithm
		smidx_exp	0.2 to 0.8	Exponent in nonlinear surface runoff contribution area algorithm
		soil2gw_max	0 to 5	Maximum rate of soil water excess moving to groundwater, inches
		soil_moist_max	0 to 20	Maximum available water holding capacity of soil profile, inches
		soil_rechr_max	0 to 4	Maximum available water holding capacity for soil recharge zone, inches
		ssr2gw_exp	0 to 3	Coefficient in equation used to route water from the subsurface reservoirs to the groundwater reservoirs
		ssr2gw_rate	0 to 1	Coefficient in equation used to route water from the subsurface reservoirs to the groundwater reservoirs
		x_coef	0 to 0.5	Weighting factor for streamflow routing

$$OF = \sum_{m=1}^{12} abs(MSD_m - SIM_m), \quad (3)$$

where

OF is the objective function,

m is the month,

MSD are the mean monthly measured values of either SR or PET, and

SIM are the mean monthly simulated values of either SR or PET.

After these four subareas were calibrated for SR and PET, the PRMS variables **swrad** and **potet** were written to individual files used as input files to the **climate_hru** module in PRMS; that is, SR and PET were preprocessed and output by HRU. These values were then read in by HRU for the second phase of the PRMS calibration.

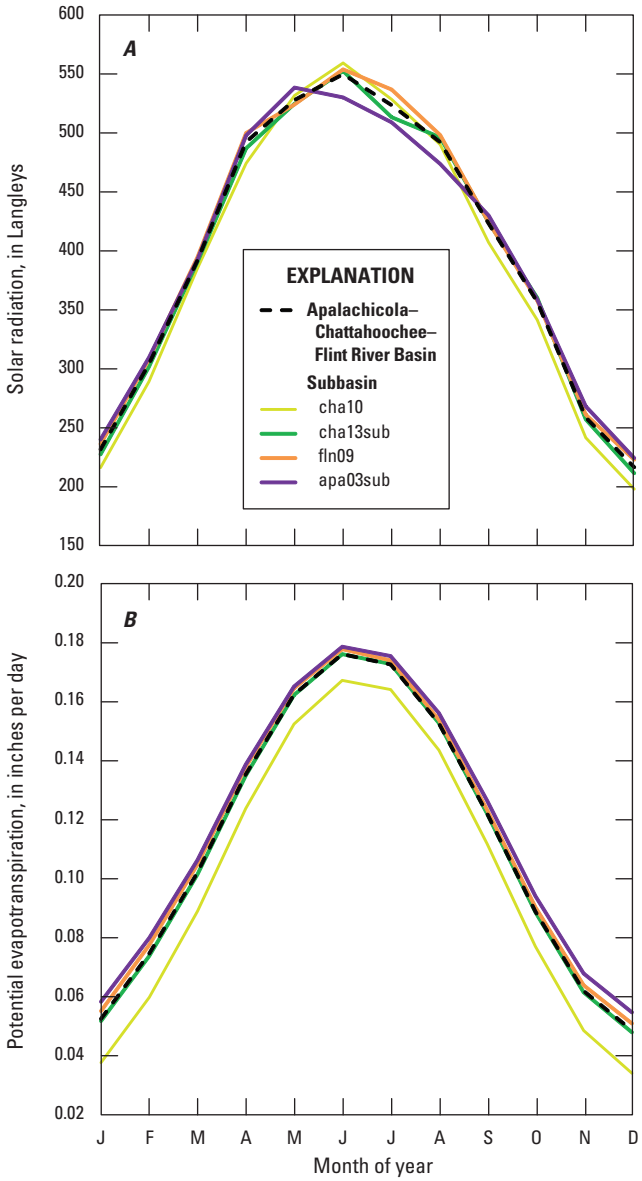

Figure 13. Historical *A,* solar radiation and *B,* potential evapotranspiration by calibration subbasin.

Phase 2: Streamflow Volume and Timing Calibration

This phase of the calibration involved matching simulated and measured streamflow in 35 subbasins of the ACFB (fig. 14). These 35 subbasins were divided into seven calibration rounds (fig. 14). Round 1 subbasins had to be calibrated first because these subbasins are nested within subbasins of subsequent rounds. Similarly, subbasins in Round 2 were calibrated before subbasins in Round 3, and so forth. Beginning with the headwater subbasins and moving downstream in a stepwise manner, the 35 subbasins were calibrated throughout the ACFB (fig. 14). As each successive round of subbasins was calibrated, the subbasins from previous rounds were not recalibrated, but instead those parameters were locked to preserve the previous calibrations. When the calibration encountered a large reservoir, simulated flow was replaced with measured flow data downstream of the reservoir so the calibration could continue downstream.

During this phase, the parameters that influence streamflow volume and timing were calibrated using (1) annual and monthly water balances and (2) a 3-day moving average of daily streamflow. The moving average of streamflow was used to lessen the effect of the smoothed precipitation forcings discussed in the Limitations of Gridded Climate Data section. This phase of model calibration compared USGS streamflow data to PRMS simulated streamflow for the historical period 1989–99; other time periods were used in several subbasins because of water-use impacts or limited measured streamflow records (table 2).

For this study, a split-sample test was used for calibration and evaluation of PRMS. Yapo and others (1996) found that approximately 8 years of data were needed to achieve model calibrations that are insensitive to the period selected. Figure 15 shows the calibration and evaluation years chosen for each subbasin. Water years (defined as October 1 of one year to September 30 of the following year) 1989–99 were chosen for model calibration when available; other time periods were used in several subbasins because of water-use impacts or limited measured-streamflow records. The chk01, ich02, and nik01 subbasins (table 2) had data only from the mid-1990s forward, so only 4 years (1996–99) of data were used for those calibrations.

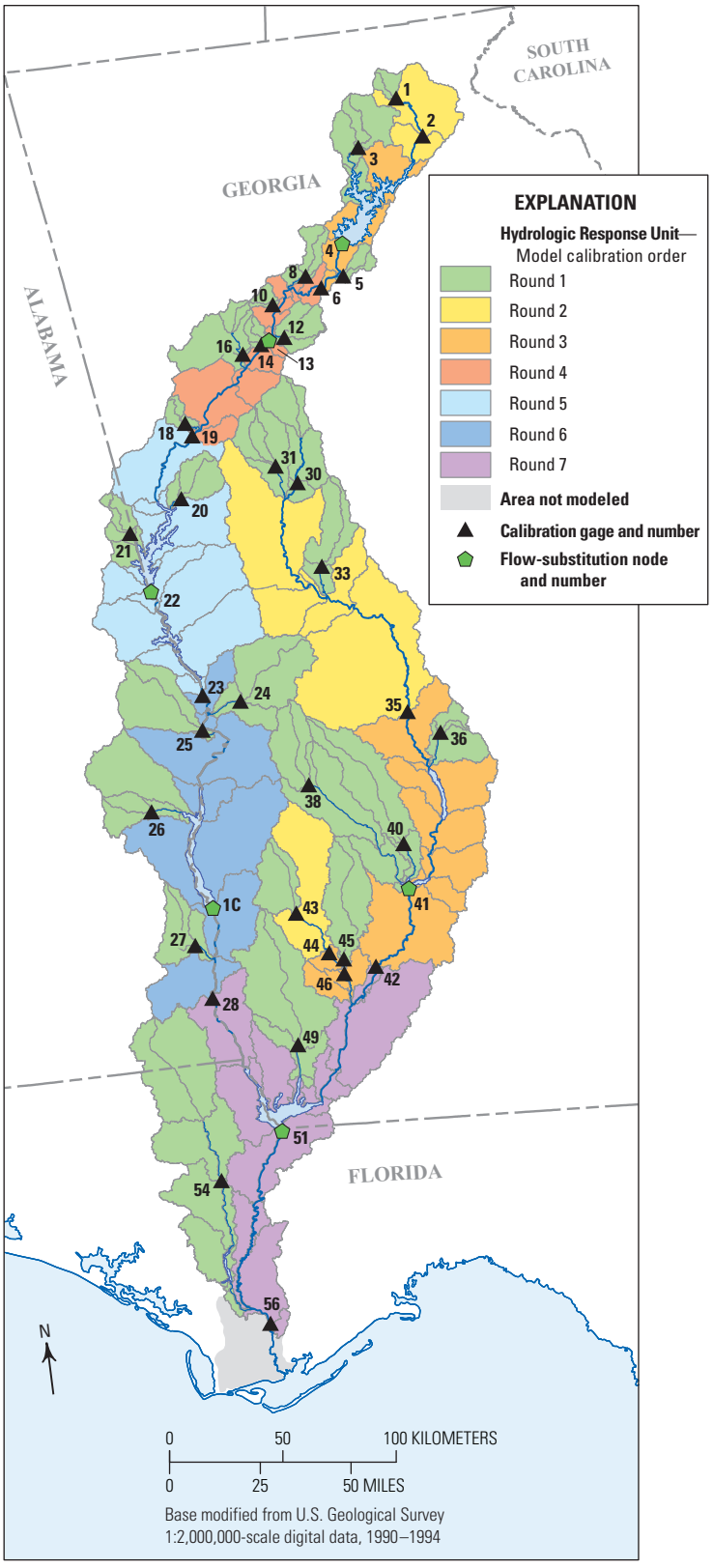

Figure 14. Apalachicola–Chattahoochee–Flint River Basin calibration gages, flow substitution gages, and calibration rounds. [HRU, hydrologic response unit]

Water Use

Flow alterations caused by substantial water use and by reservoir management were addressed by using substitution and augmentation of the measured streamflow record within the modeling process. Flow alterations of most concern in the calibration process were those that impacted the timing and magnitude of flows. With the operation of large reservoirs in the basin, peak flows are dampened and low flows are supplemented according to storage and release schedules for these impoundments. These flow adjustments may cause parameters to be unrealistically adjusted during calibration.

Using the parameters **obsin_segment** and **segment_type**, streamflow records were inserted into the model application at six locations, indicated by the flow substitution nodes in figure 14. Four of the locations were USACE reservoir projects in the ACFB (Lake Sidney Lanier, West Point Lake, Walter F. George Reservoir, and Lake Seminole). One substitution was made downstream of Atlanta (at USGS streamgage 02336490) to account for substantial water withdrawals from the Chattahoochee River. Another substitution was made downstream of Lake Worth on the Flint River (at USGS streamgage 02352500). Five of the streamflow records used were from USGS streamgages and the other was from a USACE streamgage. Instead of using simulated streamflow from those stream segments at the six locations, the measured runoff values stored in the Data File were used as the simulation values for those segments. By using this process, the model supplied the calibration software streamflows that were affected by flow regulation and water use. This was necessary to avoid calibrating natural flow model parameters to mimic regulated flows. After the calibration process was complete, however, these flow substitutions were removed from the model, and basin hydrology was computed as if there were no impoundments or water use affecting streamflow.

Flow augmentation was used in subbasins where anthropogenic effects were substantial, mostly in the form of irrigation withdrawals, and where either pre-impact historical streamflow data were not available or the previously mentioned strategy of flow substitution was not an option. Subbasins in the lower Flint River Basin, particularly in Ichawaynochaway Creek, were calibrated using USGS streamflow data augmented with estimates of monthly water withdrawals for irrigation, derived from a simulation by Wen and Zhang (2009). This study used a coupled surface-water/groundwater model that incorporated information from Jones and Torak (2006) to estimate the effects of irrigation withdrawals (both surface water and groundwater) on streamflow in the lower Flint River Basin for drought and normal precipitation years. Because irrigation in the lower Flint River Basin began to increase substantially in the 1970s (Rugel and others, 2009), several subbasins in this part of the ACFB that had USGS streamflow data for the period 1960–70 were calibrated during this period.

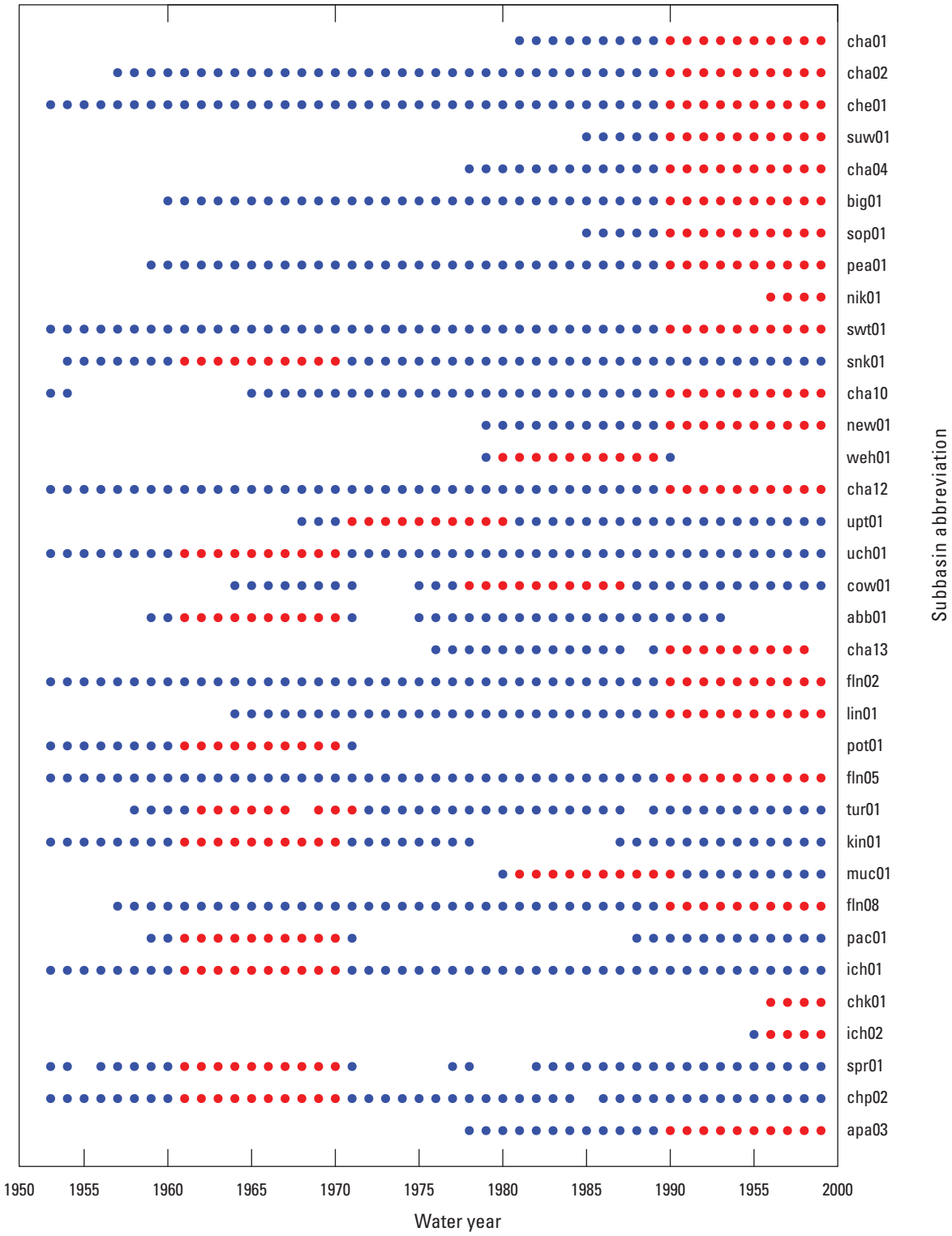

Figure 15. Calibration (red) and evaluation (blue) years for each of the 35 calibration subbasins.

Streamflow Volume

The streamflow volume step in the calibration procedure used three calibration datasets calculated from the designated USGS streamflow gaging station for each of the 35 subbasins: annual mean, monthly mean, and mean monthly streamflow (table 10). Monthly mean values are monthly averages of daily values for each month of each year for the period of interest whereas mean monthly values are average values of all the values of a particular month throughout the period of interest (that is, the average of all January values for the period of interest). The **rain_adj** parameter was adjusted to obtain the optimal water balance using the streamflow volume objective function, OF_{wb}, which was calculated using the following equation:

$$OF_{wb} = OF_{annmean} + OF_{mthmean} + OF_{meanmth}, \quad (4)$$

where

$OF_{annmean}$ is the annual volume,
$OF_{mthmean}$ is the monthly mean volume, and
$OF_{meanmth}$ is the mean monthly volume.

These objective functions were computed using the normalized root mean square error (NRMSE):

$$NRMSE = \sqrt{\frac{\sum_{n=0}^{nstep}(MSD_n - SIM_n)^2}{\sum_{n=0}^{nstep}(MSD_n - MN)^2}} \quad (5)$$

where

n is the time step,
$nstep$ is the total number of time steps,
MSD_n are the measured streamflow values,
SIM_n are simulated streamflow values, and
MN is the mean of all streamflow values for the objective function time period.

If NRMSE=0, then measured streamflow values are equal to simulated values (MSD=SIM). A value of NRMSE>1 indicates that the predictive capability of the simulated streamflow values is no more accurate than the average value of all the measured data.

Streamflow Timing

The streamflow timing step in the calibration procedure used a 3-day moving average of streamflow volume, which is calculated from the designated USGS streamgaging station for each of the 35 subbasins. The parameters listed in table 10 were adjusted to obtain the optimal streamflow timing for each subbasin based on the corresponding 3-day moving average. This average was used instead of daily streamflow because of limitations in the gridded climate data developed by Maurer and others (2002), described earlier herein. A 3-day moving average of flow appears to prevent the optimization process from overcompensating for the difference in flow timing and from adjusting the model parameters to unrealistic values. The NRMSE (eq. 3) was used as the objective function to optimize streamflow timing.

The Nash-Sutcliffe model efficiency index (NS; Nash and Sutcliffe, 1970; McCuen and others, 2006; Jain and Sudheer, 2008) was computed for each of the 35 subbasin as follows:

$$NS = 1.0 - \frac{\sum_{n=1}^{nstep}(MSD_n - SIM_n)^2}{\sum_{n=1}^{nstep}(MSD_n - MN)^2}. \quad (6)$$

An NS value of 1.0 indicates a perfect fit between the simulated and measured values, an NS value of zero indicates the goodness-of-fit is as good as using the mean of the simulated values for the period, and a negative NS value indicates that the mean of the simulated values for the period provides a better fit than the individual simulated results. In addition, the percent bias (P_{bias}) was computed for the 35 subbasins as follows:

$$P_{bias} = \frac{(MSD_n - SIM_n)}{MSD_n} \times 100. \quad (7)$$

A negative or positive P_{bias} value indicates, respectively, an overestimation or underestimation of streamflow.

Model Calibration Results and Evaluation

Four PRMS outputs were calibrated as part of the two-phase, stepwise, multiple-objective automated procedure described previously. Phase 1 includes the monthly mean SR and PET and Phase 2 includes streamflow volume and timing. Results for each phase are described in the following sections.

Phase 1: Solar Radiation and Potential Evapotranspiration Results

Calibration of SR is the first step of Phase 1 in the step-wise procedure. Figure 16 shows the subarea mean monthly SR values for measured, calibrated, and evaluated SR for the four subareas shown in figure 12 (apa03, cha10, cha13, fln09, respectively). The mean monthly average of simulated SR values during the calibration period (water years 1989–99) closely match the mean monthly average of historical measured SR data, whereas the evaluation period values of SR (water years 1952–88) for three of the four subareas (apa03, cha10, and fln09) deviate a bit more from the historical measured SR data. In each subarea, the mean

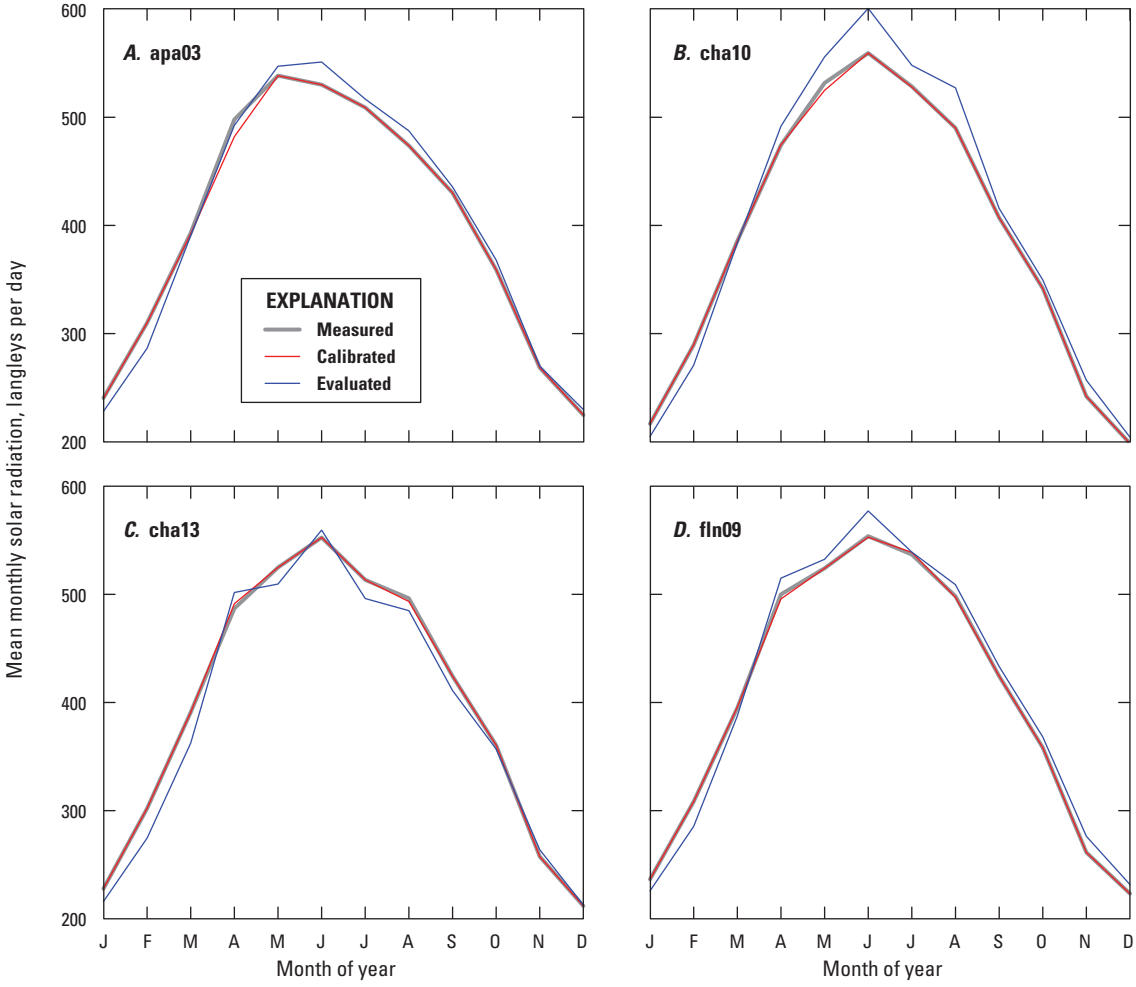

Figure 16. Solar radiation calibration and evaluation results for *A*, apa03, *B*, cha10, *C*, cha13, and *D*, fln09 subbasins for calibration period (water years 1989–99) and evaluation period (water years 1952–88).

monthly average of the evaluation period observations has somewhat higher values of simulated SR than measured SR from May to August and somewhat lower values of simulated SR from January to February. Differences may be due to the use of long-term observed data during calibration of a later, shorter period as well as assumptions made in the model algorithm for computing SR.

Calibration of PET is the second step of Phase 1 in the step-wise procedure. Figure 17 shows the subarea mean monthly PET values for measured, calibrated, and evaluated PET for the four subareas in figure 12 (apa03, cha10, cha13, fln09, respectively). Results for PET are similar to those shown for SR. The calibration period values of PET (water years 1989–99) closely match the historical measured PET data, whereas the evaluation period values of PET (water years 1952–88) for each of the four subareas deviate a bit more from the historical measured PET data. Results for PET are similar to those shown for SR for each subarea in that the evaluation period has somewhat higher values of simulated PET than measured PET in the months April to June and somewhat lower values of simulated SR in the months of January to March. The computation of PET depends on values of SR and, therefore, differences observed in the SR evaluation period play a role in the differences shown for the PET evaluation period. Again, differences may also be due in part to the use of long-term observed data during calibration of a later, shorter period.

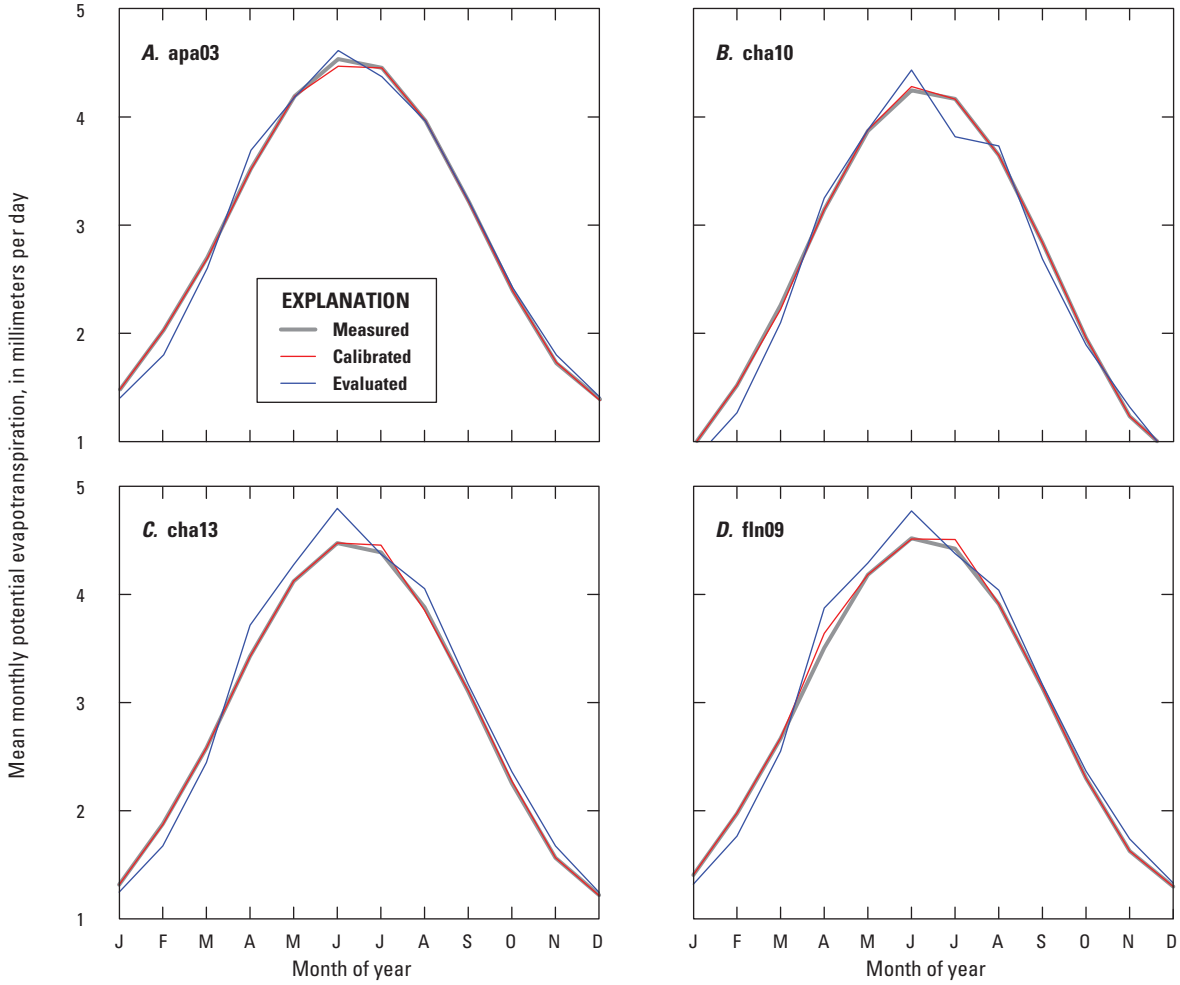

Figure 17. Potential evapotranspiration calibration and evaluation results for: *A*, apa03, *B*, cha10, *C*, cha13, and *D*, fln09 subbasins for calibration period (water years 1989–99) and evaluation period (water years 1952–88).

Phase 2: Streamflow Volume and Timing Results

To summarize the streamflow volume and timing results, the 35 subbasins were separated into the following five classes based on physiography, stream type, and urbanization: Coastal Plain located mostly or completely in the Floridan aquifer system outcrop area (CF), Coastal Plain located outside of the Floridan aquifer system outcrop area (CR), Mainstem Apalachicola, Chattahoochee, and Flint Rivers (MS), Piedmont and Blue Ridge developed (PD), and Piedmont and Blue Ridge rural (PR) (table 11 and fig. 18). The PR class includes subbasins having less than 10 percent impervious area, and the PD class includes subbasins with more than 10 percent impervious area. Subbasins in the Coastal Plain did not require differentiating between developed and rural areas. A distinction was made, however, between Coastal Plain subbasins within and outside of the Floridan aquifer system outcrop area because of karst physiography present only within the outcrop area. In the Floridan aquifer system outcrop area, the groundwater aquifer is highly productive and incised by many of the streams in the area. Subbasin distributions of P_{bias} and NS values for each of the five classes for all years between 1953–99 having measured streamflow (fig. 15) were used to evaluate streamflow volume and timing, as described next.

Streamflow Volume

Plots of measured and simulated (1) mean monthly, (2) monthly mean, and (3) annual mean streamflow for the calibration and evaluation periods for each of the 35 subbasins are provided in appendix 1. Figure 19 shows the distributions of P_{bias} across subbasins within each physiographic class, calculated using annual mean, mean monthly, and monthly mean streamflow for the years shown in figure 15. The PD class subbasins have a median bias of –4.3 percent, indicating a slight overestimation of streamflow volume in these subbasins. Of the 35 subbasins, there are 20 with a negative bias and 15 with a positive bias. The median bias for all five classes ranges from –4.3 to 0.8 percent for annual mean streamflow, –6.3 to 0.5 percent for mean monthly streamflow, and –9.2 to 1.3 percent for monthly mean streamflow.

Figure 20 shows the subbasin distributions of NS calculated using annual mean streamflow, mean monthly streamflow, and monthly mean streamflow for each of the five classes for the years shown in figure 15. The lowest NS values are rarely below 0.6, whereas the median NS for all five classes ranges from 0.74 to 0.96 for annual mean streamflow, 0.89 to 0.98 for mean monthly streamflow, and 0.82 to 0.98 for monthly mean streamflow. These results combined with the P_{bias} results presented in figure 19 indicate a good to very good streamflow volume simulation for all subbasins.

Table 11. Description of five physiographic classes used to summarize the PRMS simulation results.

[km^2, square kilometer; <, less than; >, greater than]

Class	Description	Number of subbasins	Subbasin area (km^2)			Physiographic province	Percent impervious area range
			Median	Minimum	Maximum		
CF	Coastal Plain in Floridan aquifer outcrop	4	1,230	828	2,590	Coastal Plain	<10
CR	Coastal Plain outside of Floridan aquifer outcrop	9	510	116	937	Coastal Plain	<10
MS	Mainstem Apalachicola, Chattahoochee, Flint	7	12,100	3,030	49,700	Blue Ridge/Coastal Plain/ Piedmont	<10
PD	Blue Ridge/Piedmont developed	6	154	75.6	704	Blue Ridge/Piedmont	>10
PR	Blue Ridge/Piedmont rural	9	329	91.9	815	Blue Ridge/Piedmont	<10

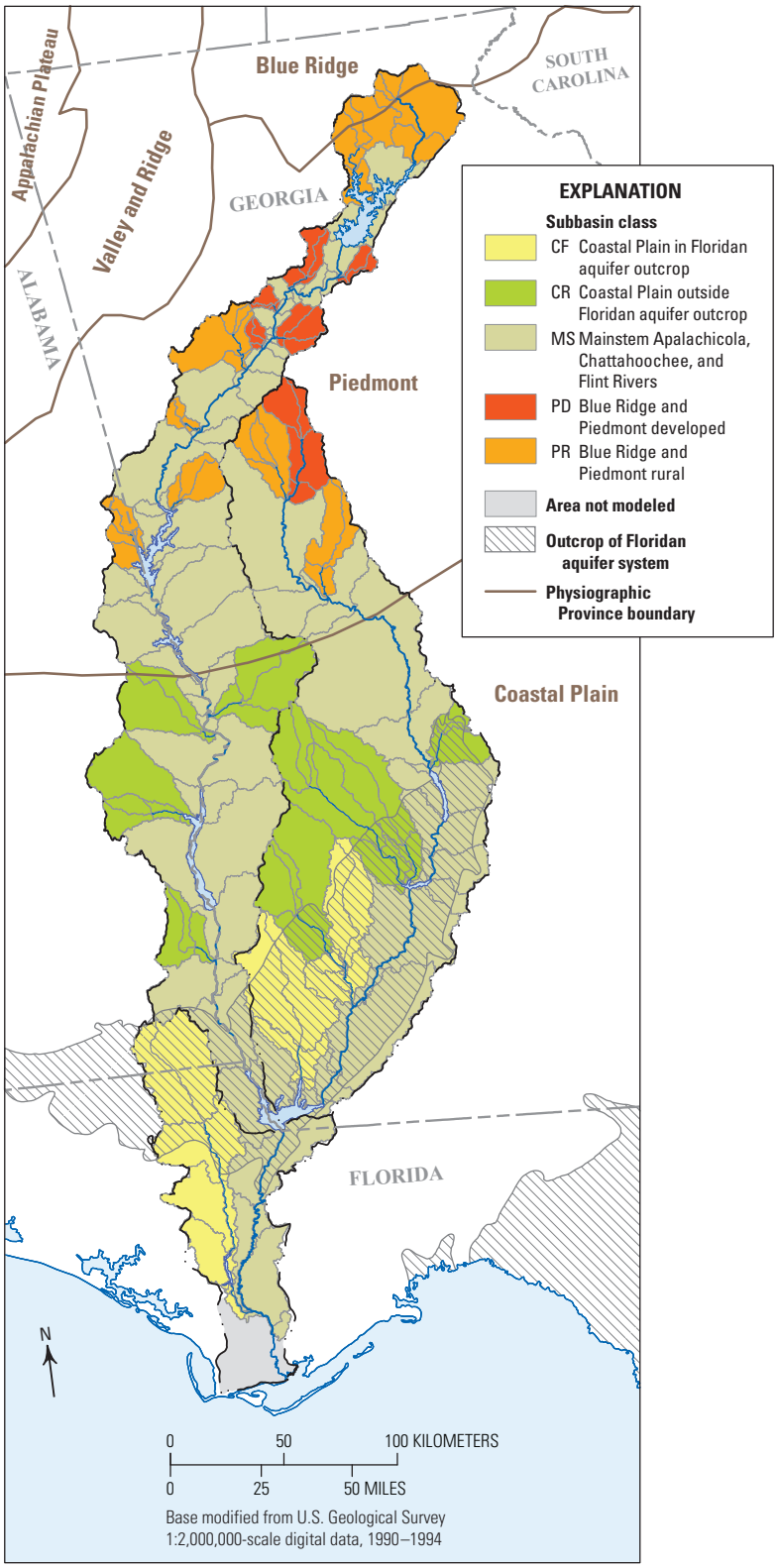

Figure 18. Locations of subbasins within the five physiographic classes. [CF, Coastal Plain in Floridan aquifer system outcrop area; CR, Coastal Plain outside Floridan aquifer system outcrop area; MS, Mainstem Apalachicola, Chattahoochee, and Flint Rivers; PD, Blue Ridge and Piedmont developed; PR, Blue Ridge and Piedmont rural]

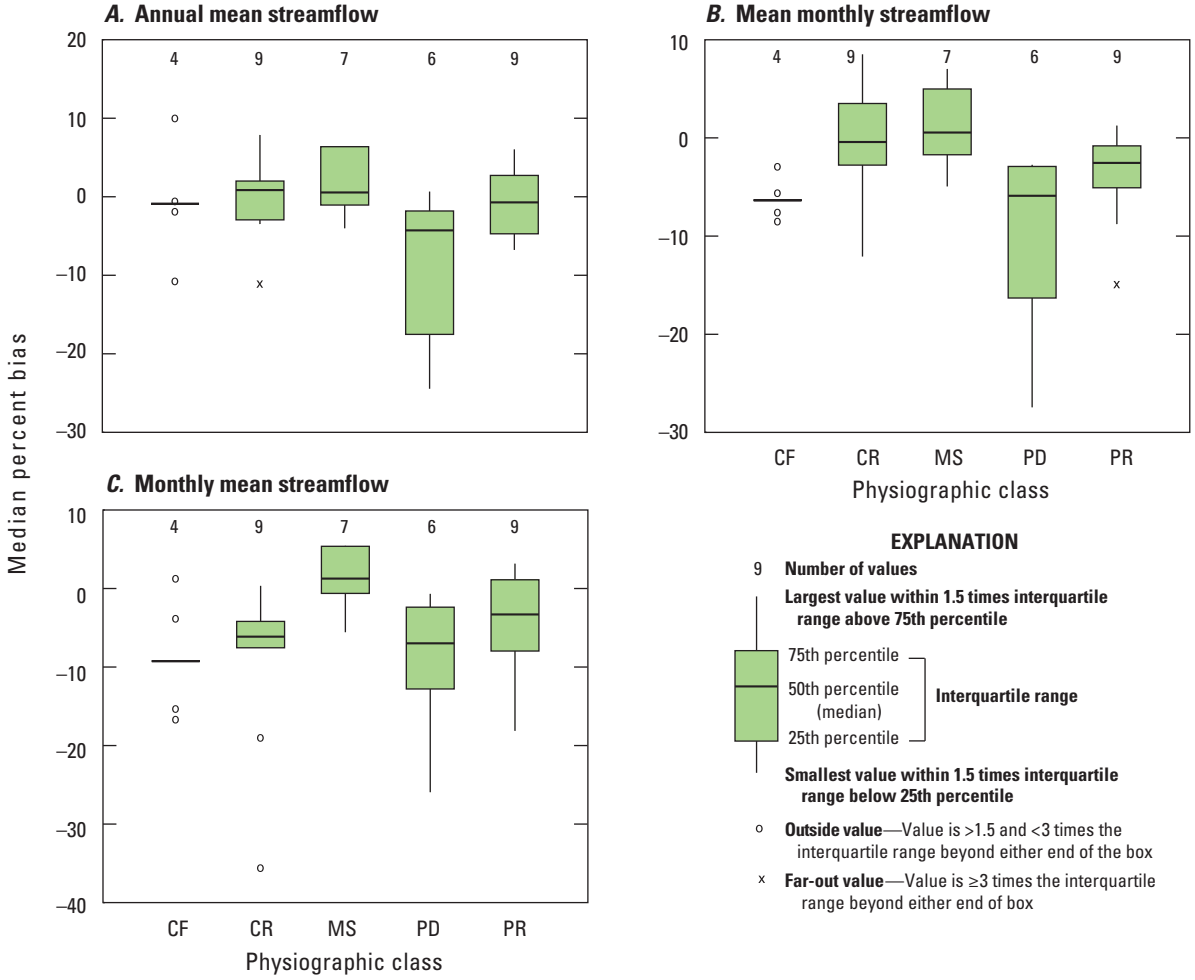

Figure 19. Boxplots showing median percent bias of simulation versus measured streamflow by subbasin class for *A*, annual mean streamflow, *B*, mean monthly streamflow, and *C*, monthly mean streamflow volumes. [CF, Coastal Plain in Floridan aquifer system outcrop area; CR, Coastal Plain outside Floridan aquifer system outcrop area; MS, Mainstem Apalachicola, Chattahoochee, and Flint Rivers; PD, Blue Ridge and Piedmont developed; PR, Blue Ridge and Piedmont rural]

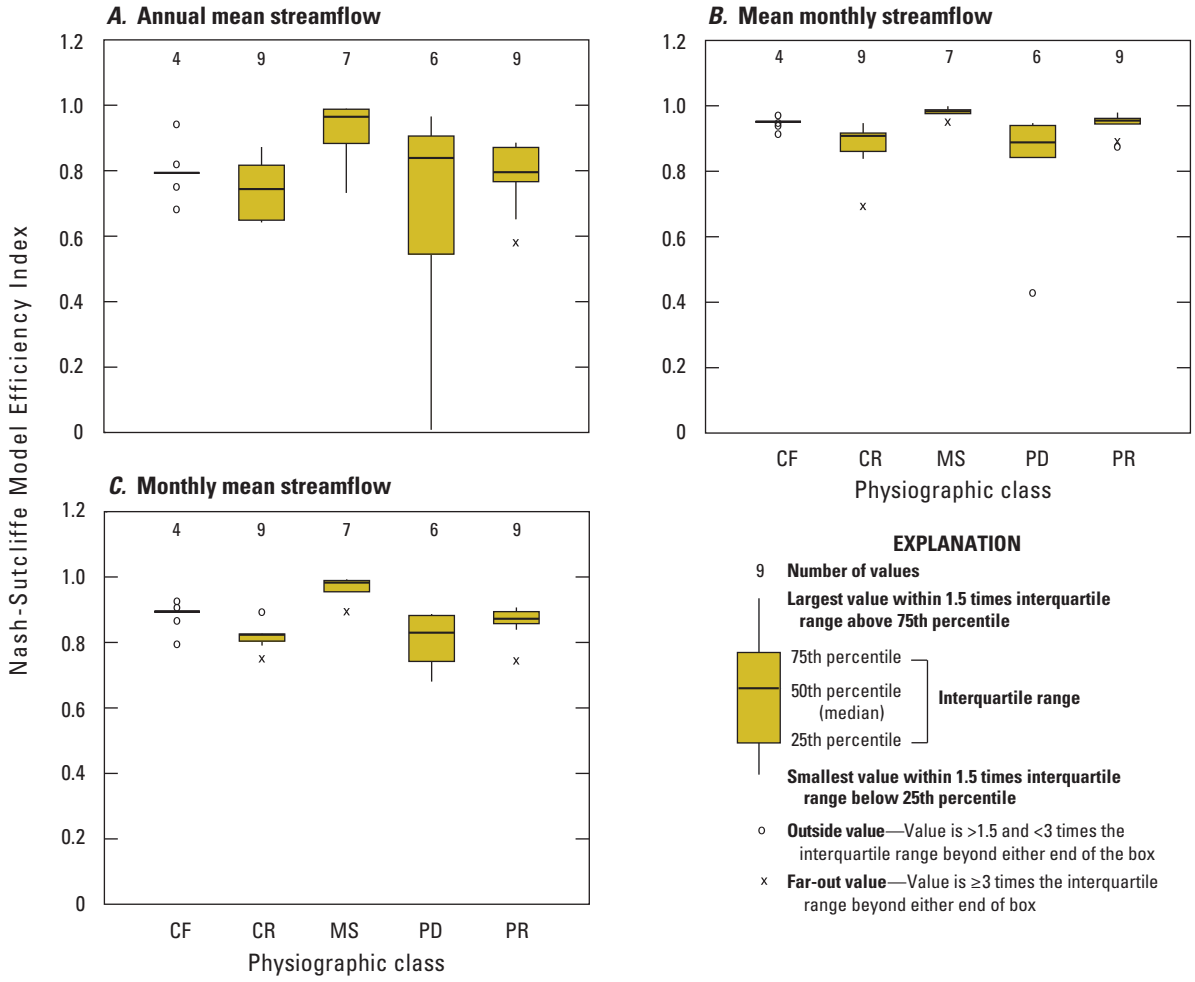

Figure 20. Boxplots showing Nash-Sutcliffe Model Efficiency Index of simulated streamflow by subbasin class for *A*, annual mean streamflow, *B*, mean monthly streamflow, and *C*, monthly mean streamflow volumes. [CF, Coastal Plain in Floridan aquifer system outcrop area; CR, Coastal Plain outside Floridan aquifer system outcrop area; MS, Mainstem Apalachicola, Chattahoochee, and Flint Rivers; PD, Blue Ridge and Piedmont developed; PR, Blue Ridge and Piedmont rural]

Streamflow Timing

Plots of measured versus simulated streamflow, annual NS values, and flow duration curves for calibration and evaluation periods are provided in appendix 2. Annual NS results obtained using the daily time series results are summarized in table 12, which also lists the subbasin area, percentage of impervious area, altitude, slope, percent depression storage area, and permeability. The mean NS refers to the NS value calculated from simulated and measured streamflow for calibration and evaluation periods. The minimum and maximum NS values are the minimum and maximum annual NS values, indicating the annual NS value associated with the worst and best years of the entire period. Most of the subbasins have mean and maximum NS values above 0.6 for the calibration and evaluation periods, a rigorous test of the simulated streamflow accuracy considering the model was calibrated using the 3-day running mean.

All but four subbasins have mean NS values of at least 0.6 for the calibration period (table 12). The four subbasins having a mean NS value lower than 0.6 (lin01, nik01, pea01, sop01) are developed or developing watersheds, with relatively large percentages of impervious area. These four subbasins are also some of the smallest in the study area having drainage areas ranging from 75.6 to 261 km^2. A combination of factors may result in a less optimal simulation of small watersheds than larger ones. The daily time step used in the model may be too coarse to accurately match the timing of the processes that occur in these watersheds, and the smoothed precipitation forcing data previously mentioned may have a substantial impact on the model's ability replicate hydrographs of daily measured data. Hydrographs of simulated storm events, generated using smoothed forcings of precipitation, rise earlier, do not peak as high, and decline slower than hydrographs of measured data. This combination of timing issues may substantially affect evaluation measures, with simulated flows overestimating pre- and post-storm flows and underestimating peak flows. Larger subbasins having multiday travel times can better match the measured streamflow using the smoothed forcings of precipitation because the routing module has more flexibility in moving water downstream; however, flow timing is a pervasive issue with this configuration of model forcings.

Figures 21 and 22 show that the large mainstem subbasins have, on average, P_{bias} values closer to zero and higher NS values when compared to the other smaller subbasins for all flow regimes. This may in part be due to the challenge of simulating flows in smaller, flashier watersheds using smoothed precipitation forcings. Almost all non-mainstem subbasins have a negative P_{bias} for all flows in the low and medium flow regimes whereas the high flow subgroups show a positive P_{bias} for all non-mainstem classes (fig. 21). The developed subbasins in the PD class tend to have the lowest NS values overall, with the largest range of biases in the high flow regime when compared to the other classes. This outcome is related to the timing issues described in the Limitations of Gridded Climate Data section. A possible substantial source of the differences between measured and simulated flows is that the simulated flows do not include the effects of water use like the measured streamflows. Low flows may be greatly affected by water use, which could help explain why the simulated low flows do not match the measured flows as well as the medium and high flow-regime values. Another possible source of inaccuracy in the simulation of the lower flows is groundwater flow direction. The hydrologic model assumes that groundwater flows according to land-surface topography like surface water. If the groundwater flows across HRU, subbasin, or basin boundaries, this could be a source of the large discrepancies between the simulated and measured flows for subbasins in the CF and CR classes.

To provide some perspective on how the statistical measures of the ACFB model results compare with previous modeling studies, a report by Moriasi and others (2007) is referenced that documents a review of past modeling studies to determine recommended model evaluation techniques and to establish guidelines for model evaluation based on the review results. The authors conclude that three quantitative statistics with thresholds, $NS>0.5$, $P_{bias}<\pm25$ percent, and the ratio of the root mean square error to the standard deviation of measured data less than 0.7, be used to assign a rating of "good" to a simulation.

The analysis of the ACFB model has employed two of these three statistics in the model evaluation process, namely, NS and P_{bias}. Table 12 is color coded to reflect a more stringent analysis of NS than Moriasi and others (2007), using a threshold of 0.6 to assess goodness-of-fit. All but two of the calibration subbasins have a mean NS higher than 0.5. The two subbasins having a mean NS lower than 0.5 are urbanized watersheds whose simulated data have a less-optimal fit compared to measured data because of stream infrastructure that is not considered in the streamflow simulations. The median streamflow of all classes is below the 25-percent maximum bias threshold for annual and monthly measures of flow. Some subbasins in the CF, CR, and PD classes exceed this threshold on a monthly mean basis. For these classes, model fit between simulated and measured data is poor because of urbanization in the PD class, water use in the CR class, and water use in combination with complex groundwater dynamics in the CF class.

Table 12. Subbasin characteristics and Nash-Sutcliffe Model Efficiency Index ranges using daily time series results for calibration subbasins.

[ID, identifier; km², square kilometer; %, percent; dprst pct area, percent of subbasin area covered by depression storage; K, permeability, m², square meter; NS, Nash-Sutcliffe; Class: CF, Coastal Plain in Floridan aquifer outcrop; CR, Coastal Plain outside of Floridan aquifer outcrop; MS, Mainstem Apalachicola, Chattahoochee, Flint; PD, Blue Ridge/Piedmont developed; PR, Blue Ridge/Piedmont rural; min, minimum; max, maximum; green shading, NS>0.6; yellow shading, 0<NS<0.6; orange shading, NS<0; gray shading, no data available; <, less than; na, no data available]

Steam-gage number (fig. 14)	USGS gage ID	Sub-basin ID	Area (km²)	Impervious % area	Altitude (meters)[1]	Slope (%)	dprst pct area	K (m²)	Class	Calibration period NS			Evaluation period NS		
										Mean	Min	Max	Mean	Min	Max
1	02330450	cha01	116	0.3	644	22.6	0.62	8.8E-15	PR	0.70	0.58	0.85	0.71	0.16	0.88
2	02331600	cha02	815	1.0	715	29.8	0.92	8.7E-15	PR	0.80	0.71	0.88	0.78	0.49	0.98
3	02333500	che01	396	0.8	456	13.8	0.37	8.9E-15	PR	0.79	0.67	0.85	0.78	0.35	0.88
5	02334885	suw01	122	13.4	314	6.5	1.50	8.7E-15	PD	0.67	0.22	0.77	0.22	<0	0.43
6	02335000	cha04	3,030	3.3	475	16.1	0.75	8.8E-15	MS	0.96	0.71	0.97	0.95	0.71	0.97
8	02335700	big01	186	11.6	340	9.2	0.68	8.9E-15	PD	0.74	0.28	0.82	0.58	<0	0.77
10	02335870	sop01	75.6	19.3	296	9.3	1.95	8.9E-15	PD	0.56	0.24	0.75	0.58	0.37	0.67
12	02336300	pea01	225	30.7	285	8.7	0.76	8.9E-15	PD	0.46	0.23	0.64	0.41	<0	0.61
14	02336635	nik01	81.5	18.3	294	8.2	1.67	9E-15	PD	0.49	0.20	0.69	na	na	na
16	02337000	swt01	637	8.0	299	8.0	0.64	8.9E-15	PR	0.88	0.49	0.93	0.81	0.01	0.93
18	02337500	snk01	91.9	1.2	287	5.2	2.21	8.9E-15	PR	0.60	<0	0.85	0.75	<0	1.00
19	02338000	cha10	6,290	7.8	381	11.9	0.87	8.8E-15	MS	0.83	0.48	0.86	0.75	0.56	0.88
20	02338660	new01	329	1.6	248	7.0	0.86	1.02E-14	PR	0.76	0.54	0.88	0.66	0.46	0.86
21	02339225	weh01	156	0.6	225	8.2	0.50	8.9E-15	PR	0.63	0.34	0.81	0.64	0.70	0.75
23	02341505	cha12	12,100	4.8	293	9.8	0.82	2.516E-13	MS	0.94	0.74	0.96	0.89	0.71	0.94
24	02341800	upt01	885	0.6	166	6.9	0.64	4.784E-13	CR	0.77	0.64	0.84	0.65	0.05	0.87
25	02342500	uch01	834	1.2	126	3.7	0.57	1.58E-13	CR	0.79	0.36	0.90	0.75	0.33	0.93
26	02342933	cow01	290	0.3	80	6.2	3.81	1.0083E-12	CR	0.63	0.38	0.72	0.60	0.22	0.72
27	02343300	abb01	378	1.0	63	1.4	0.99	6.849E-13	CR	0.82	0.70	0.91	0.76	0.35	0.86
28	02343801	cha13	21,300	3.2	208	7.5	1.27	1.344E-12	MS	0.95	0.79	0.97	0.96	0.92	0.97
30	02344500	fln02	704	12.0	251	6.6	0.62	9.7E-15	PD	0.87	0.48	0.93	0.73	0.19	0.91
31	02344700	lin01	261	7.1	266	8.4	1.24	8.8E-15	PR	0.59	<0	0.77	0.52	<0	0.78
33	02346500	pot01	482	2.3	236	3.9	0.89	9.2E-15	PR	0.82	0.44	0.90	0.78	0.61	0.89
35	02349605	fln05	7,560	2.2	213	6.8	0.81	3.31E-14	MS	0.91	0.48	0.96	0.85	0.45	0.94
36	02349900	tur01	116	0.6	122	6.1	1.93	3.1682E-12	CR	0.77	0.18	0.89	0.67	<0	0.88
38	02350600	kin01	510	0.2	122	9.0	2.13	9.254E-13	CR	0.80	0.33	0.88	0.72	0.32	1.00
40	02351890	muc01	937	1.1	120	2.6	2.10	5.903E-12	CR	0.75	0.50	0.87	0.82	0.42	0.84
42	02353000	fln08	14,900	1.8	155	5.4	1.58	1.4735E-12	MS	0.97	0.94	0.98	0.97	0.88	0.99
43	02353400	pac01	487	0.4	93	1.5	5.29	2.7678E-12	CR	0.78	0.47	0.86	0.75	0.40	0.85
44	02353500	ich01	1,600	0.4	82	5.1	3.15	2.1633E-12	CR	0.79	0.07	0.87	0.79	<0	0.93
45	02354500	chk01	828	0.5	74	2.2	2.12	7.944E-13	CF	0.83	0.14	0.92	na	na	na
46	02354800	ich02	2,590	0.5	78	4.1	2.78	1.6892E-12	CF	0.86	0.63	0.90	0.82	0.97	0.97
49	02357000	spr01	1,260	0.8	55	5.1	2.98	1.622E-12	CF	0.77	<0	0.90	0.74	0.04	0.93
54	02359000	chp02	1,200	0.8	43	2.9	1.58	1.1733E-12	CF	0.78	0.12	0.89	0.73	<0	0.90
56	02359170	apa03	49,700	2.1	149	5.7	1.50	1.12409E-06	MS	0.92	0.66	0.96	0.91	0.74	0.93

[1]Relative to North American Vertical Datum of 1988.

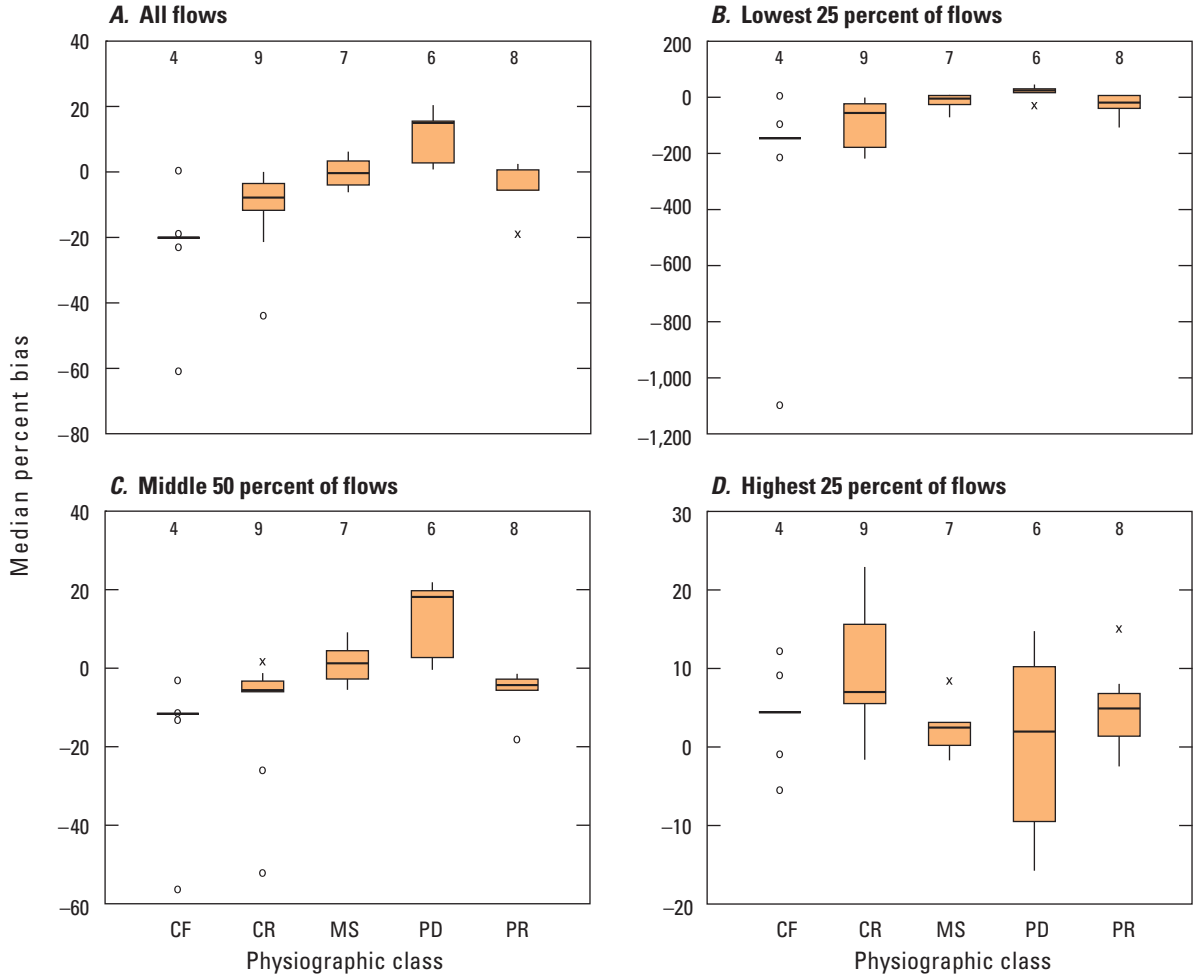

Figure 21. Boxplots showing percent bias (P_{bias}) of simulation versus measured streamflow by subbasin for daily streamflow timing. Plots of individual subbasin streamflow comparisons are provided in appendix 2. [CF, Coastal Plain in Floridan aquifer system outcrop area; CR, Coastal Plain outside Floridan aquifer system outcrop area; MS, Mainstem Apalachicola, Chattahoochee, and Flint Rivers; PD, Blue Ridge and Piedmont developed; PR, Blue Ridge and Piedmont rural]

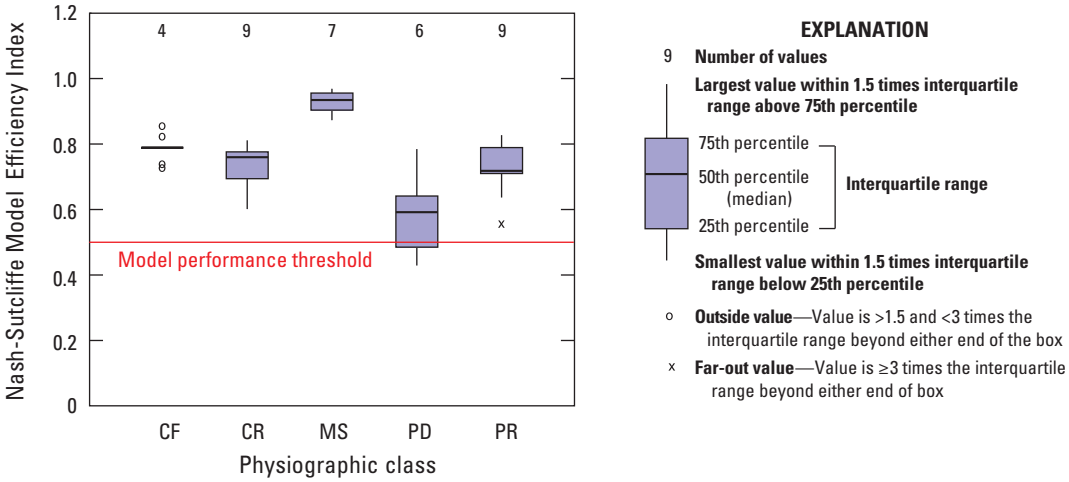

Figure 22. Boxplot showing Nash-Sutcliffe Model Efficiency Index of simulated streamflow by subbasin class for daily mean streamflow timing. Plots of individual subbasin streamflow comparisons are provided in appendix 2. [CF, Coastal Plain in Floridan aquifer system outcrop area; CR, Coastal Plain outside Floridan aquifer system outcrop area; MS, Mainstem Apalachicola, Chattahoochee, and Flint Rivers; PD, Blue Ridge and Piedmont developed; PR, Blue Ridge and Piedmont rural]

Potential Improvements to the ACFB PRMS Model

A PRMS model was developed to provide simulations of streamflow conditions throughout the ACFB. The experiences gained from this modeling effort indicate that improvements could be made by (1) exploring an understanding of the uncertainties associated with climate forcings and propagation of these uncertainties through the SERAP, (2) using dynamic land cover parameters, (3) further discretizing basin-wide parameters to the HRU level, (4) merging routing modules with methods to account for large reservoir storage, (5) incorporating additional algorithm sophistication in simulating regional groundwater flow, and (6) enhancing the calibration procedure for basins having internal calibration points. These issues are described in detail in the following sections.

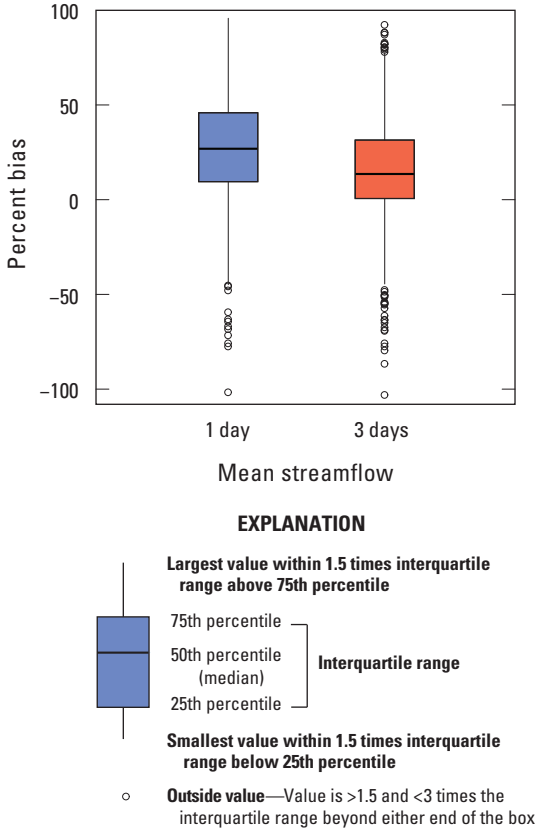

Figure 23. Boxplot showing percent bias in annual peak flow estimation for the 35 calibration subbasins for 1-day and 3-day mean flows.

Climate Forcings

Figure 23 shows the distribution of P_{bias} in daily and 3-day peak flows calculated on an annual basis for all 35 subbasins. For each water year, the highest daily and 3-day observed flow was compared to the simulated flow on that day or 3-day period, respectively. On average, daily peak flows are underestimated by 25 percent and 3-day peak flows are underestimated by 12 percent.

Streamflow timing was calibrated in PRMS using a 3-day running mean to prevent the calibration process from overcompensating for the difference in flow timing as a result of the gridded inputs. Therefore, evaluating streamflow on a daily basis may not be appropriate. Figure 24 shows the relation between the NS values calculated with daily versus 3-day time series for all 35 calibration subbasins for the period of simulation. As expected, NS results based on a 3-day time step are always higher than those on a daily time step (and greater than 0.6). If the hydrologic model output will be used to drive other simulation models, then the uncertainty associated with the gridded inputs and the propagation of this uncertainty through the SERAP workflow (fig. 1) must be considered.

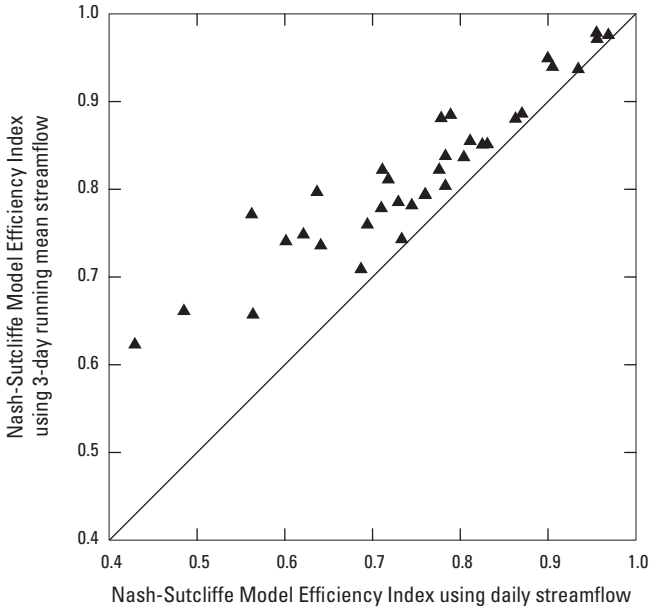

Figure 24. Comparison of annual Nash-Sutcliffe Model Efficiency Index using daily versus a 3-day running mean streamflow values for the Apalachicola–Chattahoochee–Flint River Basin subbasins.

Dynamic Parameters

The ACFB PRMS simulation was parameterized using land cover data from 2001, and the parameter values were held constant through time. Although newer land cover data were available for 2006, the 2001 land cover data were used because they were temporally closer to the calibration period of 1989–99. Although this static land cover may not pose much of an issue for rural basins, it can cause large simulation errors in basins that undergo substantial urbanization during the period of interest.

The calibration process removed, or at least minimized, the effects of water use from simulated flows, but still retained the effects of landscape development, primarily described in the model by the percentage of impervious surface in an HRU. The modeling simulation is sensitive to the amount of impervious area in a basin, and runoff is overestimated if the current extent of impervious area is used for historical simulations when the basin was less developed. This observation is supported by analysis of the annual mean streamflow for the big01 (USGS streamgage 02335700) and pea01 (USGS streamgage 02336300) subbasins, which have percent impervious areas of 11.6 and 30.7, respectively, for 2001. Figure 25 shows the difference between measured and simulated mean annual streamflow by water year for the calibration and evaluation periods for the two subbasins. The regression line is based on the evaluation period only on each plot. The positive slopes of both regression lines indicate a gradual reduction in the overestimation of simulated streamflow with time at these two sites. This finding demonstrates that as the parameter-indicated level of imperviousness approaches actual conditions, simulated streamflow more closely matches the measured data.

This application of PRMS incorporated surface depressions for the historical simulations, and the parameters describing these depressions were also held constant—no indication of change in water storage caused by changing surface depressions for historical conditions was considered. Because the surface depressions remained static, the magnitude of their effect on streamflow may only be properly produced for the calibration period or during previously observed conditions. Properly characterizing this relatively fine-scale geographic feature, and any change in this feature over time, is important for supporting effective natural resource management.

Dynamic land cover capabilities should be developed to provide a way to account for both historical and future land cover change. Land cover changes that may occur over several decades, such as conversion of forest lands to agriculture or to developed lands, have substantial impacts on basin hydrology and would need to be considered to more accurately represent actual conditions. Figure 25 demonstrates the errors induced by using current land cover in developed areas to simulate historical hydrology. From a resource management perspective, future projections of land cover are equally, if not more, important in simulating changes in hydrologic response as the landscape changes. PRMS projections for future conditions in the Flint River Basin (Viger and others, 2011) indicate increases in surface runoff caused by projected increases in urbanization, although such increases might be offset if the corresponding changes in depression storage were considered. Research using remotely sensed data to develop relations between historical changes in land cover and associated changes in depression storage would be useful for current and future simulations of water availability.

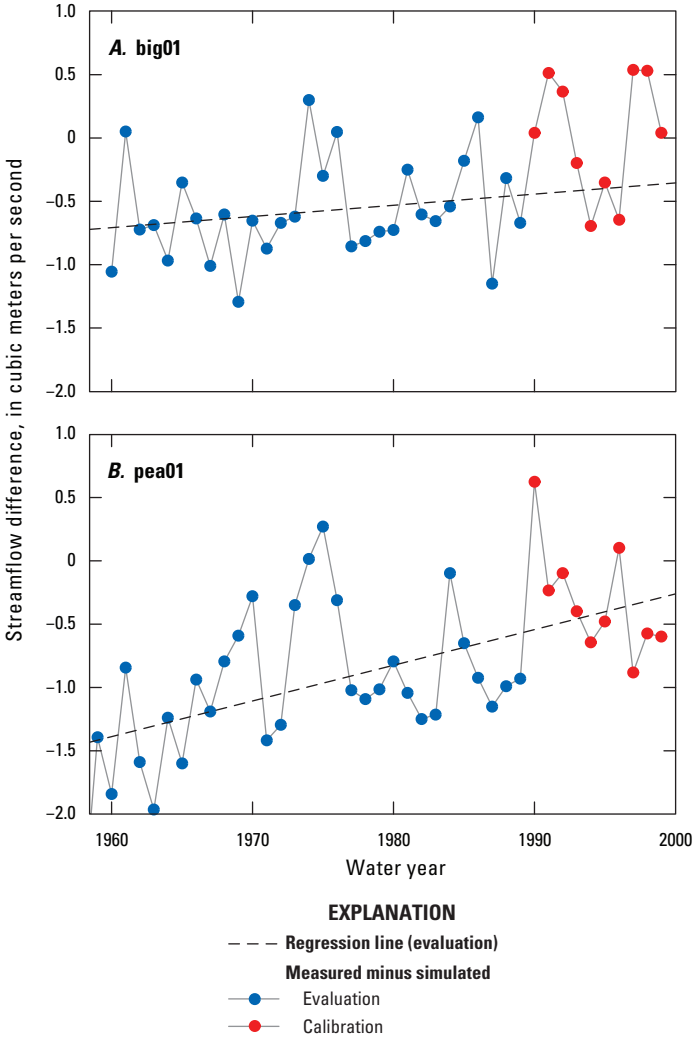

Figure 25. Measured minus simulated mean annual streamflow for the *A*, big01 and *B*, pea01 subbasins. The regression lines are based on the evaluation period only on each plot.

Spatial Parameters

Several parameters in the version of PRMS used for this study describe basin characteristics using a single value. Although this may be valid for smaller watersheds, model simulations that involve larger scales may render this assumption invalid. In past simulations, for example, SR and PET were described by mean-monthly values for the entire basin. In this application, the ACFB was split into four subareas (fig. 12) and each subarea was calibrated independently. These subareas were then simulated individually and daily values of SR and PET were output and combined as input files for the larger model of the entire basin. Further discretization of these basin-wide parameters to the HRU level would allow each HRU to have its own description of SR and PET. This methodology could be applied to other parameters as well to increase the flexibility and potential use of the modeling structure in larger areas without undue burden on the user.

Routing and Reservoirs

This PRMS model was developed to provide simulations of streamflow throughout the ACFB. In its current form, this model does not account for storage in large mainstem reservoirs nor the effects of operations at those impoundments. Flow substitutions were used at the reservoir outlets during calibration of the model and then were removed so that the model would provide simulated streamflow volumes.

Accounting for storage in large mainstem reservoirs while still routing streamflow through the basin is informative from a resource management perspective. The current modeling structure has separate modules that can either keep track of lake dynamics on the stream network or route the streamflow for multiday travel times; however, it is not currently able to do both as part of the same simulation. By combining these processes, the conceptual model would become more representative of actual processes and may reduce biases noted in the current simulation. In addition, by simulating actual impacted flows and volumes of water stored in reservoirs instead of just unregulated flows, future simulations may better inform resource managers about impacts of possible changes to operations on hydrology. This next step could be accomplished through development of a new module within the existing modeling structure or coupling the model with another modeling platform.

Groundwater Flow

Surface, subsurface, and groundwater flow components were computed for each HRU and were routed to adjacent stream segments in the network. The PRMS model used the Muskingum routing method to route streamflow throughout the stream network. This routing scheme for the flow components was based on DEM-based topography in the basin. This method did not consider regional groundwater flowpaths within the basin or from adjacent basins. Existing routing modules within PRMS, as discussed in Viger and others (2010), can account for flows traveling between HRUs before entering the stream network but may not be appropriate for the scale of the current model units. There are also ways of maintaining minimum flows during extended low flow periods by using thresholds. Because this model was developed to run future simulations, however, a constraint or threshold on minimum flows may hinder the ability of the model to account for possible future decreases in low flows compared to current conditions. It would be useful to develop new modules or enhance existing modules of PRMS to better account for groundwater flows independent of topography and across basin boundaries without exponentially increasing modeling effort or coupling with other models.

Automated Model Calibration

The Luca software (Hay and Umemoto, 2006) was developed to automate the calibration of a PRMS model with one streamflow gage. This application of PRMS had 35 calibration streamflow gages, requiring redevelopment of the calibration methodology. Beginning with the headwater subbasins, and moving downstream in a stepwise manner, the 35 subbasins were calibrated throughout the ACFB. As each of the 35 subbasins was calibrated, the subbasins upstream of the next location were not recalibrated, but instead those parameters were held constant to preserve the previous calibrations. Much of this preservation of previous calibrations was done manually for this study, which is both time consuming and prone to errors. A software application to automate the building of progressively bigger PRMS models as the calibration moves downstream, informing the Luca software about which HRUs to calibrate, would be a very effective tool for calibrating basins with multiple streamgages.

Summary

As part of the U.S. Geological Survey (USGS) National Climate Change and Wildlife Science Center's effort to provide integrated science that is useful to resource managers for understanding the impact of climate change on a range of ecosystem responses, a hydrologic model of the Apalachicola–Chattahoochee–Flint River Basin (ACFB) has been developed. The hydrologic model was developed as part of the Southeast Regional Assessment Project (SERAP) using the Precipitation Runoff Modeling System (PRMS), a deterministic, distributed-parameter, process-based system that simulates the effects of precipitation, temperature, and land use on basin hydrology.

The ACFB PRMS model simulates streamflow throughout most of the approximately 50,700-square-kilometer basin on a daily time step for the period 1950–99 using gridded forcings of air temperature and precipitation, and parameters derived from spatial data layers of altitude, land cover, soils, surficial geology, depression storage (small water bodies), and data from 56 USGS streamgages. Of the 56 streamgages used, 35 were used as calibration locations, 5 were used as flow replacement locations, with the remaining 16 used only for model delineation. The model matched the measured daily streamflow at 31 of the 35 calibration gages with a Nash-Sutcliffe Model Efficiency Index (NS) greater than 0.6; the remaining 4 gages matched with NS values ranging from 0.46 to 0.59. Three of these four gages drain urbanized subbasins and the fourth gage is in a subbasin that is not as developed but has a substantial streamflow diversion in its watershed.

Simulated flow matched measured streamflow reasonably well throughout most of the ACFB, especially for the larger subbasins. Simulations were less than optimal for smaller, more developed subbasins and in subbasins located in the southern part of the ACFB where the Floridan aquifer system crops out. Static parameters describing land cover limited the ability of the simulation to match historical runoff in the more developed subbasins. The Floridan aquifer system outcrop area posed challenges for the simulation of extended periods of low flows. A consistent underestimation of peak storm streamflow was observed as a result of the smoothing process used in the development of the gridded precipitation data. In general, storm hydrographs simulated using the gridded data began earlier and peaked lower than simulations using station data. Although other climate forcings could have been used to better simulate basin hydrology, this gridded product was selected because it provided coverage of the conterminous United States and a consistent framework for all major SERAP tasks.

Overall, the PRMS simulation of the ACFB provides a good representation of basin hydrology at annual and monthly time steps. The calibration subbasins were analyzed by separating the 35 subbasins into five classes based on physiography, land use, and stream type (tributary or mainstem). These five classes are Coastal Plain located in the Floridan aquifer system outcrop area (CF), Coastal Plain located outside of the Floridan aquifer system outcrop area (CR), Mainstem Apalachicola, Chattahoochee, and Flint Rivers (MS), Piedmont and Blue Ridge developed (PD), and Piedmont and Blue Ridge rural (PR). The lowest NS values were rarely below 0.6 whereas the median NS for all five classes ranged from 0.74 to 0.96 for annual mean streamflow, 0.89 to 0.98 for mean monthly streamflow, and 0.82 to 0.98 for monthly mean streamflow. The median bias for all five classes ranged from –4.3 to 0.8 percent for annual mean streamflow, –6.3 to 0.5 percent for mean monthly streamflow, and –9.3 to 1.3 percent for monthly mean streamflow. The NS results combined with the P_{bias} results indicate a good to very good streamflow volume simulation for all subbasins.

The analysis of the differences between simulated and measured flows in the basin revealed opportunities to further refine the modeling approach. Distributed parameter hydrologic models have historically been used to simulate relatively small watersheds. Moving into the realm of creating distributed parameter hydrologic models for larger basins and regional areas introduces new challenges that can only be addressed with further research and development. A new component, the **climate_hru** module, was developed for PRMS to deal with this increasing spatial scope. This module was developed to provide the PRMS with new functionality to use climate data distributed outside of PRMS. For this study, gridded climate data were transferred to the hydrologic response units using an area-weighted averaging algorithm, for each time step, for daily maximum and minimum temperature and precipitation using the USGS Geo Data Portal. Other data sources, such as weather stations or radar-based products, could also be used with this module. By preprocessing the climate forcings, model run times and calibration time can be substantially reduced, especially when dealing with larger watersheds.

This simulation of the ACFB provides a foundation upon which other models and future studies can be done. Simulated streamflow and other parts of the hydrologic cycle computed by PRMS can be used to inform other types of simulations; water temperature, hydrodynamic, and ecosystem dynamics simulations are three examples. In addition, possible future hydrologic conditions could be studied using this model in combination with land cover projections and downscaled general-circulation-model results.

Acknowledgments

The development of this model was supported through the USGS National Climate Change and Wildlife Science Center and the Department of Interior Southeast Climate Science Center. The authors thank all who contributed to this study. Anthony J. Gotvald and Richard A. Rebich provided thorough reviews and comments that improved the quality of this report. Jamie A. Painter provided geographic information system support.

References Cited

Albertson, P.N., and Torak, L.J., 2002, Simulated effects of groundwater pumpage on stream-aquifer flow in the vicinity of federally protected species of freshwater mussels in the lower Apalachicola–Chattahoochee–Flint River Basin (Subarea 4), southeastern Alabama, northwestern Florida, and southwestern Georgia: U.S. Geological Survey Water-Resources Investigations Report 02–4016, 23 p.

Blodgett, D.L., Booth, N.L., Kunicki, T.C., Walker, J.I., and Viger, R.J., 2011, Description and testing of the Geo Data Portal: A data integration framework and web processing services for environmental science collaboration: U.S. Geological Survey Open-File Report 2011–1157, 9 p.

Chapman, M.J., and Peck, M.F., 1997a, Groundwater resources of the Middle Chattahoochee River Basin in Georgia and Alabama, and upper Flint River Basin in Georgia—Subarea 2 of the Apalachicola–Chattahoochee–Flint and Alabama–Coosa–Tallapoosa River Basins: U.S. Geological Survey Open-File Report 96–492, 48 p.

Chapman, M.J., and Peck, M.F., 1997b, Groundwater resources of the Upper Chattahoochee River Basin in Georgia and Subarea 1 of the Apalachicola–Chattahoochee–Flint and Alabama–Coosa–Tallapoosa River Basins: U.S. Geological Survey Open-File Report 96–363, 43 p.

Couch, C.A., Hopkins, E.H., and Hardy, S.P., 1995, Influences of environmental settings on aquatic ecosystems in the Apalachicola–Chattahoochee–Flint River Basin: U.S. Geological Survey Water-Resources Investigations Report 95–4278, 58 p.

Dalton, M.S., and Jones, S.A., comps., 2010, Southeast Regional Assessment Project for the National Climate Change and Wildlife Science Center, U.S. Geological Survey: U.S. Geological Survey Open-File Report 2010–1213, 38 p.

Daly, C., Neilson, R.P., and Phillips, D.L., 1994, A statistical-topographic model for mapping climatological precipitation over mountainous terrain: Journal of Applied Meteorology, v. 33, no. 2, p. 140–158.

Daly, C., Taylor, G.H., and Gibson, W.P., 1997, The PRISM approach to mapping precipitation and temperature: Preprints, 10th Conference on Applied Climatology, Reno, Nev., American Meteorological Society, p. 10–12.

Duan, Q.Y., Gupta, V.K., and Sorooshian, Soroosh, 1993, Shuffled complex evolution approach for effective and efficient global minimization: Journal of Optimization Theory and Applications, v. 76, no. 3, p. 501–521.

Duan, Q.Y., Sorooshian, S., and Gupta, V., 1992, Effective and efficient global optimization for conceptual rainfall-runoff models: Water Resources Research, v. 28, no. 4, p. 1015–1031.

Duan, Q.Y., Sorooshian, S., and Gupta, V.K., 1994, Optimal use of the SCE-UA Global Optimization Method for calibrating watershed models: Journal of Hydrology, v. 158, no. 3–4, p. 265–284.

Fanning, J.L., and Trent, V.P., 2009, Water use in Georgia by county for 2005; and water-use trends, 1980–2005: U.S. Geological Survey Scientific Investigations Report 2009–5002, 186 p.

Farnsworth, R.K., and Thompson, E.S., 1982, Mean monthly, seasonal, and annual pan evaporation for the United States: National Oceanic and Atmospheric Administration Technical Report, NWS 34, 82 p.

Frick, E.A., Buell, G.R., and Hopkins, E.H., 1996, Nutrient sources and analysis of nutrient water-quality data, Apalachicola–Chattahoochee–Flint River basin, Georgia, Alabama, and Florida, 1972–90: U.S. Geological Survey Water-Resources Investigations Report 96–4101, 120 p.

Frick, E.A., Hippe, D.J., Buell, G.R., Couch, C.A., Hopkins, E.H., Wangsness, D.J., and Garrett, J.W., 1998, Water quality in the Apalachicola–Chattahoochee–Flint River basin, Georgia, Alabama, and Florida, 1992–95: U.S. Geological Survey Circular 1164, 38 p.

Georgakakos, A.P., and Yao, H., 2000, Climate change impacts on southeastern U.S. basins: U.S. Geological Survey Open-File Report 00–334, 72 p.

Gesch, D.B., ed., 2007, The National Elevation Dataset (2d ed.): Bethesda, Maryland, American Society for Photogrammetry and Remote Sensing, p. 99–118.

Gibson, C.A., Meyer, J.L., Poff, N.L., Hay, L.E., and Georgakakos, A.P., 2004, Flow regime alterations under changing climate in two river basins: Implications for freshwater ecosystems: River Research and Applications, v. 21, p. 849–864.

Gleeson, T., Smith, L., Moosdorf, N., Hartmann, J., Durr, H.H., Manning, A.H., van Beek, L.P.H., and Jellinek, A.M., 2011, Mapping permeability over the surface of the Earth: Geophysical Research Letters, v. 38, L. 02401, 6 p.

Gray, D.M., 1973, Handbook on the principles of hydrology: Water Information Center, Inc.

Hay, L.E., Leavesley, G.H., Clark, M.P., Markstrom, S.L., Viger, R.J., and Umemoto, M., 2006, Step wise, multiple objective calibration of a hydrologic model for a snowmelt dominated basin: Journal of the American Water Resources Association, v. 42, no. 4, p. 877–890.

Hay, L.E., Markstrom, S.L., Ward-Garrison, C., 2011, Watershed-scale response to climate change through the 21st century for selected basins across the United States: Earth Interactions, v. 15, no. 17, 37 p.

Hay, L.E., and Umemoto, M., 2006, Multiple-objective stepwise calibration using Luca: U.S. Geological Survey Open-File Report 2006–1323, 28 p.

Homer, C., Dewitz, J., Fry, J., Coan, M., Hossain, N., Larson, C., Herold, N., McKerrow, A., VanDriel, J.N., and Wickham, J., 2007, Completion of the 2001 National Land Cover Database for the conterminous United States: Photogrammetric Engineering & Remote Sensing, v. 73, no. 4, p. 337–341.

Horton, R.E., 1945, Erosional development of streams and their drainage basins; hydrophysical approach to quantitative morphology: Bulletin of the Geological Society of America, v. 56, p. 275–370.

Hummel, P.R., Kittle, J.L., Duda, P.B., and Patwardhan, A., 2003, Calibration of a watershed model for metropolitan Atlanta: CH2M Hill report, 27 p.

Jain, S.K., and Sudheer, K.P., 2008, Fitting of hydrologic models: A close look at the Nash-Sutcliffe Index: Journal of Hydrologic Engineering, v. 13, no. 10, p. 981–986.

Jones, L.E., and Torak, L.J., 2006, Simulated effects of seasonal ground-water pumpage for irrigation on hydrologic conditions in the lower Apalachicola–Chattahoochee–Flint River Basin, southwestern Georgia and parts of Alabama and Florida, 1999–2002: U.S. Geological Survey Scientific Investigations Report 2006–5234, 106 p.

Leavesley, G.H., Lichty, R.W., Troutman, B.M., and Saindon, L.G., 1983, Precipitation-runoff modeling system—User's manual: U.S. Geological Survey Water-Resources Investigations Report 83–4238, 207 p.

Leitman, S., Dowd, J., and Holmbeck-Pelham, S., 2003, An evaluation of observed and unimpaired flow and precipitation during drought events in the ACF Basin: Proceedings of the 2003 Georgia Water Resources Conference, April 23–24, 2003, University of Georgia, 4 p.

Light, H.M., Darst, M.R., and Grubbs, J.W., 1998, Aquatic habitats in relation to river flow in the Apalachicola River floodplain, Florida: U.S. Geological Survey Professional Paper, 1594, 77 p.

Loh, W.Y., 2008, Classification and regression tree methods, *in* Ruggeri, Kenett and Faltin eds., Encyclopedia of Statistics in Quality and Reliability: New York, Wiley.

Mannshardt-Shamseldin, E.C., Smith, R.L., Sain, S.R., Mearns, L.O., and Cooley, D., 2010, Downscaling extremes: A comparison of extreme value distributions in point-source and gridded precipitation data: The Annals of Applied Statistics, v. 4, no. 1, p. 484–502.

Markstrom, S.L., Hay, L.E., Ward-Garrison, C.D., Risley, J.C., Battaglin, W.A., Bjerklie, D.M., Chase, K.J., Christiansen, D.E., Dudley, R.W., Hunt, R.J., Koczot, K.M., Mastin, M.C., Regan, R.S., Viger, R.J., Vining, K.C., and Walker, J.F., 2012, Integrated watershed-scale response to climate change for selected basins across the United States: U.S. Geological Survey Scientific Investigations Report 2011–5077, 143 p.

Markstrom, S.L., Niswonger, R.G., Regan, R.S., Prudic, D.E., and Barlow, P.M., 2008, GSFLOW—Coupled groundwater and surface-water flow model based on the integration of the Precipitation-Runoff Modeling System (PRMS) and the Modular Ground-Water Flow Model (MODFLOW–2005): U.S. Geological Survey Techniques and Methods, book 6, chap. D1, 240 p.

Mastin, M.C., and Vaccaro, J.J., 2002, Documentation of Precipitation-Runoff Modeling System modules for the Modular Modeling System modified for the Watershed and River Systems Management Program: U.S. Geological Survey Open-File Report 02–362. (Also available at *http://pubs.usgs.gov/of/2002/ofr02362/*.)

Maurer, E.P., Wood, A.W., Adam, J.C., Lettenmaier, D.P., and Nijssen, B., 2002, A long-term hydrologically-based data set of land surface fluxes for the conterminous United States: Journal of Climate, v. 15, no. 22, p. 3237–3251.

Mayer, G.C., 1997, Groundwater resources of the Lower-Middle Chattahoochee River Basin in Georgia and Alabama, and Middle Flint River Basin in Georgia—Subarea 3 of the Apalachicola-Chattahoochee-Flint and Alabama-Coosa-Tallapoosa River Basins: U.S. Geological Survey Open-File Report 96–483, 47 p.

McCuen, R.H., Knight, Z., and Cutter, A.G., 2006, Evaluation of the Nash-Sutcliffe Efficiency Index: Journal of Hydrologic Engineering, November/December 2006, p. 597–602.

Miller, D., 2008, Programs for DEM analysis: Earth Systems Institute, p. 20.

Moriasi, D.N., Arnold, J.G., Van Liew, M.W., Bingner, R.L., Harmel, R.D., Veith, T.L., 2007, Model evaluation guidelines for systematic quantification of accuracy in watershed simulations: American Society of Agricultural and Biological Engineers, v. 50, no. 3, p. 885–900.

Mosner, M.S., 2002, Stream-aquifer relations and the potentiometric surface of the Upper Floridan aquifer in the Lower Apalachicola-Chattahoochee-Flint River Basin in parts of Georgia, Florida, and Alabama, 1999–2000: U.S. Geological Survey Water-Resources Investigations Report 02–4244, 45 p.

National Aeronautics and Space Administration, [n.d.], The Worldwide Reference System: Accessed March 8, 2011, at *http://landsat.gsfc.nasa.gov/about/wrs.html*.

National Oceanic and Atmospheric Administration, 2009, National Weather Service Cooperative Observer Program: Accessed November 2009 at *http://www.nws.noaa.gov/om/coop*.

Nash, J.E., Sutcliffe, J.V., 1970, River flow forecasting through conceptual models part I—A discussion of principles: Journal of Hydrology, v. 10, no. 3, p. 282–290.

Peterson, J.T., Hay, L., Odom, K., Hughes, W.B., Jacobson, R.B., Jones, J., and Freeman, M., 2010, Multi-resolution assessment of potential climate change effects on biological resources: aquatic and hydrologic dynamics, *in* Dalton, M.S., and Jones, S.A., eds., Southeast Regional Assessment Project for the National Climate Change and Wildlife Science Center, U.S. Geological Survey: U.S. Geological Survey Open-File Report 2010–1213, p. 25–29.

Rugel, K., Romeis, J., Jackson, C.R., Golladay, S.W., Hicks, D.W., and Dowd, J.F., 2009, Use of historic data to evaluate effects of pumping stress on streams in southwest Georgia: Proceedings of the 2009 Georgia Water Resources Conference, April 27–29, 2009, University of Georgia, 4 p.

Rutledge, A.T., 1998, Computer programs for describing the recession of ground-water discharge and for estimating mean ground-water recharge and discharge from streamflow records—Update: U.S. Geological Survey Water-Resources Investigations Report 98–4148, 43 p.

Stoner, A.M.K., Hayhoe, K.A., Yang, X., and Wuebbles, D.J., 2012, An asynchronous regional regression model for statistical downscaling of daily climate variables: International Journal of Climatology. (Also available at *http://dx.doi.org/10.1002/joc.3603*.)

Tarboton, D.G., 1997, A new method for the determination of flow networks from digital elevation data: Water Resources Research, v. 33, no. 2, p. 309–319.

Torak, L.J., and McDowell, R.J., 1996, Groundwater resources of the Lower Apalachicola–Chattahoochee–Flint River Basin in parts of Alabama, Florida, and Georgia—Subarea 4 of the Apalachicola–Chattahoochee–Flint and Alabama–Coosa–Tallapoosa River Basins: U.S. Geological Survey Open-File Report 95–321, 145 p.

U.S. Army Corps of Engineers, 1997, ACT/ACF comprehensive water resources study, Surface water availability, Volume I, Unimpaired flow: U.S. Army Corps of Engineers report, 96 p.

Viger, R.J., Hay, L.E., Jones, J.W., and Buell, G.R., 2010, Effects of including surface depressions in the application of the Precipitation-Runoff Modeling System in the Upper Flint River Basin, Georgia: U.S. Geological Survey Scientific-Investigations Report 2010–5062, 36 p.

Viger, R.J., Hay, L.E., Jones, J.W., and Buell, G.R., 2011, Hydrologic effects of urbanization and climate change on the Flint River Basin, Georgia: Earth Interactions, v. 15, no. 20, 25 p.

Viger, R.J., and Leavesley, G.H., 2007, The GIS Weasel user's manual: U.S. Geological Survey Techniques and Methods, book 6, chap. B4, 201 p., accessed October 1, 2010, at *http://pubs.usgs.gov/tm/2007/06B04/*.

Walker, J.F., Hay, L.E., Markstrom, S.L., Dettinger, M.D., 2011, Characterizing climate-change impacts on the 1.5-yr flood flow in selected basins across the United States: A probabilistic approach: Earth Interactions, v. 15, no. 18, 16 p.

Wangsness, D.J., 1997, The National Water-Quality Assessment Program—Example of study unit design for the Apalachicola–Chattahoochee–Flint River Basin in Georgia, Alabama, and Florida, 1991–97: U.S. Geological Survey Open-File Report 97–48, 29 p.

Ward-Garrison, Christian, Markstrom, S.L., and Hay, L.E., 2009, Downsizer—A graphical user interface-based application for browsing, acquiring, and formatting time-series data for hydrologic models: U.S. Geological Survey Open-File Report 2009–1166, 27 p.

Wen, Menghong, and Zhang, Yi, 2009, Agricultural water use estimation for the Flint River Basin Regional Water Development and Conservation Plan: Proceedings of the 2009 Georgia Water Resources Conference, April 27–29, 2009, University of Georgia, 4 p.

Wen, Menghong, Zhang, Yi, and Zeng, Wei, 2007, HSPF model of the streamflow simulation for the lower Flint River watershed: Proceedings of the 2007 Georgia Water Resources Conference, March 27–29, 2007, University of Georgia, 4 p.

Wolock, D.M., 2003, Base-flow index grid for the conterminous United States: U.S. Geological Survey Open-File Report 03–263, digital data set, available at *http://ks.water.usgs.gov/pubs/abstracts/of.03-263.htm*.

Yapo, P.O., Gupta, H.V., and Sorooshian, S., 1996, Automatic Calibration of Conceptual Rainfall-Runoff Models: Sensitivity to Calibration Data: Journal of Hydrology, v. 181, p. 23–48.

Zeng, Wei, Jiang, Feng, and Zhang, Yi, 2009, Reservoir management in the Apalachicola–Chattahoochee–Flint (ACF) River system under the Interim Operations Plan (IOP) during the ongoing drought: Proceedings of the 2009 Georgia Water Resources Conference, April 27–29, 2009, University of Georgia, 4 p.

Zeng, Wei, and Wen, Menghong, 2005, Constructing a hydrologic model of the Ichawaynochaway Creek watershed, *in* Hatcher, K.J., ed., Proceedings of 2005 Georgia Water Resources Conference, April 25–27, 2003, Athens, Ga., The University of Georgia, Institute of Ecology, 4 p.

Zhang, Yi, Hawkins, David, Zeng, Wei, and Wen, Menghong, 2005, The framework of GIS-based Decision Support Systems (DSS) for water resources management at the Flint River Basin, *in* Hatcher, K.J., ed., Proceedings of 2005 Georgia Water Resources Conference, April 25–27, 2003, Athens, Ga., The University of Georgia, Institute of Ecology, 4 p.

Zhang, Yi, and Wen, Menghong, 2005, Watershed modeling and calibration for Spring Creek sub-basin in the Flint River Basin using the EPA BASINS/HSPF Modeling Tool, *in* Hatcher, K.J., ed., Proceedings of 2005 Georgia Water Resources Conference, April 25–27, 2003, Athens, Ga., The University of Georgia, Institute of Ecology, 4 p.

Appendix 1. Plots of measured and simulated mean-monthly, monthly mean, and annual mean streamflow for calibration and evaluation periods for 35 subbasins of the Apalachicola–Chattahoochee–Flint River Basin

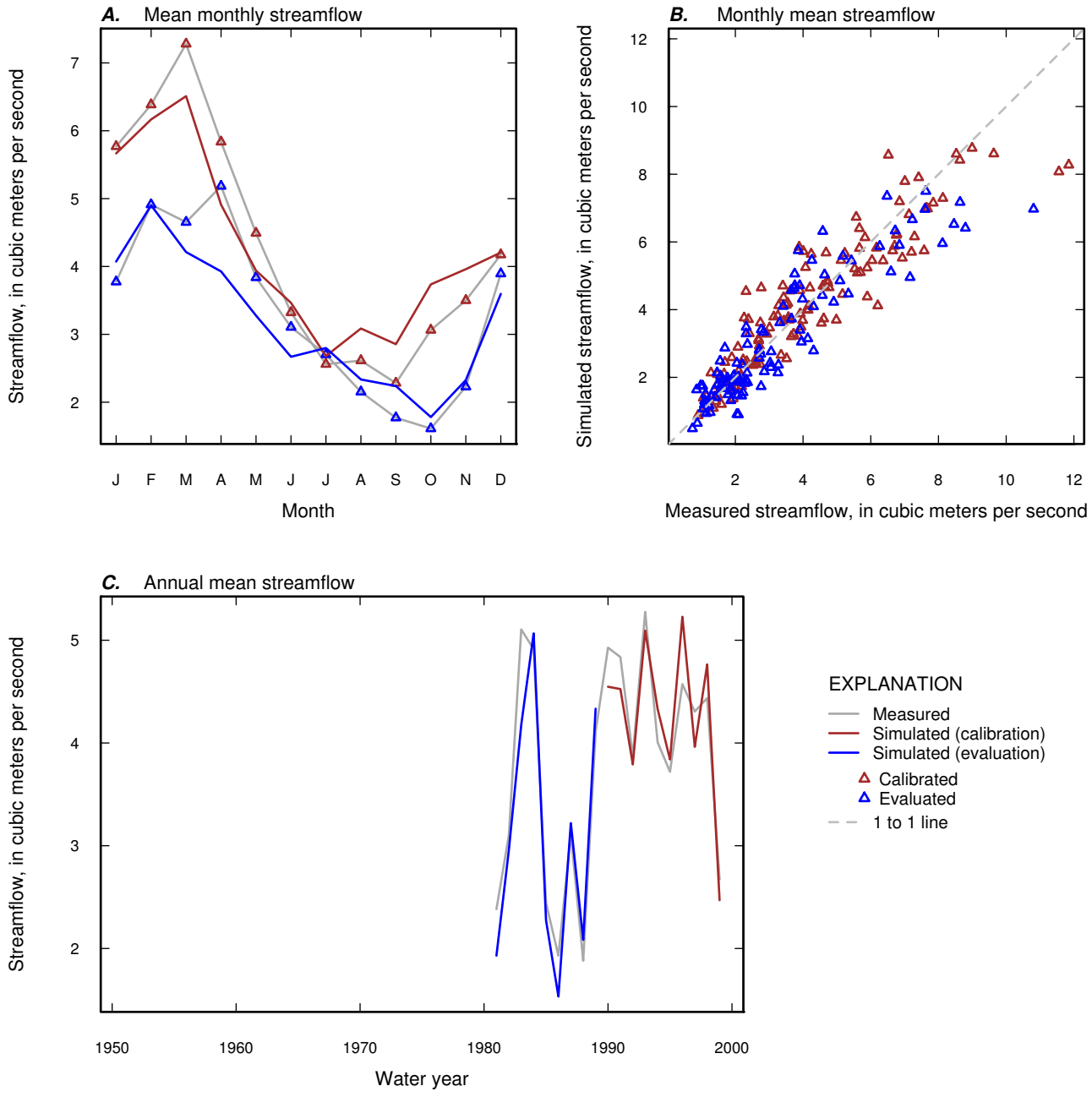

Figure 1–1. Measured and simulated mean-monthly, monthly mean, and annual mean streamflow for calibration and evaluation periods for USGS streamgage 02330450 (Chattahoochee River at Helen, GA).

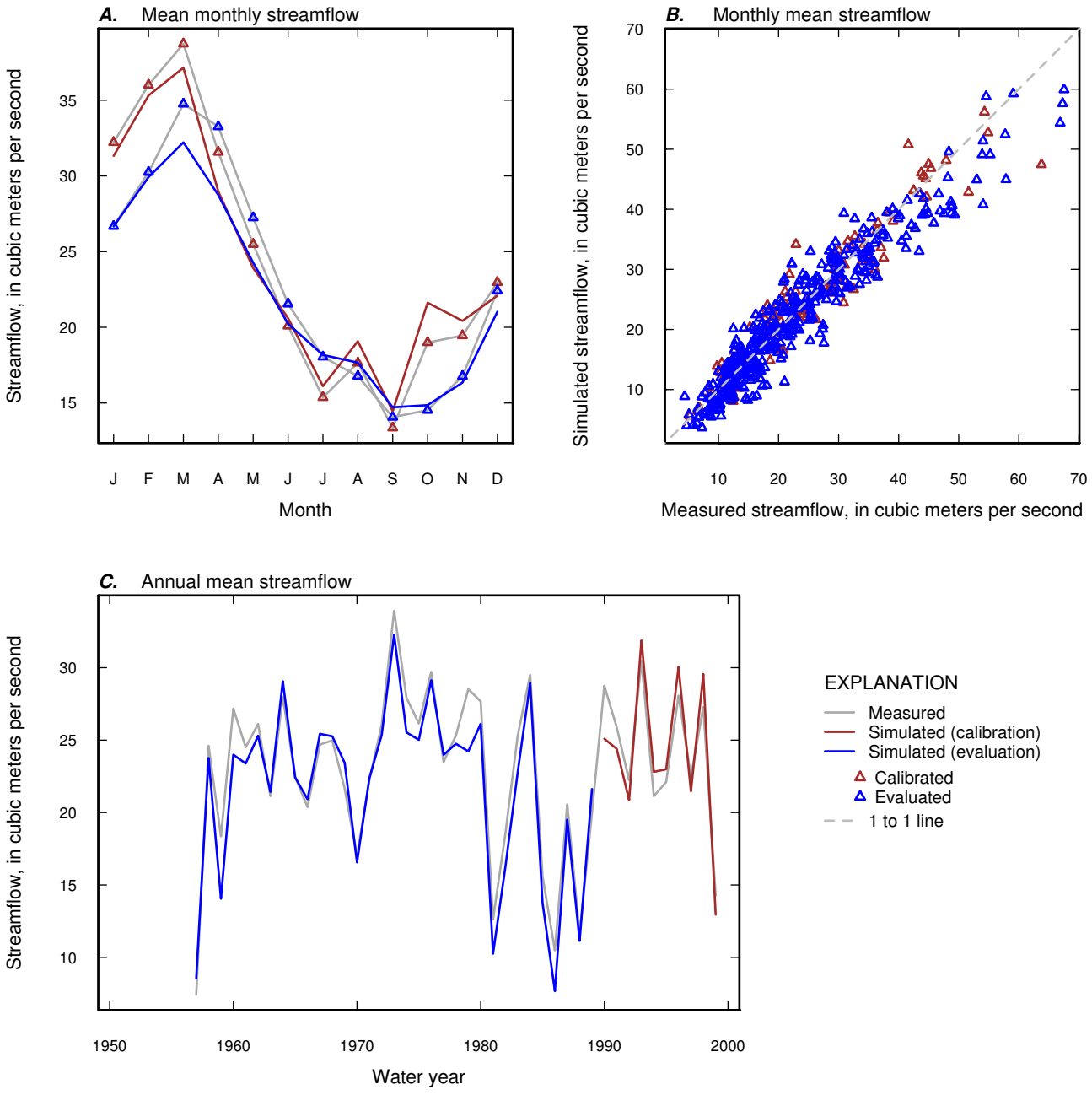

Figure 1–2. Measured and simulated mean-monthly, monthly mean, and annual mean streamflow for calibration and evaluation periods for USGS streamgage 02331600 (Chattahoochee River at Cornelia, GA).

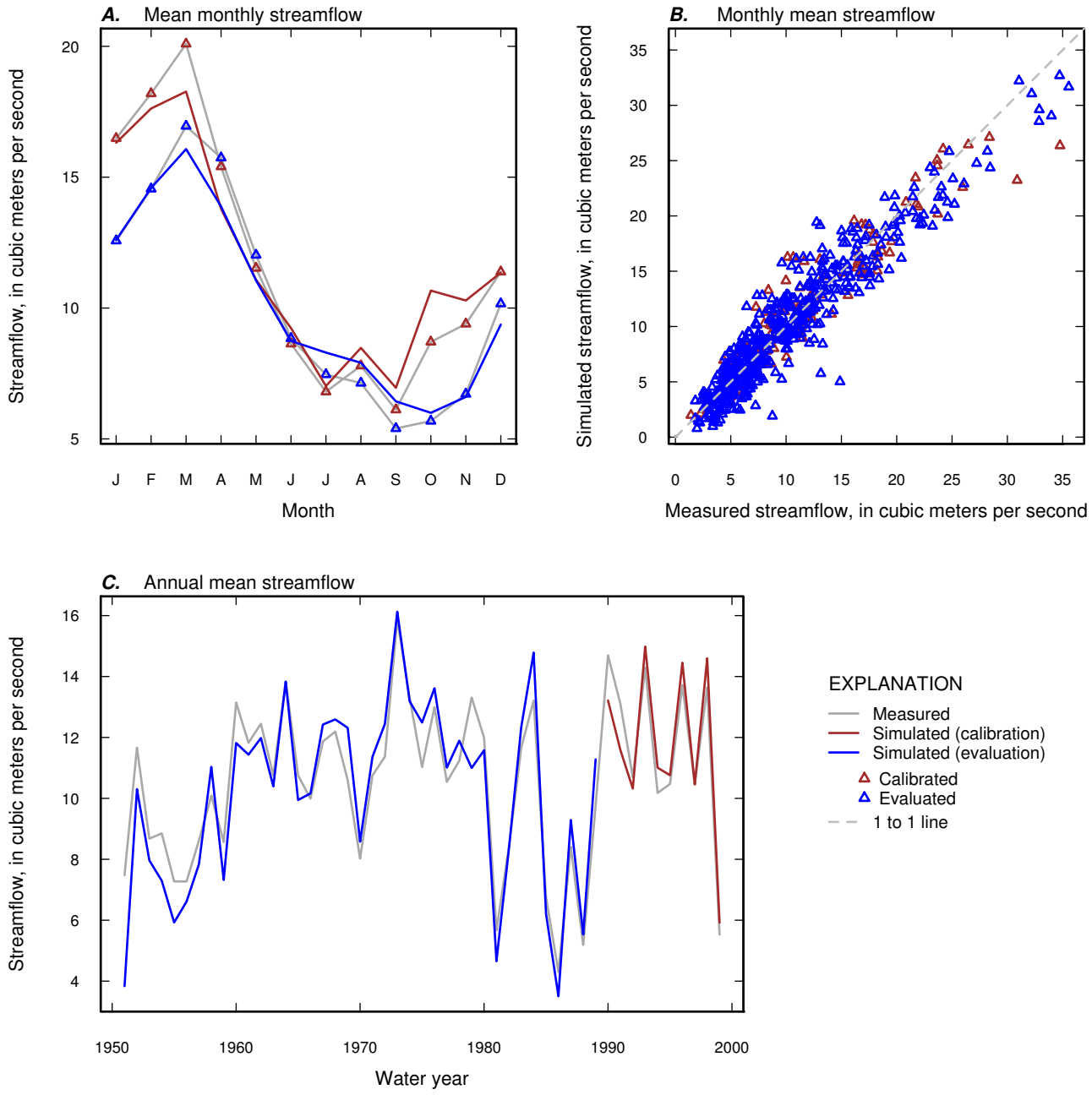

Figure 1–3. Measured and simulated mean-monthly, monthly mean, and annual mean streamflow for calibration and evaluation periods for USGS streamgage 02333500 (Chestatee River at Dahonlega, GA).

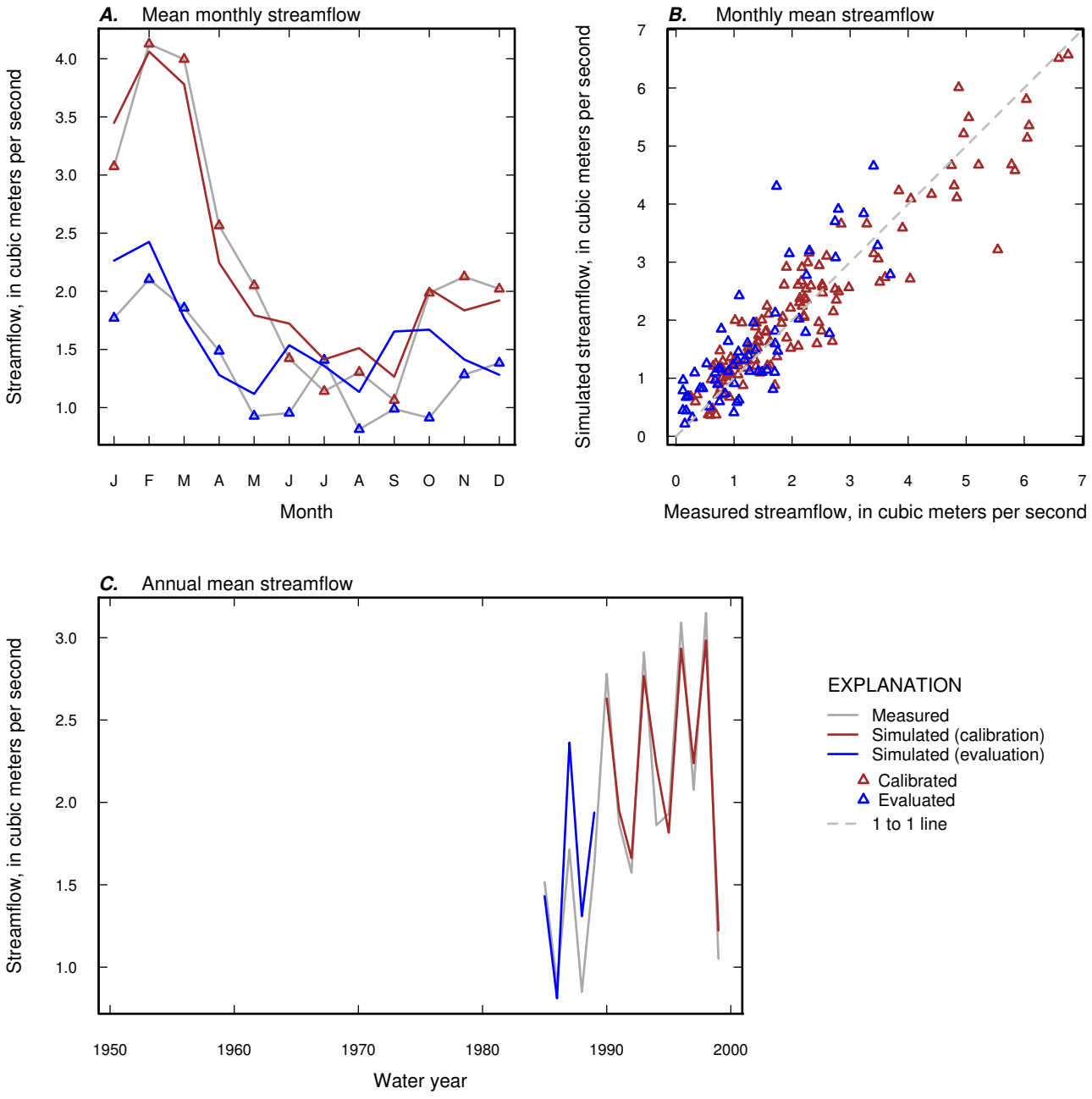

Figure 1–4. Measured and simulated mean-monthly, monthly mean, and annual mean streamflow for calibration and evaluation periods for USGS streamgage 02334885 (Suwanee Creek at Suwanee, GA).

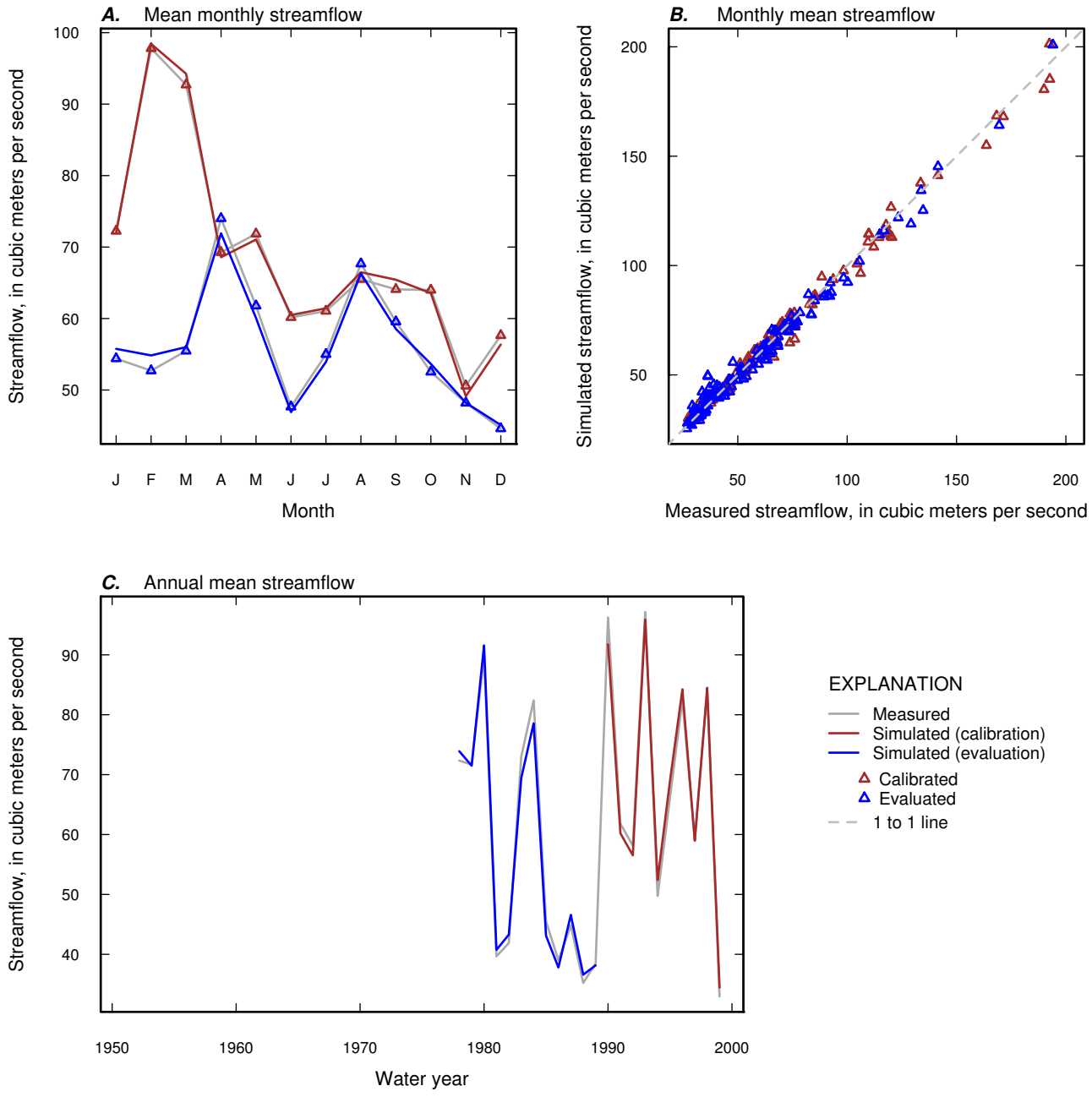

Figure 1–5. Measured and simulated mean-monthly, monthly mean, and annual mean streamflow for calibration and evaluation periods for USGS streamgage 02335000 (Chattahoochee River near Norcross, GA).

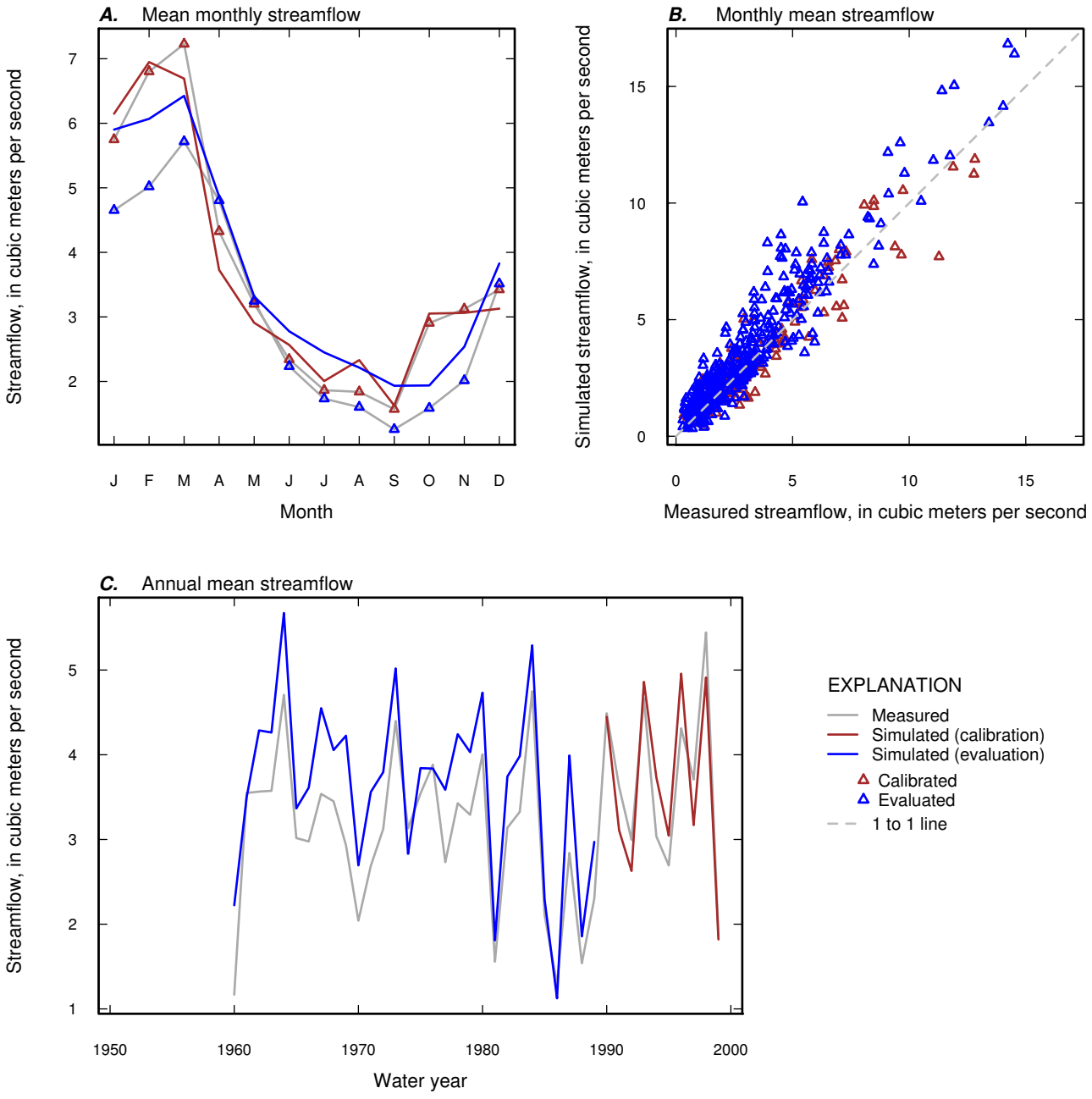

Figure 1–6. Measured and simulated mean-monthly, monthly mean, and annual mean streamflow for calibration and evaluation periods for USGS streamgage 02335700 (Big Creek near Alpharetta, GA).

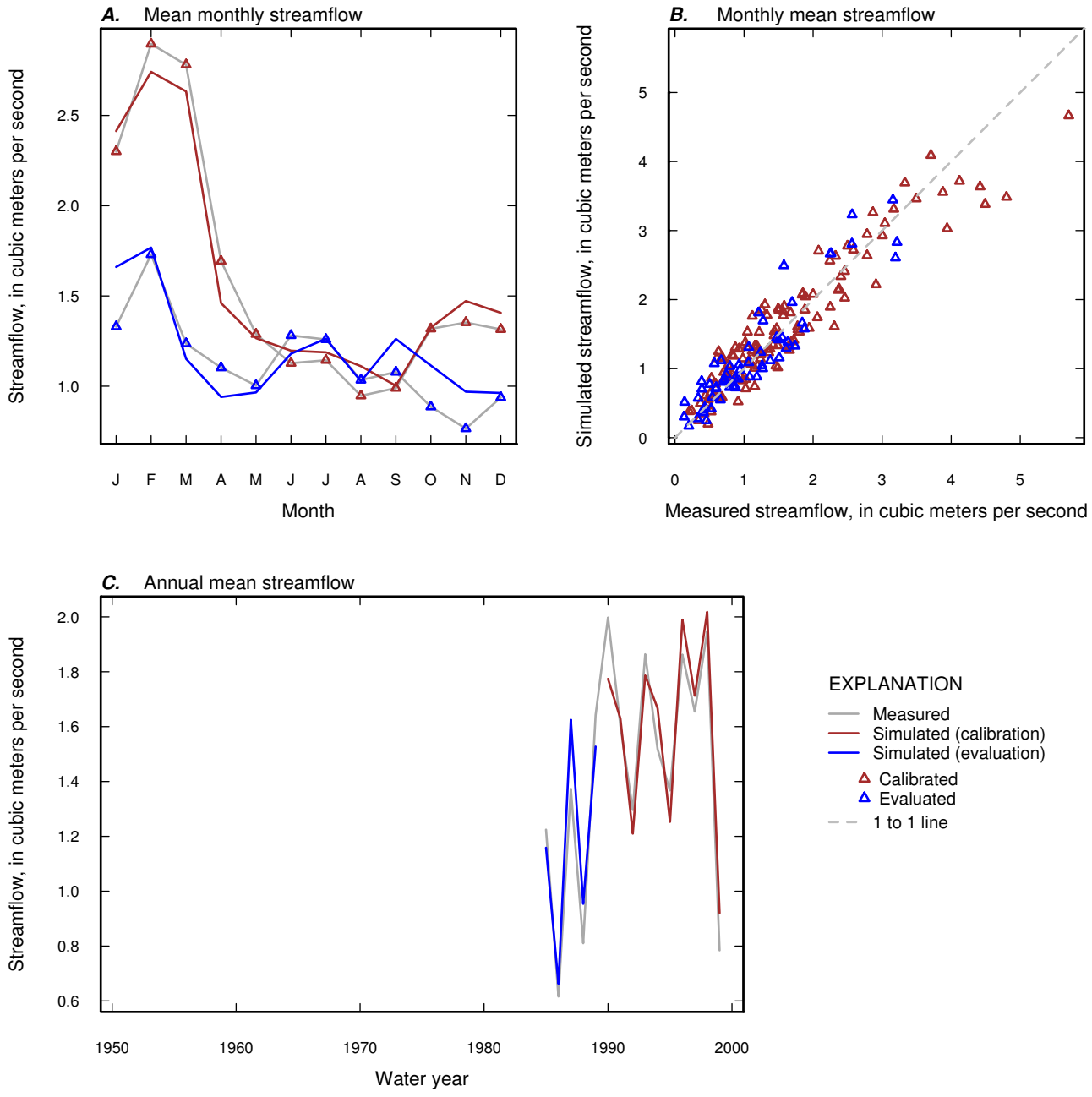

Figure 1–7. Measured and simulated mean-monthly, monthly mean, and annual mean streamflow for calibration and evaluation periods for USGS streamgage 02335870 (Sope Creek near Marietta, GA).

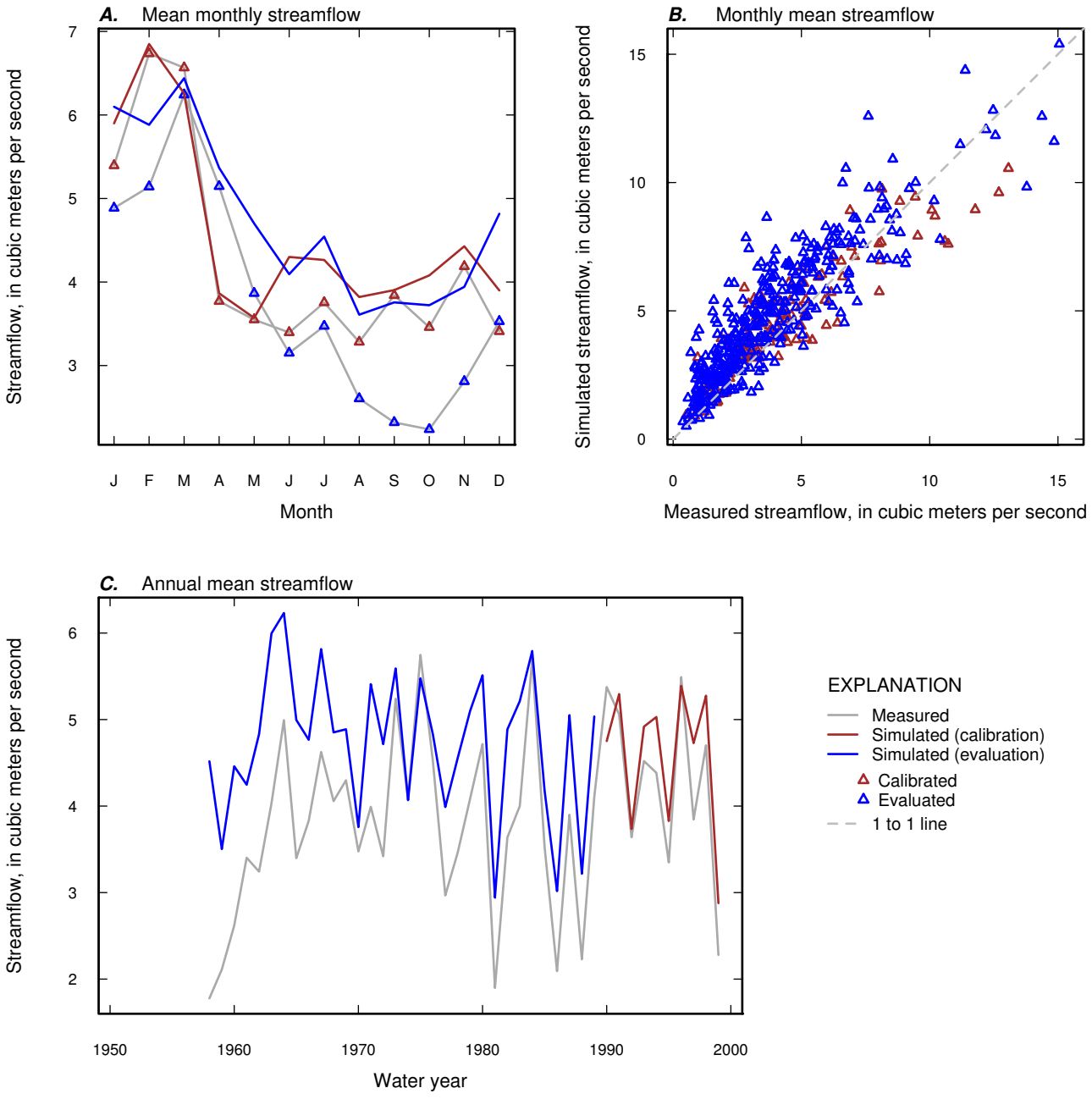

Figure 1–8. Measured and simulated mean-monthly, monthly mean, and annual mean streamflow for calibration and evaluation periods for USGS streamgage 02336300 (Peachtree Creek at Atlanta, GA).

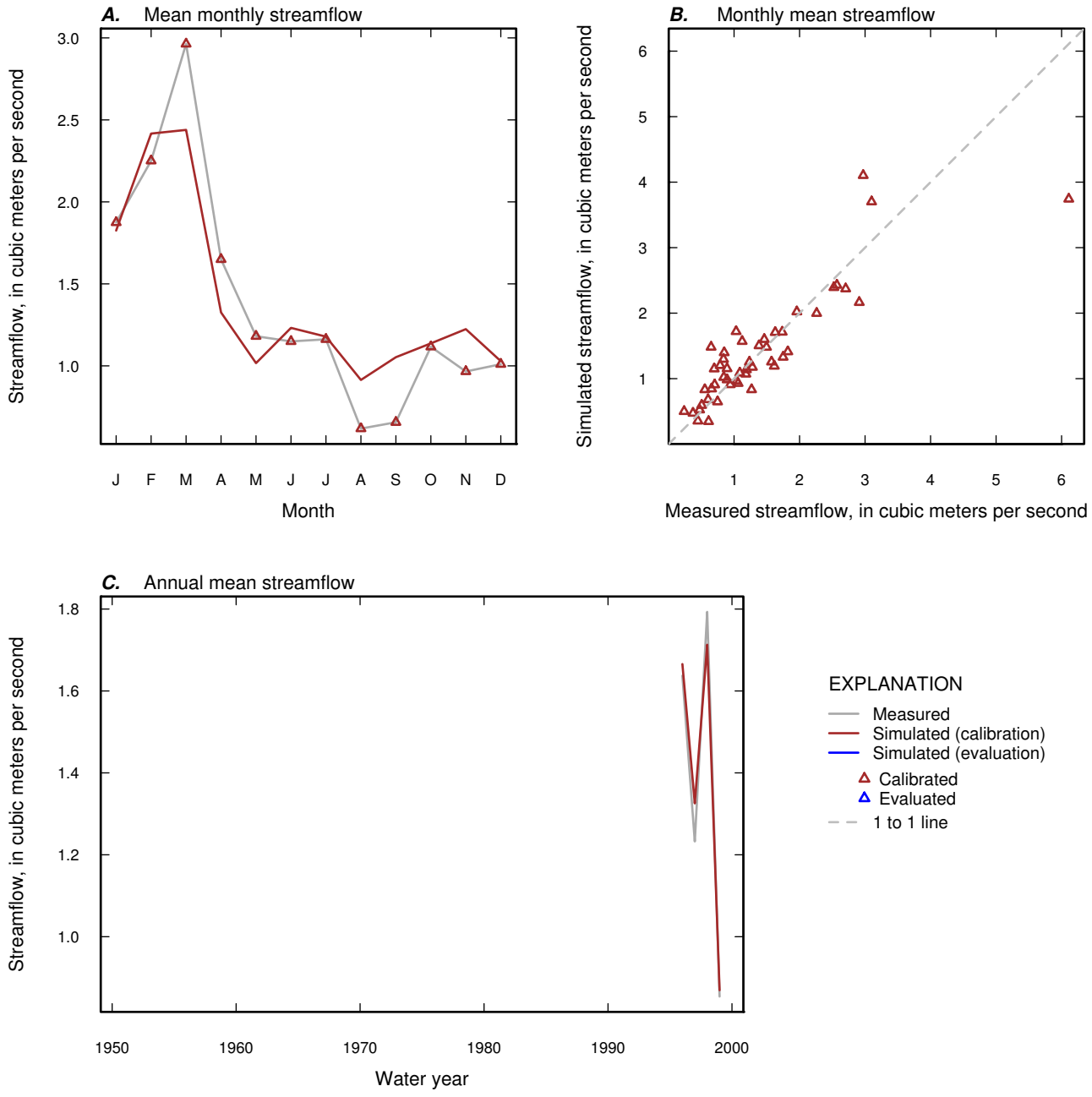

Figure 1–9. Measured and simulated mean-monthly, monthly mean, and annual mean streamflow for calibration and evaluation periods for USGS streamgage 02336635 (Nickajack Creek at US 78/278, near Mableton, GA).

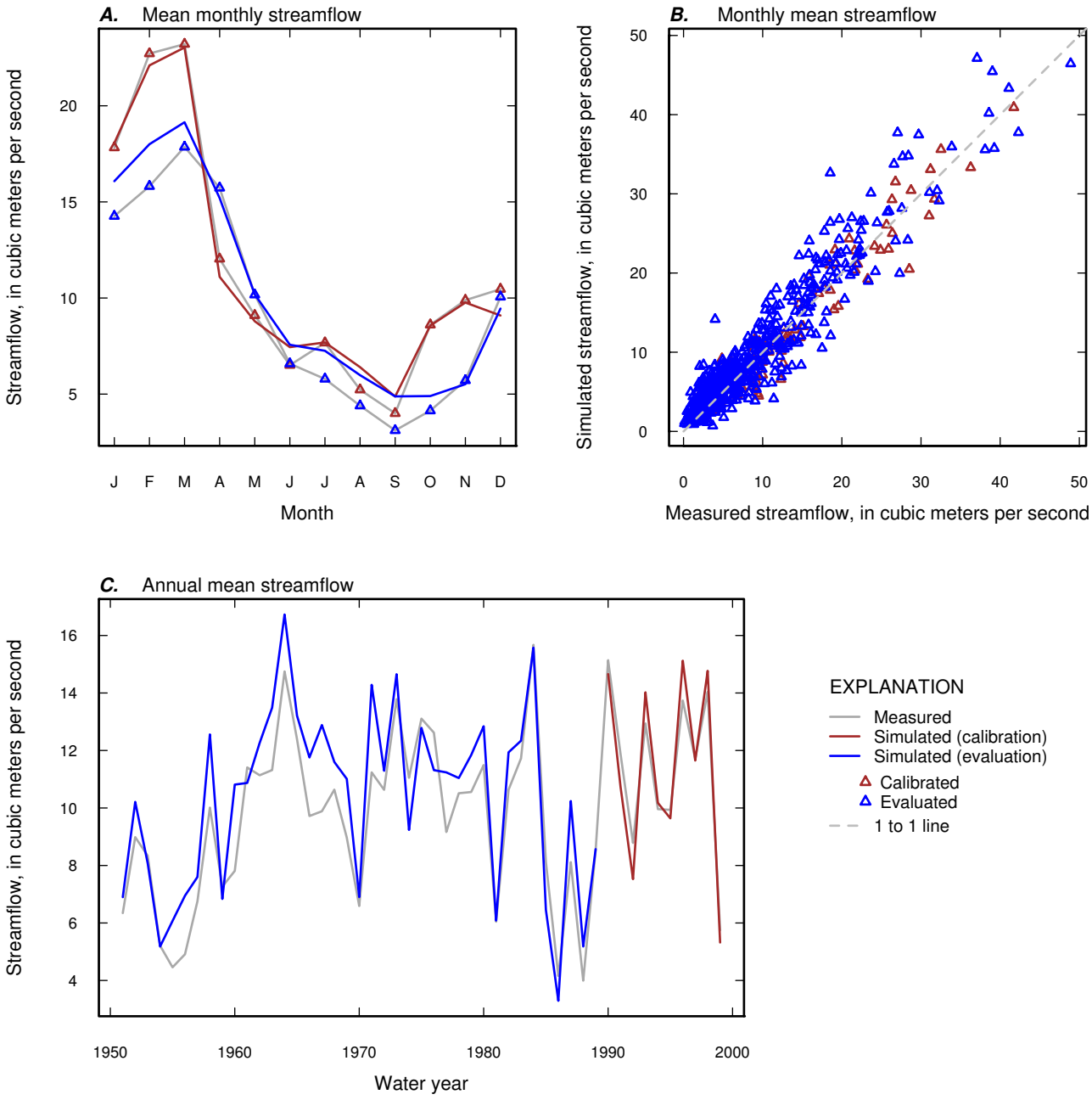

Figure 1–10. Measured and simulated mean-monthly, monthly mean, and annual mean streamflow for calibration and evaluation periods for USGS streamgage 02337000 (Sweetwater Creek near Austell, GA).

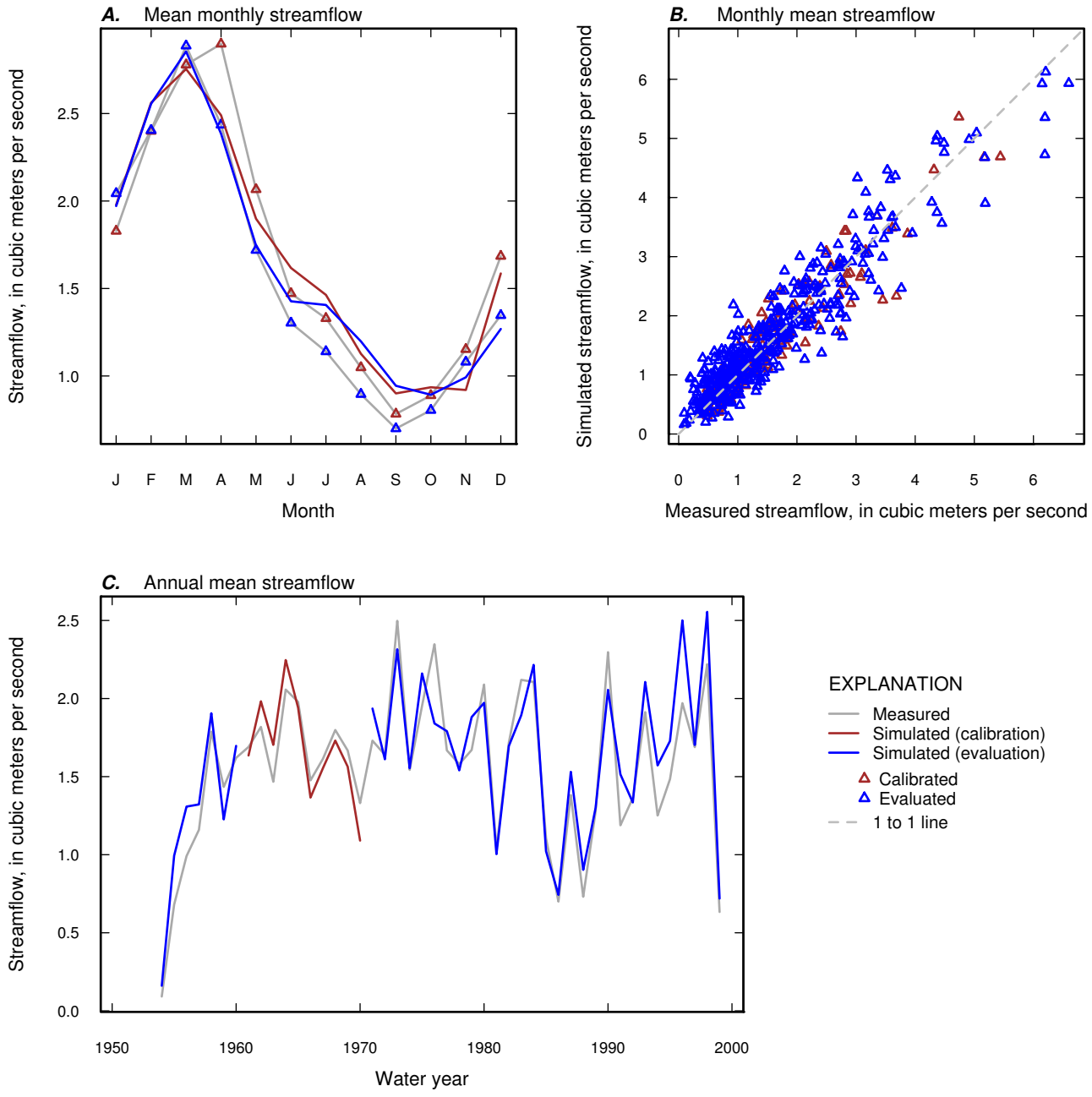

Figure 1–11. Measured and simulated mean-monthly, monthly mean, and annual mean streamflow for calibration and evaluation periods for USGS streamgage 02337500 (Snake Creek near Whitesburg, GA).

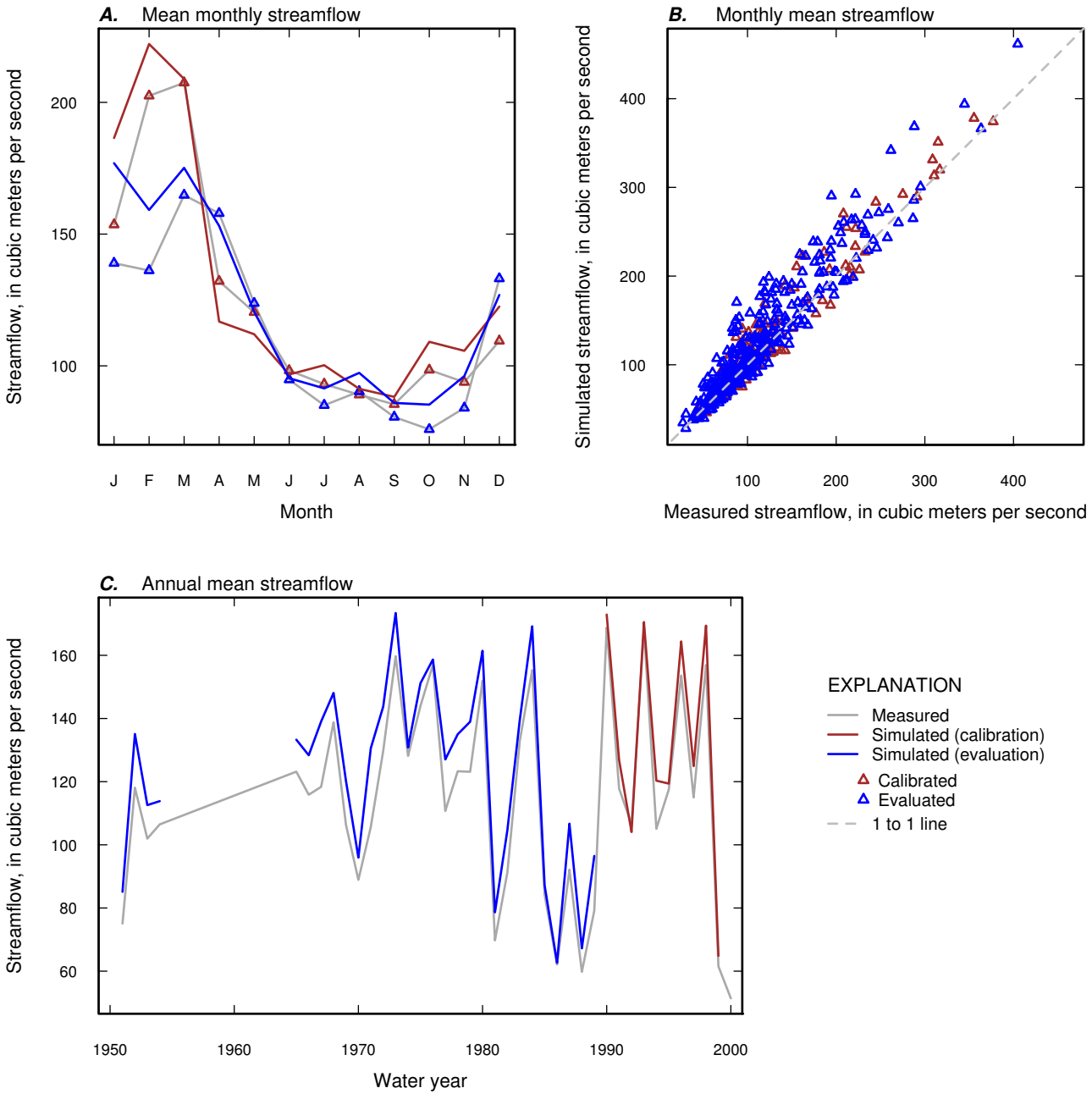

Figure 1–12. Measured and simulated mean-monthly, monthly mean, and annual mean streamflow for calibration and evaluation periods for USGS streamgage 02338000 (Chattahoochee River near Whitesburg, GA).

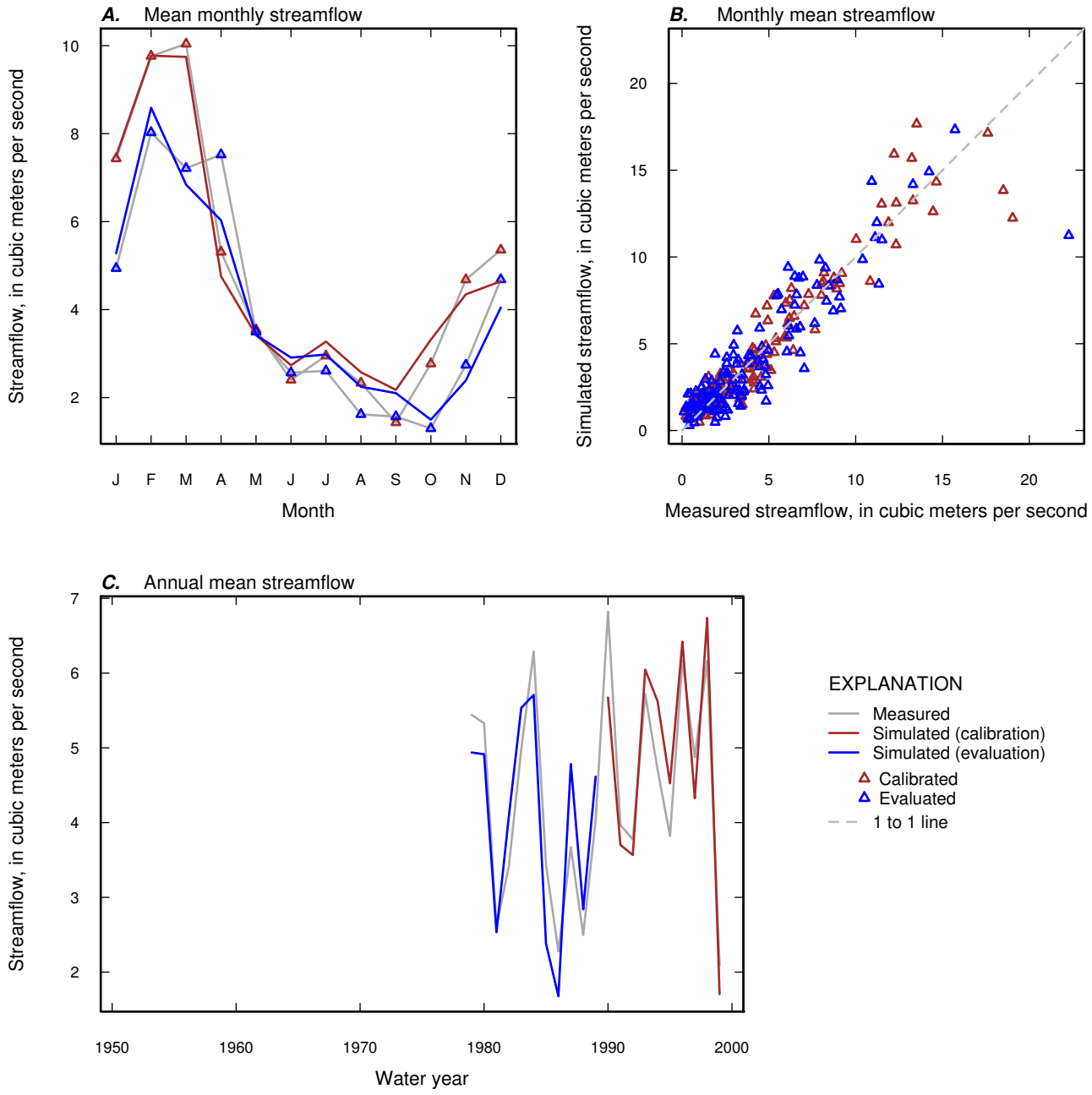

Figure 1–13. Measured and simulated mean-monthly, monthly mean, and annual mean streamflow for calibration and evaluation periods for USGS streamgage 02338660 (New River at GA 100, near Corinth, GA).

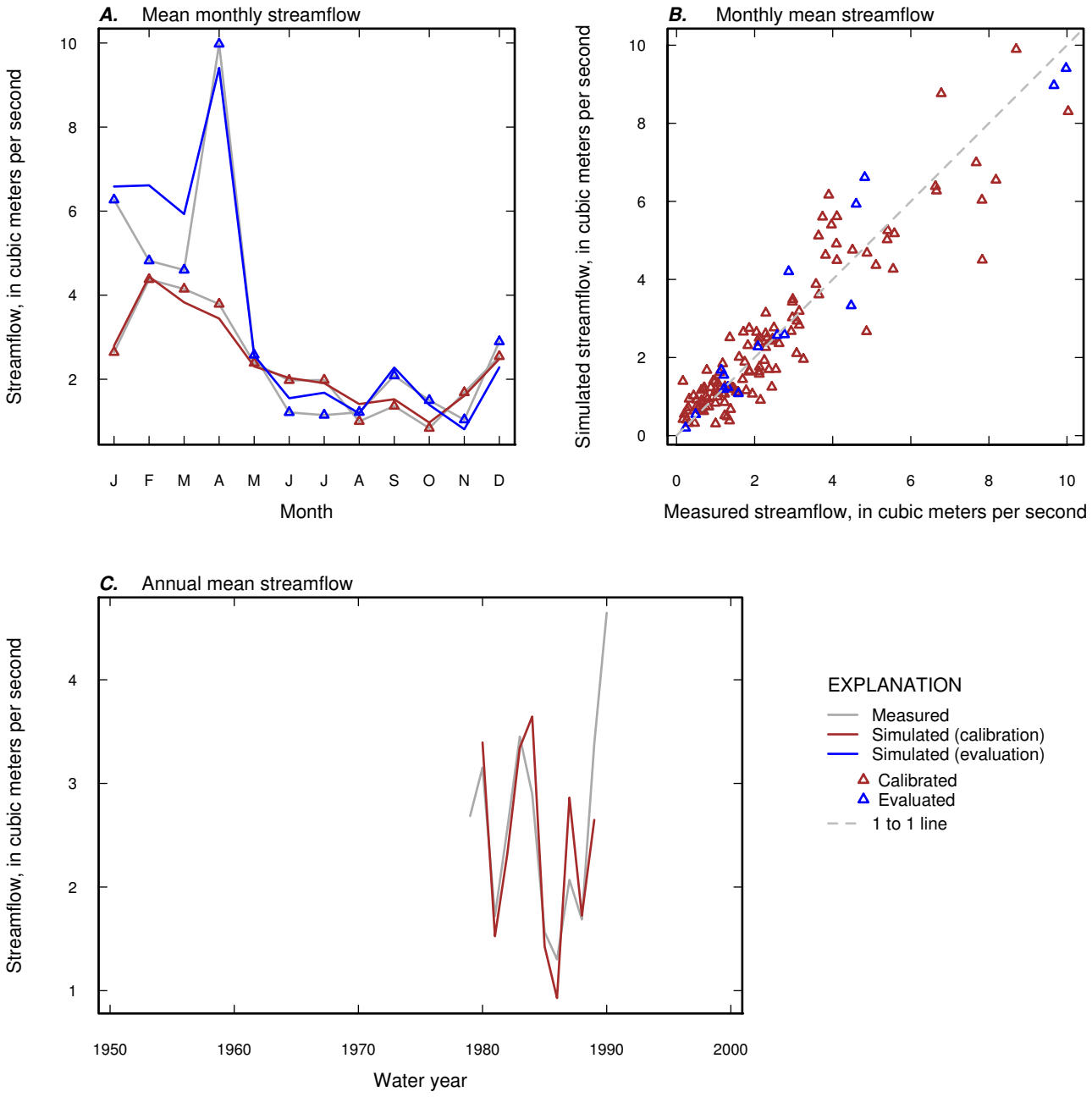

Figure 1–14. Measured and simulated mean-monthly, monthly mean, and annual mean streamflow for calibration and evaluation periods for USGS streamgage 02339225 (Wehadkee Creek below Rock Mills, AL).

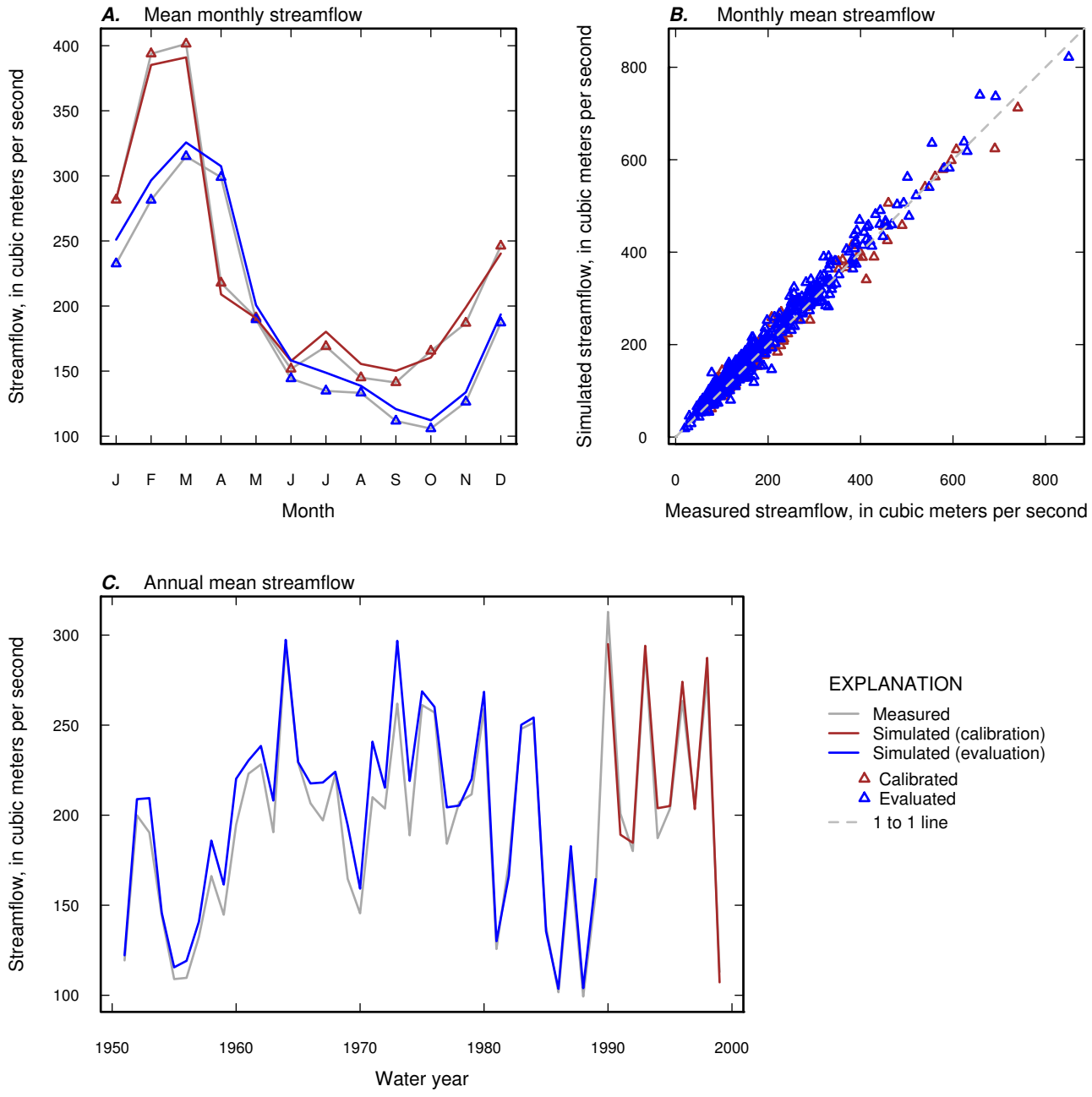

Figure 1–15. Measured and simulated mean-monthly, monthly mean, and annual mean streamflow for calibration and evaluation periods for USGS streamgage 02341505 (Chattahoochee River at US 280, near Columbus, GA).

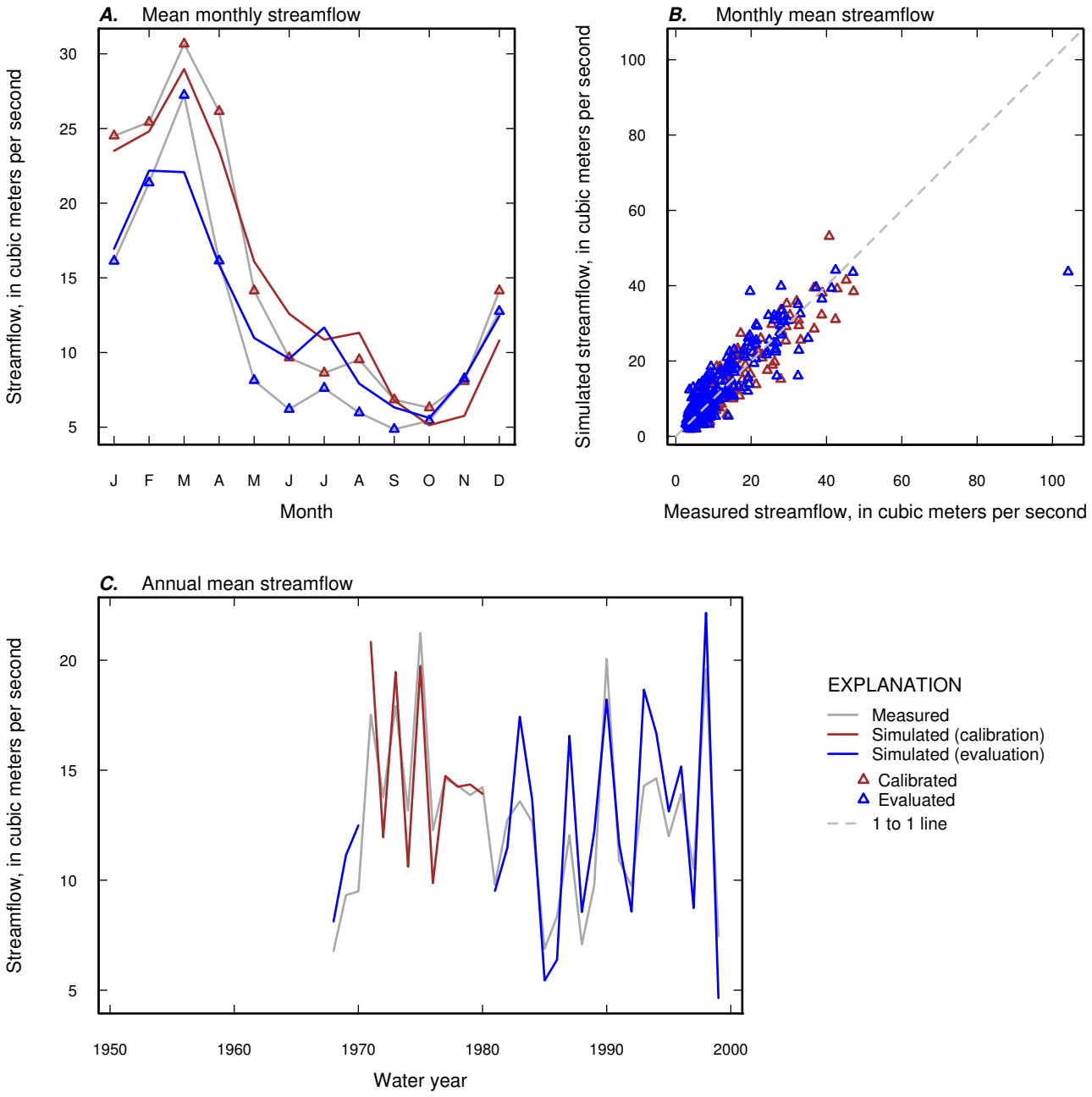

Figure 1–16. Measured and simulated mean-monthly, monthly mean, and annual mean streamflow for calibration and evaluation periods for USGS streamgage 02341800 (Upatoi Creek near Columbus, GA).

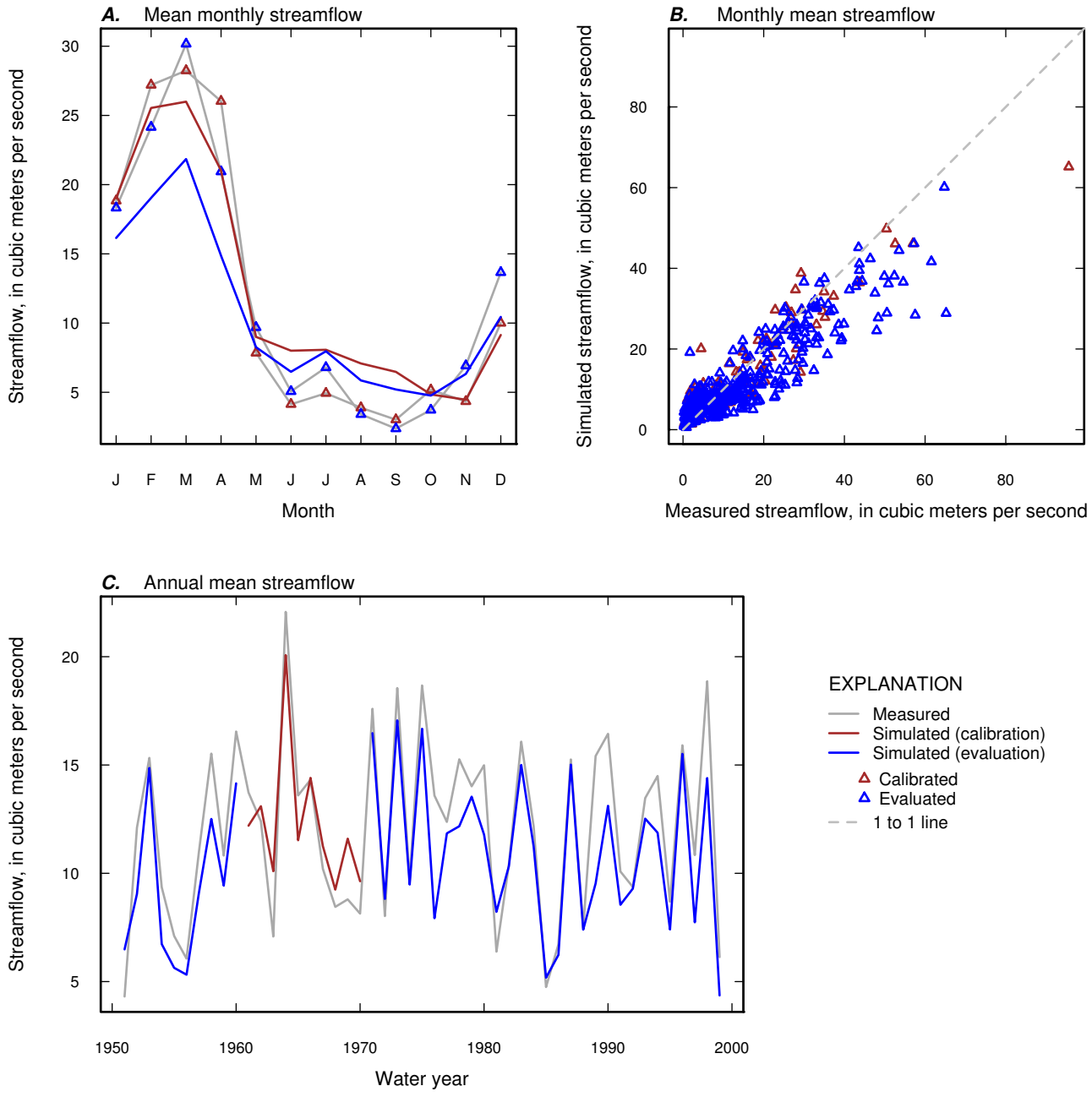

Figure 1–17. Measured and simulated mean-monthly, monthly mean, and annual mean streamflow for calibration and evaluation periods for USGS streamgage 02342500 (Uchee Creek near Fort Mitchell, AL).

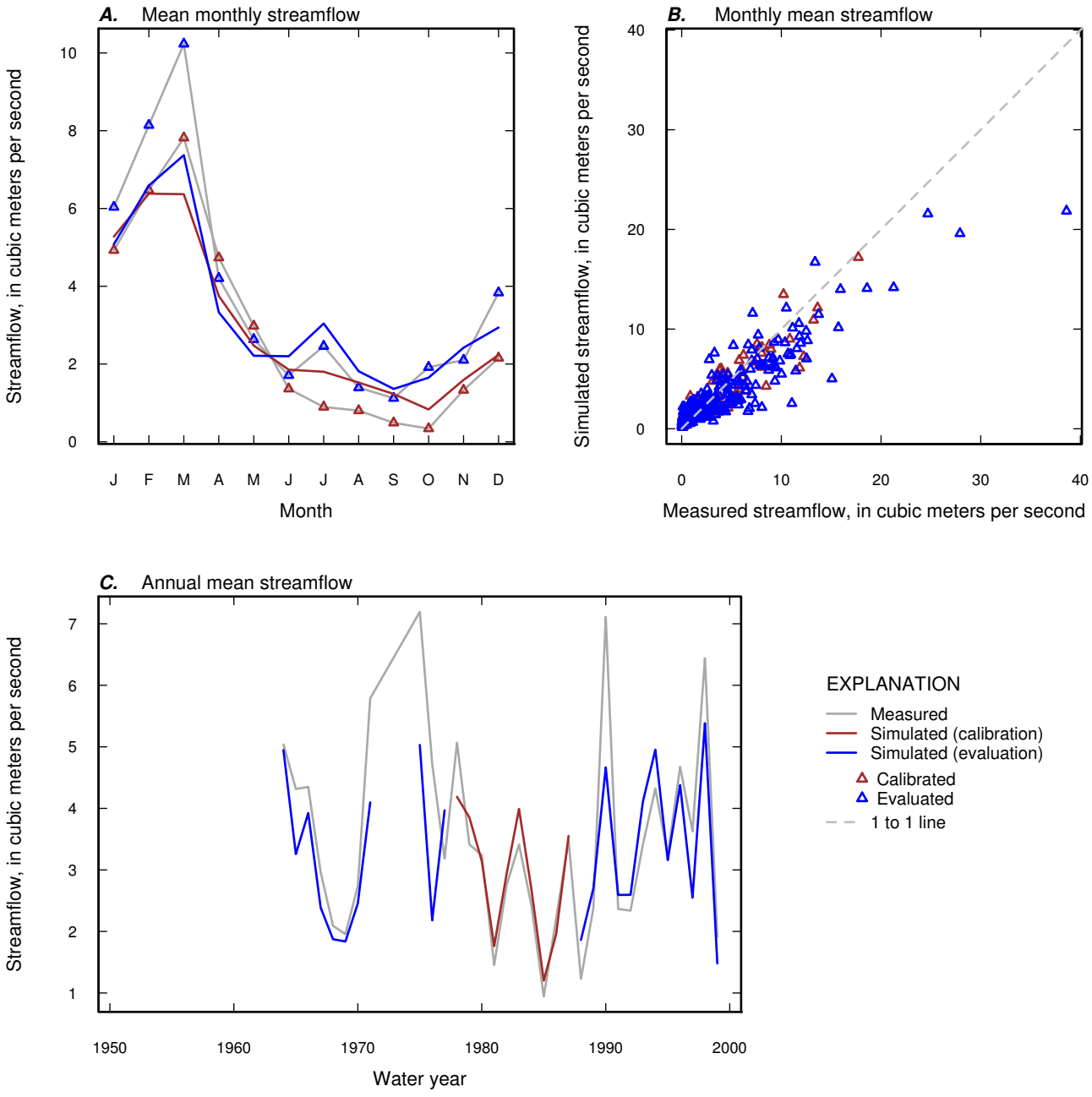

Figure 1–18. Measured and simulated mean-monthly, monthly mean, and annual mean streamflow for calibration and evaluation periods for USGS streamgage 02342933 (South Fork Cowikee Creek near Batesville, AL).

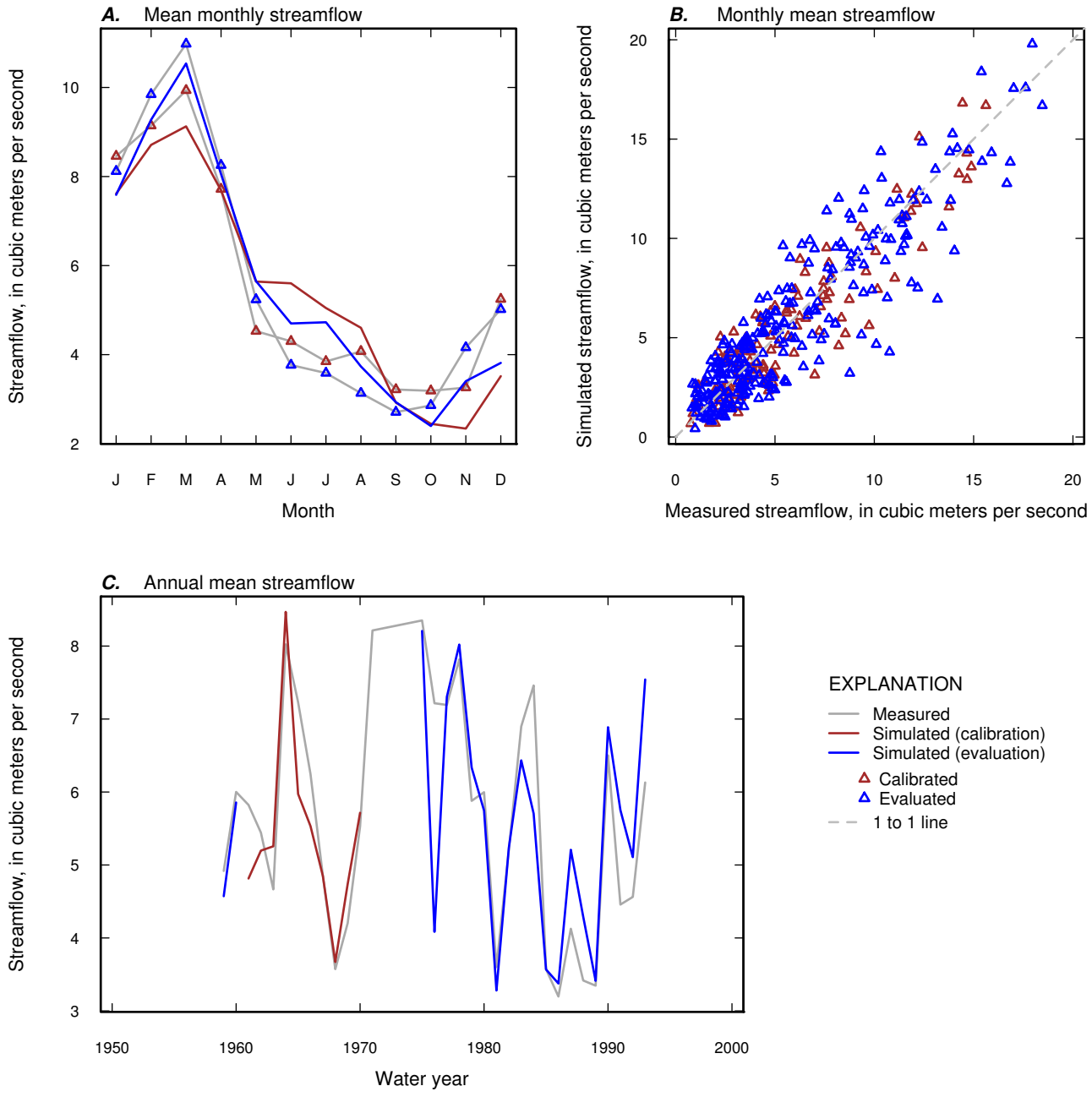

Figure 1–19. Measured and simulated mean-monthly, monthly mean, and annual mean streamflow for calibration and evaluation periods for USGS streamgage 02343300 (Abbie Creek near Haleburg, AL).

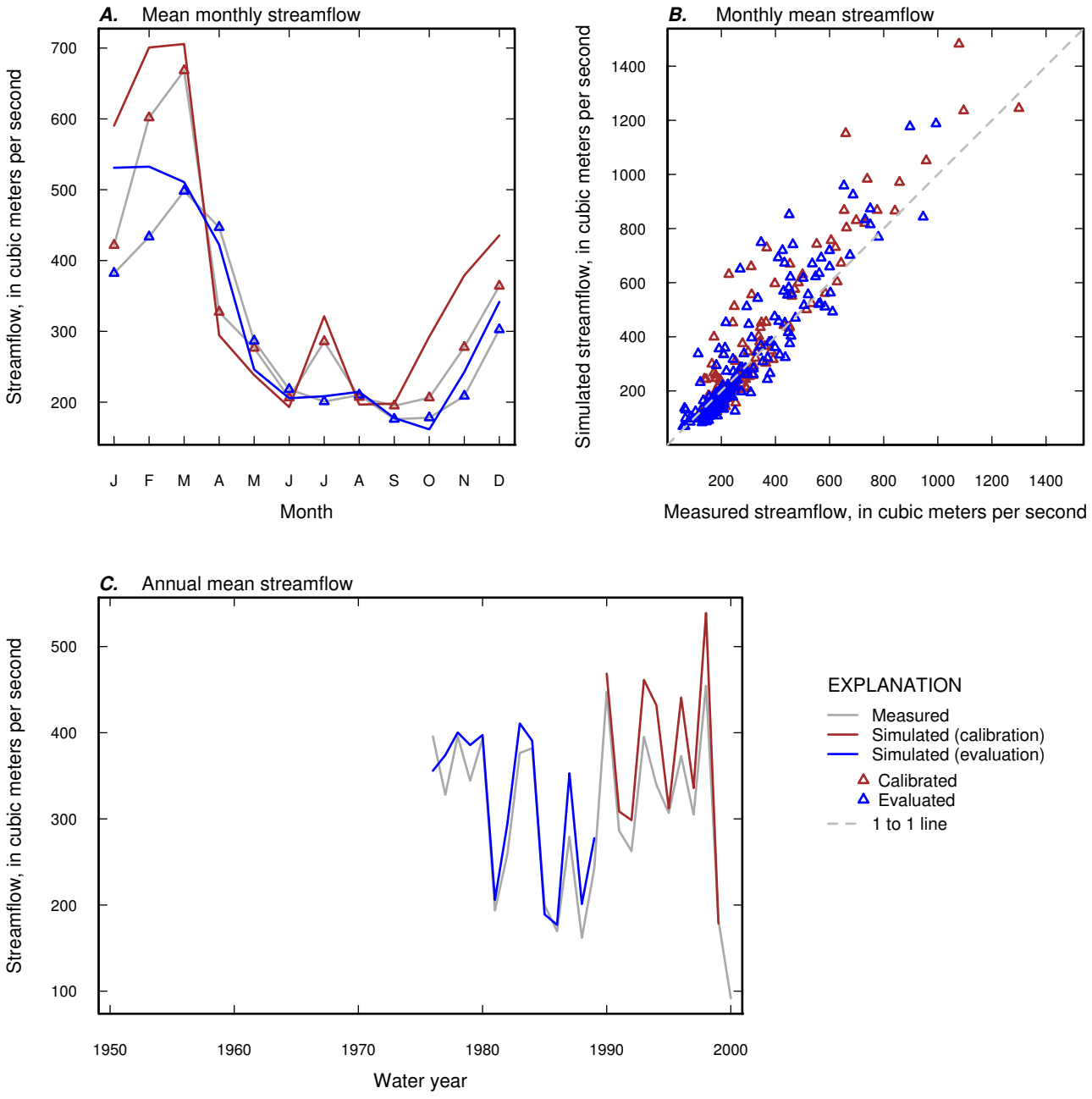

Figure 1–20. Measured and simulated mean-monthly, monthly mean, and annual mean streamflow for calibration and evaluation periods for USGS streamgage 02343801 (Chattahoochee River near Columbia, AL).

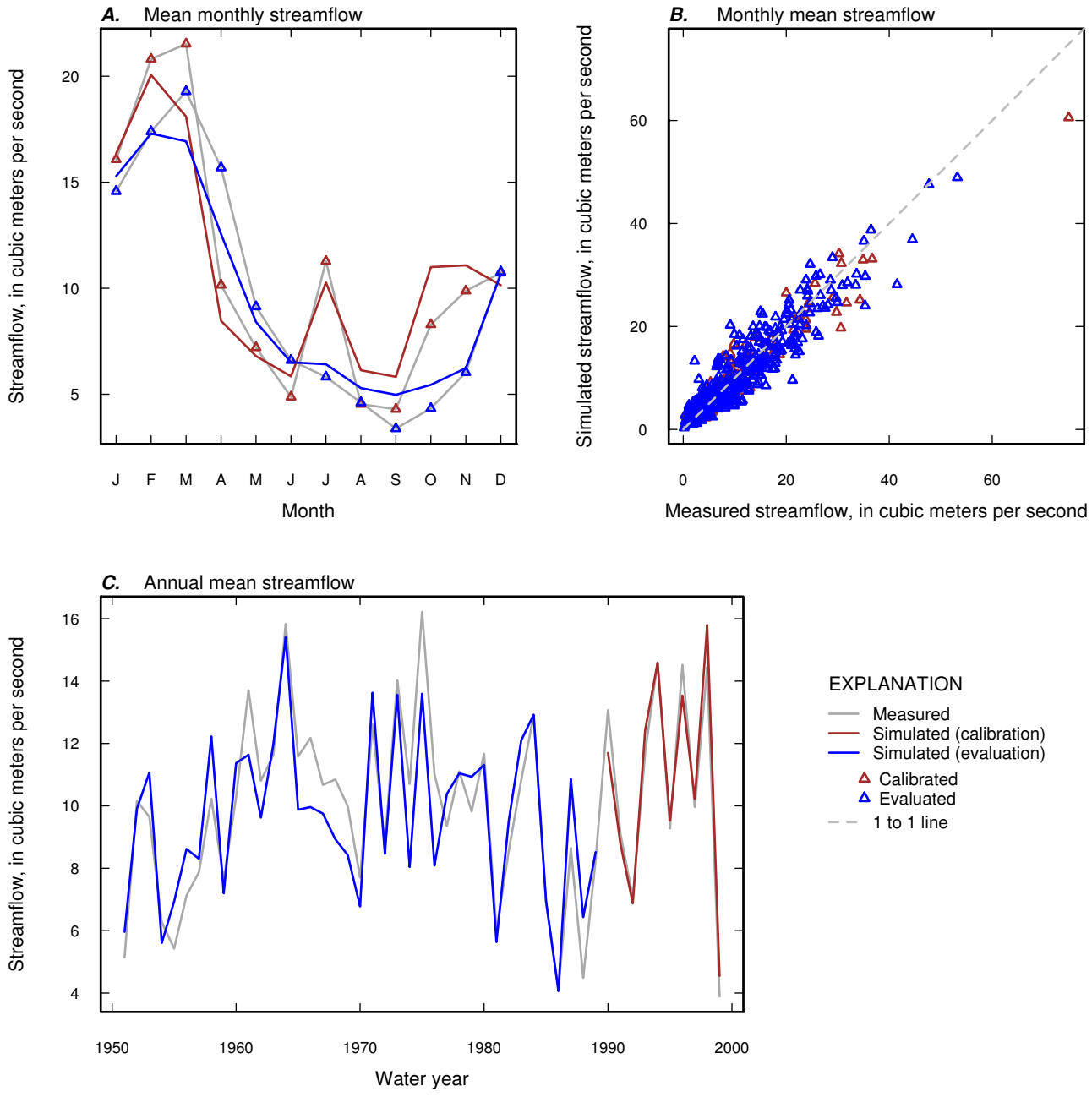

Figure 1–21. Measured and simulated mean-monthly, monthly mean, and annual mean streamflow for calibration and evaluation periods for USGS streamgage 02344500 (Flint River near Griffin, GA).

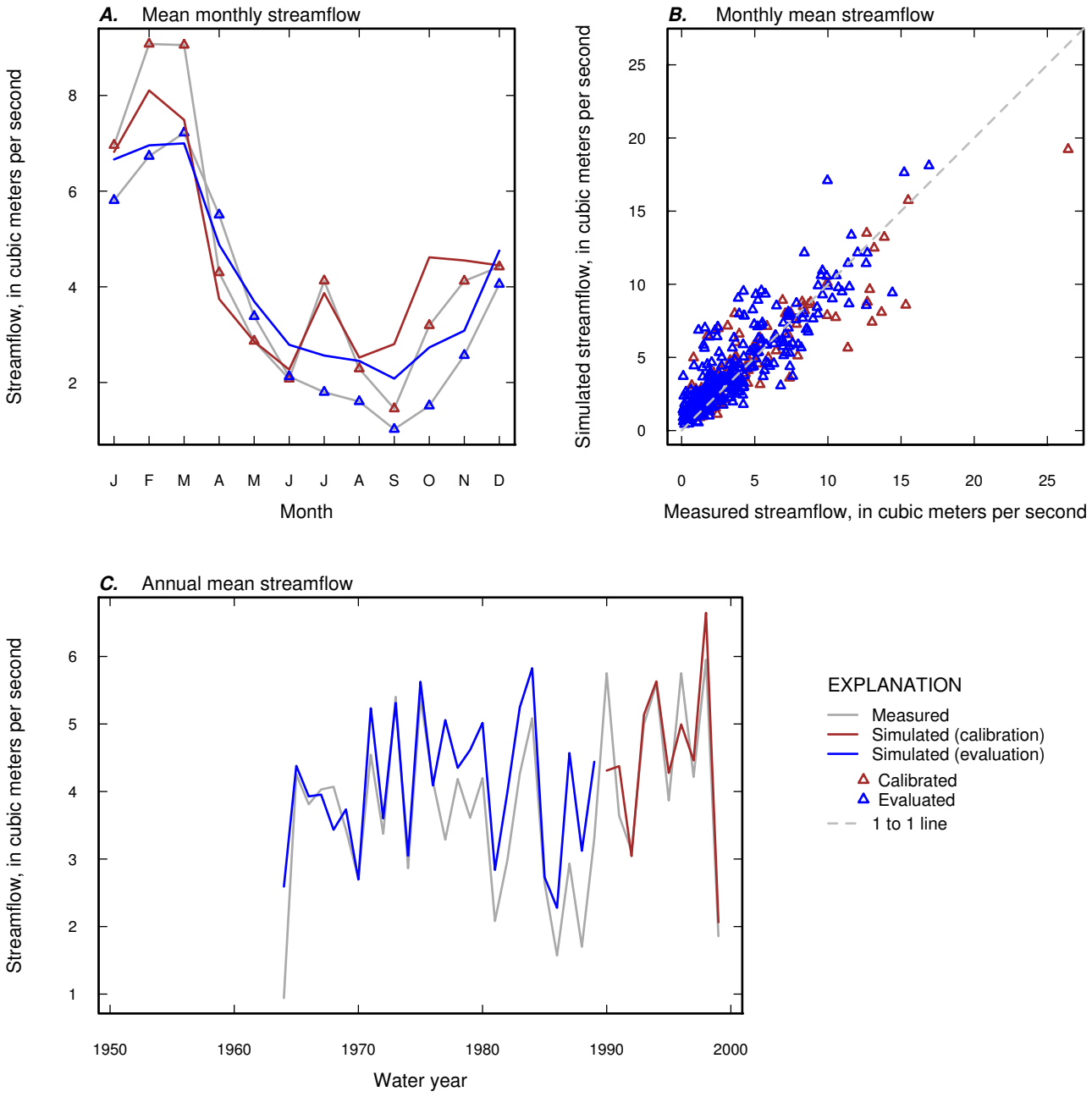

Figure 1–22. Measured and simulated mean-monthly, monthly mean, and annual mean streamflow for calibration and evaluation periods for USGS streamgage 02344700 (Line Creek near Senoia, GA).

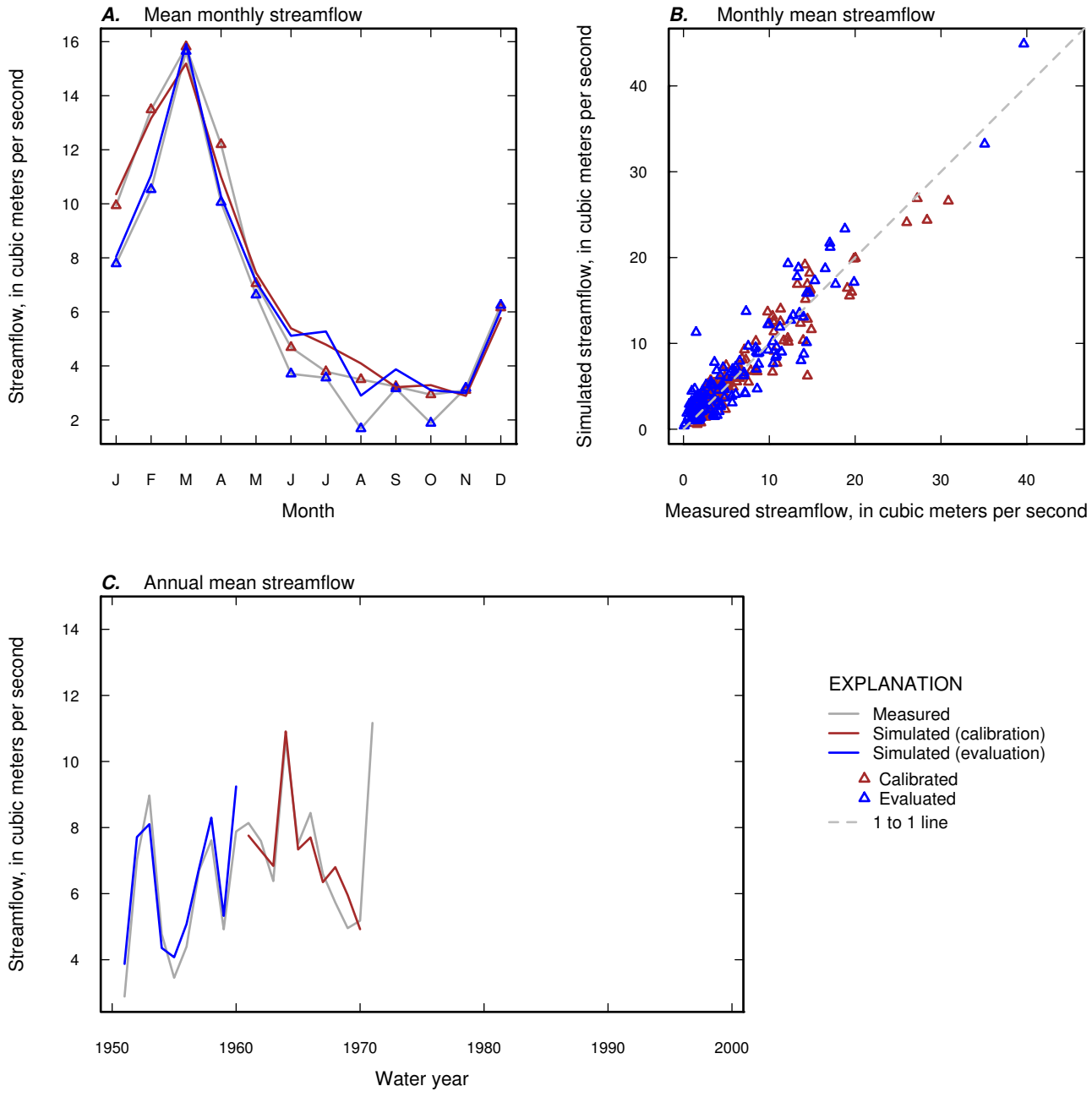

Figure 1–23. Measured and simulated mean-monthly, monthly mean, and annual mean streamflow for calibration and evaluation periods for USGS streamgage 02346500 (Potato Creek near Thomaston, GA).

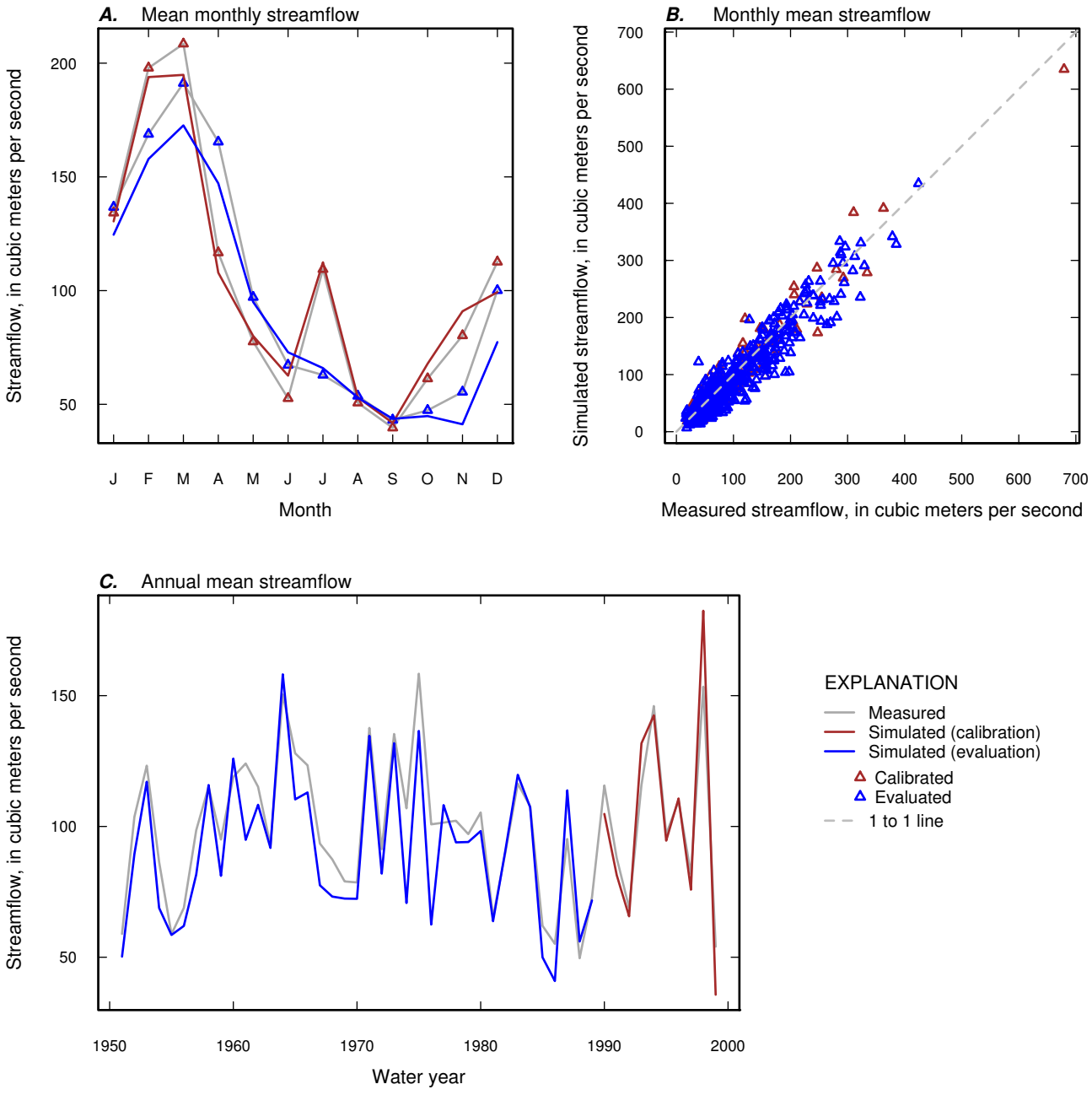

Figure 1–24. Measured and simulated mean-monthly, monthly mean, and annual mean streamflow for calibration and evaluation periods for USGS streamgage 02349605 (Flint River at GA 26, near Montezuma, GA).

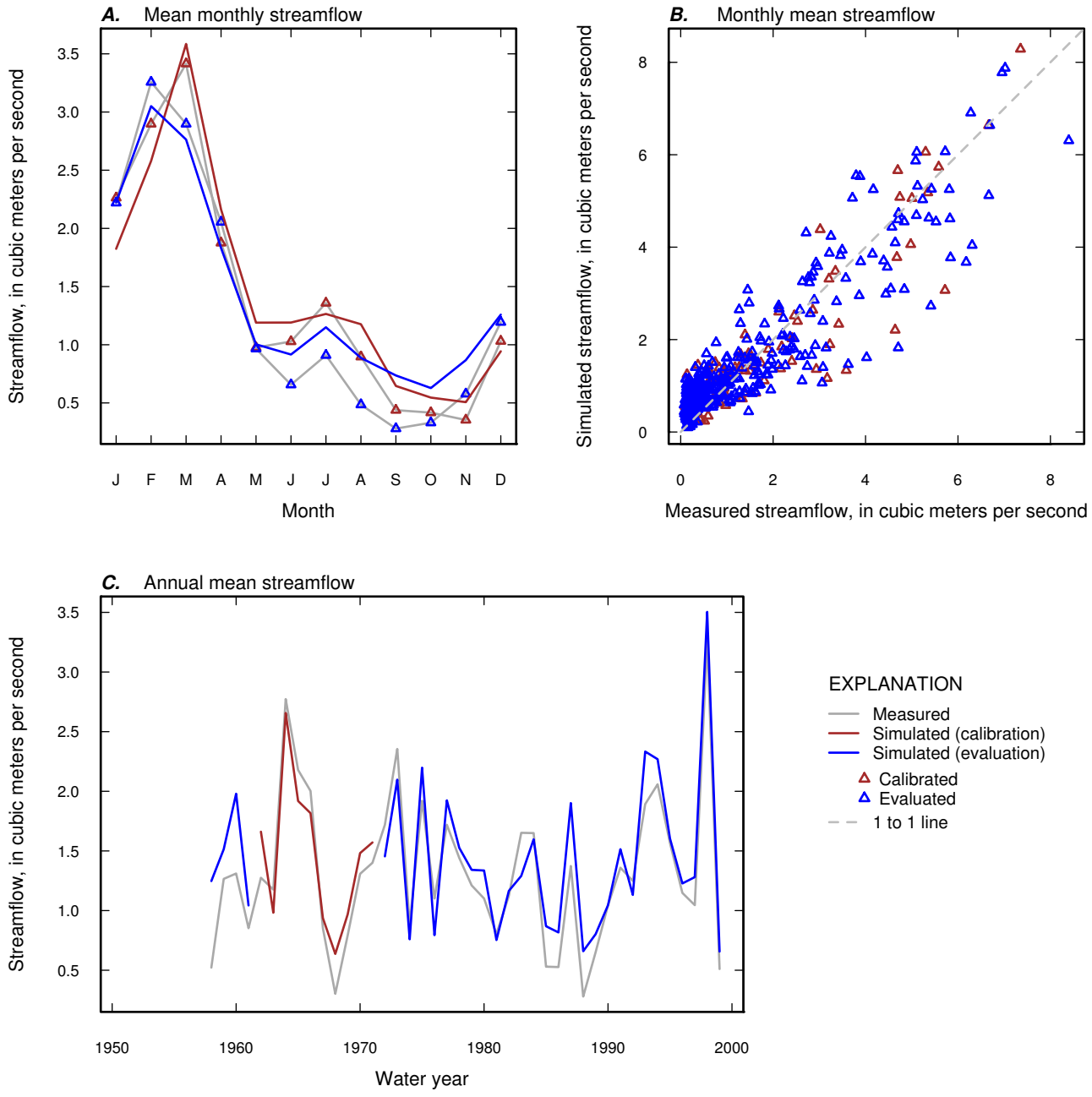

Figure 1–25. Measured and simulated mean-monthly, monthly mean, and annual mean streamflow for calibration and evaluation periods for USGS streamgage 02349900 (Turkey Creek at Byromville, GA).

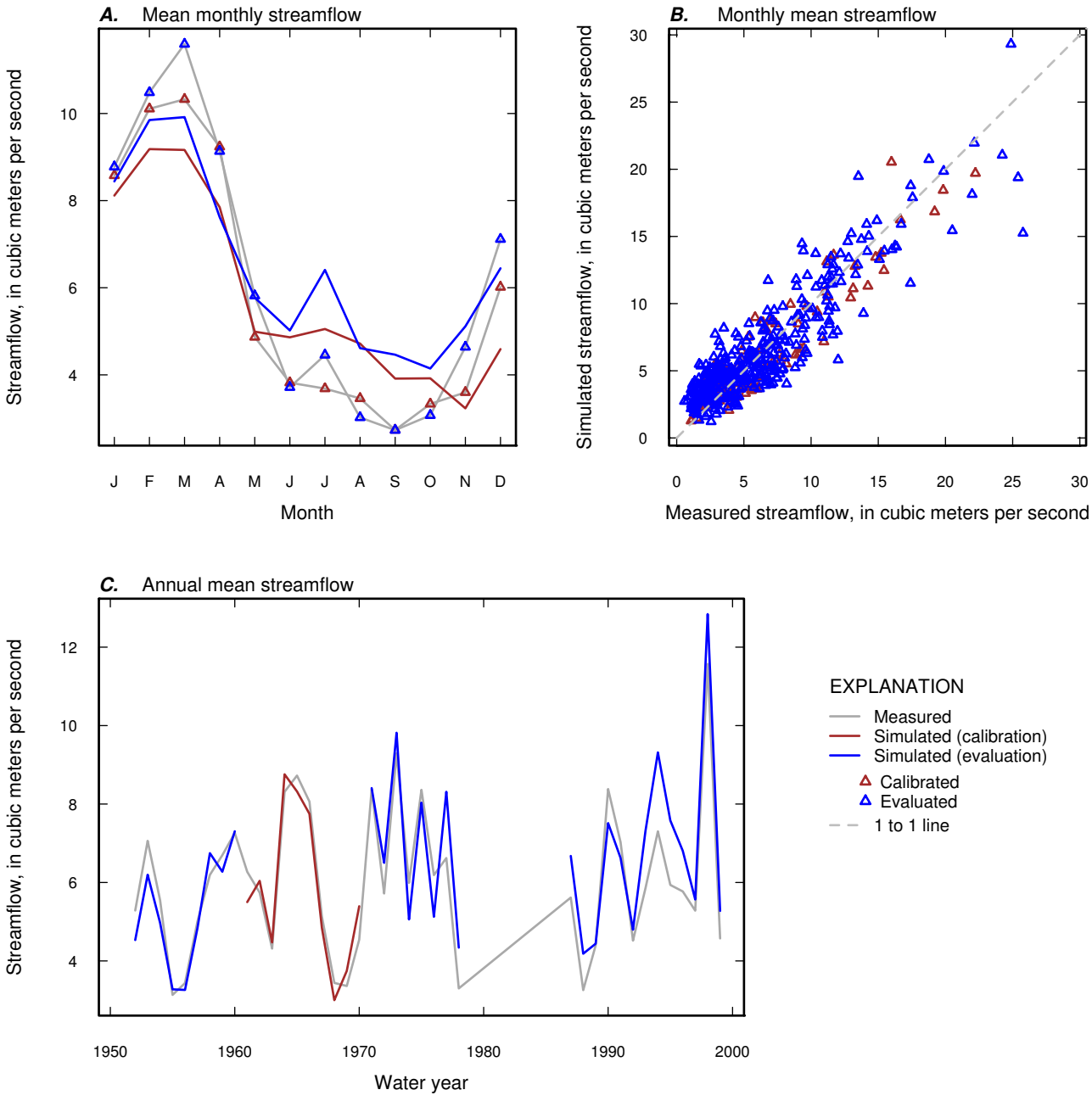

Figure 1–26. Measured and simulated mean-monthly, monthly mean, and annual mean streamflow for calibration and evaluation periods for USGS streamgage 02350600 (Kinchafoonee Creek at Preston, GA).

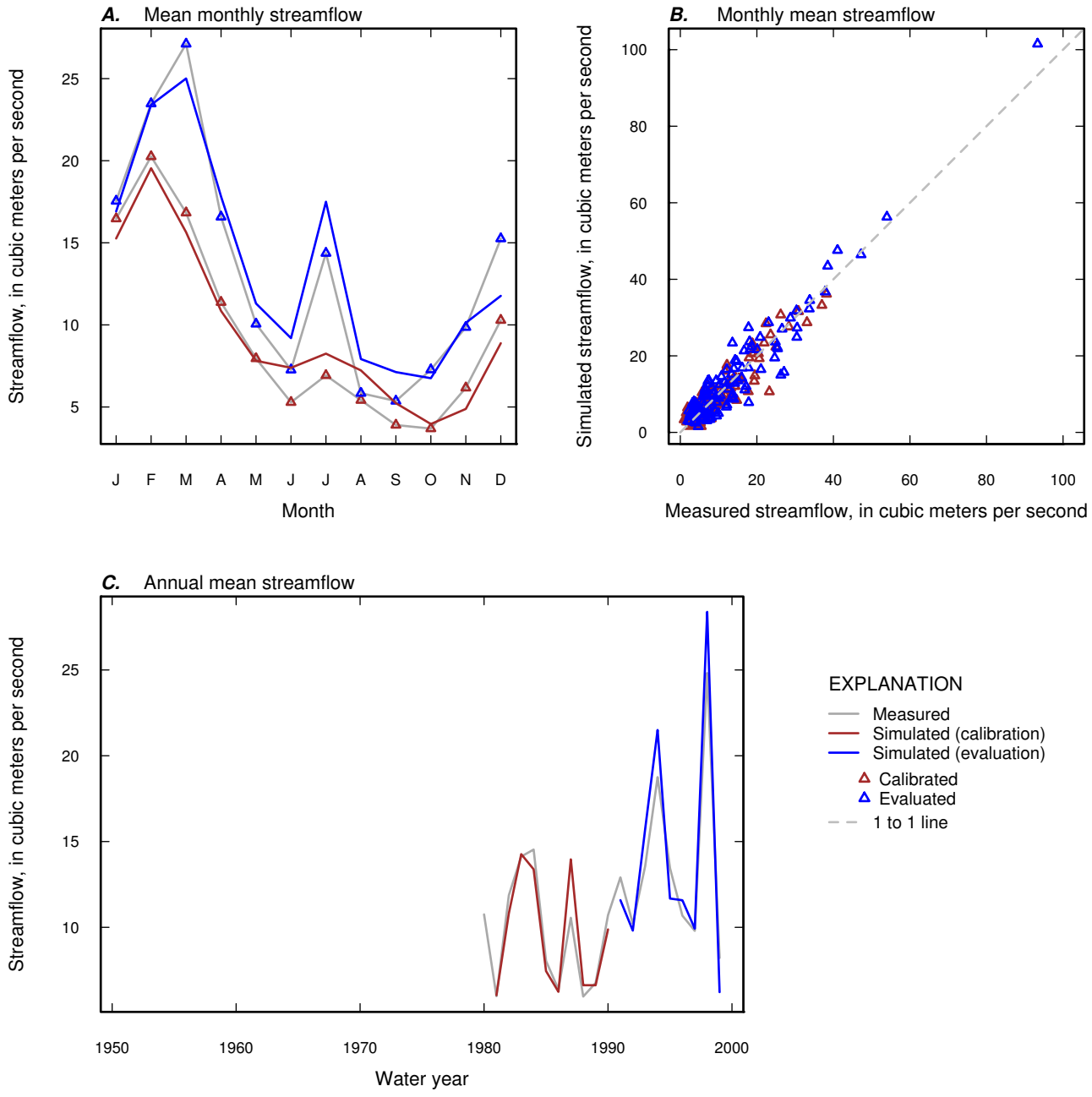

Figure 1–27. Measured and simulated mean-monthly, monthly mean, and annual mean streamflow for calibration and evaluation periods for USGS streamgage 02351890 (Muckalee Creek at GA 195, near Leesburg, GA).

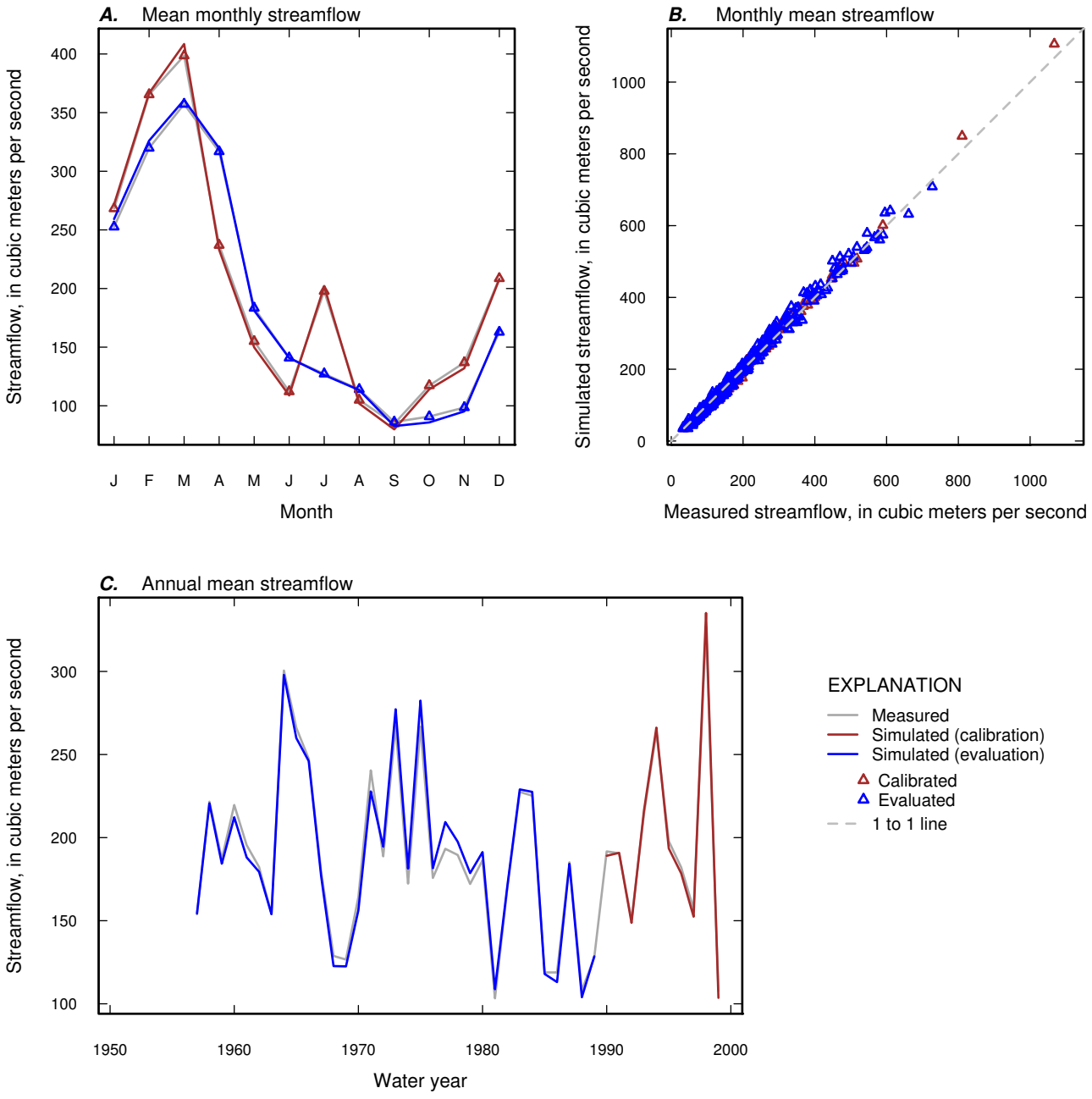

Figure 1–28. Measured and simulated mean-monthly, monthly mean, and annual mean streamflow for calibration and evaluation periods for USGS streamgage 02353000 (Flint River at Newton, GA).

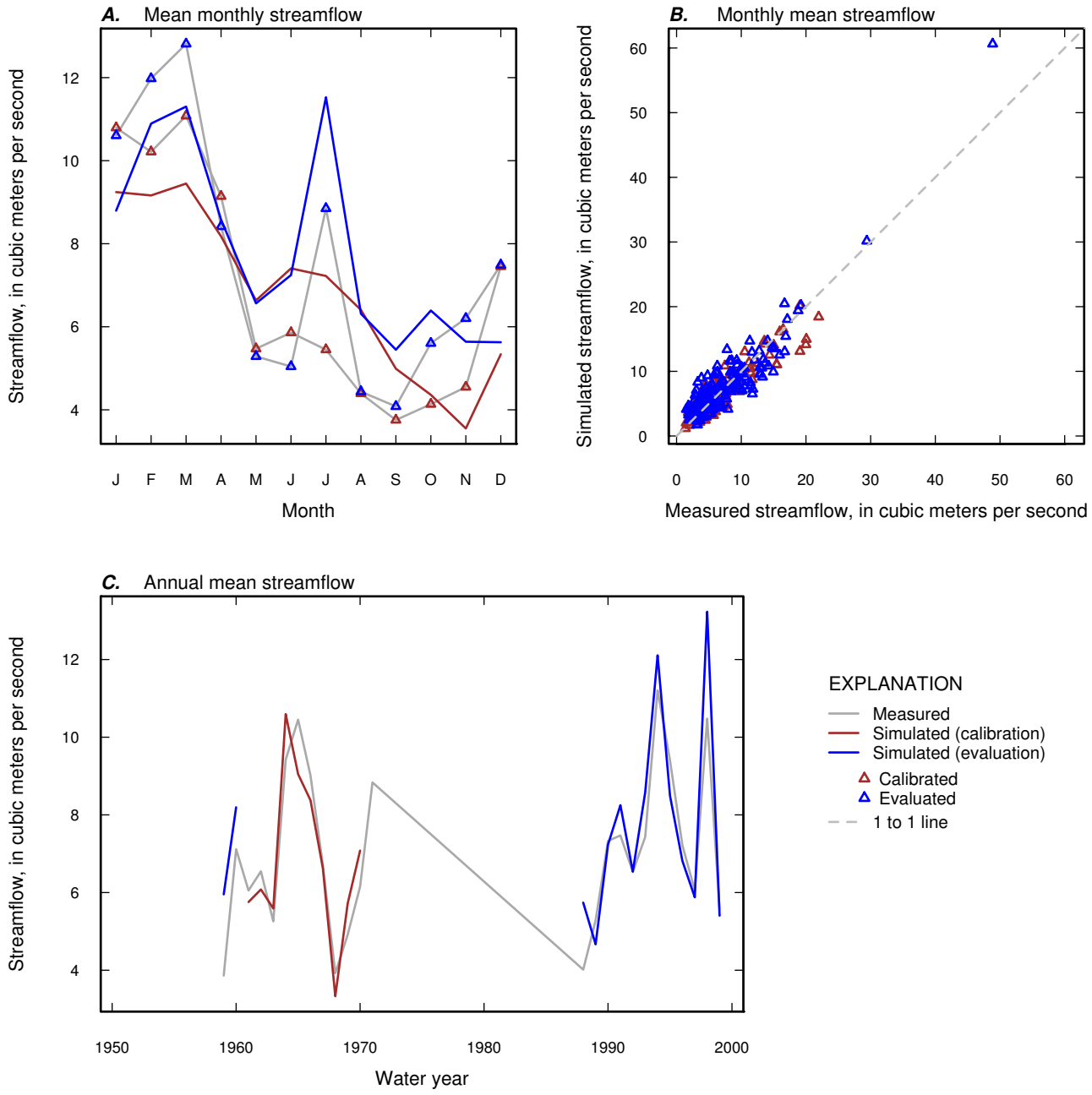

Figure 1–29. Measured and simulated mean-monthly, monthly mean, and annual mean streamflow for calibration and evaluation periods for USGS streamgage 02353400 (Pachitla Creek near Edison, GA).

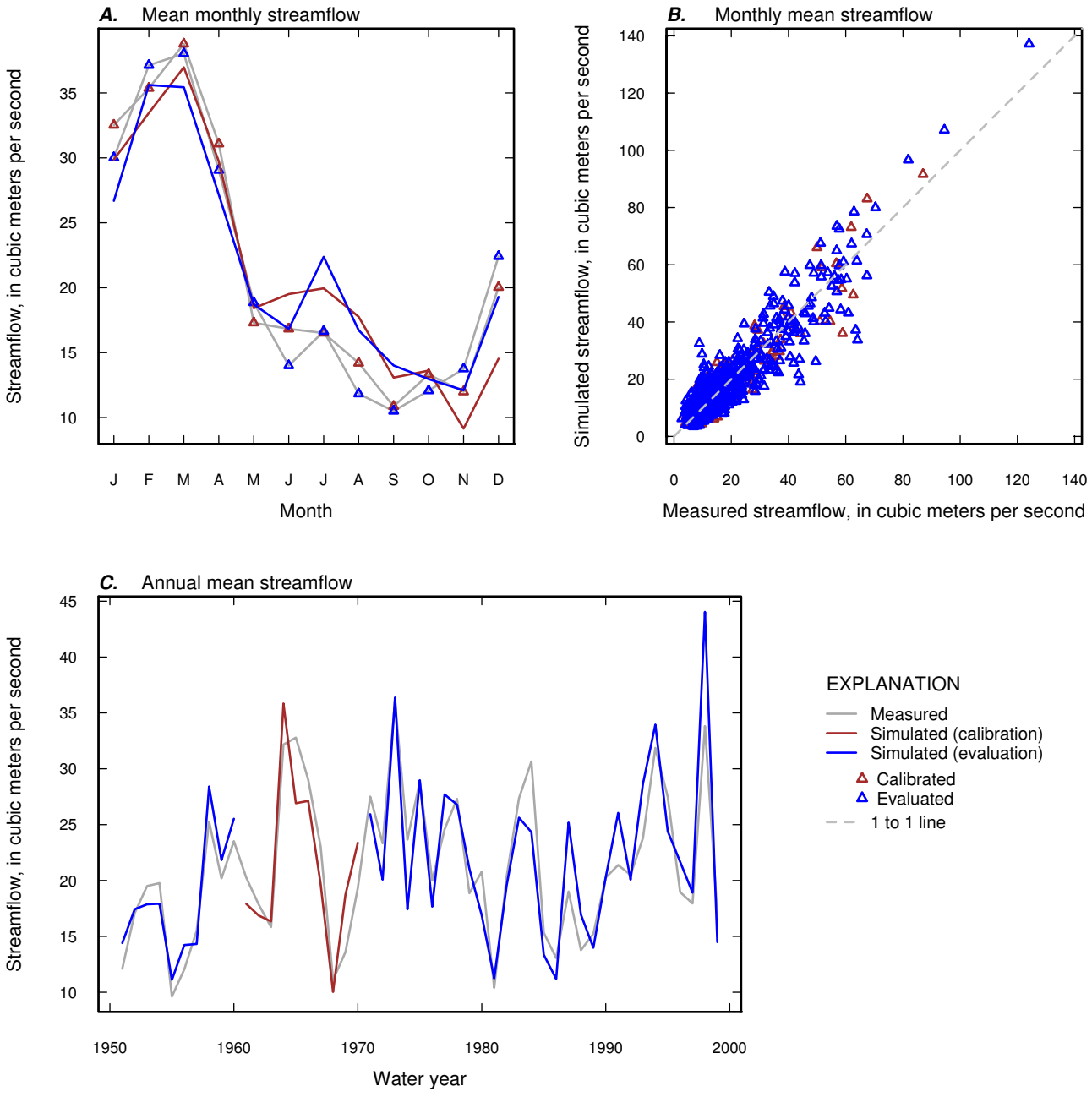

Figure 1–30. Measured and simulated mean-monthly, monthly mean, and annual mean streamflow for calibration and evaluation periods for USGS streamgage 02353500 (Ichawaynochaway Creek at Milford, GA).

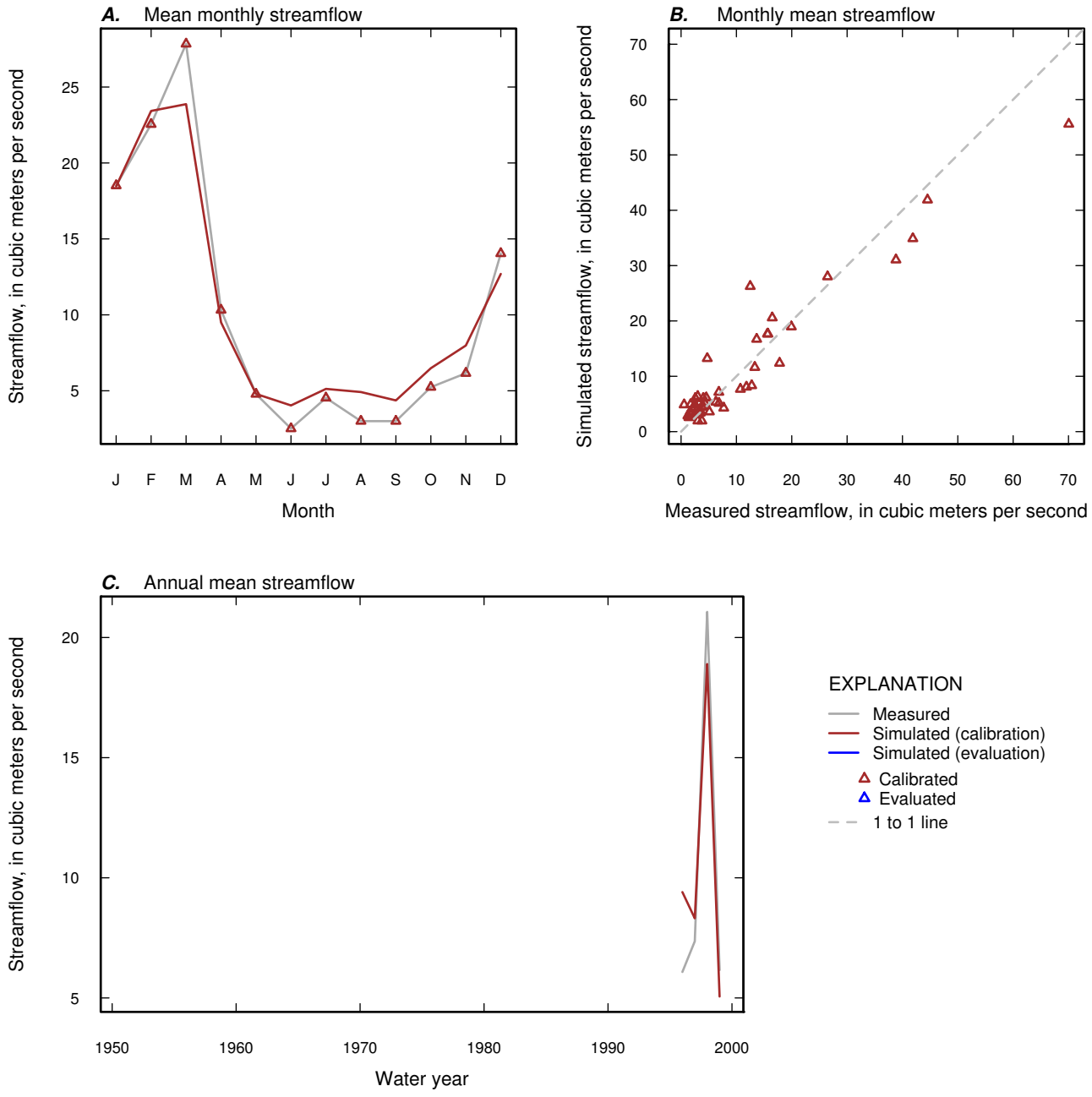

Figure 1–31. Measured and simulated mean-monthly, monthly mean, and annual mean streamflow for calibration and evaluation periods for USGS streamgage 02354500 (Chickasawhatchee Creek at Elmodel, GA).

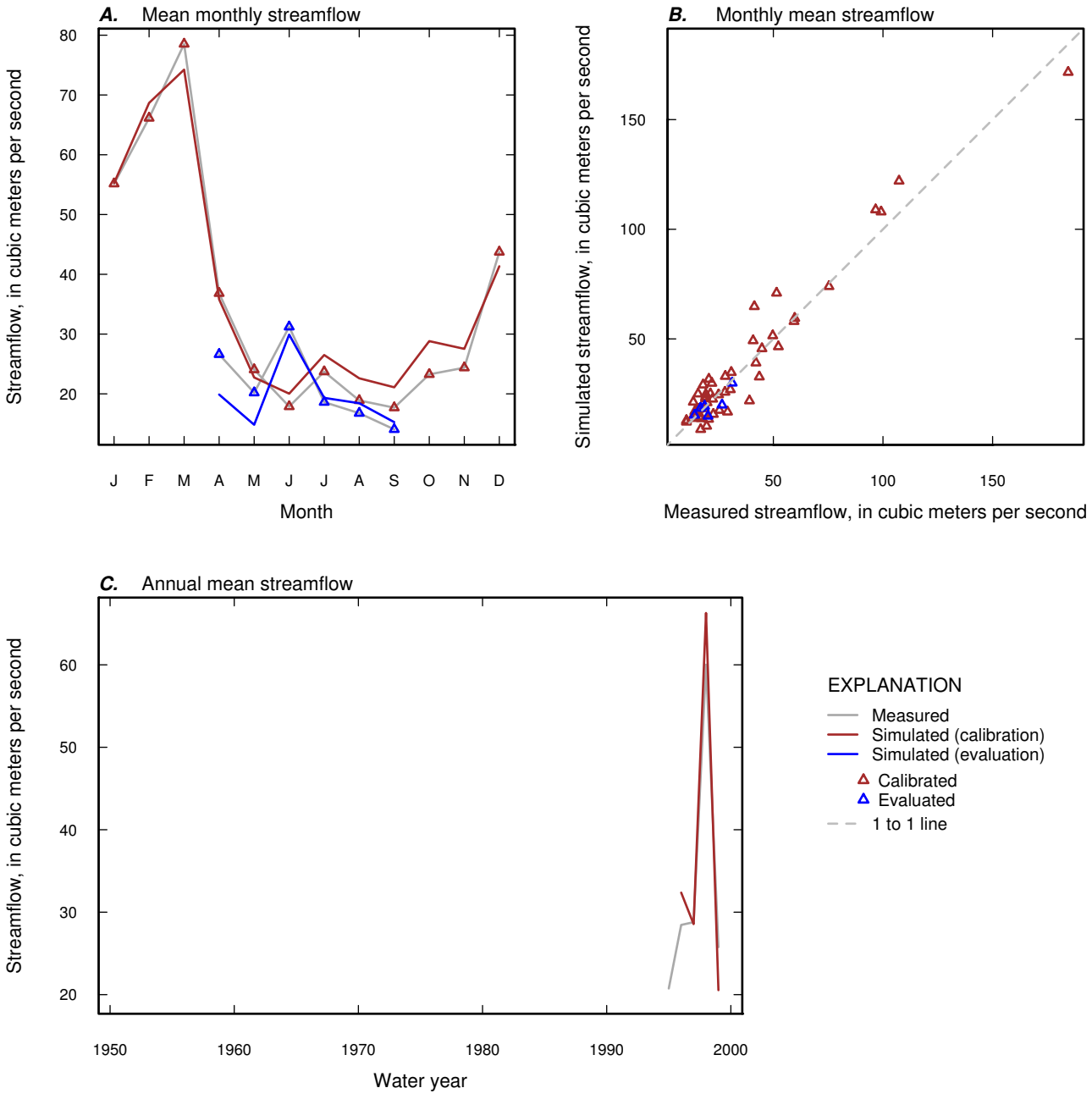

Figure 1–32. Measured and simulated mean-monthly, monthly mean, and annual mean streamflow for calibration and evaluation periods for USGS streamgage 02354800 (Ichawaynochaway Creek near Elmodel, GA).

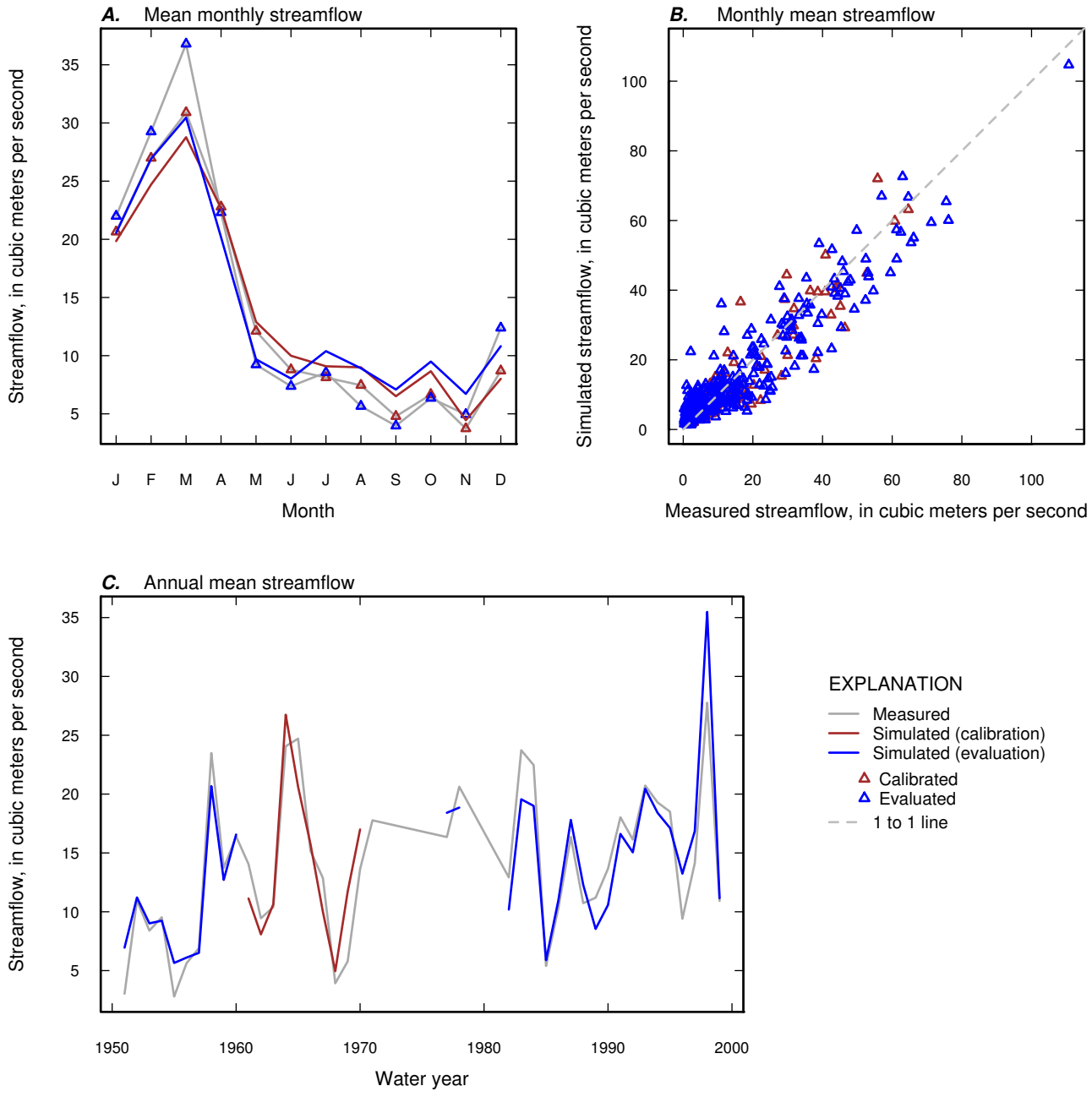

Figure 1–33. Measured and simulated mean-monthly, monthly mean, and annual mean streamflow for calibration and evaluation periods for USGS streamgage 02357000 (Spring Creek near Iron City, GA).

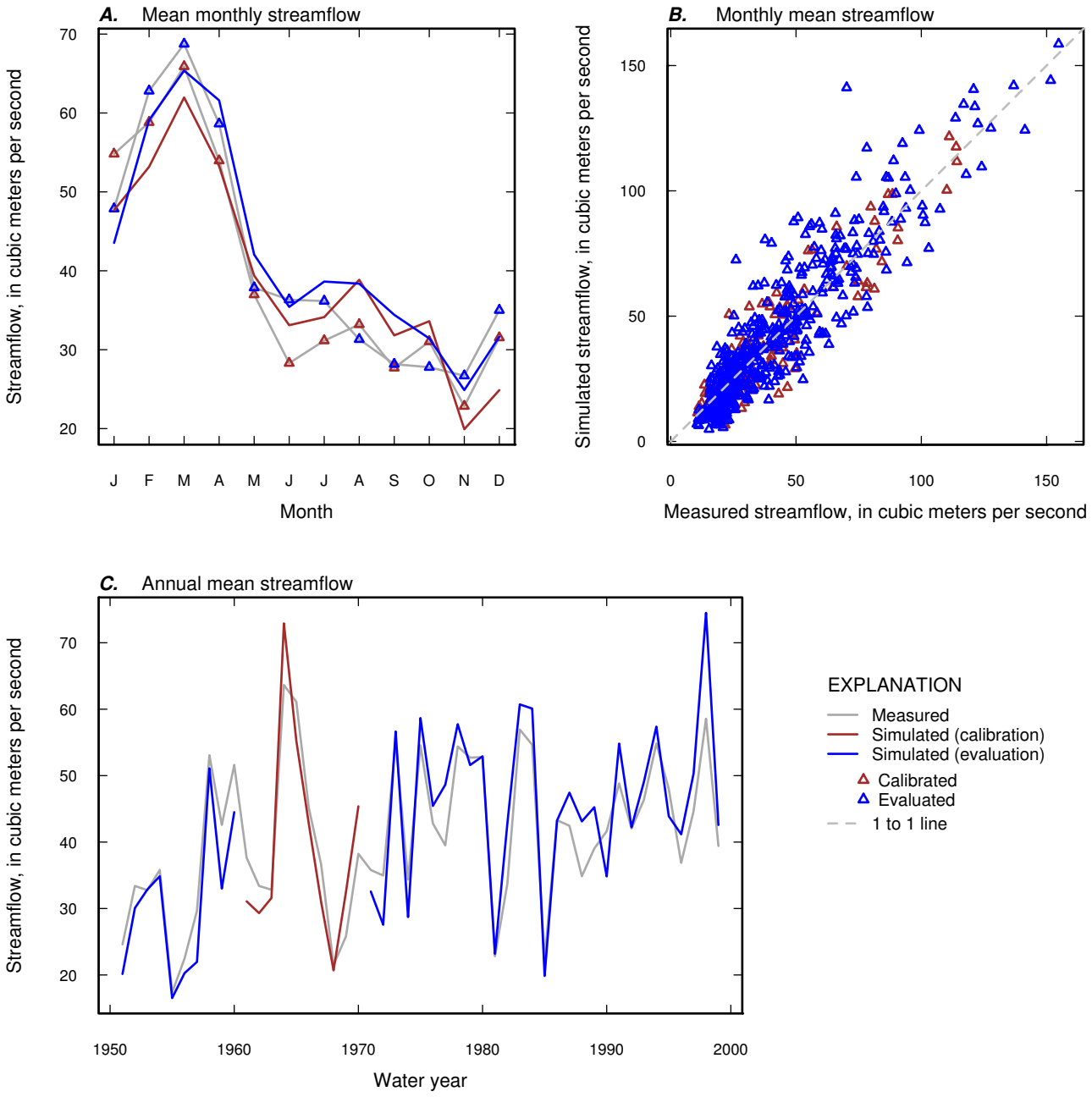

Figure 1–34. Measured and simulated mean-monthly, monthly mean, and annual mean streamflow for calibration and evaluation periods for USGS streamgage 02359000 (Chipola River near Altha, FL).

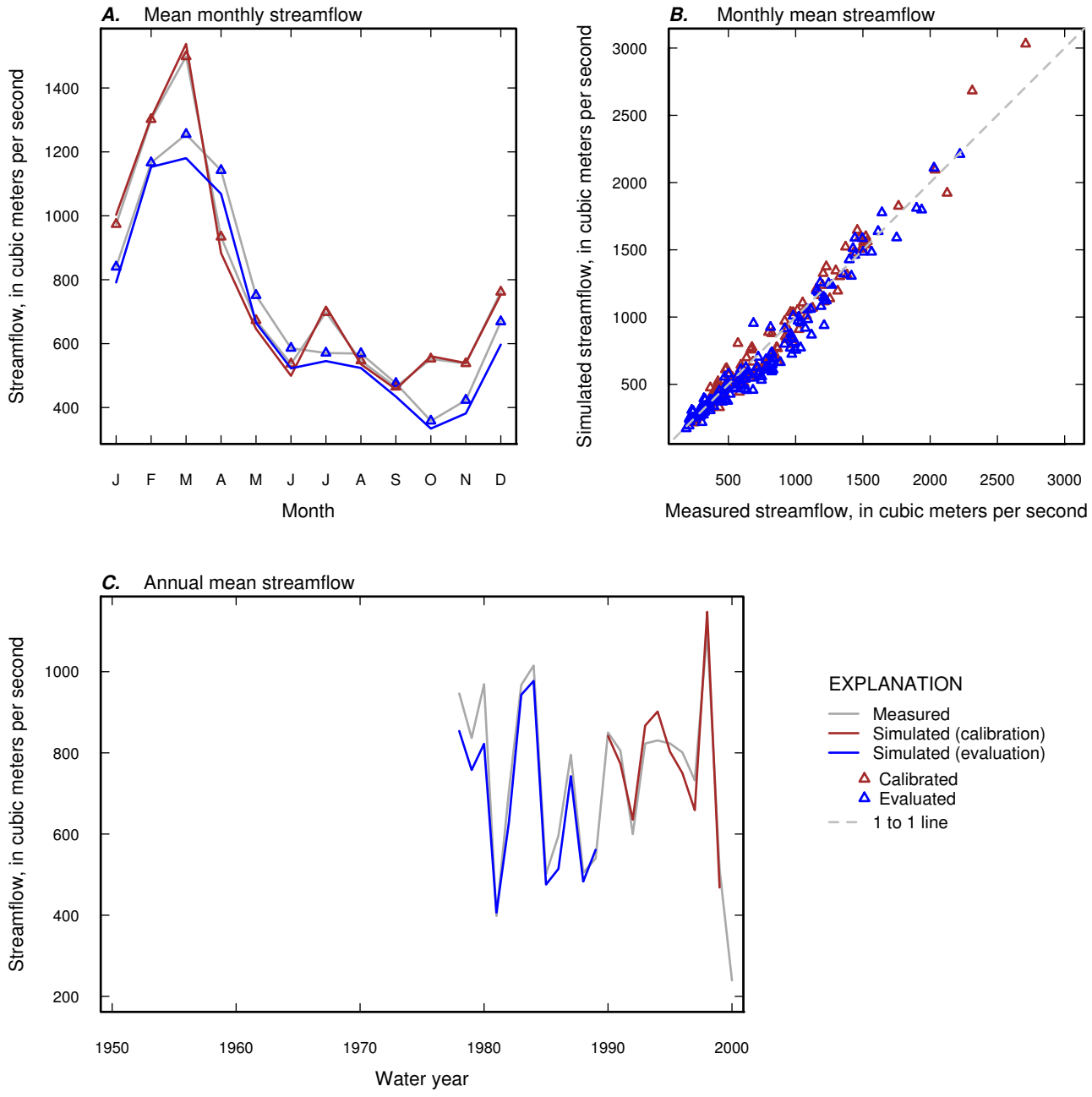

Figure 1–35. Measured and simulated mean-monthly, monthly mean, and annual mean streamflow for calibration and evaluation periods for USGS streamgage 02359170 (Apalachicola River near Sumatra, FL).

Appendix 2. Plots of measured and simulated daily streamflow, annual Nash-Sutcliffe Index, and flow duration curves for calibration and evaluation periods for 35 subbasins of the Apalachicola–Chattahoochee–Flint River Basin

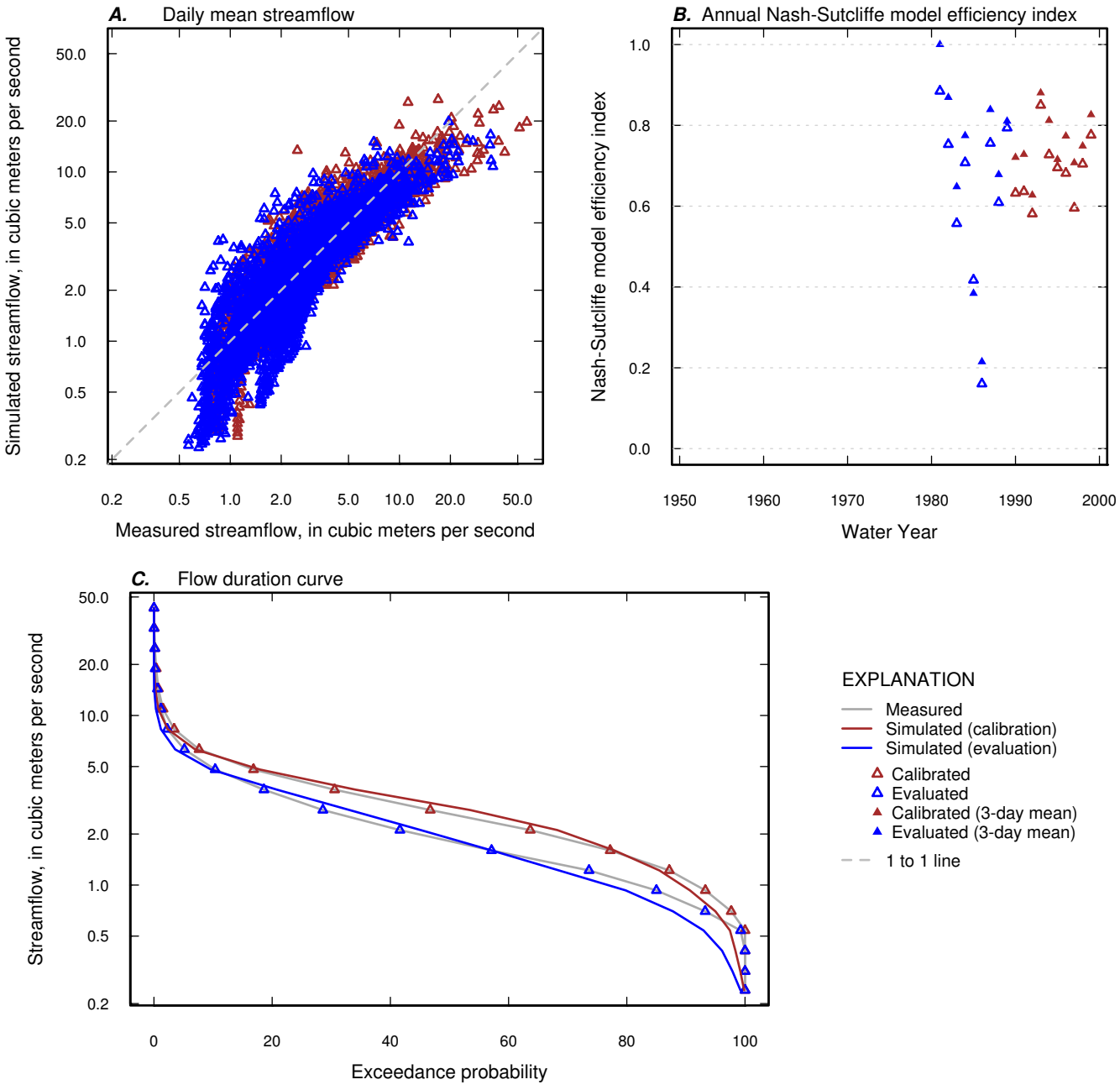

Figure 2–1. Measured and simulated daily streamflow, annual Nash-Sutcliffe Index, and flow duration curve for calibration and evaluation periods for USGS streamgage 02330450 (Chattahoochee River at Helen, GA).

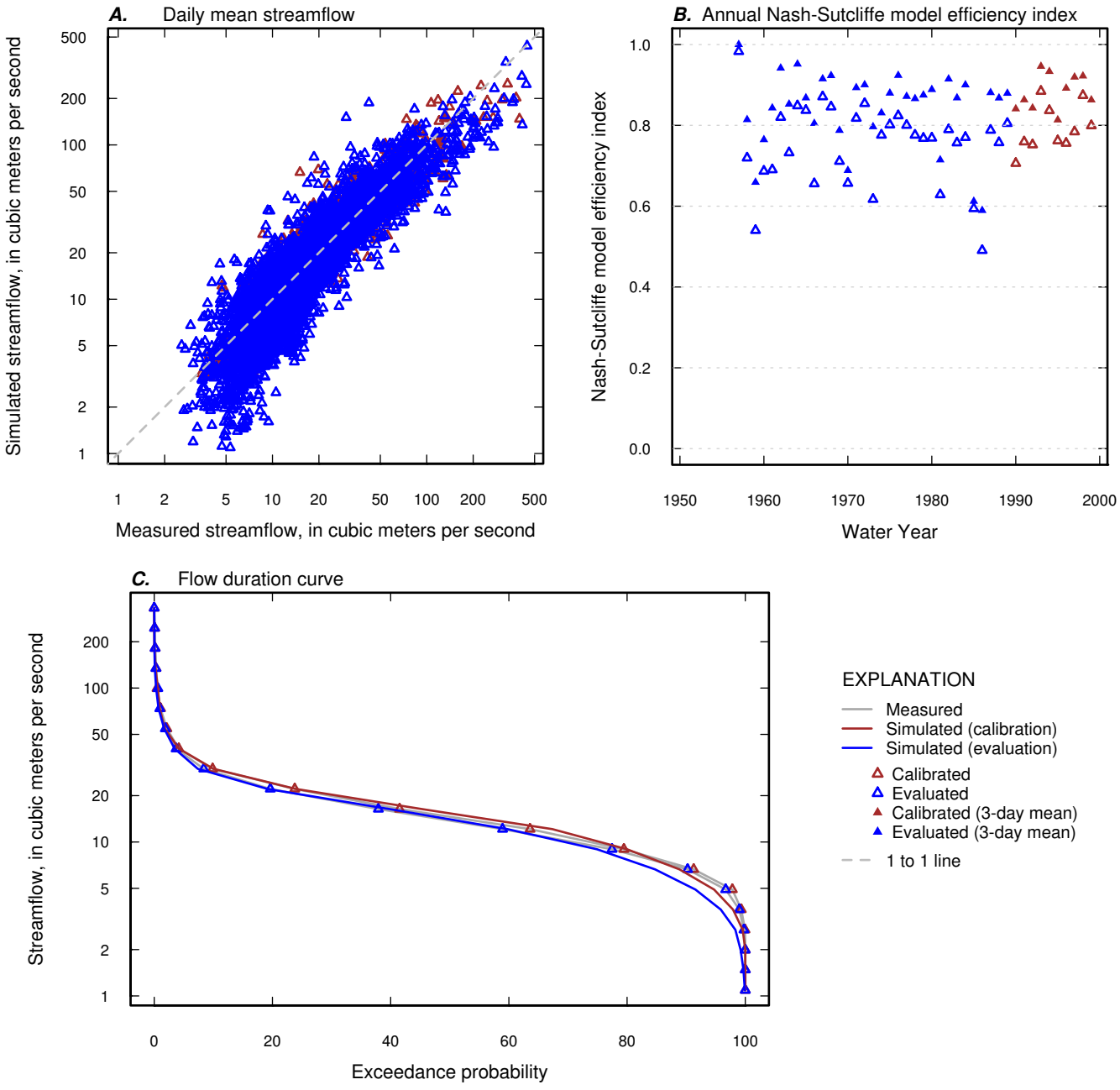

Figure 2–2. Measured and simulated daily streamflow, annual Nash-Sutcliffe Index, and flow duration curve for calibration and evaluation periods for USGS streamgage 02331600 (Chattahoochee River at Cornelia, GA).

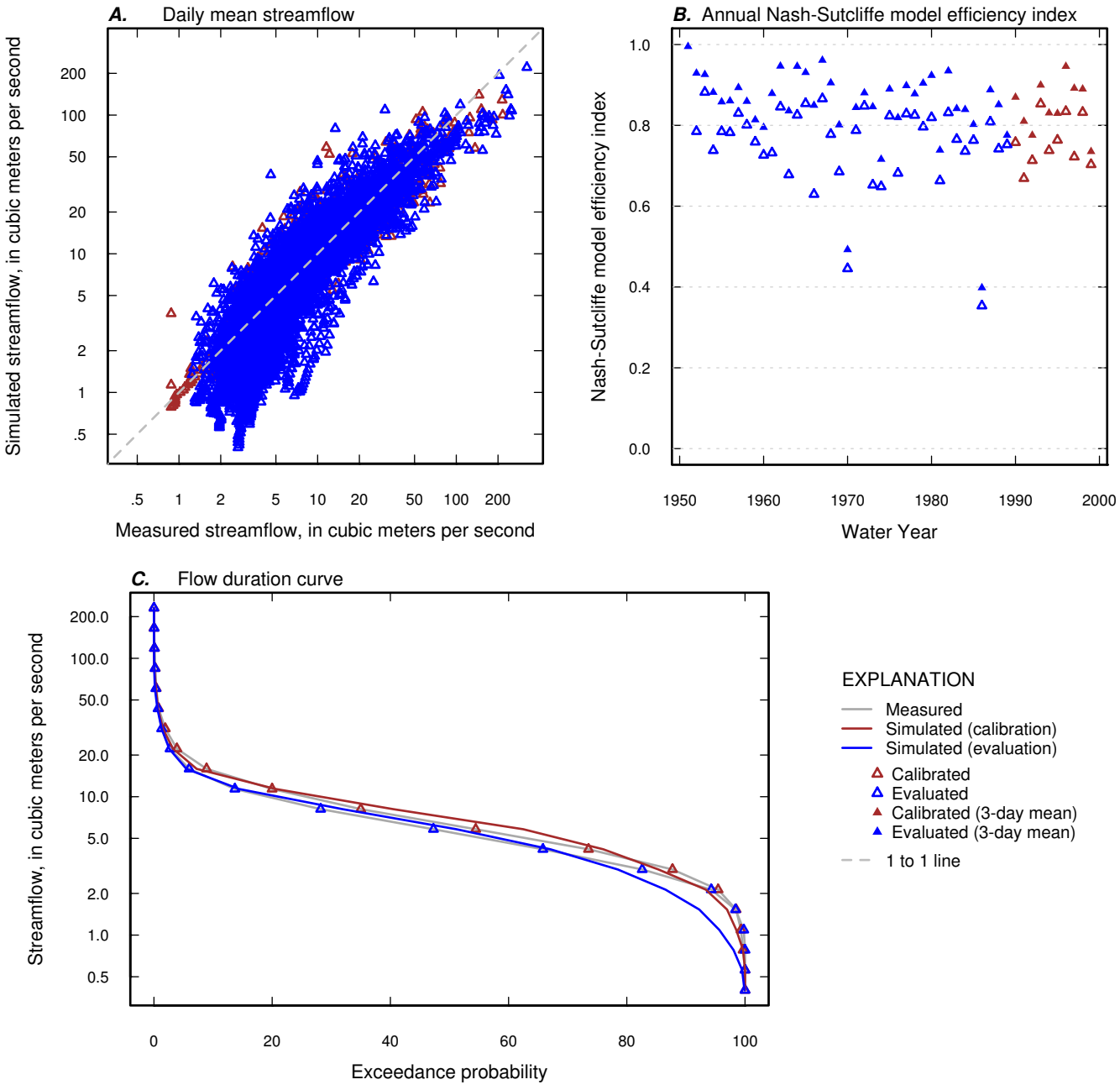

Figure 2–3. Measured and simulated daily streamflow, annual Nash-Sutcliffe Index, and flow duration curve for calibration and evaluation periods for USGS streamgage 02333500 (Chestatee River at Dahonlega, GA).

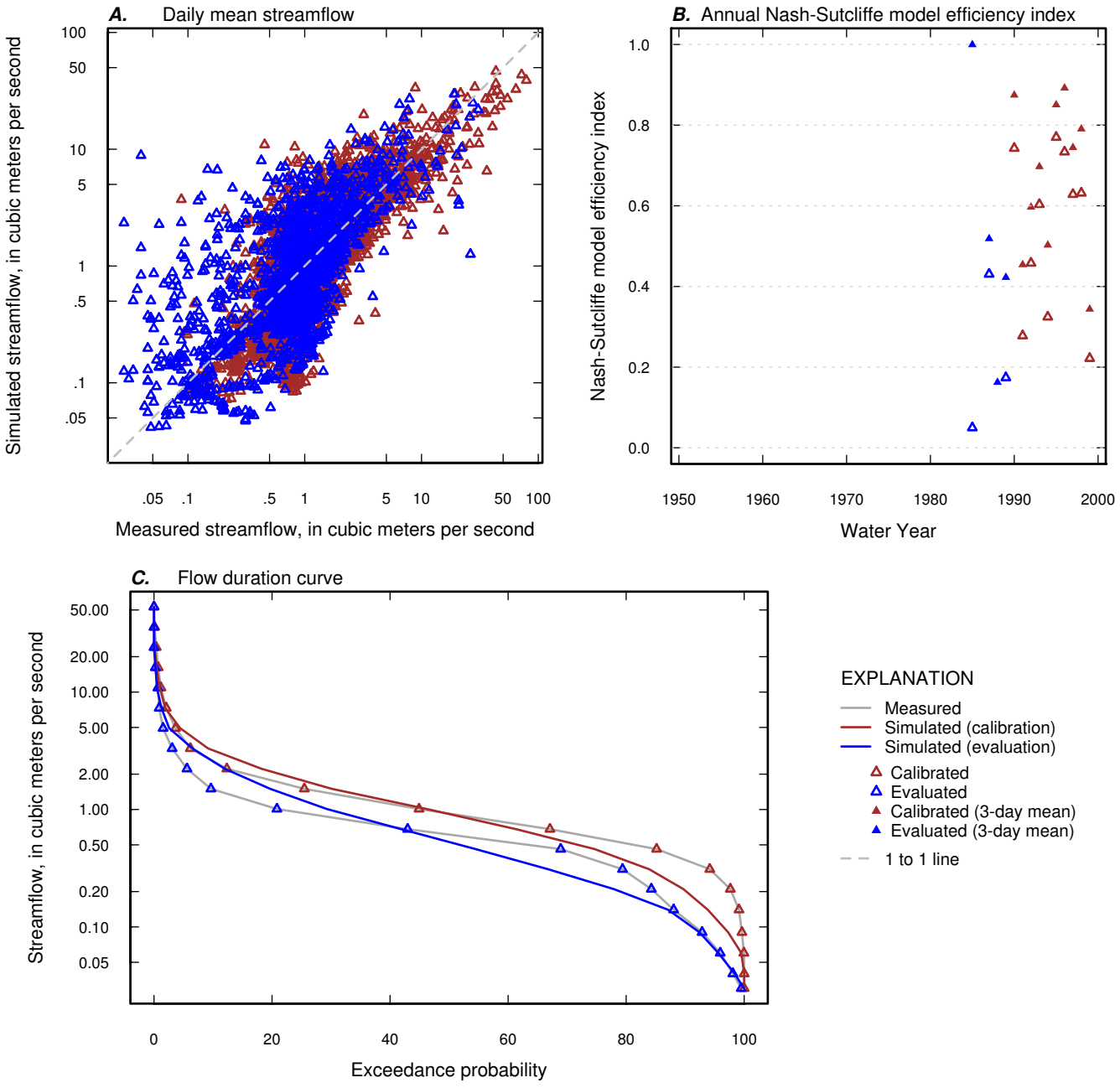

Figure 2–4. Measured and simulated daily streamflow, annual Nash-Sutcliffe Index, and flow duration curve for calibration and evaluation periods for USGS streamgage 02334885 (Suwanee Creek at Suwanee, GA).

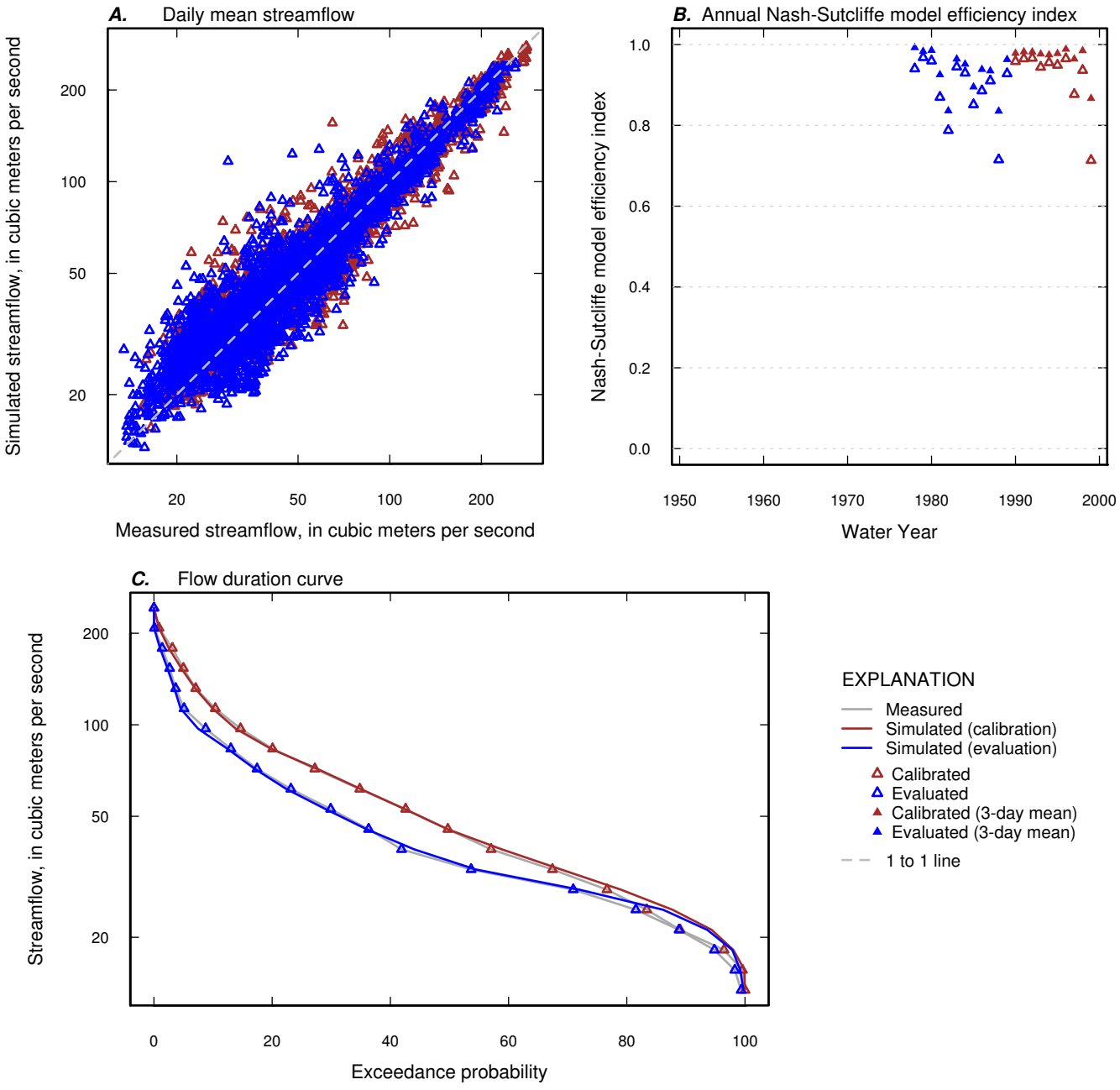

Figure 2–5. Measured and simulated daily streamflow, annual Nash-Sutcliffe Index, and flow duration curve for calibration and evaluation periods for USGS streamgage 02335000 (Chattahoochee River near Norcross, GA).

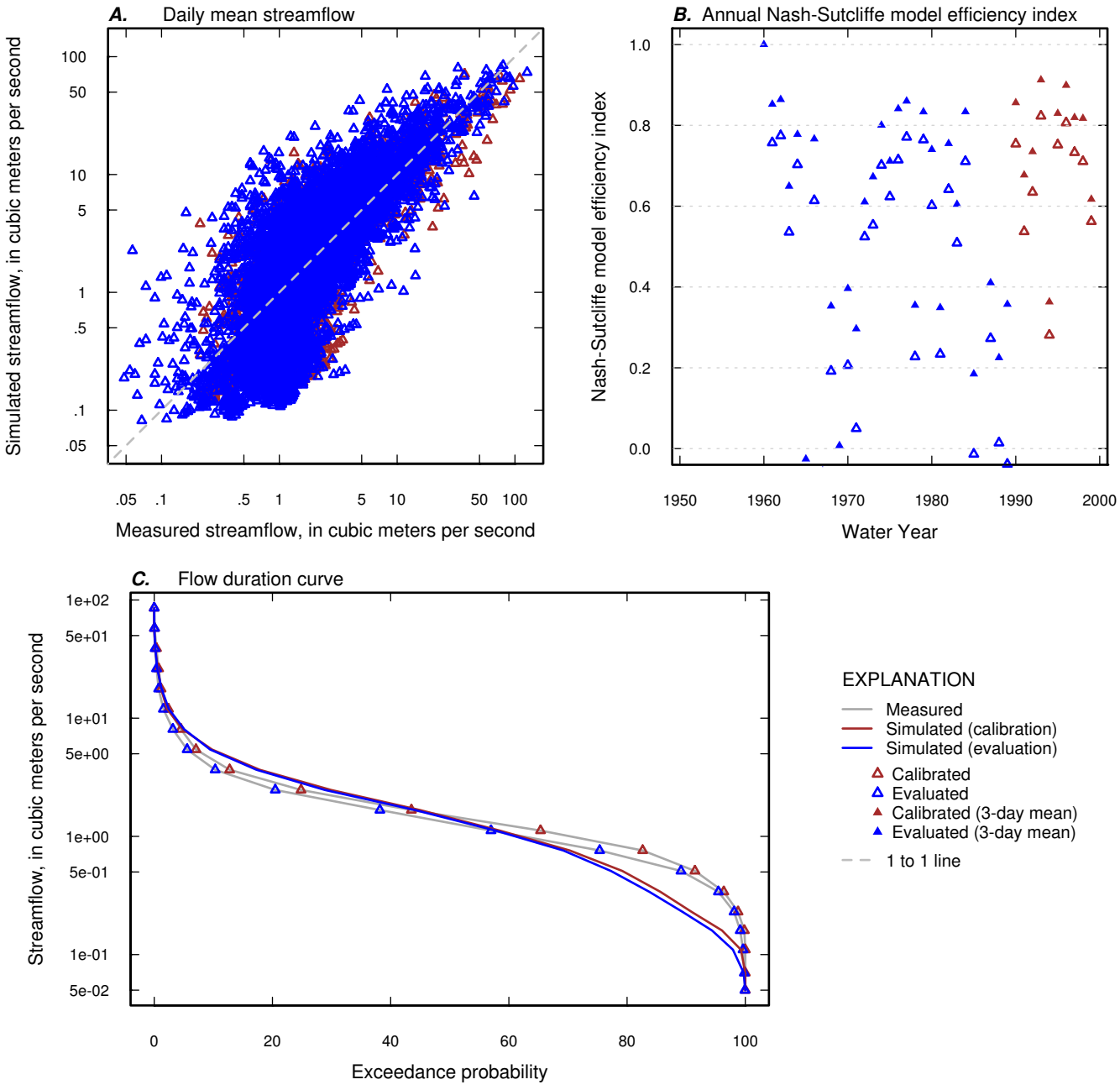

Figure 2–6. Measured and simulated daily streamflow, annual Nash-Sutcliffe Index, and flow duration curve for calibration and evaluation periods for USGS streamgage 02335700 (Big Creek near Alpharetta, GA).

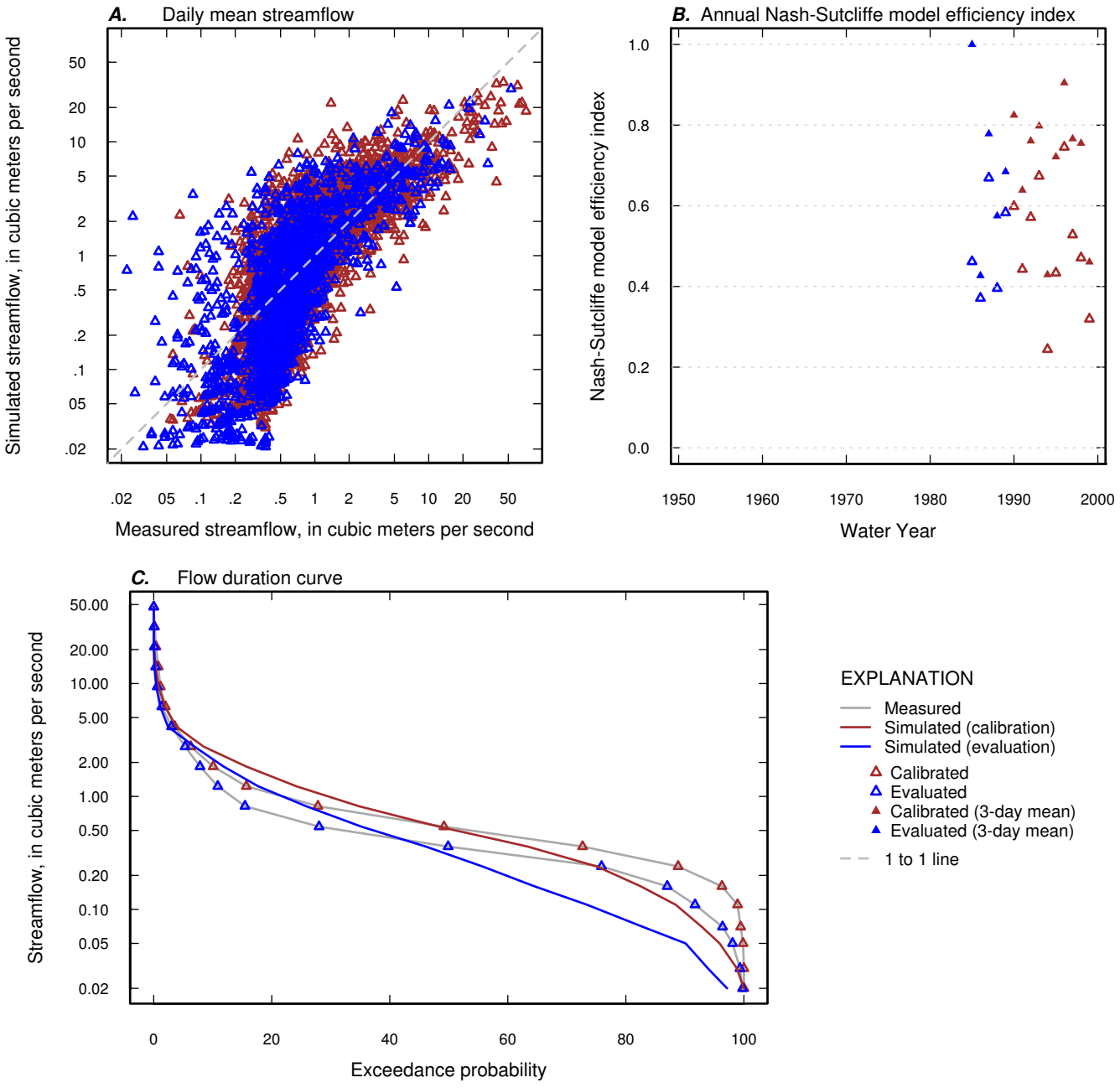

Figure 2–7. Measured and simulated daily streamflow, annual Nash-Sutcliffe Index, and flow duration curve for calibration and evaluation periods for USGS streamgage 02335870 (Sope Creek near Marietta, GA).

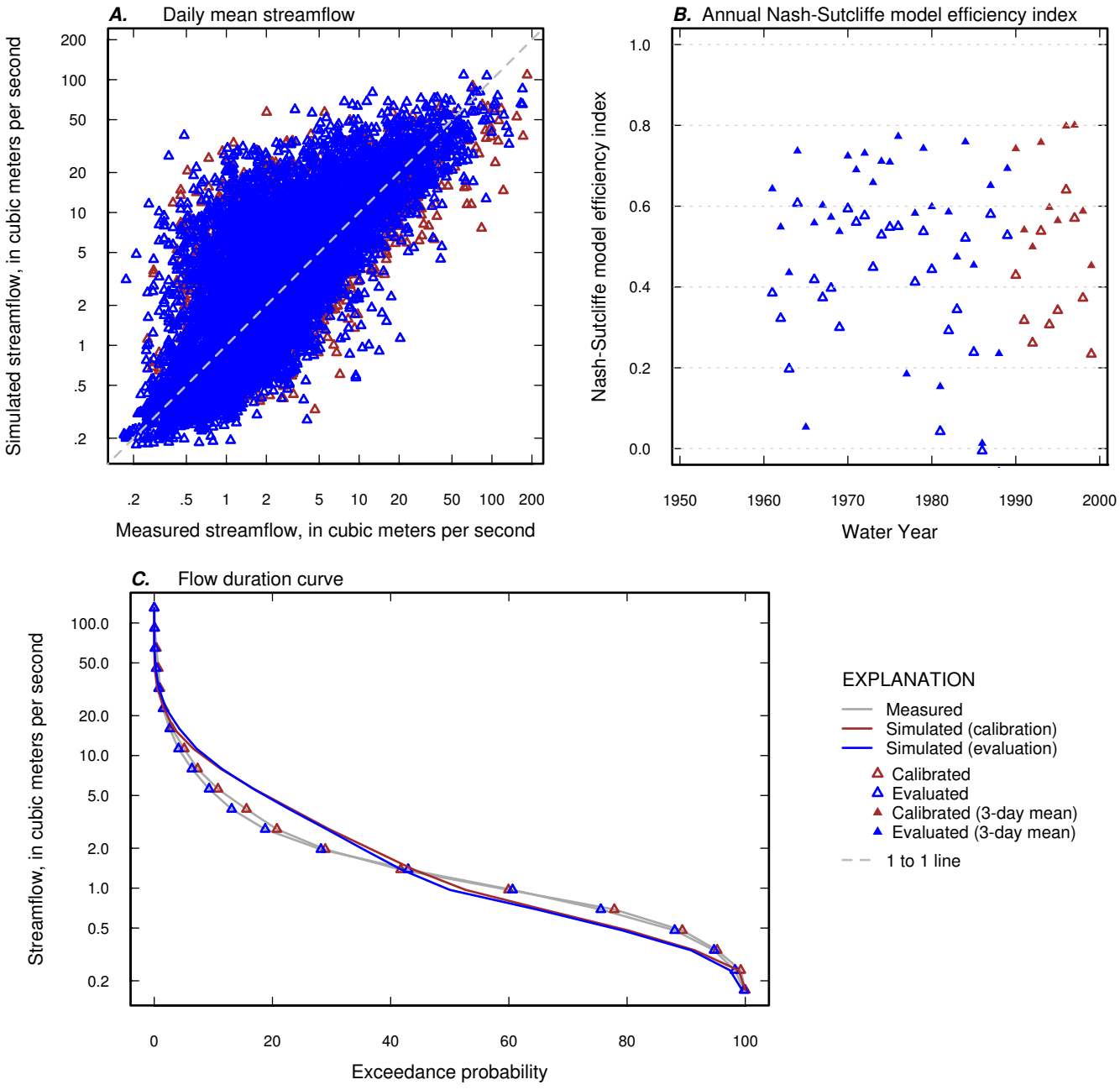

Figure 2–8. Measured and simulated daily streamflow, annual Nash-Sutcliffe Index, and flow duration curve for calibration and evaluation periods for USGS streamgage 02336300 (Peachtree Creek at Atlanta, GA).

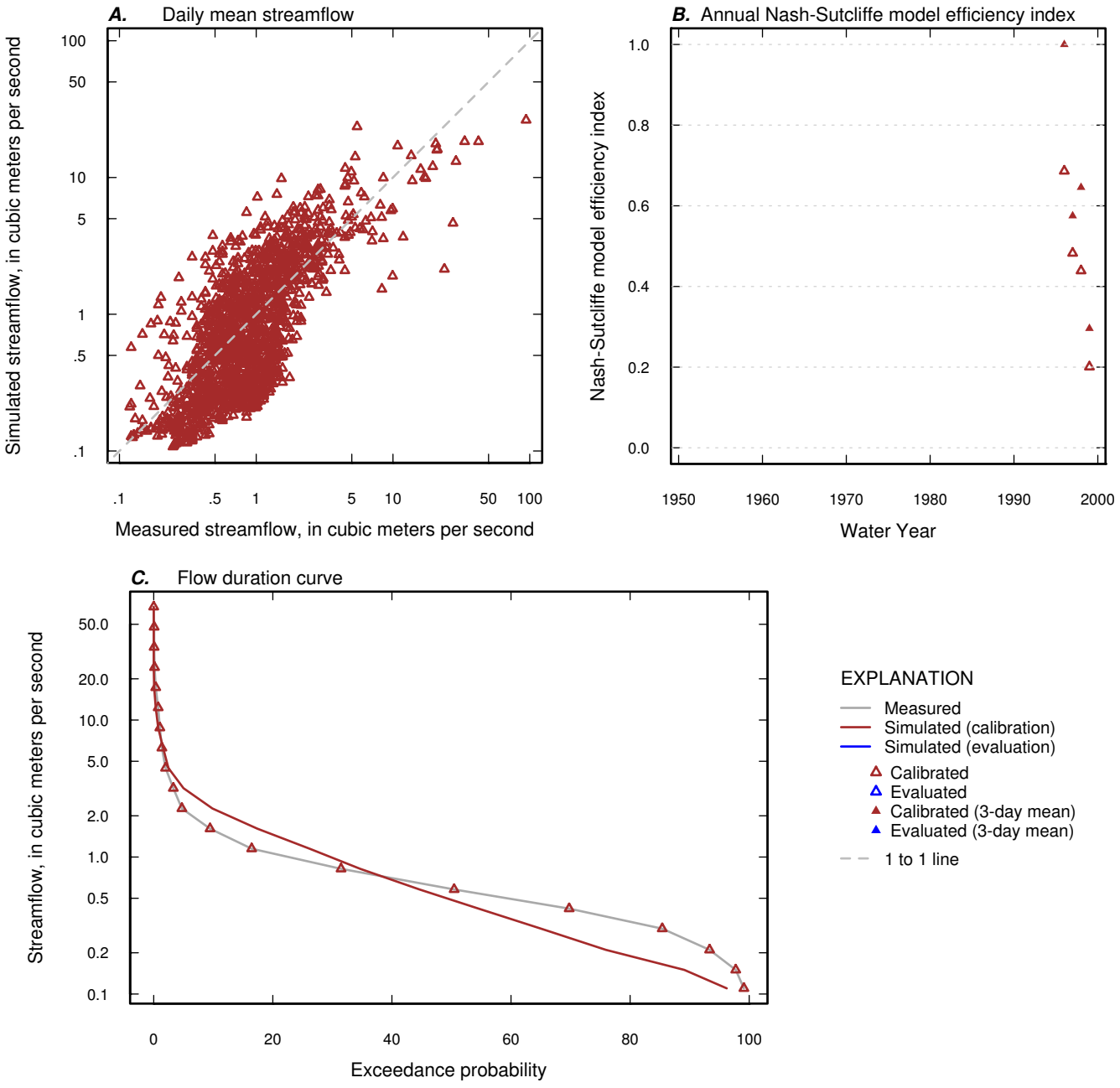

Figure 2–9. Measured and simulated daily streamflow, annual Nash-Sutcliffe Index, and flow duration curve for calibration and evaluation periods for USGS streamgage 02336635 (Nickajack Creek at US 78/278, near Mableton, GA).

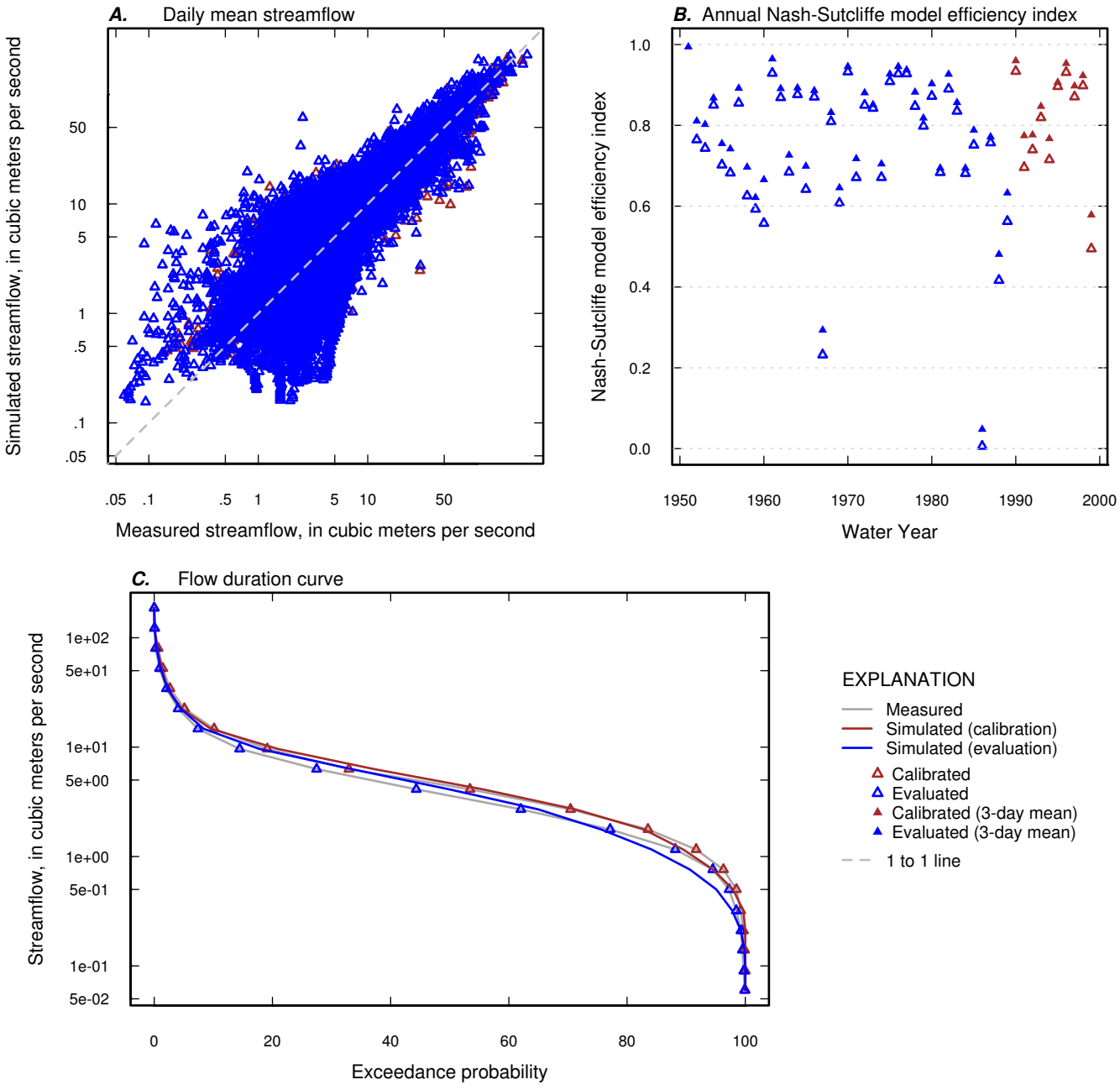

Figure 2–10. Measured and simulated daily streamflow, annual Nash-Sutcliffe Index, and flow duration curve for calibration and evaluation periods for USGS streamgage 02337000 (Sweetwater Creek near Austell, GA).

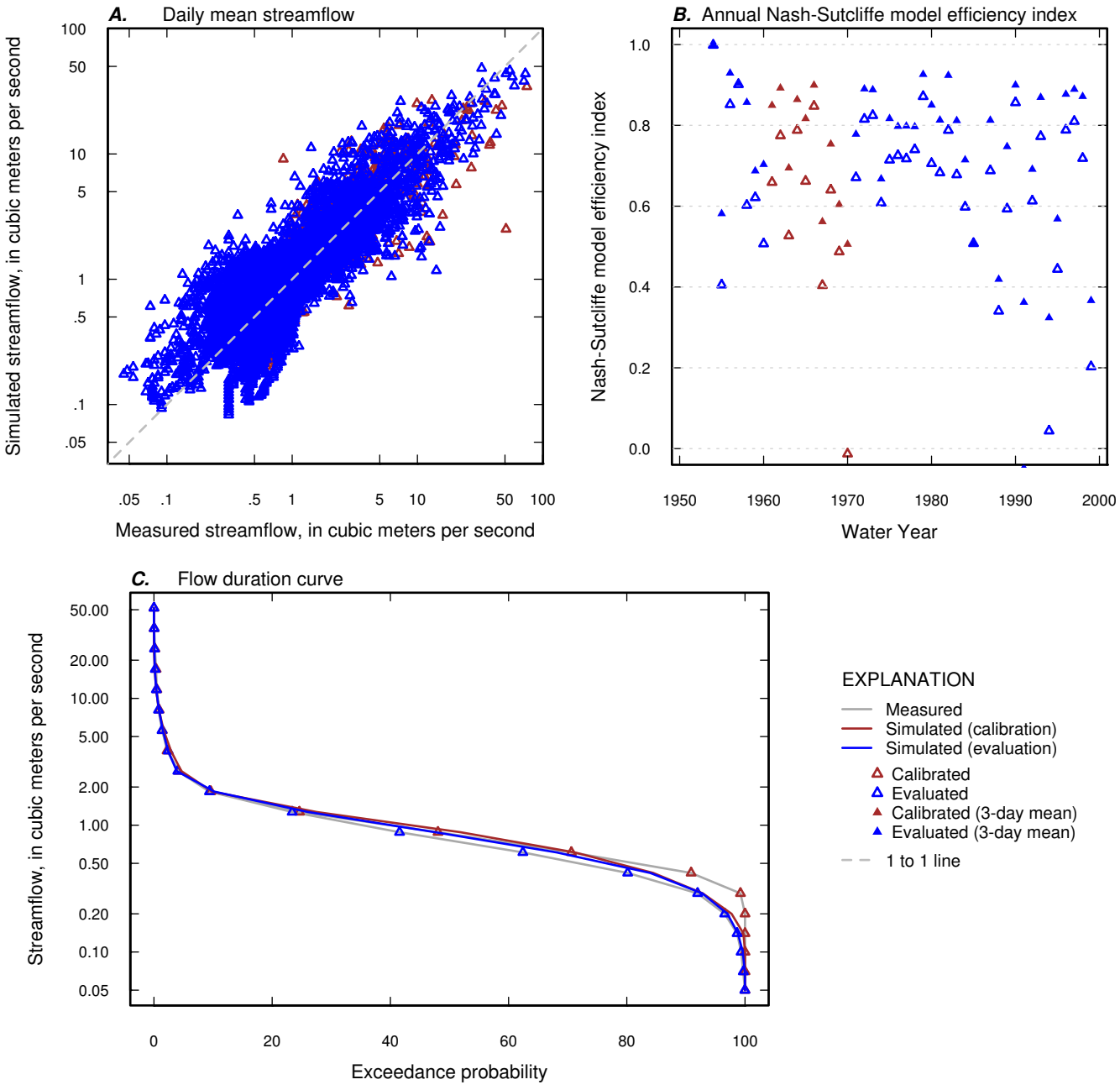

Figure 2–11. Measured and simulated daily streamflow, annual Nash-Sutcliffe Index, and flow duration curve for calibration and evaluation periods for USGS streamgage 02337500 (Snake Creek near Whitesburg, GA).

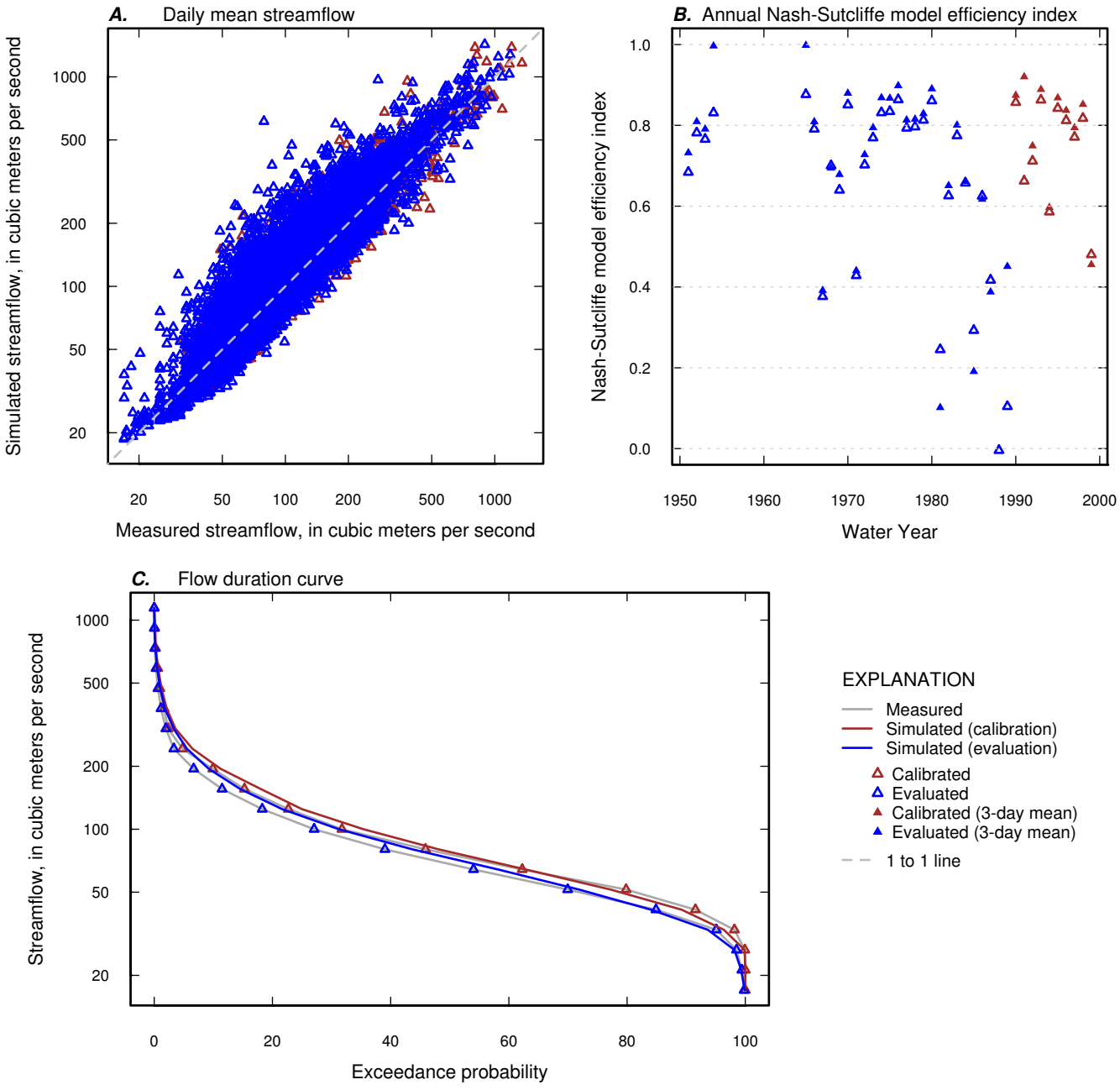

Figure 2–12. Measured and simulated daily streamflow, annual Nash-Sutcliffe Index, and flow duration curve for calibration and evaluation periods for USGS streamgage 02338000 (Chattahoochee River near Whitesburg, GA).

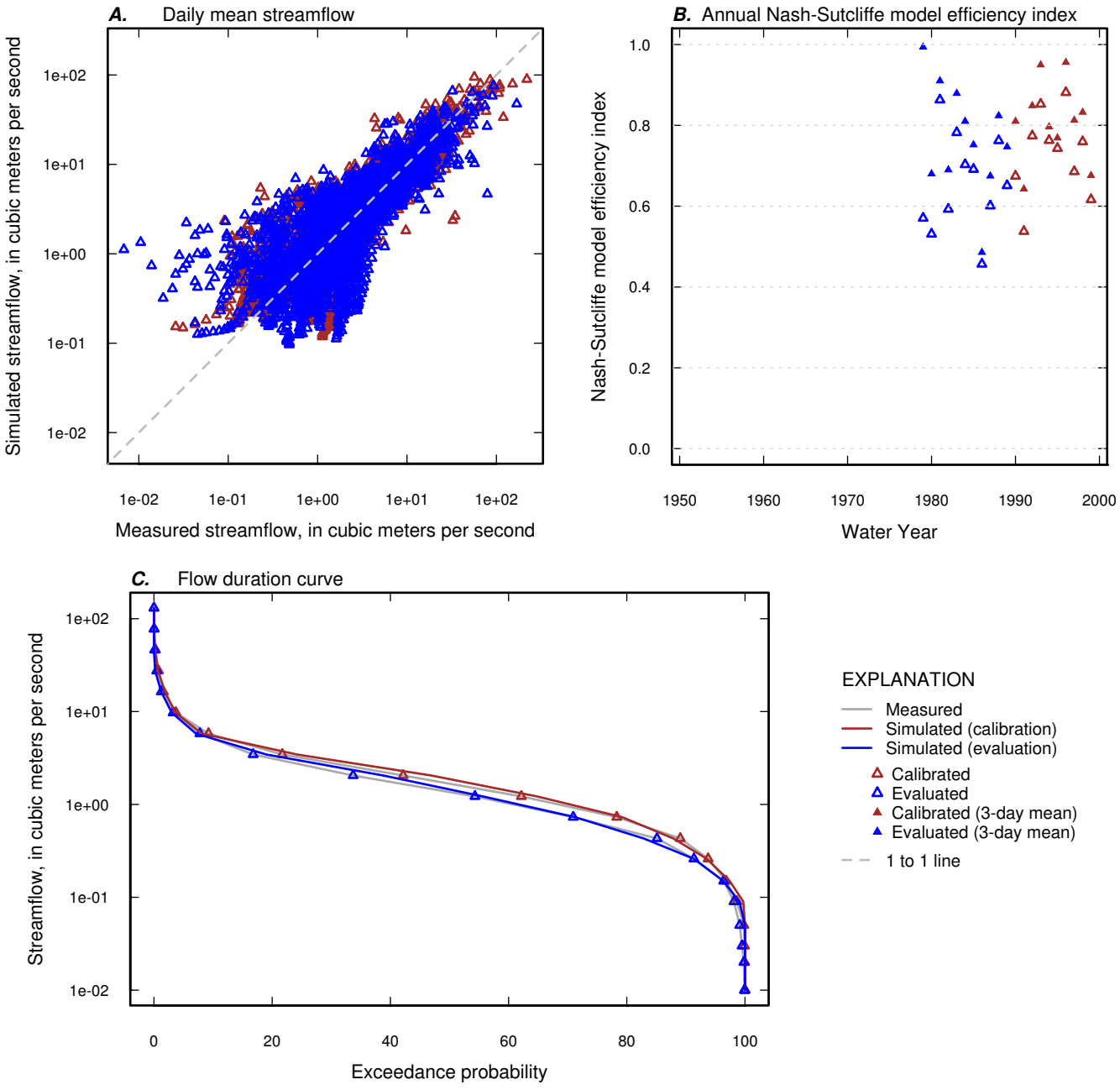

Figure 2–13. Measured and simulated daily streamflow, annual Nash-Sutcliffe Index, and flow duration curve for calibration and evaluation periods for USGS streamgage 02338660 (New River at GA 100, near Corinth, GA).

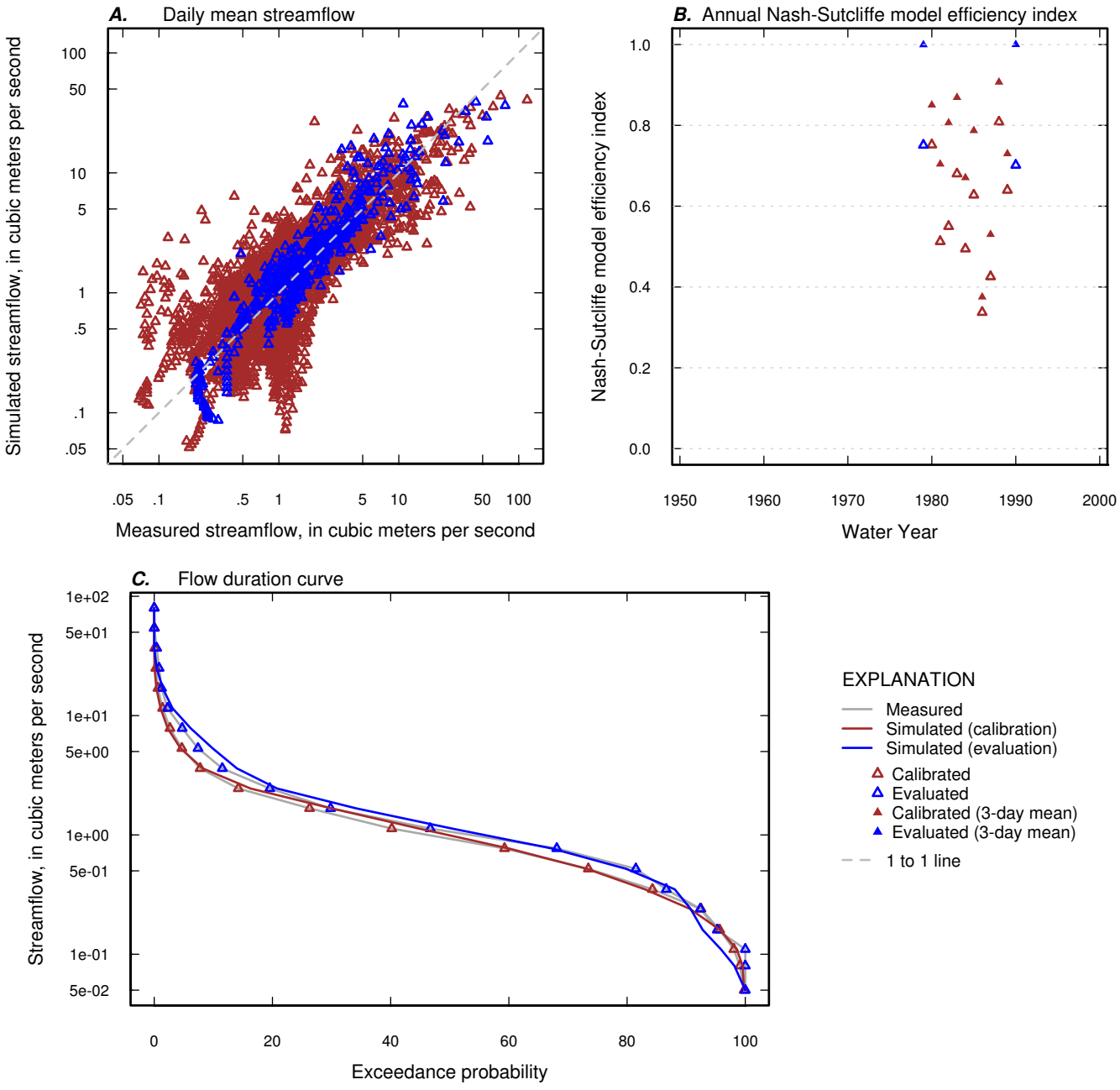

Figure 2–14. Measured and simulated daily streamflow, annual Nash-Sutcliffe Index, and flow duration curve for calibration and evaluation periods for USGS streamgage 02339225 (Wehadkee Creek below Rock Mills, AL).

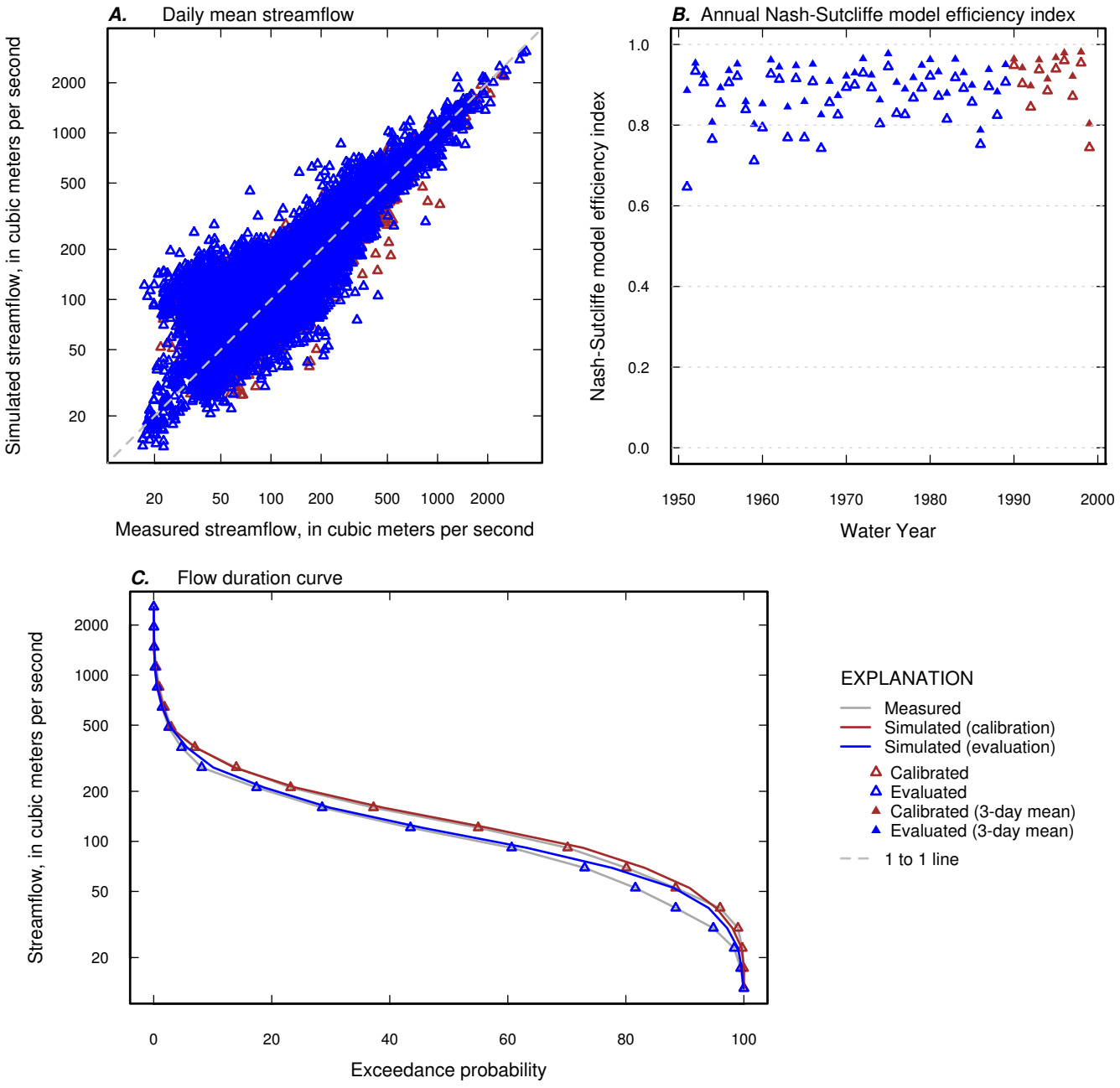

Figure 2–15. Measured and simulated daily streamflow, annual Nash-Sutcliffe Index, and flow duration curve for calibration and evaluation periods for USGS streamgage 02341505 (Chattahoochee River at US 280, near Columbus, GA).

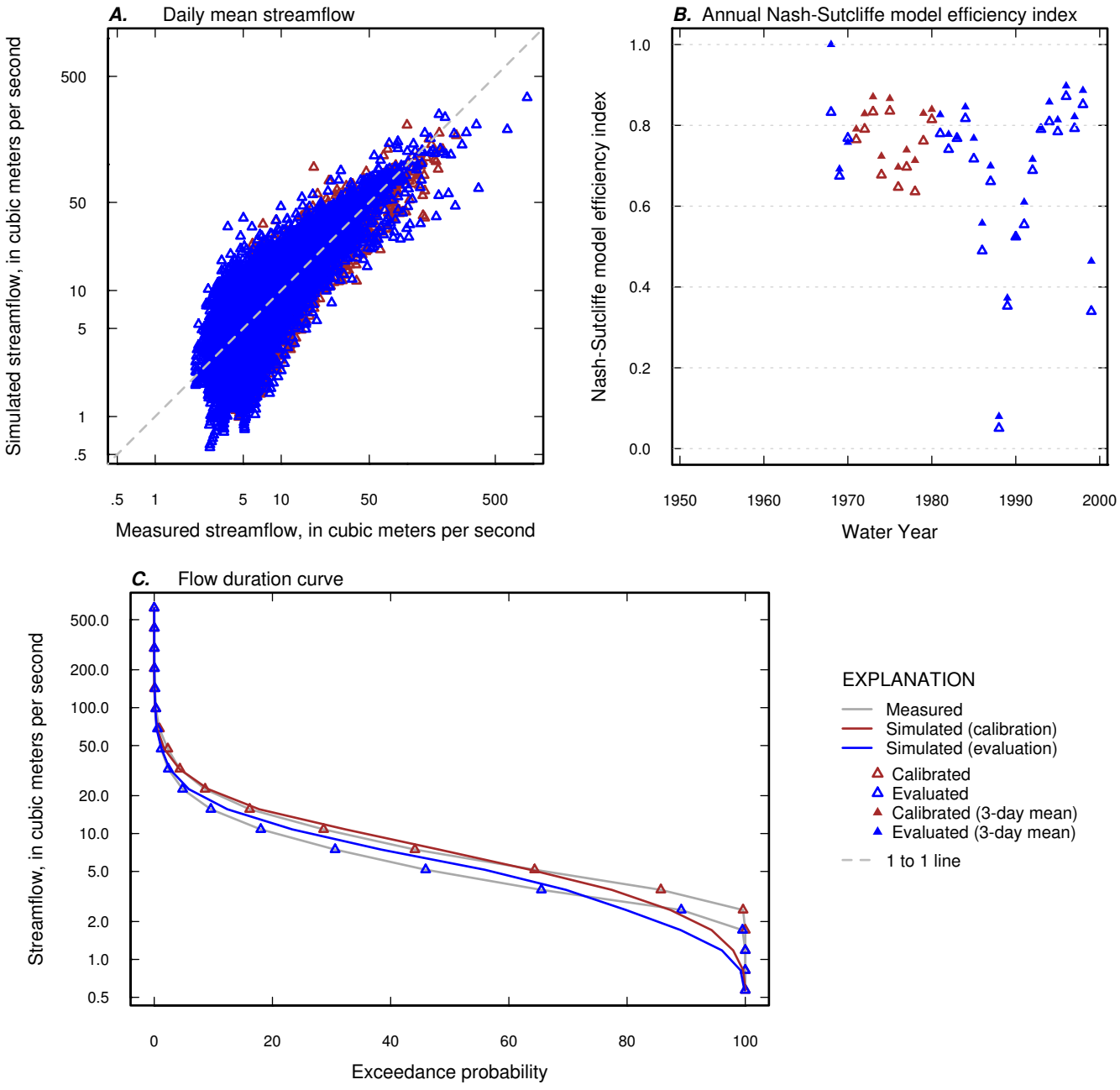

Figure 2–16. Measured and simulated daily streamflow, annual Nash-Sutcliffe Index, and flow duration curve for calibration and evaluation periods for USGS streamgage 02341800 (Upatoi Creek near Columbus, GA).

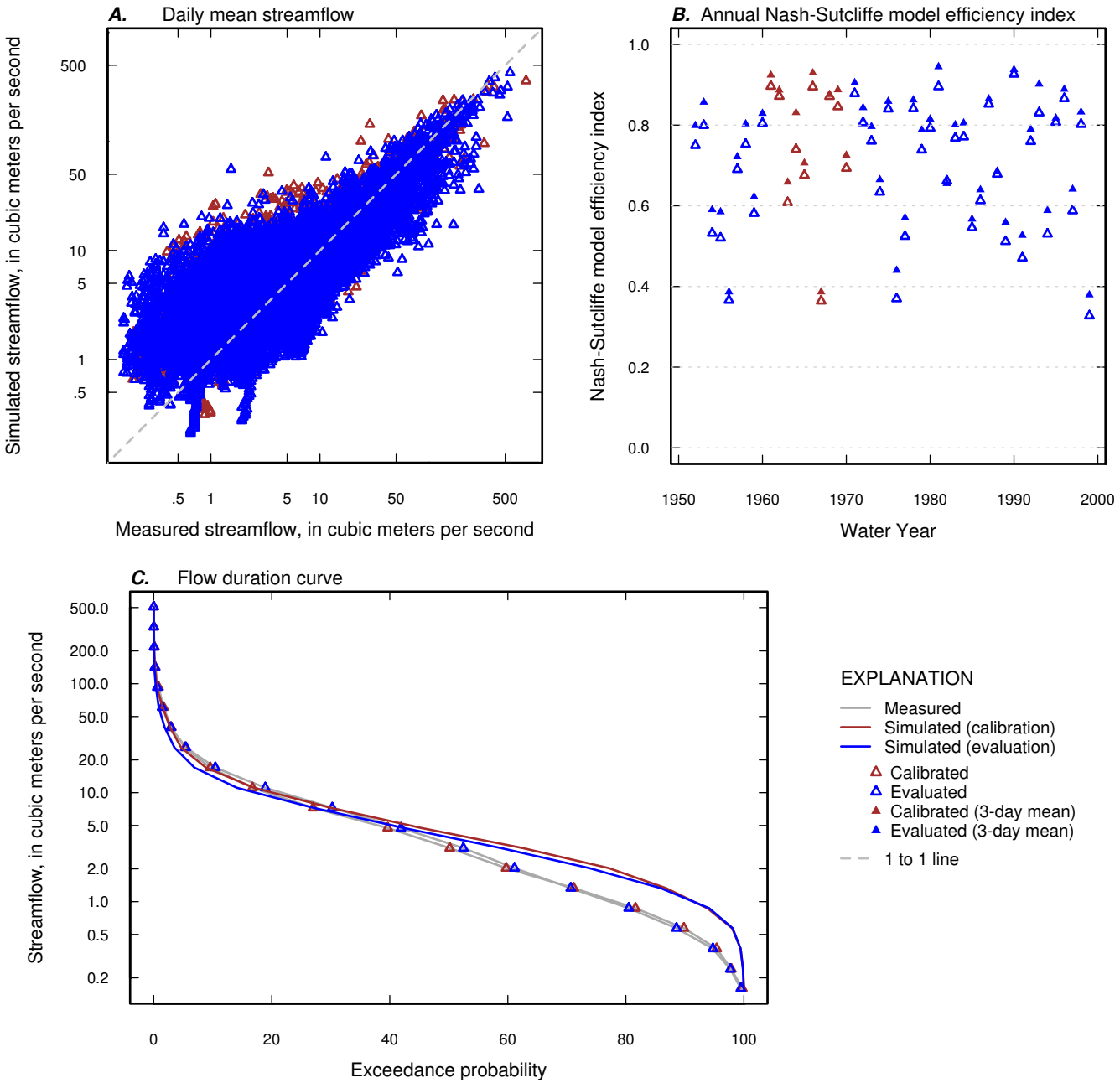

Figure 2–17. Measured and simulated daily streamflow, annual Nash-Sutcliffe Index, and flow duration curve for calibration and evaluation periods for USGS streamgage 02342500 (Uchee Creek near Fort Mitchell, AL).

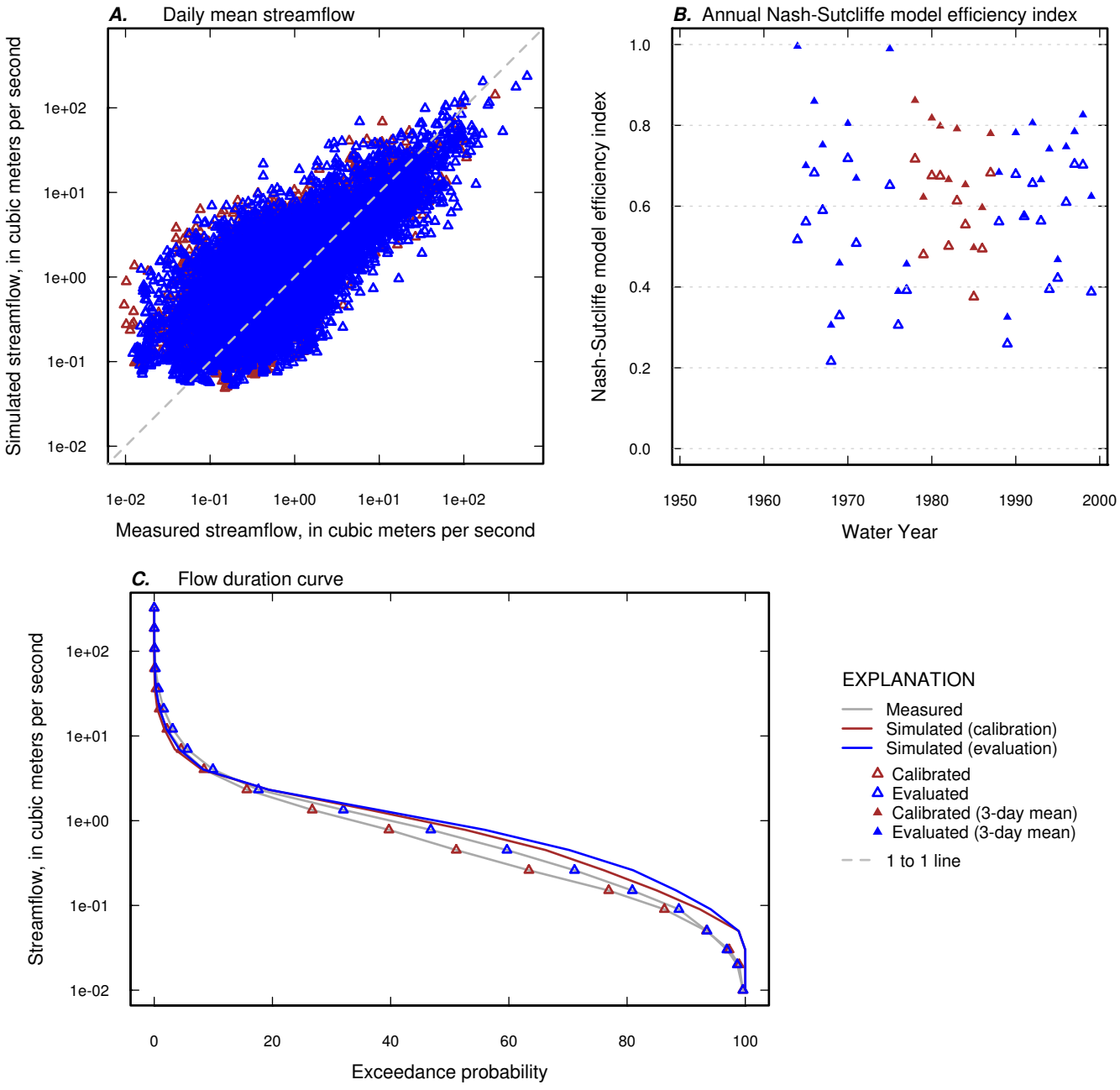

Figure 2–18. Measured and simulated daily streamflow, annual Nash-Sutcliffe Index, and flow duration curve for calibration and evaluation periods for USGS streamgage 02342933 (South Fork Cowikee Creek near Batesville, AL).

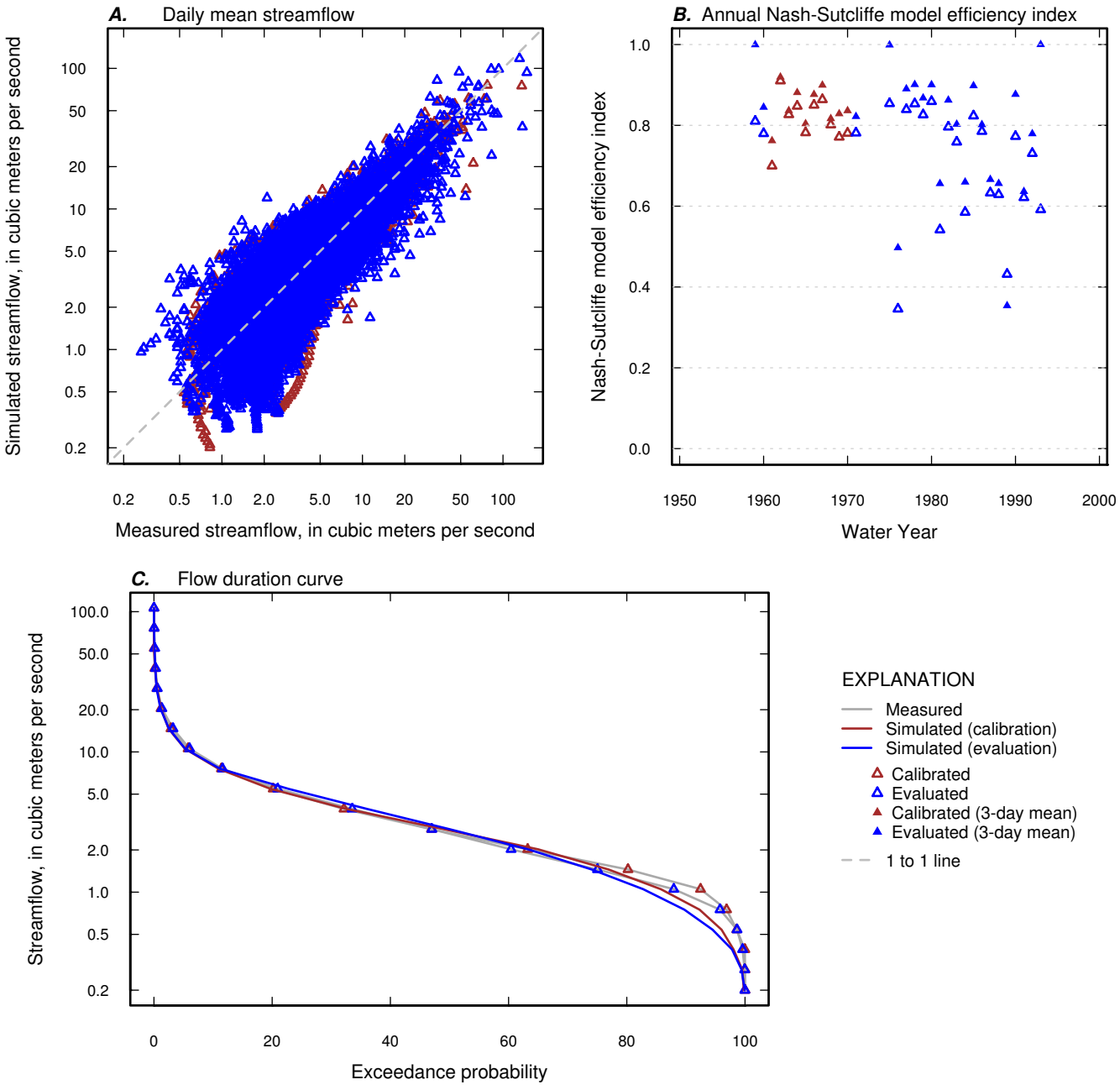

Figure 2–19. Measured and simulated daily streamflow, annual Nash-Sutcliffe Index, and flow duration curve for calibration and evaluation periods for USGS streamgage 02343300 (Abbie Creek near Haleburg, AL).

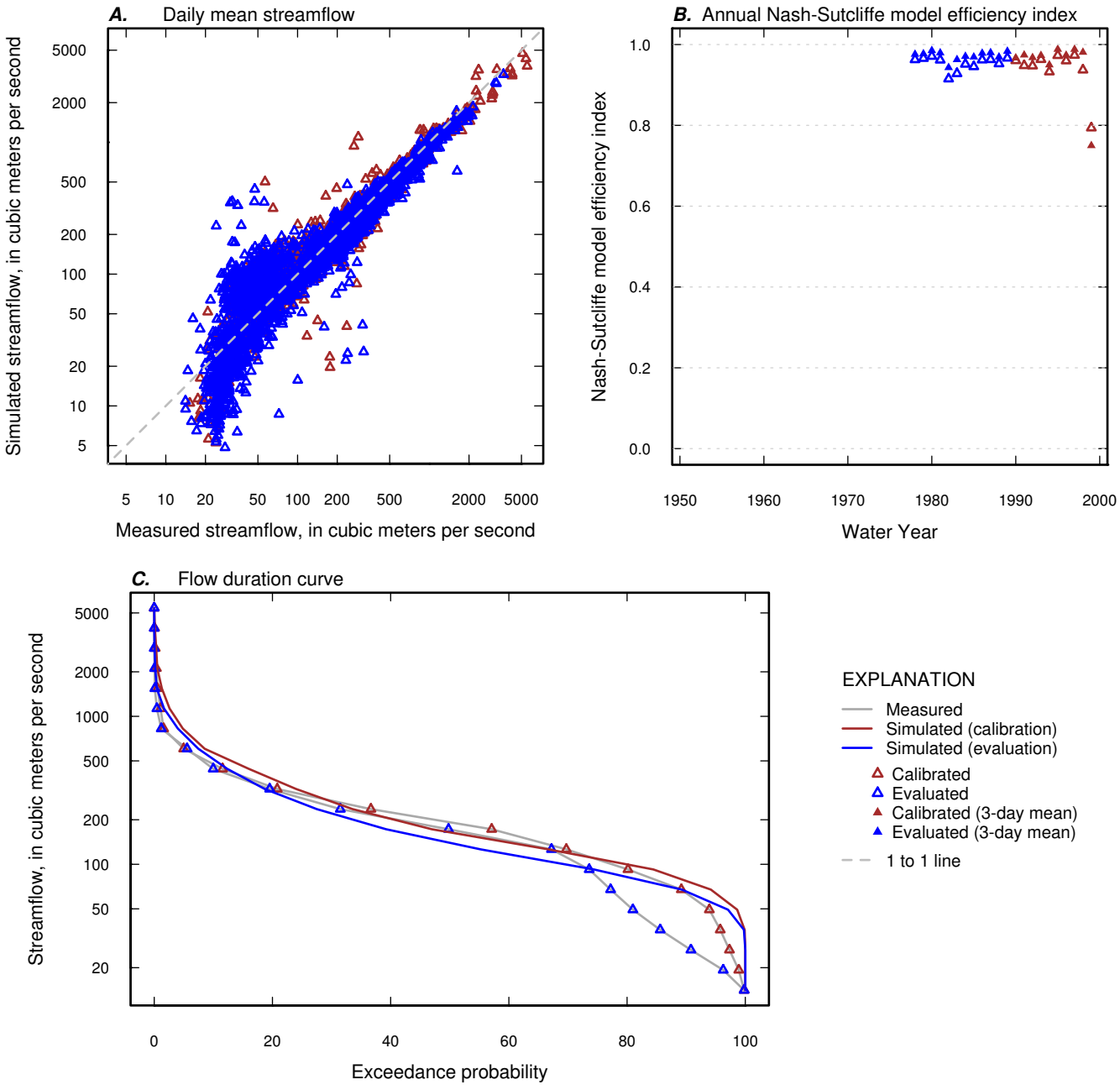

Figure 2–20. Measured and simulated daily streamflow, annual Nash-Sutcliffe Index, and flow duration curve for calibration and evaluation periods for USGS streamgage 02343801 (Chattahoochee River near Columbia, AL).

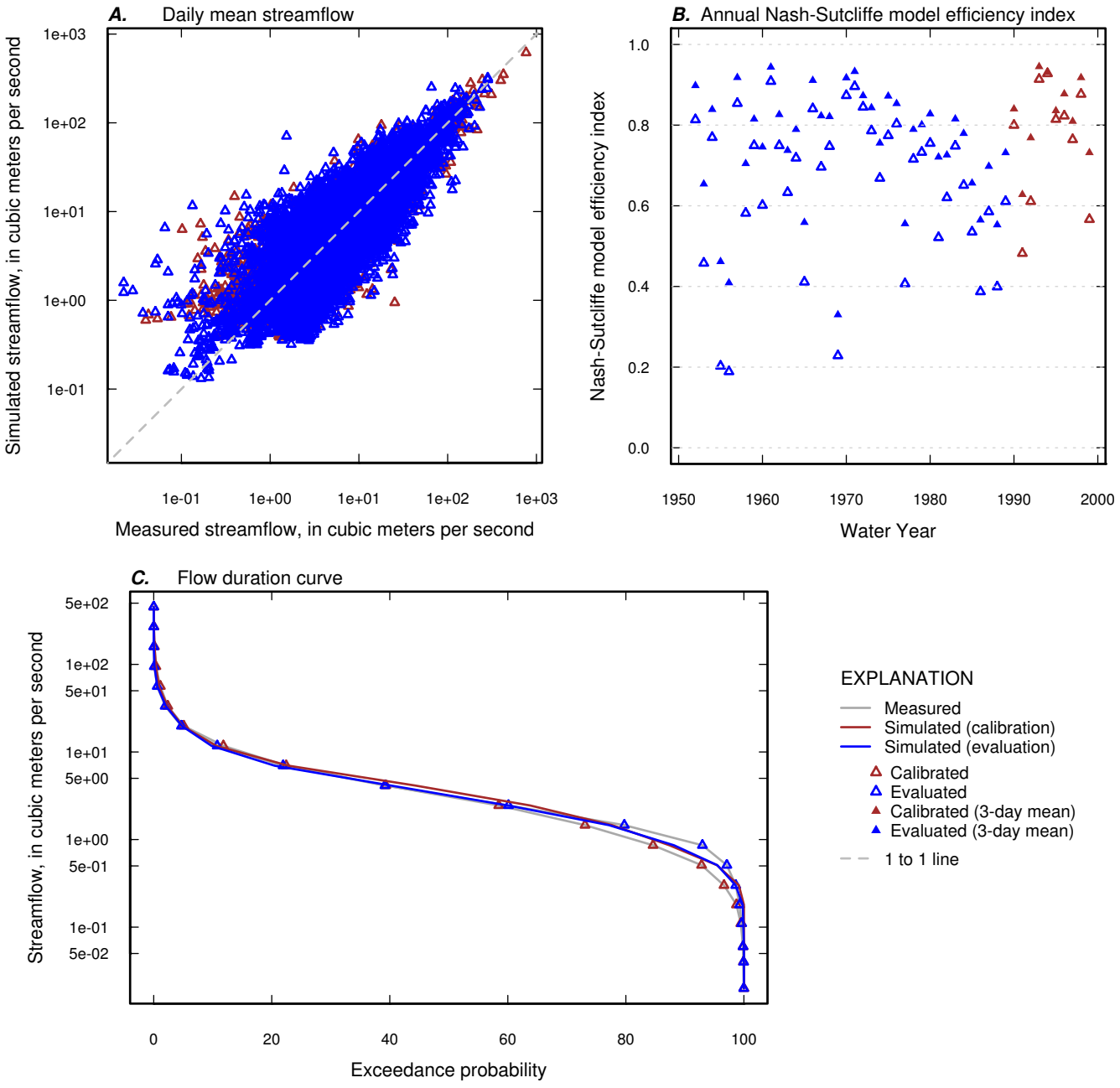

Figure 2–21. Measured and simulated daily streamflow, annual Nash-Sutcliffe Index, and flow duration curve for calibration and evaluation periods for USGS streamgage 02344500 (Flint River near Griffin, GA).

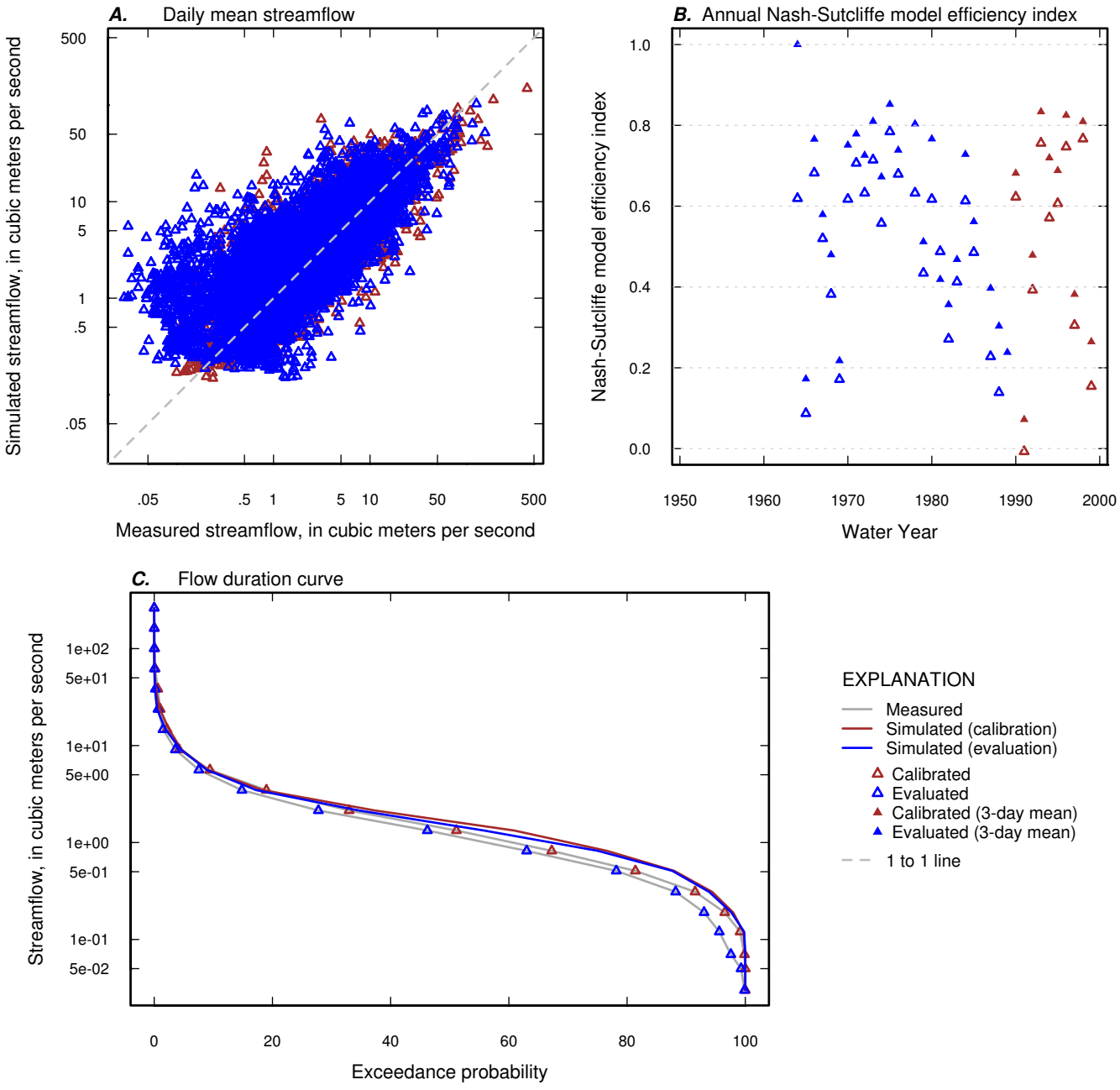

Figure 2–22. Measured and simulated daily streamflow, annual Nash-Sutcliffe Index, and flow duration curve for calibration and evaluation periods for USGS streamgage 02344700 (Line Creek near Senoia, GA).

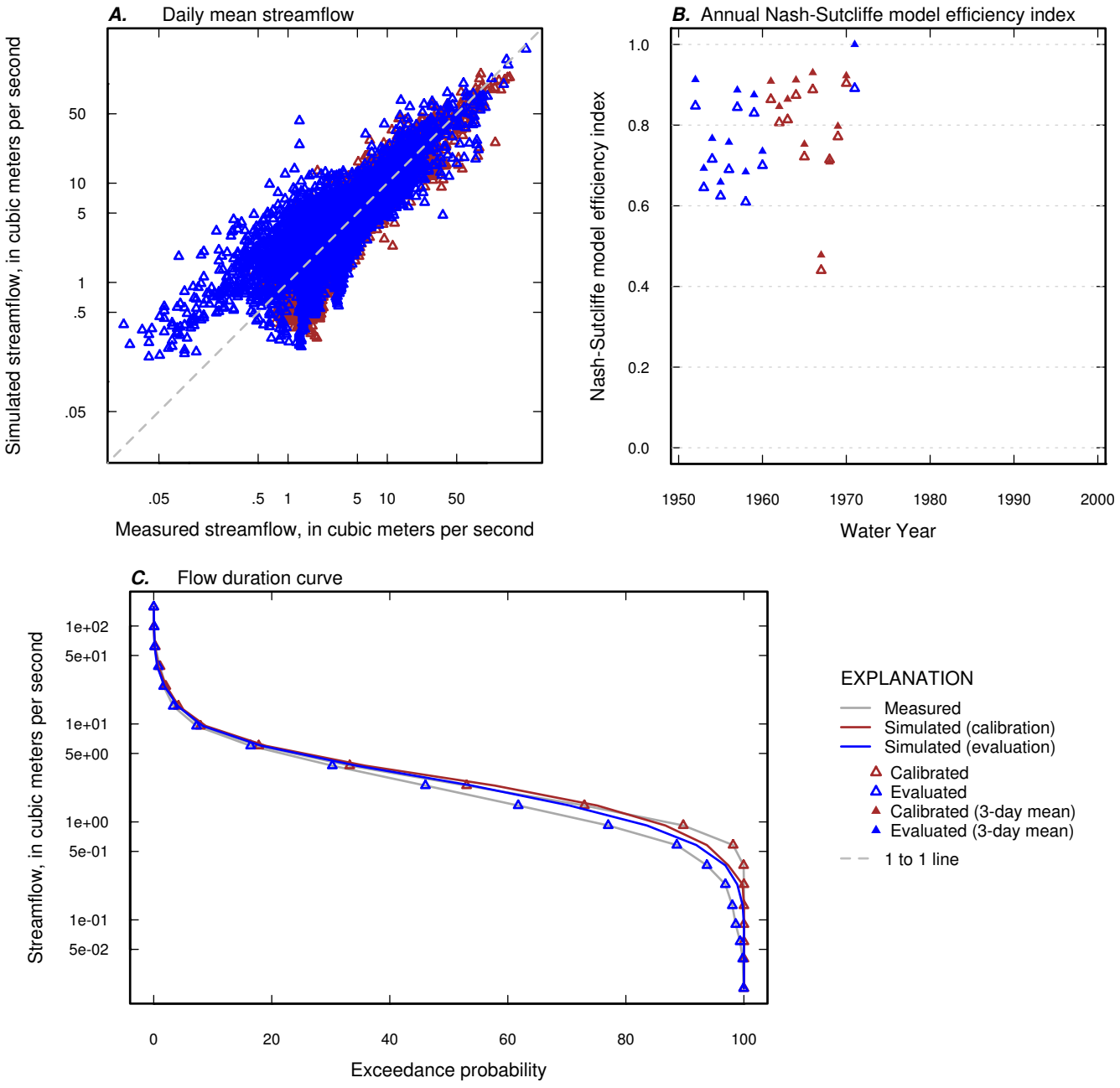

Figure 2–23. Measured and simulated daily streamflow, annual Nash-Sutcliffe Index, and flow duration curve for calibration and evaluation periods for USGS streamgage 02346500 (Potato Creek near Thomaston, GA).

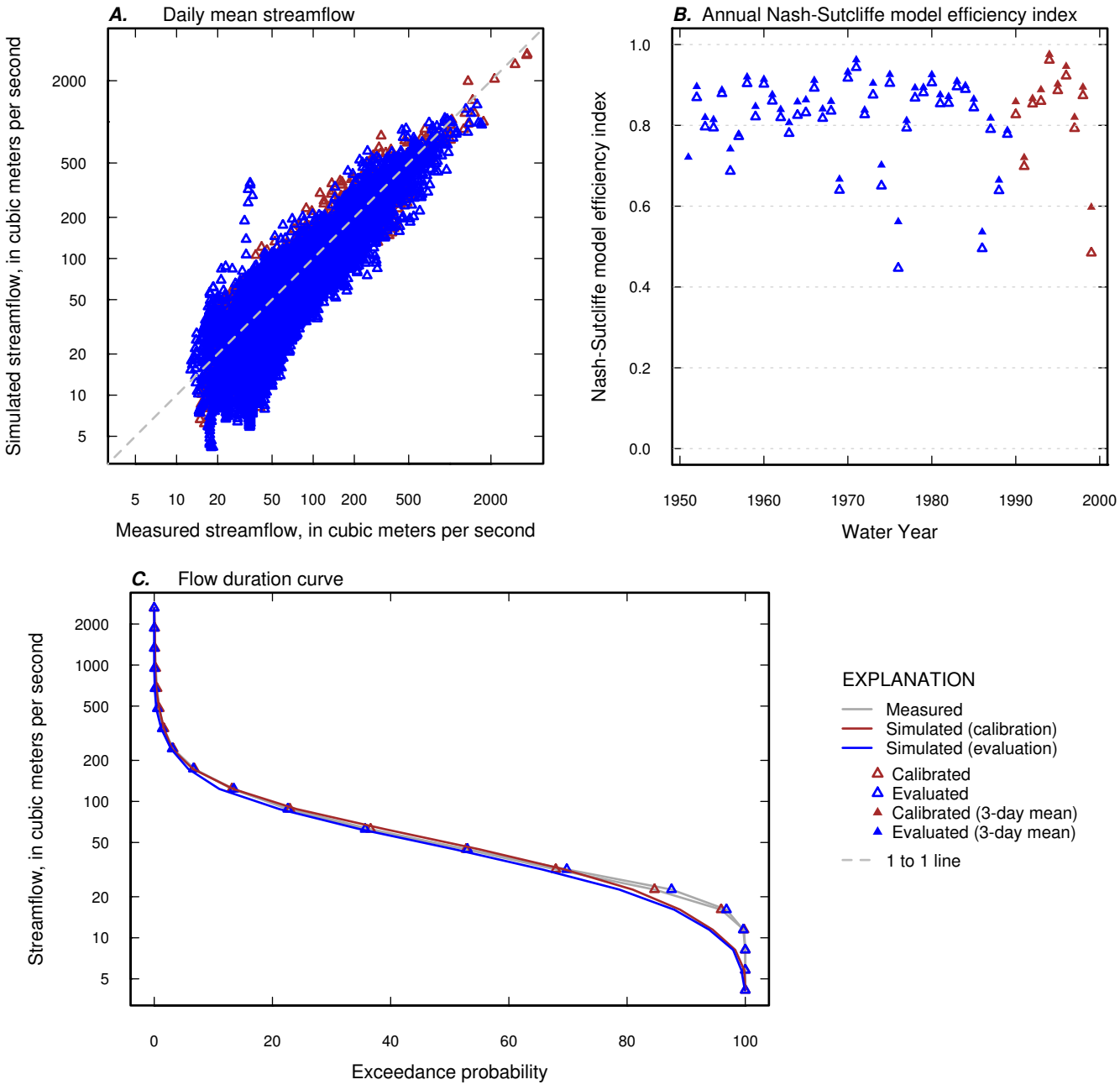

Figure 2–24. Measured and simulated daily streamflow, annual Nash-Sutcliffe Index, and flow duration curve for calibration and evaluation periods for USGS streamgage 02349605 (Flint River at GA 26, near Montezuma, GA).

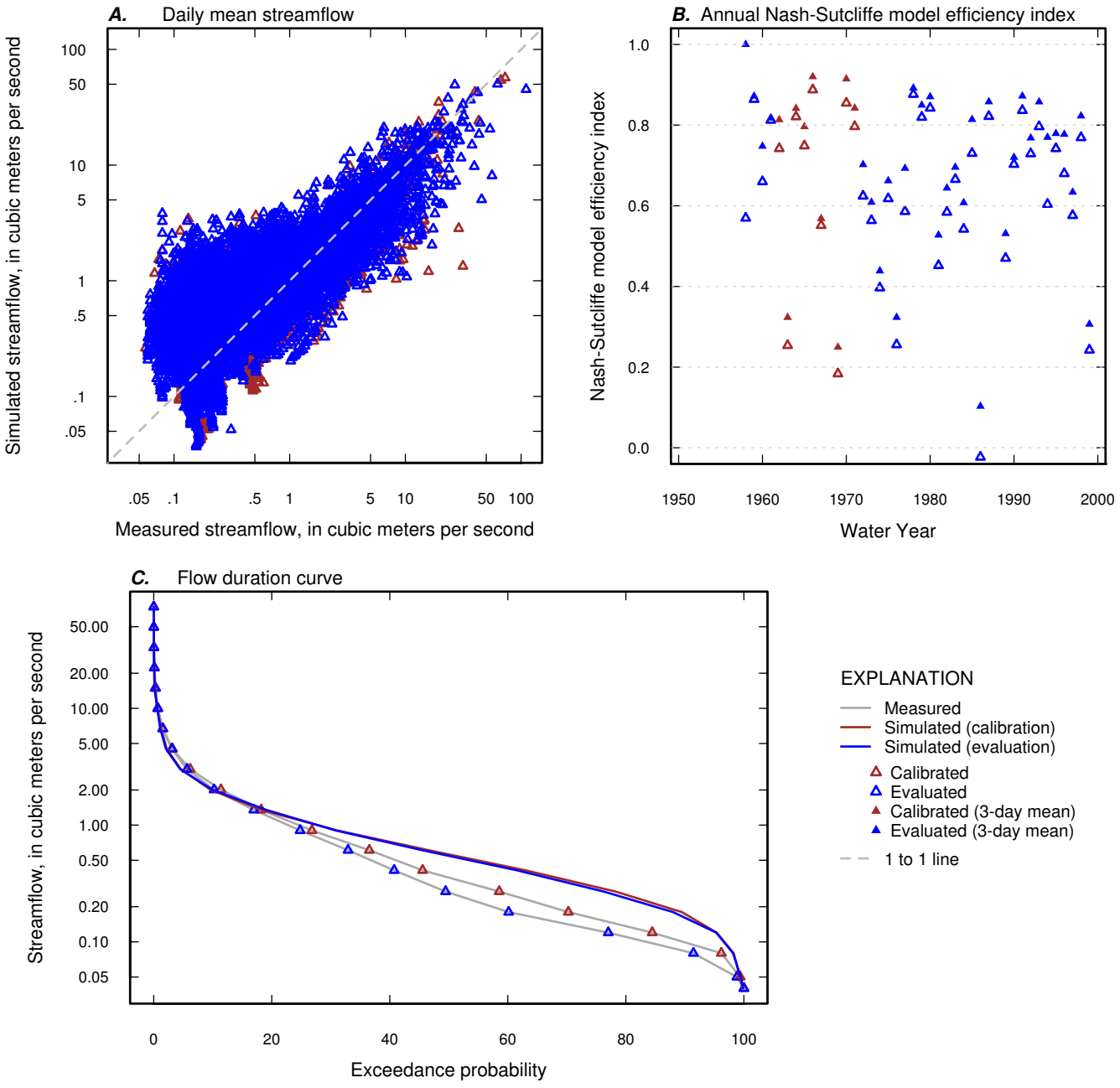

Figure 2–25. Measured and simulated daily streamflow, annual Nash-Sutcliffe Index, and flow duration curve for calibration and evaluation periods for USGS streamgage 02349900 (Turkey Creek at Byromville, GA).

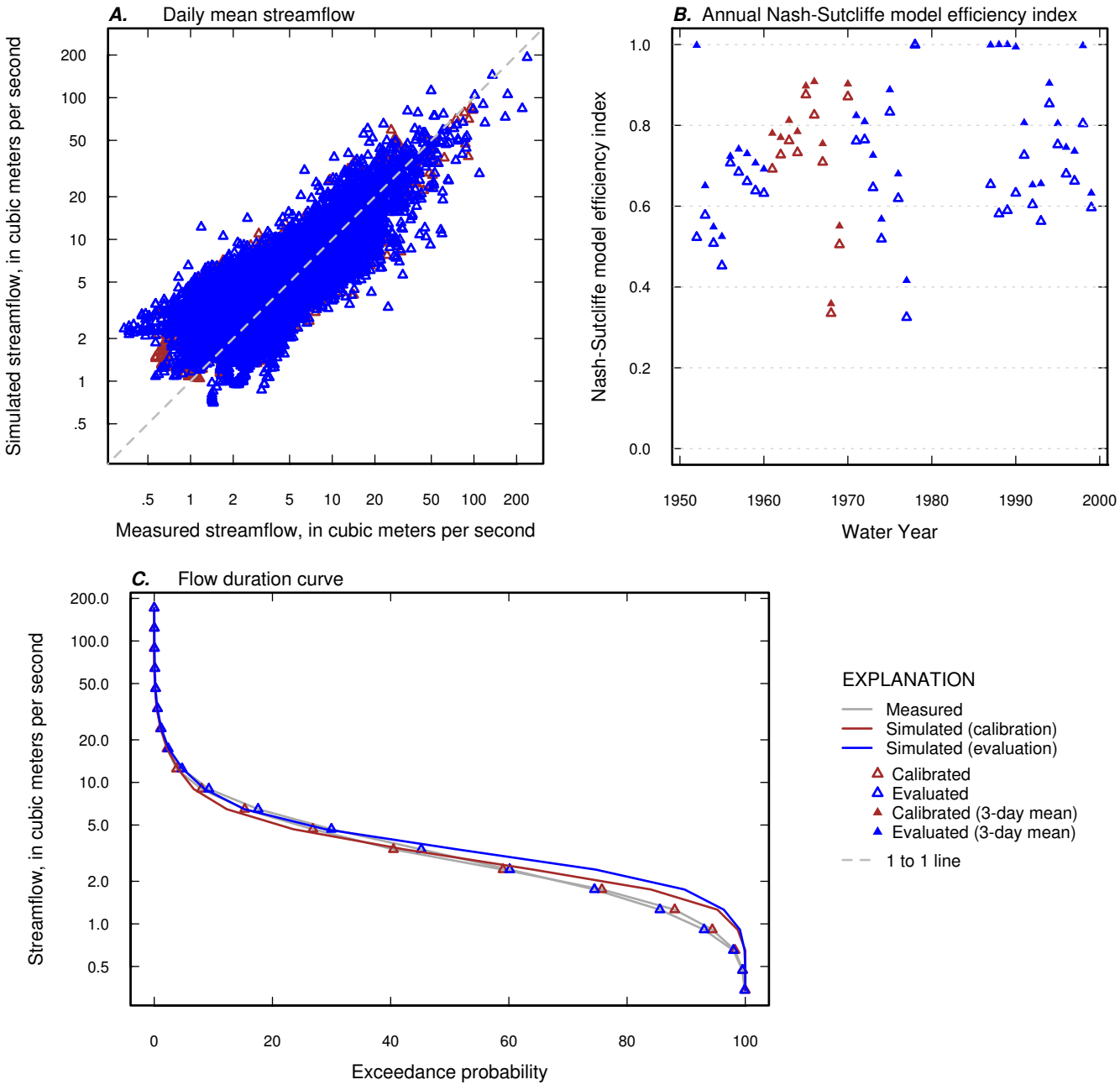

Figure 2–26. Measured and simulated daily streamflow, annual Nash-Sutcliffe Index, and flow duration curve for calibration and evaluation periods for USGS streamgage 02350600 (Kinchafoonee Creek at Preston, GA).

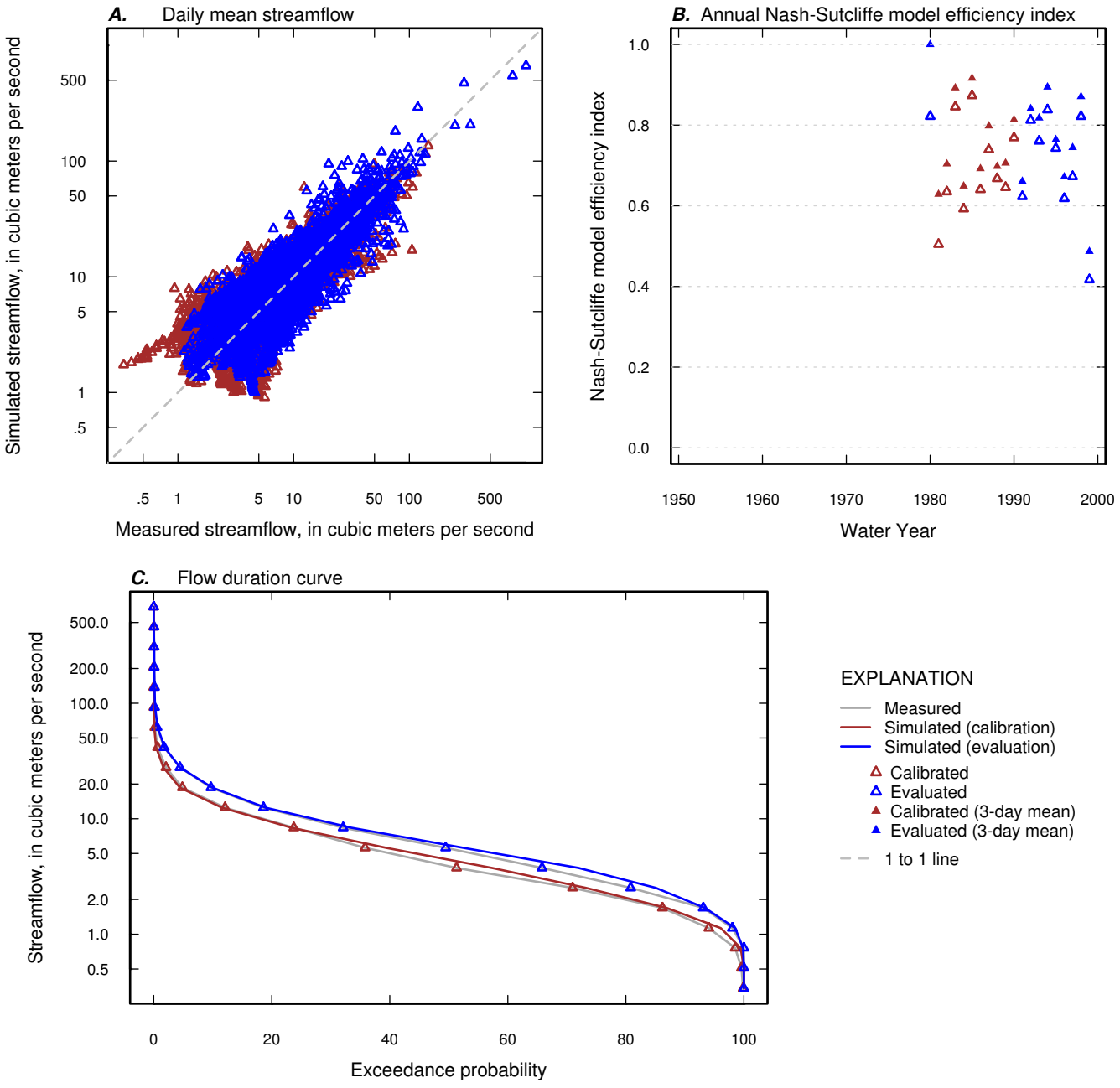

Figure 2–27. Measured and simulated daily streamflow, annual Nash-Sutcliffe Index, and flow duration curve for calibration and evaluation periods for USGS streamgage 02351890 (Muckalee Creek at GA 195, near Leesburg, GA).

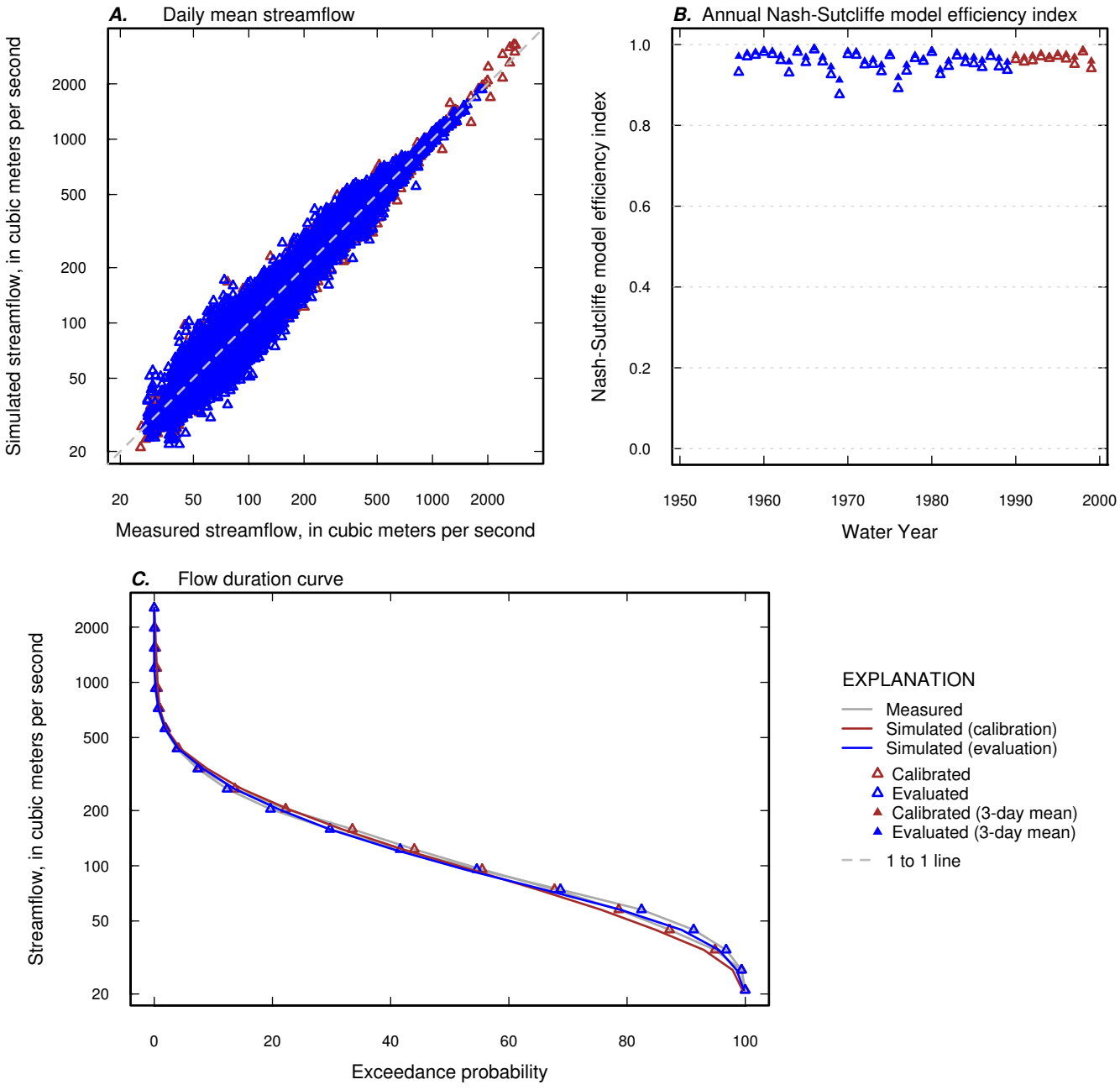

Figure 2–28. Measured and simulated daily streamflow, annual Nash-Sutcliffe Index, and flow duration curve for calibration and evaluation periods for USGS streamgage 02353000 (Flint River at Newton, GA).

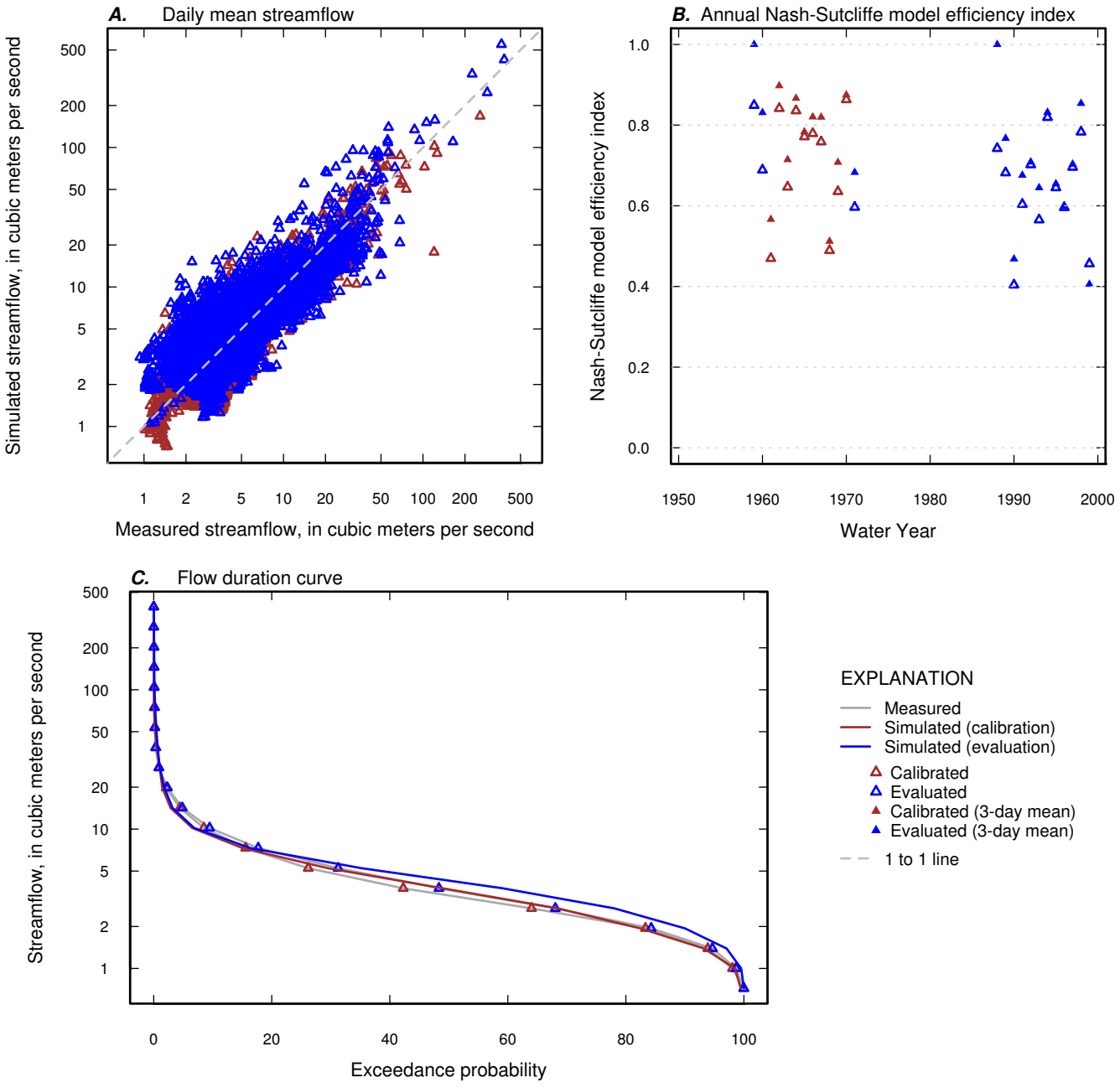

Figure 2–29. Measured and simulated daily streamflow, annual Nash-Sutcliffe Index, and flow duration curve for calibration and evaluation periods for USGS streamgage 02353400 (Pachitla Creek near Edison, GA).

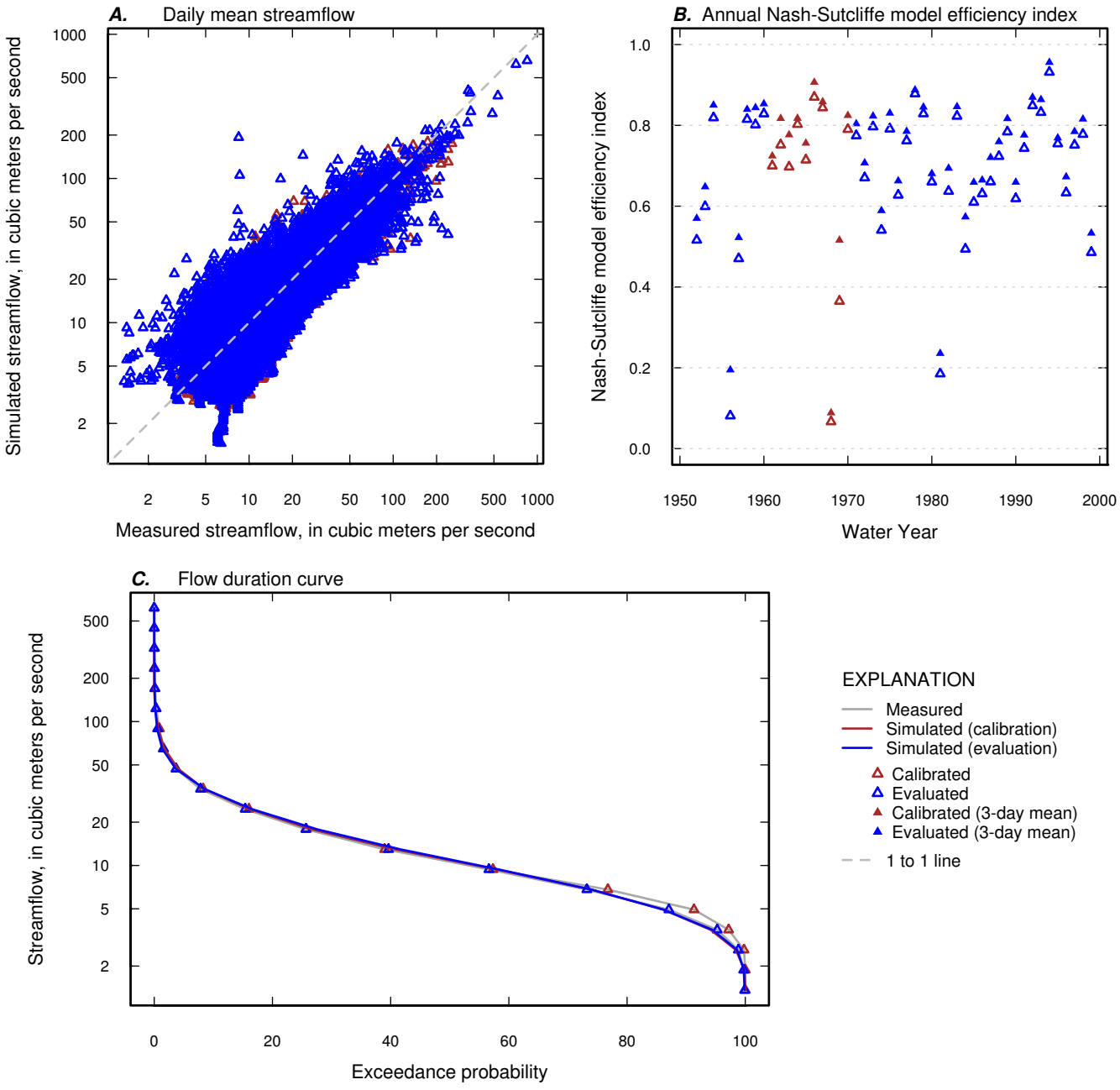

Figure 2–30. Measured and simulated daily streamflow, annual Nash-Sutcliffe Index, and flow duration curve for calibration and evaluation periods for USGS streamgage 02353500 (Ichawaynochaway Creek at Milford, GA).

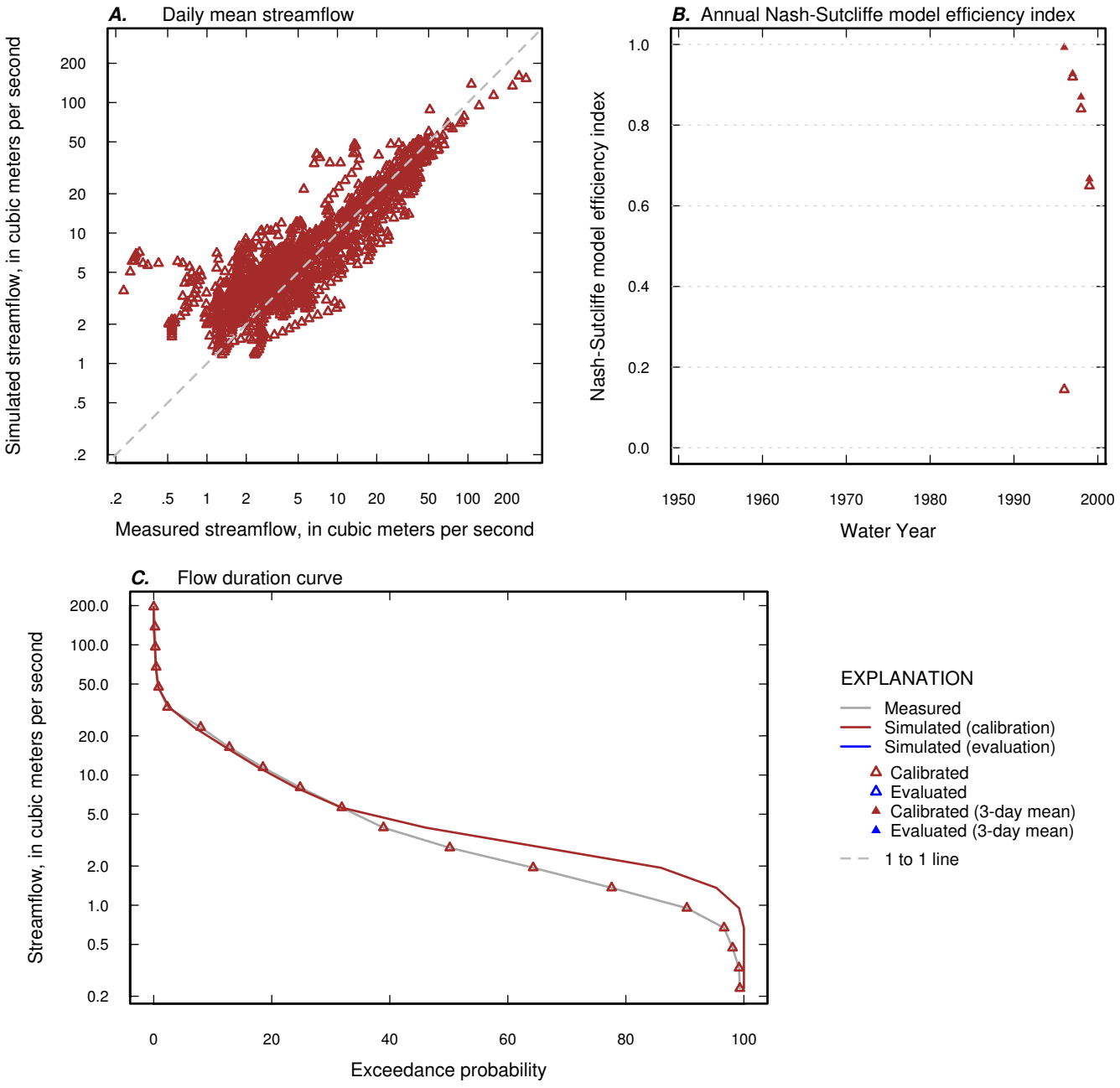

Figure 2–31. Measured and simulated daily streamflow, annual Nash-Sutcliffe Index, and flow duration curve for calibration and evaluation periods for USGS streamgage 02354500 (Chickasawhatchee Creek at Elmodel, GA).

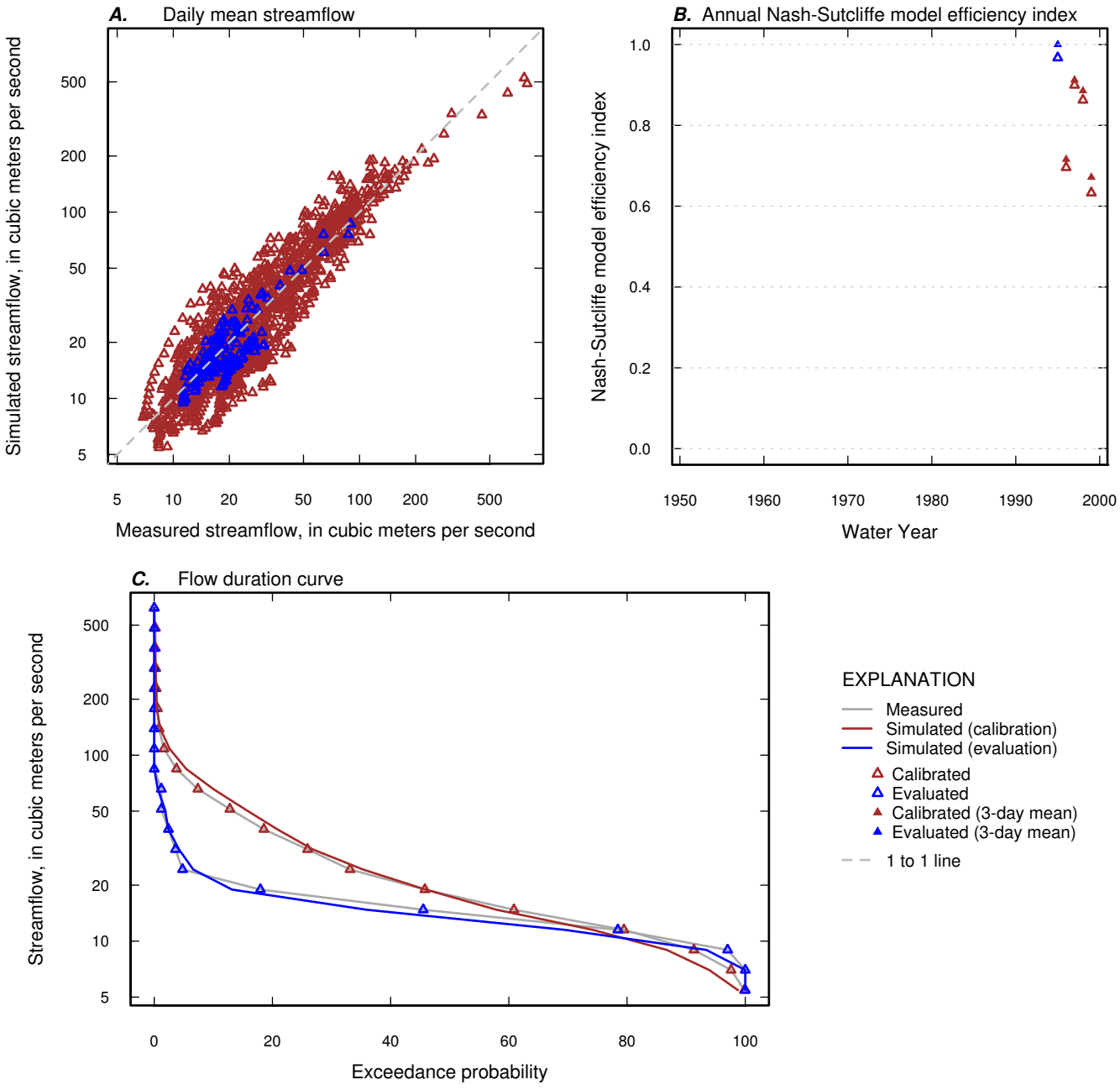

Figure 2–32. Measured and simulated daily streamflow, annual Nash-Sutcliffe Index, and flow duration curve for calibration and evaluation periods for USGS streamgage 02354800 (Ichawaynochaway Creek near Elmodel, GA).

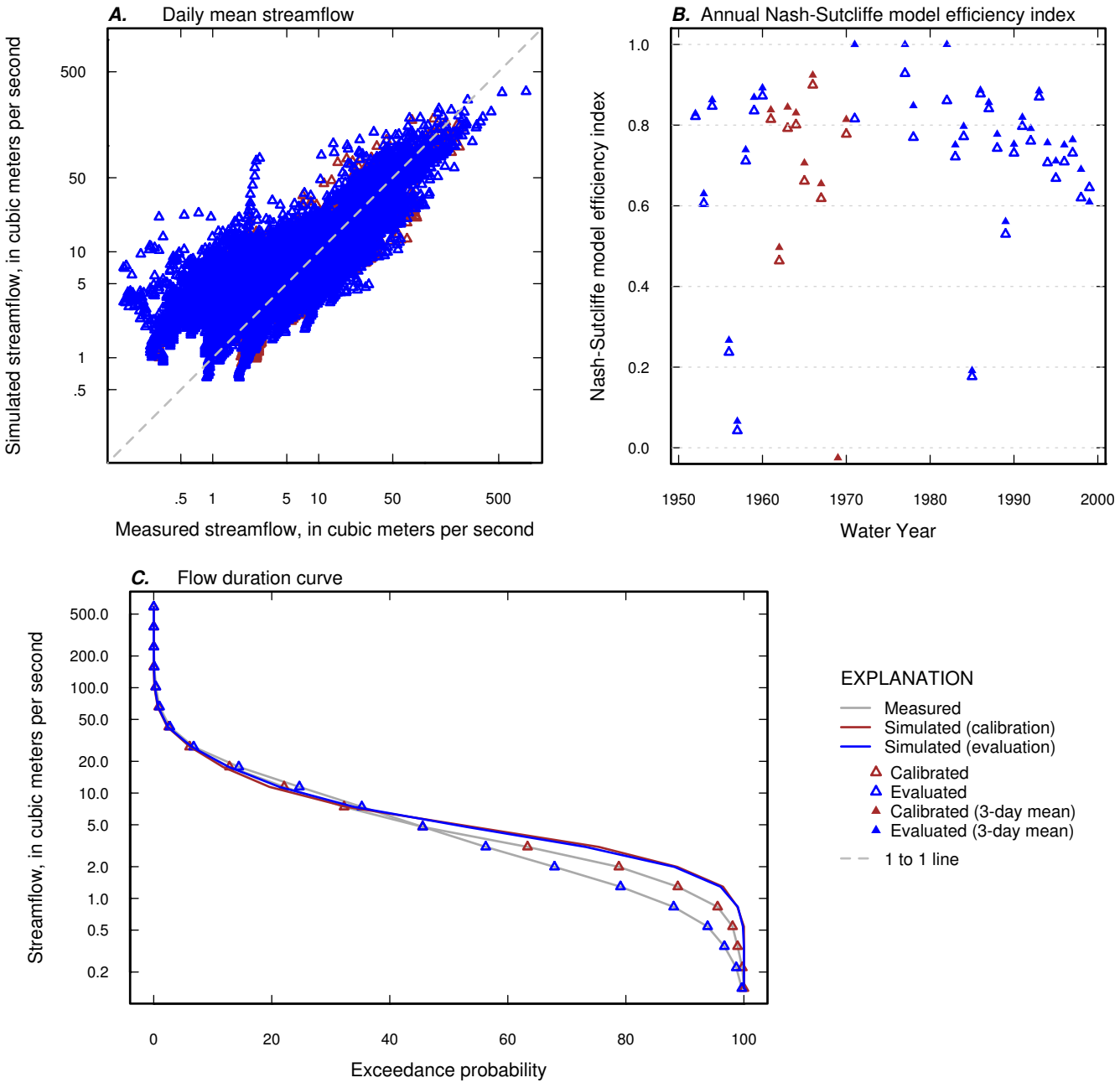

Figure 2–33. Measured and simulated daily streamflow, annual Nash-Sutcliffe Index, and flow duration curve for calibration and evaluation periods for USGS streamgage 02357000 (Spring Creek near Iron City, GA).

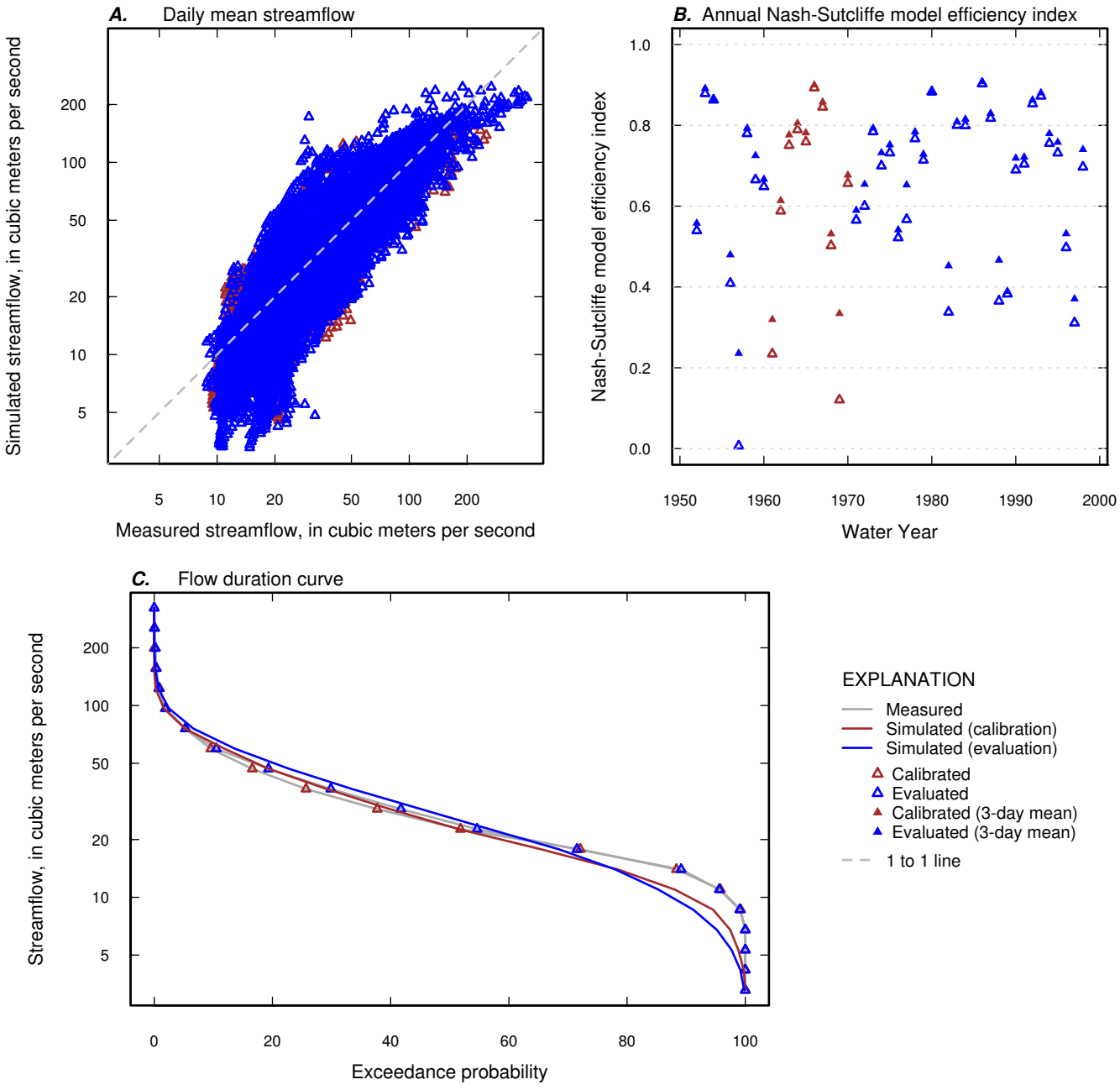

Figure 2–34. Measured and simulated daily streamflow, annual Nash-Sutcliffe Index, and flow duration curve for calibration and evaluation periods for USGS streamgage 02359000 (Chipola River near Altha, FL).

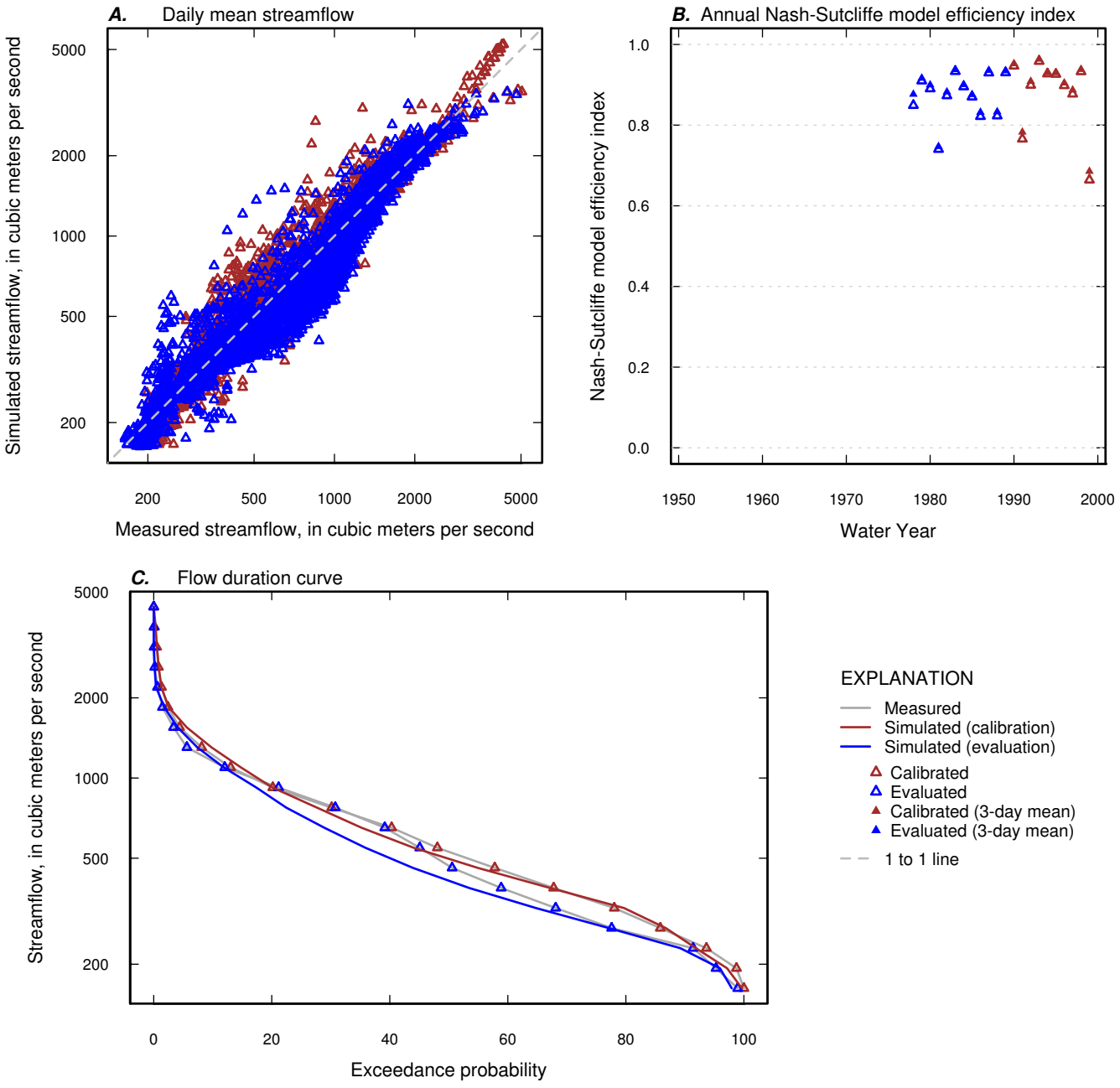

Figure 2–35. Measured and simulated daily streamflow, annual Nash-Sutcliffe Index, and flow duration curve for calibration and evaluation periods for USGS streamgage 02359170 (Apalachicola River near Sumatra, FL).

Approved August 15, 2013

Prepared by the USGS Science Publishing Network
Raleigh Publishing Service Center
Edited by Michael Deacon
Illustrations and layout by Caryl J. Wipperfurth

For more information concerning this report, contact:
Director
U.S. Geological Survey
Georgia Water Science Center
1770 Corporate Drive, Suite 500
Norcross, Georgia 30093
dc_ga@usgs.gov

or visit our Web site at:
http://ga.water.usgs.gov/